國立中央大學天文研究所
鹿林天文台年報

2005

NO.3

國立中央大學天文研究所編

This page intentionally left blank.

序言

這一年充滿歡喜與感傷！！！

中大大家長劉全生校長於 2006 年初退休，劉校長三年前剛到任時即到訪鹿林天文台，退休前再次蒞臨，帶給我們莫大鼓舞，在此祝福他老人家身體健康、萬事如意。

成功大學物理系紅色精靈團隊在鹿林天文台設置 ELF 系統偵測極低頻電波 3 年，首篇科學論文出爐，然作者王雲慶博士不幸於 2004 年因癌症過世，痛失良師益友，令人不勝欷噓！

2005 年最受注目的 9P/Tempel 1 彗星深撞計畫(Deep Impact)，我們與日本國立天文台合作，特地空運儀器來台用鹿林一米望遠鏡進行偏振光觀測，是深撞號太空船所沒有的科學項目。連年參與 WET、WEBT 全球望遠鏡聯測更成為我們必行之事，讓我們與全球天文台接軌，協力觀測，完成單一天文台所不可能達成的任務。累積了多年觀測能量，鹿林的科學成果開始陸續展現，目前已有多篇重要科學論文發表。而在 2005 年物理年會、天文年會及 Star & Telescope XI 會議上，更有許多鹿林觀測的科學報告。新天體發現方面，2005 年發現超新星 3 顆，累計 10 顆；在此年報編輯同時，又發現了第 11 顆。2005 年發現小行星 1 顆，累計 2 顆；此外還發現了一顆新的 Mira 變星。

研究計畫方面，中美合作的 TAOS 觀測進行順利，資料正緊鑼密鼓地分析中，結果可期。LELSI 系統全面更新，正待再次出擊。值得一提的是中大大氣所與環工所在鹿林辛勤採樣 3 載，環保署終於今年在鹿林設置空氣品質背景測站，為基地拓展了另一科學領域。

在國科會鹿林營運計畫的支持下，2005 年開始有觀測專員常駐，負責望遠鏡與儀器的維護及運作，提升了觀測效率及品質。望遠鏡與儀器方面，減焦系統開始投入觀測，提供廣域天區觀測的需求。40 公分遠距遙控望遠鏡的設置，滿足了更多科學觀測的需求。此外一些周邊設備的設立，如雲雨偵測器、夜空監視系統、網路即時氣象系統，則提供了觀測所需的天氣訊息，並為未來遠距遙控及自動觀測做準備。2005 年鹿林 LOT 的總觀測時數 1655 小時，比前兩年平均值略低，大環境的天氣因素我們無能為力，只有更積極的提升觀測效率及研究成果來彌補天候的不足。

除了科學研究外，累積多年辦理中大大學部與研究生鹿林天文觀測實習的經驗，我們也開始開放校外申請，提供國內高等天文觀測教育訓練之需要。並適度地對學校社團開放參訪，其中有遠從新加坡的 Catholic Junior College 慕名而來，訪問了中大天文所及鹿林、墾丁天文台。配合 2005 校慶辦理了校友參訪鹿林活動，體驗校外站台大自然環境，深受好評。

「亮燈密度、全球第一、物理年點燈、台灣光耀世界」鹿林天文台參與 2005 世界物理年/相對論 100 年點燈活動，台灣得到全球第一的殊榮，我們與有榮焉。鹿林喜訊頻傳，同仁石俊雄於今年完成終身大事、石皓偉妻子也懷了第二胎，在此一併祝福他們。

最後要感謝全體工作同仁的後勤支援，您們的辛勤付出，提供了無虞的工作環境。感謝各科學團隊的利用與參與，天文台因您們而存在。感謝教育部、國科會及中大校方的支持，鹿林才能永續發展。感謝同仁張明新先生毫無怨言地連續三年主編年報，沒有他的殷殷催促，這本年報不會出現在各位面前。

20060208

目錄

This page intentionally left blank.

研究報告

IL NUOVO CIMENTO Vol. 28 C, N. 4-5 Luglio-Ottobre 2005
DOI 10.1393/ncc/i2005-10072-x

GRBs Optical follow-up observation at Lulin observatory, Taiwan(*)

K. Y. Huang(1), Y. Urata(2)(3), W. H. Ip(1), T. Tamagawa(2), K. Onda(2) and K. Makishima(2)(4)

(1) *Institute of Astronomy, National Central University Chung-Li 32054, Taiwan, Republic of China*
(2) *RIKEN (Institute of Physical and Chemical Research) 2-1 Hirosawa, Wako, Saitama 351-0198, Japan*
(3) *Department of Physics, Tokyo Institute of Technology 2-12-1 Oookayama, Meguro-ku, Tokyo 152-8551, Japan*
(4) *Department of Physics, University of Tokyo 7-3-1 Hongo, Bunkyo-ku, Tokyo 113-0033, Japan*

(ricevuto il 23 Maggio 2005; pubblicato online il 20 Ottobre 2005)

Summary. — The Lulin GRB program, using the Lulin One-meter Telescope (LOT) in Taiwan started in July 2003. Its scientific aims are to discover optical counterparts of XRFs and short and long GRBs, then to quickly observe them in multiple bands. Thirteen follow-up observations were provided by LOT between July 2003 and Feb. 2005. One host galaxy was found at GRB 031203. Two optical afterglows were detected for GRB 040924 and GRB 041006. In addition, the optical observations of GRB 031203 and a discussion of the non-detection of the optical afterglow of GRB 031203 are also reported in this article.

PACS 95.55.Cs – Ground-based ultraviolet, optical and infrared telescopes.
PACS 98.70.Rz – γ-ray sources; γ-ray bursts.
PACS 01.30.Cc – Conference proceedings.

1. – Introduction

A parallel effort based on the Kiso GRB optical observation system [1,2], was started in July 2003 using the Lulin One-meter Telescope (LOT) at Taiwan. The scientific aims of our Lulin GRB program are: 1) to discover optical counterparts of XRFs, and short- and long-duration GRBs; 2) to perform multi-band observations that will unlock the temporal and spectral evolution of the corresponding optical afterglows. The Lulin observatory is located in Nantou County, Taiwan, at $120°52'25''E$, $23°28'07''N$, on a 2862-m high peak. The sky background levels in the $UBVRI$ bands are: $U = 21.8$; $B = 22.0$; $V = 21.3$; $R = 20.9$; $I = 19.5$ mag arcsec^{-2}, respectively. From statistical

(*) Paper presented at the "4th Workshop on Gamma-Ray Burst in the Afterglow Era", Rome, October 18-22, 2004.

TABLE I. – *Basic characteristics of LOT with PI1300B and AP8 CCD*

Filter	PI1300B CCD			AP8 CCD		
	Zero point[a]	Color term	Extinction	Zero point	Color term	Extinction
B	22.34±0.02	0.199±0.018	0.19±0.02	21.99±0.03	0.035±0.005	0.28±0.02
V	22.68±0.02	−0.058±0.017	0.11±0.01	21.97±0.02	0.069±0.004	0.20±0.02
R	22.66±0.01	−0.049±0.021	0.09±0.01	21.87±0.02	0.113±0.007	0.15±0.02
I	21.99±0.04	0.040±0.029	0.06±0.01	21.27±0.03	0.043±0.005	0.12±0.02

[a]Units: Zero point (mag), Color term (mag), Extinction (mag/airmass)

measurements at Lulin site, it was found that the typical accumulative observation time is 1700 hours per year and the typical seeing is 1.5 arcsec. The LOT is a Cassegrain telescope ($f/8$) with an ACE filter system and a main CCD camera— PI1300B (1340 × 1300, F.O.V.∼ 11.5′ × 11.2′) as well as a spare CCD camera—Ap8 ($1k \times 1k$, F.O.V. ∼ 10.6′× 10.6′). Table I shows the characteristics of LOT with AP8 and PI1300B CCD [3].

Due to the fact that there are only a very few telescopes for GRB follow-up observations in East Asia, and that the observational range can reach up to Dec. −40 degree, Lulin enjoys a unique position for GRB study. The fast PI1300B read out time that allows small cadence multi-band time series photometry is another distinct advantage. Due to the nature of GRBs detection, the Lulin GRB project is included as a part of the Target of Opportunity (TOO) program. We have developed two approaches to search for GRB optical afterglows, according to the dimensions of the burst error box provided by such satellites as *HETE-2*, INTEGRAL, and SWIFT. First, if the error range is larger than the FOV of the LOT, we can dither the field and search for the optical counterpart in the B or R band. Second, if the error range is smaller than the FOV, we can quickly locate the counterpart and monitor the temporal variation of the brightness of the optical afterglow in several wavelengths.

During the analysis procedure, the positions and coordinates of the detected objects in our images are compared with the USNO stellar coordinates. These physical coordinates are then transformed to equatorial coordinates using the WCS (World Coordinate System). After this, our images compared with DSS2 images, to look for likely candidates.

2. – Summary of observed events

Between July 2003 and Feb. 2005 (table II), thirteen follow-up observations were provided by LOT. We could provide upper limits to the magnitude for ten events. Two optical afterglows were detected for GRB 040924 and GRB 041006 and the host galaxy of GRB 031203 was identified. We will focus on the GRB 031203 case in the following.

GRB 031203 was detected by the IBIS instrument on *INTEGRAL* on December 3, 2003 at 22:01:28 UT as a single peaked burst with a duration of 30s [4]. Newton-XMM detected two sources named S1 and S2 within the INTEGRAL error circle. The brightest source S1, which faded throughout the observation period, was interpreted to be the afterglow [5]. Its position coincided with that of a fading radio source [6].

A new source was detected by Lulin I-band observations [7]; see fig. 1. Bloom *et al.* [8] have pointed out that this new source could either be a galaxy in the foreground or the

TABLE II. – *Log of Lulin GRB follow-up observations.*

GRB	Delay time (hr)	Triggered Spacecraft	Limit mag. (3σ)	Results	Publications
GRB 030823	3.3	*HETE-2*	$R \sim 19$	Upper limit	GCN 2360
GRB 031026	6.0	*HETE-2*	$R \sim 21$	Upper limit	GCN 2436
GRB 031203	19.6	*INTEGRAL*	$I \sim 20$	Host Galaxy	GCN 2470
GRB 031220	8.0	*HETE-2*	$R \sim 20$	Upper limit	GCN 2494
GRB 040422	9.6	*INTEGRAL*	$R \sim 20$	Upper limit	GCN 2577
GRB 040916	16.3	*HETE-2*	$I \sim 20$	Upper limit	GCN 2721
GRB 040924	2.3	*HETE-2*	–	OT	GCN 2744
GRB 041006	9.0	*HETE-2*	–	OT	GCN 2785
GRB 041211	3.4	*HETE-2*	$R \sim 20$	Upper limit	GCN 2840
GRB 041219	9.6	*SWIFT*	$R \sim 21$	Upper limit	GCN 2891
GRB 050123	5.5	*HETE-2*	$I \sim 19$	Upper limit	GCN 2971
GRB 050124	4.4	*SWIFT*	$R \sim 20$	Upper limit	GCN 2976
GRB 050215B	13.1	*SWIFT*	$V \sim 19$	Upper limit	GCN 3030
			$I \sim 20$	Upper limit	GCN 3030

host of GRB 031203. A radio afterglow was detected at the same position. From spectroscopic observations, Prochaska *et al.* [9] found this to be an active star-forming galaxy, with $z = 0.105$ and that should be the host galaxy of GRB 031203, designated HG 031203.

The LOT follow-up observations in combination with other I-band data [10-12], indicated that the source did not show variability in terms of its brightness (fig. 2). Thus, the optical source detected was the host galaxy, HG 031203, and no variable source brighter than $I = 20.0$ was found during our observations. The astrometry of the GRB 031203 field was corrected by matching with stars in the USNO A2 catalog. This resulted in the following astrometric position of HG 031203: R.A. $= 08^{\rm h}02^{\rm m}30^{\rm s}.177 \pm 0.175$ arcsec, Dec. $= -39°51'03''.960 \pm 0.164$ arcsec (J2000.0). It is important to note that optical and spectroscopic observations made by several groups have revealed that SN 2003lw was associated with GRB 031203. It had a brightness peak between 26 and 34 days after the gamma-ray burst [10-13].

In order to explore the reason behind the absence of optical afterglow, we have analyzed the X-ray Newton-XMM afterglow data. Using the power law plus absorption model, we found that the best fit of the photon index is 1.8 ± 0.1 ($\chi^2 = 14.07$ with 22 dof) with $N_H = 7.73 \pm 0.04 \times 10^{21}\,\mathrm{cm}^{-2}$ for the energy between 0.6 keV to 10 keV. Our results are consistent with those found by Watson *et al.* [14]. Assuming no break in the lightcurve, the spectral flux distribution follows $F_\nu \propto \nu^{-\beta} (\beta = 0.8 \pm 0.1)$ and the

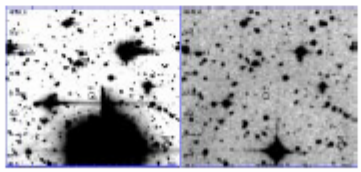

Fig. 1. – LOT I-band image of XMM-Source: S1 and S2. By comparing this with the DSS I-band image, we found a source near S1.

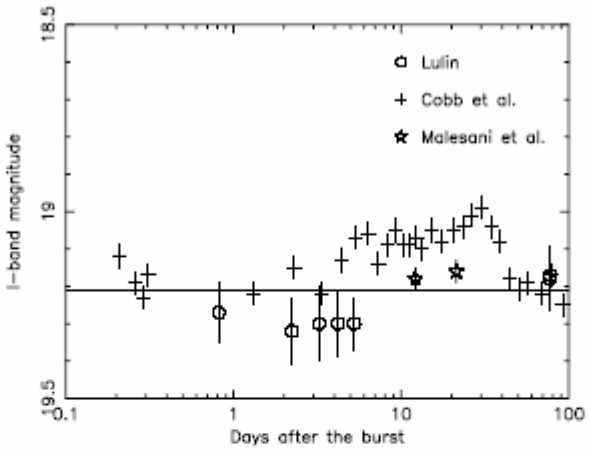

Fig. 2. – Lightcurve of HG 031203 at the I-band. The solid line shows the magnitude of the host galaxy ($I = 19.21$).

extrapolation of the X-ray flux to the optical range yields $I = 20.65$ and $R = 21.13$, at 0.26 days after the burst.

In comparison with the value of $N_H = 7.73 \pm 0.04 \times 10^{21}\,\mathrm{cm}^{-2}$, the neutral hydrogen column density along the line-of-sight to GRB 031203, is on the order of $N_H = 6.21 \times 10^{21}\,\mathrm{cm}^{-2}$ within the Galaxy [15]. This means that most of the extinction of the optical emission of this gamma-ray burst should have come from the Galactic interstellar medium. This effect alone is enough to reduce the optical brightness by 2 magnitudes from 20.65 to about 22.65 at the I-band [15]. This might explain why GRB 031203 shows no optical afterglow.

* * *

We thank all those of Lulin users for helping with the GRB follow-up observations. This work is supported by NSC 93-2752-M-008-001-PAE and NSC 93-2112-M-008-006. K. Y. Huang acknowledges support from from Foundation For the Advancement of Outstanding Scholarship.

REFERENCES

[1] Urata, Y. *et al.*, these proceedings (2005).
[2] Urata, Y. *et al.*, *A.S.P Con. Ser.*, Vol. **312** (2004) 243.
[3] Kinosuita, D. *et al.*, in press (2005).
[4] Sazonov, S. Y. *et al.*, *Nature*, **430** (2004) 646.
[5] Vaughan, S. *et al.*, *ApJ*, **603** (2004) L5.
[6] Soderberg, A. M. *et al.*, *Nature*, **430** (2004) 648.
[7] Hsia, C. H. *et al.*, *GCN Circ.*, (2003) 2470.
[8] Bloom, J. S. *et al.*, *GCN Circ.*, (2003) 2481.
[9] Prochaska, J. X. *et al.*, *ApJ*, **611** (2004) 200.
[10] Thomsen, B. *et al.*, *A&A*, **419** (2004) L21.
[11] Cobb, B. E. *et al.*, *ApJ*, **608** (2004) L93.
[12] Malesani, D. *et al.*, *ApJ*, **609** (2004) L5.
[13] Gal-Yam, A. *et al.*, *ApJ*, **609** (2004) L59.
[14] Watson, D. *et al.*, *ApJ*, **605** (2004) L101.
[15] Dickey, J. M. and Lockman, F. J. , *Annu. Rev. Astron. Astrophys.*, **28** (1990) 215.

Astronomy & Astrophysics manuscript no. pap2 December 20, 2005
(DOI: will be inserted by hand later)

Testing the inverse-Compton catastrophe scenario in the intra-day variable blazar S5 0716+71

I. Simultaneous broadband observations⋆ during November 2003

L. Ostorero[1,2], S. J. Wagner[1], J. Gracia[3], E. Ferrero[1], T. P. Krichbaum[4], S. Britzen[4], A. Witzel[4], K. Nilsson[2], M. Villata[5], U. Bach[5,4], D. Barnaby[6], S. Bernhart[4], M. T. Carini[6], C. W. Chen[7], W. P. Chen[7,8], S. Ciprini[2,9], S. Crapanzano[5], V. Doroshenko[10], N. V. Efimova[11], D. Emmanoulopoulos[1], L. Fuhrmann[9,4], K. Gabanyi[4], A. Giltinan[12], V. Hagen-Thorn[11], M. Hauser[1], J. Heidt[1], A. S. Hojaev[7,13,14], T. Hovatta[15], F. Hroch[16], M. Ibrahimov[13], V. Impellizzeri[4], R. Z. Ivanidze[17], D. Kachel[1], A. Kraus[4], O. Kurtanidze[17,1,18], A. Lähteenmäki[15], L. Lanteri[5], V. M. Larionov[11], Z. Y. Lin[7], E. Lindfors[2], F. Munz[16], M. G. Nikolashvili[17], G. Nucciarelli[9], A. O'Connor[12], J. Ohlert[19], M. Pasanen[2], C. Pullen[20], C. M. Raiteri[5], T. A. Rector[21], R. Robb[22], L. A. Sigua[17], A. Sillanpää[2], L. Sixtova[16], N. Smith[12], P. Strub[1], S. Takahashi[23], L. O. Takalo[2], C. Tapken[1], J. Tartar[24], M. Tornikoski[15], G. Tosti[9], M. Tröller[15], R. Walters[6], B. A. Wilking[24], W. Wills[6], I. Agudo[4], H. D. Aller[25], M. F. Aller[25], E. Angelakis[4], J. Klare[4], E. Körding[4], R. G. Strom[26,27], H. Teräsranta[15], A. Ungerechts[28], and B. Vila-Vilaro[29]

[1] Landessternwarte Heidelberg-Königstuhl, Königstuhl, 69117 Heidelberg, Germany
[2] Tuorla Observatory, University of Turku, Väisäläntie 20, 21500 Piikkiö, Finland
[3] Section of Astrophysics, Astronomy & Mechanics, Department of Physics, University of Athens, Panepistimiopolis, 157 84 Zografos, Athens, Greece
[4] Max-Planck-Institut für Radioastronomie, Auf dem Hügel 69, 53121 Bonn, Germany
[5] Istituto Nazionale di Astrofisica (INAF), Osservatorio Astronomico di Torino, via Osservatorio 20, 10025 Pino Torinese (TO), Italy
[6] Department of Physics and Astronomy, Western Kentucky University, 1 Big Red Way, Bowling Green, KY 42104, USA
[7] Institute of Astronomy, National Central University, 300 Jungda Road, Jungli City 320-54, Taoyuan, Taiwan, ROC
[8] Department of Physics, National Central University, 300 Jungda Road, Jungli City 320-54, Taoyuan, Taiwan, ROC
[9] Osservatorio Astronomico, Università di Perugia, Via B. Bonfigli, I-06126 Perugia, Italy
[10] Crimean Laboratory of the Sternberg Astronomical Institute, University of Moscow, Russia; P/O Nauchny, 98409 Crimea, Ukraine
[11] Astronomical Institute, St. Petersburg State University, Universitetsky pr. 28, Petrodvoretz, 198504 St. Petersburg, Russia
[12] Cork Institute of Technology, Dept. of Applied Physics & Instrumentation, Rossa Avenue, Bishoptown, Cork, Ireland
[13] Ulugh Beg Astronomical Institute, Center for Space Research, Uzbek Academy of Sciences, Astronomicheskaya 33, 700052 Tashkent, Uzbekistan
[14] Isaac Newton Institute, Uzbekistan Branch, Astronomicheskaya 33, 700052 Tashkent, Uzbekistan
[15] Metsähovi Radio Observatory, Helsinki University of Technology, Metsähovintie 114, 02540 Kylmälä, Finland
[16] Institute of Theoretical Physics and Astrophysics, Faculty of Science, Masaryk University, Kotlárská 2, 611 37 Brno, Czech Republic
[17] Abastumani Astrophysical Observatory, 383762 Abastumani, Georgia
[18] Astrophysikalisches Institut Potsdam, An der Sternwarte 16, 14482 Potsdam, Germany
[19] Michael Adrian Observatory, Astronomie Stiftung Trebur, Fichtenstrasse 7, 65468 Trebur, Germany
[20] Coyote Hill Observatory, P.O. Box 930, Wilton, CA 95693, USA
[21] Department of Physics and Astronomy, University of Alaska Anchorage, 3211 Providence Dr., Anchorage, AK 99508, USA
[22] Department of Physics and Astronomy, University of Victoria, BC, Canada
[23] Faculty of Information Sciences, Hiroshima-City University, 3-4-1, Ozuka-Higashi, Asa-minami-ku, Hiroshima, 731-3194, Japan
[24] Department of Physics and Astronomy, University of Missouri–St. Louis, 8001 Natural Bridge Road, St. Louis, MO 63121
[25] Department of Astronomy, Dennison Building, University of Michigan, Ann Arbor, MI 48109 USA
[26] ASTRON, Postbus 2, 7990 AA Dwingeloo, The Netherlands
[27] Astronomical Institute, University of Amsterdam, Kruislaan 403, 1098 SJ Amsterdam, The Netherlands
[28] IRAM, Avd. Div. Pastora 7NC, 18012 Granada, Spain
[29] University of Arizona, Steward Observatory, 933 N. Cherry Ave., Tucson, AZ 85721, USA

Received...; accepted...

Abstract.

Key words. galaxies: active – galaxies: BL Lacertae objects: general – galaxies: BL Lacertae objects: individual: S5 0716+71

Send offprint requests to: L.Ostorero@lsw.uni-heidelberg.de

⋆ Partially based on observations obtained with INTEGRAL, an ESA project with instruments and science data centre funded by ESA member states (especially the PI countries: Denmark, France, Germany, Italy, Switzerland, Spain, Czech Republic and Poland), and with the participation of Russia and the USA. Partially based on observations by the Whole Earth Blazar Telescope (WEBT); for questions regarding the availability of the data from the WEBT campaign, please contact Massimo Villata (villata@to.astro.it). **Partially based on observations with the 100-m telescope of the MPIfR (Max-Planck-Institut für Radioastronomie) in Effelsberg, Germany.**

Abstract. The BL Lacertae object S5 0716+71 was the target of a multifrequency observing campaign during the period October 2003–May 2004. The observations, organized **under the framework** of the European Network for the Investigation of Galactic nuclei through Multifrequency Analysis (ENIGMA) together with a campaign by the Whole Earth Blazar Telescope (WEBT), involved a pointing by the soft-γ–ray satellite INTEGRAL, optical, near-infrared, sub-millimeter, millimeter and radio monitoring, as well as Very Long Baseline Array (VLBA) monitoring. We here report on the results of the core campaign, carried out in the period November 06–20, 2003 simultaneously with the INTEGRAL observation. Its aim was the search for broadband signatures of inverse-Compton (IC) catastrophes possibly occurring in the source. S5 0716+71 was very bright at radio frequencies and in a rather faint optical state ($R = 14.17 - 13.64$) during the INTEGRAL pointing; significant inter-day and low intra-day variability was recorded in the radio regime, while typical fast variability features were observed in the optical band. No obvious correlation was found between the radio and optical emission. The source was not detected by INTEGRAL, neither by the X-ray monitor JEM-X nor by the gamma-ray imager ISGRI, but upper limits to the source emission in the 3–200 keV energy band were estimated. A brightness temperature $T_b > 2.1 \times 10^{14}$ **K (violating the IC limit)** was inferred from the variability observed in the radio regime, but no corresponding signatures of IC avalanches were recorded at higher energies.

1. Introduction

The phenomenon of intra-day variability (IDV; Wagner & Witzel 1995) has been a long-standing problem since its discovery in the late 1960s (see e.g. Racine et al. 1970; Witzel et al. 1986; Heeschen et al. 1987). **The occurrence of IDV appears to be more common in flat-spectrum extragalactic sources dominated by a very compact core in Very Long Baseline Interferometry (VLBI) maps (Quirrenbach et al. 1992, 2000). With recent Very Long Baseline Array (VLBA) measurements, Kovalev et al. (2005) showed that IDV sources typically exhibit a higher compactness and core-dominance on sub-milliarcsecond scales than non-IDV ones; they also found that a higher amplitude of intraday variations characterizes sources with a higher flux density in an unresolved VLBA component, and that the most variable sources tend to have the most compact structure.**

Rapid variations in flux may be caused by **mechanisms intrinsic to the source**. In this case, causality arguments would imply **that the variability originates** from very compact regions of the AGN, thus characterized by high photon densities and brightness temperatures. In sources of incoherent synchrotron radiation, very high photon densities would lead to catastrophic cooling via inverse-Compton (IC) scattering of the synchrotron radiation by the high-energy electrons, with a production of high-energy radiation much higher than **observed** (Hoyle et al. 1966). Kellermann & Pauliny-Toth (1969) showed that the onset of catastrophic radiation losses, occurring when the photon energy density in the emission region exceeds the energy density of the magnetic field, limits the maximum observed brightness temperature to the so-called 'IC limit' $T_b \lesssim 10^{12}$ K (see also Readhead 1994). They also noticed, however, that this limit may be significantly exceeded under non-stationary conditions. Evidence of severe violations of the IC limit was reported for many compact IDV radio sources (see e.g. Quirrenbach et al. 1989; Wagner & Witzel 1995; Kedziora-Chudczer et al. 1997), although no information about corresponding IC-scattered emission is available for any of them.

Alternatively, propagation effects, like variations of the absorption along the line of sight, deflection of the light in the potential **well** of foreground stars (microlensing; Chang & Refsdal 1979), and, in the radio regime, interstellar scintillation (ISS; Rickett 1990; Rickett et al. 1995), are possible extrinsic-source mechanisms which have been invoked to explain IDV. On the one hand, microlensing was shown to be an unlikely explanation of the rapid variability in the best-studied IDV sources, due to the frequency of the flaring activity, the statistical asymmetry of the light curves, the short time scales of variability, and the non-zero lag measured between optical and radio variations (see Wagner 1992 and references therein). On the other hand, ISS is not expected to play a major role at millimeter and sub-millimeter wavelengths, the transition between weak and strong scintillation regimes occurring in the centimeter domain (Rickett et al. 1995).

In order to reconcile intrinsic variations with the theoretical limit, different explanations, like beaming of the emission due to bulk relativistic motion (Rees 1967), coherent radiation mechanisms (Baker et al. 1988; Benford 1992; Lesch & Pohl 1992), propagation of a shock in an underlying, stable relativistic jet (Qian et al. 1991), were proposed. Neither the broadband nature of the spectral energy distribution (SED) observed in IDV sources (see e.g. Quirrenbach et al. 1989; Wagner et al. 1993, 1996) nor the VLBI observations strongly support **any** of them, leaving the alternative explanation that the IC limit might actually be violated and inverse-Compton catastrophes occur during transient periods (Kellermann & Pauliny-Toth1969; Slysh 1992). In this paper, this hypothesis is explored for a prototypical source, S5 0716+71.

This source is one of the brightest and best-studied BL Lacertae objects in the sky. It was one of the prime targets for investigating the mechanism responsible for IDV, and the first source in which simultaneous variations in the radio and optical bands, indicating a possible intrinsic origin of the observed IDV, were reported (Wagner et al. 1990; Quirrenbach et al. 1991). Moreover, it exhibited IDV during all the past optical studies and almost all the radio campaigns carried out during the last two decades (Heeschen et al. 1987; Wagner et al. 1990, 1996; Ghisellini et al. 1997; Sagar et al. 1999; Quirrenbach et al. 2000; Villata et al. 2000; Nesci et al. 2002; Kraus et al. 2003; Raiteri et al. 2003). The IDV duty cycle of the source (the fraction of time in which the object is variable) derived from these studies is ~ 90%.

Deep maps of the source obtained with the Very Large Array (VLA) show a core-halo structure on **the** arcsecond scale. VLBI observations over more than 20 years at centimeter wavelengths reveal a very compact source, with evidence of a core-dominated jet structure extending several tens of milliarc-

seconds to the North (Eckart et al. 1986, 1987; Witzel et al. 1988; Polatidis et al. 1995; Jorstad et al. 2001). The milliarcsecond jet is misaligned with respect to the VLA jet by ~ 75° (Britzen et al. 2005; see also Eckart et al. 1987).

Controversial scenarios, involving a wide range of proper motions (0.05–1.2 mas/year), were proposed for the kinematics of the S5 0716+71 jet components, the more recent ones pointing towards apparent velocities which are atypically fast for BL Lac objects (see Bach et al. 2005a, and references therein).

The redshift of the source is still unknown, although the starlike appearance and the absence of any signature of a host galaxy in deep images had set a lower limit of $z > 0.3$ (Quirrenbach et al. 1991; Stickel et al. 1993; Wagner et al. 1996). **More recently, Sbarufatti et al. (2005) suggested a higher lower limit of $z > 0.52$**. The exact brightness temperature of the source can therefore not be determined: lower limits up to $T_b \sim 10^{17}$ K were inferred from radio IDV at 5 GHz (Quirrenbach et al. 1991; Wagner et al. 1996), whereas a limit of $T_{b,z=0} = \mathbf{1.85 \times 10^{13}}$ K was estimated from the constraints on the core size derived through interferometric measurements performed in August 2003 with the Very Long Baseline Array (VLBA) at 15 GHz (Kovalev et al. 2005). This source is hence an ideal target for the investigation of radiative signatures of IC catastrophes.

S5 0716+71 has been detected at GeV energies with a steep γ-ray spectrum (Hartman et al. 1999), but the soft-γ–ray part of its spectral energy distribution is poorly known: only upper limits to the emission provided by OSSE (McNaron-Brown et al. 1995) and COMPTEL (Schönfelder et al. 2000) are available in the literature.

Synchrotron-self-Compton (SSC) emission models, which can reproduce the GeV γ-ray emission of the source (see e.g. Ghisellini et al. 1997), predict the SED peak to occur in the MeV–GeV domain. A recent reanalysis of the COMPTEL data (Collmar **2005**) resulted in a source detection in the 3–10 MeV energy range, which is consistent with this scenario. The above SSC modelling involves a wide range of Lorentz factors of the radiating particles, up to $\gamma \sim 10^5$, in order to explain the high-energy component of the spectrum.

In a Compton catastrophe, the main role is expected to be played by electrons responsible for the bulk of the radio emission in the GHz regime, where the violations of the IC limit have been observed. Assuming an observed peak frequency of the radio spectrum of a few GHz, and a magnetic field $B \gtrsim 10^{-3}/\delta$ μG (δ being the Doppler factor of the emitting region), the above electrons would be characterized by Lorentz factors not greater than a few **times** 10^2. First-order IC scattering by these particles would generate bursts of radiation at $\sim 10^{14} - 10^{15}$ Hz, which might blend with the synchrotron radiation **produced** by the high-energy tail of the same distribution of particles. The dominant loss-term would be second-order IC scattering (see e.g. Kellermann & Pauliny-Toth 1969; Bloom & Marscher 1996), also responsible for the onset of the catastrophe, and would boost photons into the $10^{18} - 10^{20}$ Hz frequency range. Flares of IC-scattered radiation should therefore be observed in this energy range whenever the Compton limit is violated. The efficient cooling associated with a Compton catastrophe would then rapidly restore the actual brightness temperature of the source.

The advent of the soft-γ–ray INTEGRAL satellite offers an unprecedented chance of investigating this effect.

A multifrequency campaign involving an INTEGRAL pointing of the source and simultaneous radio, millimeter, submillimeter, near-infrared, and optical photometric monitoring, as well as VLBA observations, was organized and carried out during November 2003. For the first time, constraints on the brightness temperature and on the IC emission of the source were tested simultaneously against each other.

The first results of the ground-based observing campaign are presented in Sect. 2 of this paper; the INTEGRAL observations are described in Sect. 3; the simultaneous spectral energy distribution of the source is presented in Sect. 4; in Sect. 5 we discuss our results and draw conclusions.

2. Ground-based multifrequency observations

The multiwavelength observations, organized **under the framework** of the ENIGMA[1] collaboration together with a WEBT[2] campaign were scheduled for the period November 06–20, 2003 (hereafter referred to as core campaign) to provide the low-energy counterpart of the INTEGRAL observation of S5 0716+71. Since the source underwent an unprecedented outburst phase at radio and millimeter frequencies during September–October 2003, the campaign was started earlier. When the core campaign began on November 06 (JD = 2452949.5), S5 0716+71 was still brighter than in all past studies in the radio and millimeter domain. A rather faint optical state ($R \sim 14.17 - 13.64$) characterized the source in this band for the whole duration of the INTEGRAL pointing. During the last two days of the core campaign the source entered a brightening phase, and the ground-based monitoring was continued.

We here present the results of the core campaign in terms of radio light curves at 32 and 37 GHz, and an optical R-band light curve. Flux variation ranges at other radio, millimeter and sub-millimeter frequencies are included in the simultaneous SED presented in Sect. 4; the corresponding light curves will be discussed in Agudo et al. (2005) and Fuhrmann et al. (in prep.). The ground-based observing facilities whose contribution to the core campaign is presented in this paper are listed in Table 1.

2.1. Radio data

2.1.1. Observations, data reduction and calibration

The radio observations of S5 0716+71 at 32 GHz were performed during JD = 2452954.889–2452961.251 with the 100-m radio telescope in Effelsberg. The measurements were carried out using repeated scans, each of them consisting of 4–8 cross-scans in azimuth and elevation, resulting in typical single

[1] http://www.lsw.uni-heidelberg.de/projects/enigma/

[2] http://www.to.astro.it/blazars/webt/
(see e.g. Mattox et al. 1998; Villata et al. 2004, Raiteri et al. 2005, and references therein)

Table 1. List of the ground-based observing facilities whose contribution to the core campaign is presented in this paper in the form of light curves and/or flux variation ranges in the SED. a: Radio, millimeter and submillimeter antennas, listed in ascending order of the lowest observing frequency. b: Optical telescopes, listed in order of longitude, and their contribution to the core campaign in terms of *R*-band useful data (and observing nights). The offsets indicate the corrections applied to the data sets in order to eliminate instrumental inconsistencies (when a range is given, different offsets were used in different nights).

a. Radio, millimeter and sub-millimeter observatories			
Observatory (telescope)	Location	Telescope diameter (m)	Observing frequencies (GHz)
Westerbork	The Netherlands	14 × 25	1.392, 1.67
UMRAO	Michigan, USA	26	4.8, 8.0, 14.5
Effelsberg	Germany	100	4.85, 10.45, 32.0
Metsähovi	Finland	13.7	22.2, 36.8
IRAM	Spain	30	86.0, 230.0
HHT-SMTO	Arizona, USA	10	345.0
JAC (JCMT)	Hawaii	15	350.0, 664.0

b. Optical observatories				
Observatory	Location	Telescope diameter (cm)	*R*-band data (nights)	Offsets
Lulin	Taiwan	100	153 (7)	0.
Mt. Maidanak	Uzbekistan	150	2 (1)	0.
Abastumani	Georgia	70	655 (6)	[−0.03;0.]
Crimean	Ukraine	70	3 (2)	+0.03
Tuorla	Finland	103	102 (2)	[+0.01;+0.02]
MonteBoo	Czech Republic	62	59 (2)	[+0.05;+0.07]
Perugia	Italy	40	7 (4)	0.
Heidelberg	Germany	70	333 (8)	[+0.03;+0.06]
Michael Adrian	Germany	120	90 (4)	+0.03
Torino	Italy	105	19 (3)	−0.02
Hoher List	Germany	106	41 (2)	+0.14
Calar Alto	Spain	220	374 (3)	[+0.01;+0.02]
Roque de los Muchachos (KVA)	Spain	35	58 (5)	−0.01
Roque de los Muchachos (WHT)	Spain	420	751 (1)	0.
Bell	Kentucky, USA	60	3 (1)	0.
St. Louis	Missouri, USA	36	3 (1)	0.
Kitt Peak (WIYN)	Arizona, USA	90	21 (6)	0.
Coyote Hill	California, USA	28	73 (1)	0.
University of Victoria	Canada	50	102 (1)	0.

flux-density exposure times of 120–480 s. The antenna temperature on the source was measured through the averaged pointing-corrected amplitude of the Gaussian-shaped cross-scans and with the standard data reduction software of the 100-m telescope. Regular measurements of the system temperature were used to determine the time-dependent fluctuation of the atmospheric opacity, which was used to correct the measured antenna temperature for each scan. Several non-variable secondary calibrators (within 10°–20° of S5 0716+71) were observed with the same sampling of the target source, in order to ensure an accurate calibration of the residual gain fluctuations, mainly due to atmospheric effects. The total flux density scale was fixed using the standard primary calibrators (e.g. 3C 286, 3C 295, NGC 7027), whose fluxes are given in Baars et al. (1977) and Ott et al. (1994). Further details on the observing method and data reduction scheme can be found in Kraus et al. (2003) and references therein.

The measurements at 37 GHz were obtained in the period JD = 2452951.878–2452962.838 with the 13.7-m diameter radome-enclosed antenna of the Metsähovi Radio Observatory. The 37-GHz receiver is a dual horn, Dicke-switched receiver with a HEMT preamplifier, and it is operated at room temperature. *On-on* observations were performed, alternating the source and the sky in each feed horn, and adopting typical integration times of 1200–1400 s. The source DR 21 was used as primary flux calibrator, whereas 3C 84 was used as secondary calibrator. Errors on the calibrated fluxes were computed by taking both the contribution of the measurement rms and the uncertainty on the absolute calibration into account. More details about the Metsähovi observing system and data reduction can be found in Teräsranta et al. (1998) and references therein.

2.1.2. The light curves

Fig. 1a shows a superposition of the 32 GHz (black symbols) and 37 GHz (grey symbols) radio light curves. In spite of the different measurement accuracy and scatter which characterize the two data sets, a rise of the source flux over the observing period, with some shorter-term fluctuations superimposed, is clearly visible at both wavelengths.

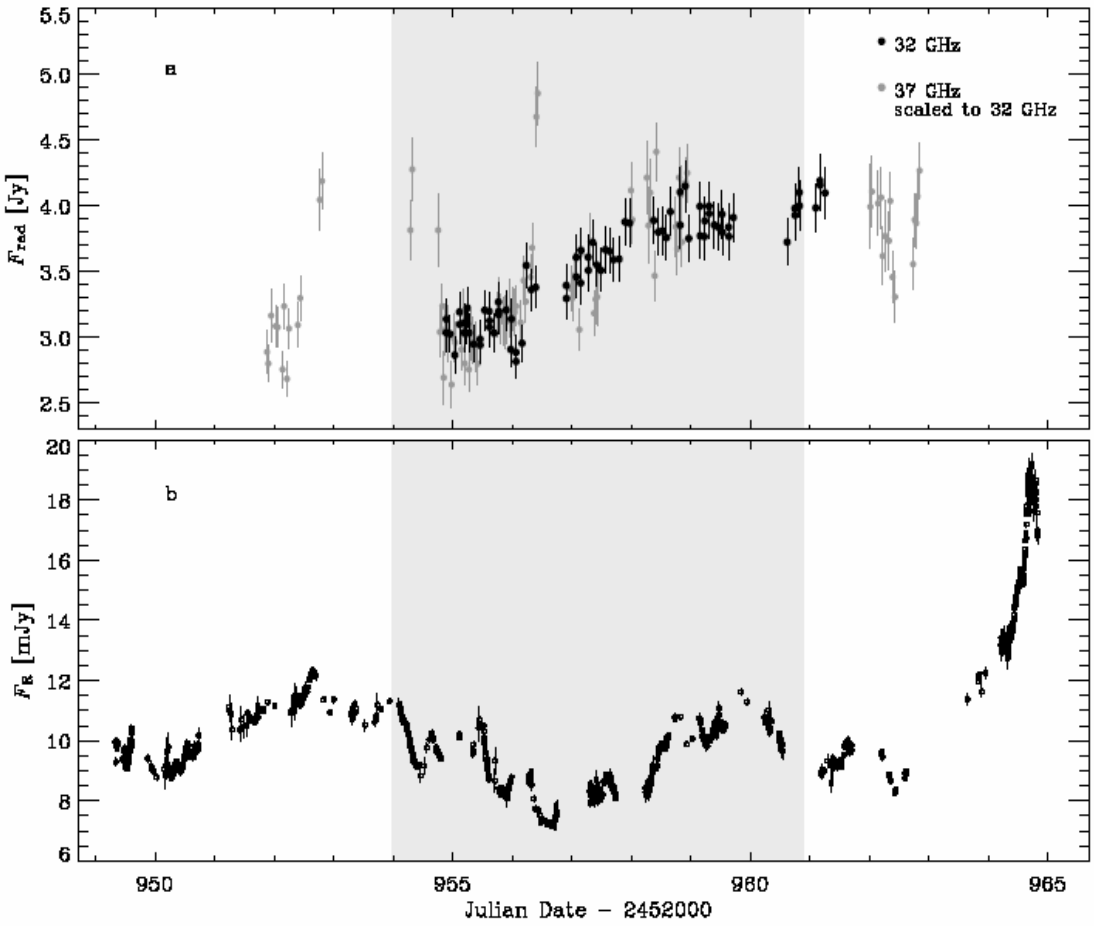

Fig. 1. Radio-optical light curve of S5 0716+71 during the core campaign. Panel a: 32 GHz radio light curve, and 37 GHz radio light curve scaled to the 32 GHz one (scaling factor: $< F_{32\,GHz}/F_{37\,GHz} >=0.89$). Panel b: *R*-band optical light curve. The shaded strip indicates the period of the INTEGRAL pointing. The two radio light curves, consistent with each other, exhibit significant inter-day variability but low-amplitude IDV. The optical light curve displays a weekly modulation of the emission with typical IDV features superimposed.

A variability test was performed on the two data sets by checking their consistency with a constant flux level at 0.1% significance level: the test yielded a negative result, meaning that the light curves clearly exhibit variability.

The overall increase of the brightness was approximated by a linear slope: the 32-GHz data can be represented by a linear increase of the flux of 41% in 6.4 days, whereas the 37-GHz data can be described by a flux rise of 39% in 10.7 days (see Table 2a).

A consistency check of the two light curves was performed for the period in which they overlap, namely JD = 2452954.878–2452958.962 . In this period, the data at 32 and 37 GHz were characterized by a sampling of ~ 12 and ~ 15 data-points per day, and average flux uncertainties of 4.6% and 5.0%, respectively. The difference in scatter of the two data trains is reflected in the fractional root-mean-square variability amplitude F_{var} (Vaughan et al. 2003, and references therein), which is 9.1% at 32 GHz and 13.9% at 37 GHz. However, a Kolmogorov-Smirnov test showed that the differences between the 32-GHz and the 37-GHz data (rescaled to the 32-GHz frequency) are normally distributed at 95% significance level, confirming that the measurement errors can well account for the discrepancies between the two curves. The light curves are hence consistent with each other.

The period of overlap of the two light curves covers the inter-day flux variation recorded in the source during the core campaign: the rise in flux is consistent at both frequencies with the linear increase of 35% in 4.1 days which best fits the 32-GHz data (see Table 2b).

A search for faster variations was then performed in both light curves for the whole core-campaign period, during which the sampling of each light curve is such that it is easy to identify subsets of data separated in time by gaps of ~ 8 hours.

At 32 GHz, four subsets of light curve can be fitted by a linear trend, whose slope is significantly variable. The result of the variability test **(made by assuming the slope equal to zero)** and the best-fit value of the slope are reported, for each subset, in Table 2c. **Seven subsets of data at 37 GHz can also be approximated by linear slopes (see Table 2c), with the exception of seven measurements during JD = 2452952, 2452954,**

Table 2. Results of the linear fits to the radio light curves at 32 and 37 GHz over different periods during the core-campaign (see text for details). Col 1: time interval relevant to the fit; Col. 2: observing frequency [and size of the time bin applied to the light curve in order to make the linear fit acceptable at 5% significance level]; Col. 3: linear slope; Col. 4: reduced χ^2 of the fit; Col. 5: Fit significance.

Time interval (JD-2452000.00)	ν (GHz) [bin (h)]	Slope (Jy/d)	χ^2_{red}	Sign. (%)
		a		
954.889–961.251	32	+0.19 ± 0.01	1.00	47.53
951.878–962.838	37 [12.4]	+0.12 ± 0.03	1.38	19.04
		b		
954.878–958.962	32	+0.25 ± 0.02	0.96	55.30
	37 [3.]	+0.35 ± 0.15	1.22	22.71
		c		
954.889–956.391	32	0.	1.21	19.97
	32	+0.08 ± 0.06	1.17	24.08
956.904–957.968	32	0.	0.86	61.50
	32	+0.35 ± 0.13	0.38	98.50
958.372–959.711	32	0.	0.36	99.67
	32	−0.01 ± 0.09	0.38	99.45
960.614–961.251	32	0.	0.60	77.58
	32	+0.48 ± 0.28	0.28	96.36
951.878–952.437	37	0.	3.19	0.39
	37	0.42 ± 0.27	2.26	1.61
954.782–955.419	37	0.	1.13	32.26
	37	−0.24 ± 0.22	1.12	33.46
955.743–956.310	37	0.	0.49	92.96
	37	0.42 ± 0.27	0.33	98.37
956.980–957.423	37	0.	1.67	9.96
	37	−0.10 ± 0.37	1.88	6.87
957.990–958.938	37	0.	2.09	1.16
	37	0.05 ± 0.17	2.24	0.79
962.010–962.428	37	0.	2.23	1.73
	37	−1.86 ± 0.57	1.09	36.32
962.729–962.839	37	0.	2.23	6.30
	37	6.75 ± 2.38	0.27	84.51
		d		
952.213–952.803	37	+2.61 ± 0.33	3.58	46.52
954.286–954.980	37	−2.14 ± 0.30	2.32	2.32
956.225–956.428	37	+8.86 ± 1.21	2.88	3.47

and 2452956 (see Table 2d). The most extreme deviation was the one recorded during JD = 2452956 (which yielded a flux difference of $\sim 4\sigma$ in the distribution discussed above), corresponding to a linear increase of the flux of 42% in 0.12 days. The other two strong deviations can be described by linear flux variations of 33% in 0.41 days and 20% in 0.12 days, respectively.

The reliability of the observations can be best estimated by comparing the measurements taken simultaneously with different telescopes (see e.g. Witzel et al., 1992, for a comparison of the 5-GHz observations of S5 0716+71 performed at the same time with the VLA and the Effelsberg telescope in May 1989). Therefore, although a careful analysis of the 37-GHz data showed that the measurements characterized by extreme deviations were not affected by any obvious systematic effect, the lack of any counterpart at other radio frequencies did not allow us to consider the lower limits to the brightness temperatures inferred from those variations (up to $\boldsymbol{T_b \sim 1.5 \times 10^{17}}$ K) as a reliable constraint on the variability brightness temperature of the source.

2.2. Optical data

2.2.1. Observations

Table 1b (cols. 1–4) shows names and locations of the nineteen observatories which contributed to the core campaign with *R*-band optical data, together with the sizes of the telescopes used and the amount of useful observations provided.

The optical observers were recommended to perform intranight observations of S5 0716+71 and of the field reference stars nos. 1 to 8 whose finding chart and standard magnitudes are given in Villata et al. (1998). The choice of the exposure times was left to the observers, who found the optimal compromise between high accuracy and good time sampling.

The core-campaign period was characterized by unfavourable weather conditions in most of the observing sites. However, the high declination of the source, the long northern nights, and the large number of telescopes involved allowed a considerable overlap among observations carried out with telescopes located at very different longitudes. This led to unprecedented dense monitoring of the source over such a long period: 2849 useful observations were performed in ~ 15 days, with an average rate of ~ 8 frames per hour.

2.2.2. Data reduction, calibration and assembling

Ten out of nineteen data sets (44% of the collected data) were homogeneously analysed with aperture photometry on de-biased and flat-fielded frames. The remaining data sets were analysed with different procedures by the observers themselves.

The instrumental magnitudes were then processed in order to obtain the standard magnitudes of S5 0716+71 and the relevant errors. Due to the variety of characteristics of the telescopes and detectors involved, as well as of the collected photometric results, not all the reference stars suggested to the observers were available for the calibration. Moreover, because the source was faint during most of the core campaign, the long exposure times required often caused the saturation of reference stars 1 and 2. In order to achieve a homogeneous data calibration and minimize the instrumental offsets, we defined our calibration sequence of reference stars common to most of the data sets and free of saturation, i.e. stars 3, 5 and 6. **The uncertainty on the S5 0716+71 calibrated magnitudes was estimated, for each subset of data taken during the same night and under comparable observing conditions, as follows: the two stars of the calibration sequence closest in magnitude to the source were selected, and their magnitude difference calculated. For each frame, the deviation of this quantity with respect to its mean was found. The error was taken as the larger of this deviation and the standard deviation of the difference over the night.**

Binning (over time intervals from 5 to 20 minutes) was applied to intranight data trains affected by noise and/or low accuracy due to either non-optimal sky conditions or too short integration times.

The calibrated light curves relevant to the various telescopes were then assembled according to the procedure described in Villata et al. (2002). Instrumental offsets were computed, night by night, whenever this was allowed by the temporal overlap between two data sets, i. e. when one of the two datasets had at least two data points belonging to the time interval covered by the second data set. Each offset was defined as the mean magnitude difference of the overlapping parts of the two light curves, the difference being computed between pairs of data points separated in time by no more than 5 minutes (see Table 1b, col. 5). The data sets were then corrected by the above offsets. Data subsets characterized by both lower accuracy and worse time sampling were finally discarded when higher-accuracy and better-sampled data trains were available in the same time interval. Data points affected by errors greater than 0.05 mag were not included in the final light curve, unless no other data were available within 10 minutes. The average accuracy of the final light curve is of **order** ~ 1%.

2.2.3. The light curve

The R-band core-campaign light curve is displayed in Fig. 1b. Fluxes were derived from magnitudes using the absolute calibrations of Bessel (1979), and dereddened with the extinction laws of Cardelli et al. (1989), under the assumption of a Galactic extinction $A_B = 0.132$ mag (provided by NED; from Schlegel et al. 1998).

This light curve is characterized by a mean gap of 20 minutes through the whole core-campaign period, and of about 14 minutes during the INTEGRAL observation.

The source displayed remarkable variability during the core campaign: the overall peak-to-peak R-band variation was $\Delta F_R = 12.1$ mJy ($\Delta R = 1.07$ mag), and the fractional root mean square variability amplitude $F_{var} = 23.3\%$.

A weekly modulation of the emission with intra-day features superimposed characterized the relatively faint state of the source before JD = 2452963.0: during this period the source brightness varied between 7.2 and 12.4 mJy ($R = 14.17 - 13.58$), the mean flux was $< F_R >= 9.5$ mJy ($< R >= 13.87$), and $F_{var} = 10.6\%$. After JD = 2452963.0, a brightness rise of 7.8 mJy ($\Delta R = 0.57$ mag) occurred in 25.7 hours, and the source reached 19.2 mJy ($R = 13.10$ mag), the highest level recorded during the core-campaign period.

The IDV features do not generally show well-defined shapes, suggesting that there might be blending between **successive** flares. Their linear parts (in magnitude scale), lasting up to ~ 3.5 hours, display rising and declining rates not faster than 13% per hour. These variation rates are comparable with the steepest slopes reported by Wagner et al. (1996) (~ 10% h^{-1}) and also with the slopes found by Villata et al. (2000) (12% h^{-1}). Lower intra-day variations, on comparable time scales, were reported by Ghisellini et al. (1997), Sagar et al. (1999) and Nesci et al. (2002). Detailed temporal and spectral analysis of the optical variability will be given in forthcoming papers.

3. INTEGRAL observations and data analysis

INTEGRAL (Winkler et al. 2003) observed S5 0716+71 from 2003 November 10th, 11:20:04 UT to 2003 November 17th, 09:09:31 UT, for a total amount of ~ 539 ks.

The observations were strongly affected by the biggest ever recorded solar flare (classified as X28), which occurred on November 04, 2003. Because of this event, SPI (Vedrenne et al. 2003) underwent annealing treatment during revolutions 132–136 and was not operational for most of the granted observing time. Of the two detectors of JEM-X (Lund et al. 2003), only JEM-X 2 was used, while JEM-X 1 was switched off. IBIS/ISGRI (Ubertini et al. 2004; Lebrun et al. 2003) and IBIS/PICsIT (Ubertini et al. 2004; Di Cocco et al. 2003) were both operational.

The INTEGRAL data were analysed by means of the INTEGRAL Offline Scientific Analysis (OSA) software, whose algorithms are described in Westergaard et al. (2003) for JEM-X and Goldwurm et al. (2003) for IBIS. **Version 4.2 of the OSA software was used for the analysis of the IBIS data, whereas the improved OSA 5.0 was necessary for the JEM-X data analysis.** The PICsIT data could not be analysed due to the failure of the OSA software pipeline.

3.1. JEM-X

The JEM-X observation is split into 145 different science windows with an average exposure of ~ 3 ks each. The OSA software was used to look for sources within an offset angle of 5° to avoid spurious detections. S5 0716+71 was not detected in any of the single science windows, neither in the 3-35 keV band nor in any sub-band. There was also no other detected source in the field of view.

We combined the images from all the individual science windows into a mosaic (corresponding to a total effective exposure of ~ 381 ksec) with **the *varmosaic* routine of the FTOOL package**; however, the source remained undetected.

We estimated an upper limit to the flux of S5 0716+71 by means of the statistical variance of the mosaic intensity at the position of the source. The 3σ upper-limit intensity (cts cm $^{-2}$s $^{-1}$), with σ being the square root of the variance, was multiplied by the ratio of the flux of the Crab Nebula in the JEM-X band (Toor & Seward 1974; Nørgaard et al. 1994) and the JEM-X intensity obtained from a mosaic image of the Crab. Assuming for S5 0716+71 the spectrum of the Crab ($\Gamma = 2.1 \pm 0.03$; see Toor & Seward 1974), we obtained a **3σ flux** upper limit of $F_{3-35\ keV} = 6.12 \times 10^{-12}$ **erg cm** $^{-2}$ s^{-1} (see Table 3a), which is **lower than** the upper limit derived by Pian et al. (2005) from a shorter (189 ks) observation performed in April 2004.

3.2. IBIS/ISGRI

The ISGRI instrument data set consists of 150 science windows, corresponding to a total effective exposure of 362 ksec.

Table 3. Results of the INTEGRAL analysis: JEM-X and IBIS/ISGRI 3σ upper limits to the flux of S5 0716+71 during November 10–17, 2003.

a. JEM-X			
Energy range (keV)	**Intensity** (10^{-5} cts/cm^2/s)	Photon index Γ*	Flux (10^{-12} erg/cm^2/s)
3 – 35	**< 5.89**	2.1	**< 6.12**

b. IBIS/ISGRI			
Energy range (keV)	Count rate** (cts/s)	Photon index Γ*	Flux (10^{-11} erg/cm^2/s)
15 – 40	**< 0.176**	1.6 – 2.1	**< 1.34 – < 1.41**
40 – 100	**< 0.160**	1.6 – 2.1	**< 1.70 – < 1.72**
100 – 200	**< 0.140**	1.6 – 2.1	**< 5.58 – < 5.73**

* Photon index adopted to derive the flux from the count rate, under the assumption that $F(E) \propto E^{1-\Gamma}$

** Count rate errors are 1σ uncertainties

The standard energy binning was used for the image deconvolution, and the individual frames were accumulated into a co-added mosaic image. Several sources, including Mrk 3 and Mrk 6, were reported as significant detections by the OSA software.

S5 0716+71 was not detected by the source locator at 3σ significance in any energy bin of the mosaic image. However, the source was detected at significance greater than 1σ in at least one energy bin between 15 and 200 keV in 54% of the individual science windows. The reliability of these detections was checked by extracting, from each science window, the count rate at the sky position of S5 0716+71 and in 12 background regions located within 1° **of** the source. A two-sample Kolmogorov-Smirnov test showed that the resulting distributions of source and background count rates in each sub-band were consistent with **them** being drawn from the same parent distribution at **the** 5% significance level, confirming the non-detection of S5 0716+71 at science-window level **also**.

In order to estimate an upper limit to the source flux in the ISGRI energy band, we extracted, for each sub-band, the value of the **statistical variance** of the count rate at the position of the source from the mosaic[3] of all the science windows. **The corresponding standard deviation (σ_{stat}) was multiplied by the HWHM of the distribution of the significances of the mosaic (σ_{syst}) to take systematic errors into account (A. Goldwurm, priv. comm.). The 3σ upper limits ($\sigma = \sigma_{stat} \cdot \sigma_{syst}$) to the count rate derived with this procedure are shown in Table 3b.**

The above-mentioned result was crosschecked by estimating, for each energy sub-band, the standard deviation σ_{stat} from the statistical variances of all the science windows (A. Goldwurm, priv. comm.). The flux and variance at the nominal position of the source were extracted from each science window. The mean of these fluxes was then computed by weighing it with the inverses of the corresponding variances. The error on the mean flux, representing σ_{stat}, was found to have the same value as in the case of the mosaic, thus yielding equivalent upper limits.

The count-rate upper limits derived with these methods were converted into fluxes through XSPEC by using the results of the spectral analysis of three *Beppo*SAX observations (Giommi et al. 1999; Tagliaferri et al. 2003) above ~ 2 keV, where the source spectrum can be well represented by a power law (Γ = 1.6 – 1.96). In addition, the Crab Nebula spectrum (Γ = 2.1) was **also** considered, for consistency with the assumption made for the computation of the JEM-X flux. By varying the assumed photon index in the range Γ = 1.6 – 2.1, we obtained the 3σ flux upper limits given in **Table 3b.**

A comparison of this result with the ISGRI flux of S5 0716+71 derived by Pian et al. (2005) in the 30–60 keV range **from their ~ 30% shorter observation (256 ksec) of April 2004** was performed by computing the flux in the same energy bin, under the assumption of a spectral index equal to that of the Crab Nebula. The upper limit obtained in this way was $F_{30-60\ keV} = 1.06 \times 10^{-11}$ erg cm^{-2} s^{-1}, a factor of ~ 3 below their detection.

4. The spectral energy distribution (SED)

The broadband monitoring carried out during the INTEGRAL pointing (see Table 1 for a list of the ground-based observing facilities) allowed us to assemble, for the first time, the SED of S5 0716+71 with truly simultaneous data spanning more than 10 decades of frequency and characterized by an exceptional energy sampling.

The flux variation ranges at radio-to-optical frequencies recorded during the INTEGRAL pointing period (see Sect. 2), as well as the upper limits estimated from the non-detection of the source by INTEGRAL (see Sect. 3) are plotted with dark diamonds, and are superposed on the historical data or variation ranges, drawn with grey symbols[4].

The low-energy part of the SED, which is commonly interpreted as due to synchrotron emission, shows the unprecedented brightness of the source in the radio-millimeter energy range and the moderate emission recorded at optical frequencies. The synchrotron peak (representing the most relevant output of the synchrotron component) is likely to be located around $10^{13} – 10^{14}$ Hz.

During the core campaign, the synchrotron spectrum of S5 0716+71 was inverted ($\alpha > 0$, **with** $F_\nu \propto \nu^\alpha$) in the radio-millimeter wavelength domain, **with a turnover frequency close to 90 GHz (see Agudo et al. 2005). The spectral index of the partially opaque part of the spectrum was derived from the simultaneous radio measurements at 5 and 32 GHz (considerably below the turnover) performed on JD=2452955 and JD=2452961 with the Effelsberg 100-m**

[3] **Note that the parameter responsible for the pixel spreading in the mosaic creation was not activated in our ISGRI analysis (*OBS1_PixSpread*=0), in order to obtain a better estimate of the variance of the mosaic (A. Goldwurm, priv. comm.)**

[4] Previous studies of the SED of S5 0716+71 can be found in Wagner et al. (1996), Ghisellini et al. (1997), Giommi et al. (1999), Ostorero et al. (2001), and Tagliaferri et al. (2003).

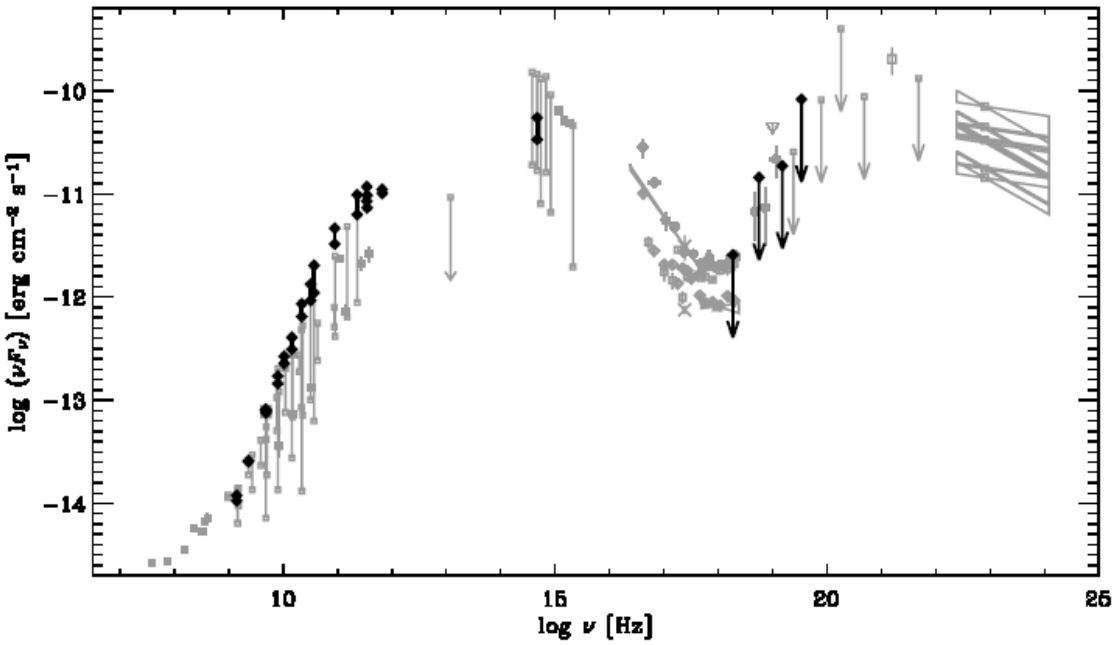

Fig. 2. Spectral energy distribution (SED) of S5 0716+71: dark diamonds represent data simultaneous with the INTEGRAL pointing, and grey symbols represent historical data; variation ranges are indicated by vertical bars. Simultaneous data are from this work: they show the exceptionally bright state of the source in the radio-to-submillimeter domain, the moderate level of the optical emission and the upper limits to the hard-X–ray brightness. Historical data are from: RATAN-600, at the wavelengths of 1.38, 2.7, 3.9, 7.7, 13 and 31 cm (Ostorero et al., in prep.); Kühr et al. (1981), Waltman et al. (1981), Eckart et al. (1982), Perley (1982), Perley et al. (1982), Lawrence et al. (1985), Saikia et al. (1987), Impey & Neugebauer (1988), Kühr & Schmidt (1990), Hales et al. (1991), Krichbaum et al. (1993), Gear et al. (1994), Hales et al. (1995), Douglas et al. (1996), Rengelink et al. (1997), Zhang et al. (1997), Riley et al. (1999), Cohen et al. (2002), Raiteri et al. (2003) and references therein, at other radio-to-optical frequencies; Pian & Treves (1993), & Ghisellini et al. (1997) in the UV band; Biermann et al. (1992), Comastri et al. (1997), Kubo et al. (1998), Giommi et al. (1999), Tagliaferri et al. (2003), & Pian et al. (2005) in the X-ray band; McNaron-Brown et al. (1995), Hartman et al. (1999), & Collmar (2005) in the gamma-ray energy range.

radio telescope (see Fuhrmann et al., in prep.) Its value is $\alpha_{5-32} = +0.3$ on JD=2452955, and $\alpha_{5-32} = +0.5$ on JD=2452961: as the millimeter-flux raised towards the end of the observing period, the radio spectrum became more inverted.

As usually found in compact radio sources, the spectrum at frequencies **lower than** the turnover was not rising **as fast as** the optically thick spectrum of a homogeneous spherical synchrotron source ($F_\nu \propto \nu^{2.5}$). Such behaviour is traditionally interpreted as the result of a superposition of **spectra characterized by different synchrotron self-absorption (SSA) frequencies, which might be produced either by a finite number of homogeneous components (Kellermann & Pauliny-Toth 1969) or by an inhomogeneous source with gradients in the magnetic field and particle density (Condon & Dressel 1973; de Bruyn 1976; Marscher 1977).**

The variability observed in the radio-millimeter energy range, of which we showed an example in the 32 and 37 GHz light curves presented in Sect. 2.1, hence occurred in a regime in which SSA processes might have played an important role.

The IDV study carried out during the fainter radio-to-optical state of the source of February 1990 (Wagner et al. 1990; Quirrenbach et al. 1991), reported a variable radio spectrum which was on average **optically thin both** in the 5.0–8.4 GHz energy range ($\alpha_{5-8.4} = -0.10$) and in the 1.4–5.0 GHz band ($\alpha_{1.4-5} = -0.35$) (Wagner et al. 1996). The long-term behaviour of the radio spectral indices indicates spectra on average inverted in the 4.8–14.5 GHz band ($\alpha_{4.8-8} = 0.72$; $\alpha_{8-14.5} = 0.16$) during 1985–1992 (Wagner et al. 1996), as well as in the 5.0–15.0 GHz band ($\alpha_{5-15} = 0.19$) during 1978–2002 (C. Raiteri, priv. comm.), where also a flatter-when-brighter trend and a weak correlation between spectral flattening and ejection of a new component were recognized by Raiteri et al. (2003) and Bach et al. (2005a), respectively. However, no truly simultaneous spectral information on the source spectrum from radio up to millimeter frequencies was available to date.

The moderate level of the optical emission recorded during the bright radio state confirms the absence of correlation, at zero time lag, between major optical and radio events in the source, as already noticed by Raiteri et al. (2003) from the inspection of the historical (1978–2002) radio-optical light curve.

As far as the high-energy part of the SED is concerned, the upper limits provided by JEM-X (see Sect. 3.1) and by IBIS/ISGRI (see Sect. 3.2) in the two lower-energy bins are consistent with the levels recorded by ASCA (Kubo et al. 1998) and *Beppo*SAX (Giommi et al. 1999; Tagliaferri et al. 2003) during past observations, and indicate that the source was fainter than during the INTEGRAL observation of April 2004

(Pian et al. 2005), represented in Fig. 2 by the grey triangle at ~ 41.4 keV (~ 10^{19} **Hz).** The two higher-energy IBIS/ISGRI upper limits are comparable with the limits derived from the OSSE observations (McNaron-Brown et al. 1995).

5. Discussion and conclusions

The known high duty cycle of S5 0716+71 was confirmed by the intensive simultaneous radio-to-optical monitoring performed during the core campaign. The source was variable in both the radio and optical bands, although the amplitude of IDV recorded in the radio regime was significantly lower than in previous studies.

Under the assumption of a stationary radio emission, and considering a Gaussian brightness distribution for the variable source region, if the event which triggers the flux fluctuations propagates isotropically through the source, the flux variability observed in the radio band allows one to estimate the brightness temperature of the source through the relation:

$$T_{\rm b} = 8.47 \times 10^4 \, F_\nu \left[\frac{\lambda \; d_{\rm L}}{t_\nu \, (1+z)^2} \right]^2 \qquad (1)$$

where F_ν is the flux density in Jy, λ is the wavelength in cm, t_ν in years is a function of the mean flux and the flux variation in the considered time interval according to the relation

$$t_\nu = \frac{< F_\nu >}{\Delta F_\nu} \frac{\Delta t}{(1+z)} \qquad (2)$$

(Wagner et al. 1996; **see also Jones et al. 1974**), z is the source redshift, and $d_{\rm L}$ is the luminosity distance of the source in Mpc, given by

$$d_{\rm L} = \frac{c(1+z)}{H_0} \int_0^z [(1+z')^2(1+\Omega_{\rm M} z') - z'(2+z')\Omega_\Lambda)]^{-1/2} {\rm d}z' \qquad (3)$$

(Carroll et al. 1992) in the case of a Λ-dominated universe (Ω_Λ = 0.7, $\Omega_{\rm M}$ = 0.3, $\Omega_{\rm k}$ = 0; see Spergel et al. 2003). Assuming H_0=72 km sec^{-1} Mpc^{-1} (Freedman 2001) and a redshift z > 0.3, the source luminosity distance would be greater than **1510** Mpc. The brightness temperature derived from the overall increase of the source flux recorded at 32 and 37 GHz during the period of overlap of the two-frequency measurements (Δt = **4.1 days**) is hence determined to be $T_{\rm b} > (2.1 \pm 0.1) \times 10^{14}$ K, if the observed flux variations are not affected by any propagation effects. **Higher lower limits to the brightness temperature can be derived under less-conservative assumptions: a uniform distribution of the source brightness, and/or an anisotropic propagation of the perturbation which causes the variability would yield values up to $T_{\rm b} > (1.2 \pm 0.1) \times 10^{15}$ K. Moreover, a redshift limit $z > 0.52$ would increase $T_{\rm b}$ by a factor of ~ 3. In any case, our brightness temperature exceeds the IC limit of ~ 10^{12} K by at least two orders of magnitude.**

If relativistic boosting of the radiation is the explanation of this excessive value, Doppler factors $\delta \gtrsim (T_{\rm b}/10^{12}\,{\rm K})^{1/3}(1+z) \gtrsim 8$ would be required in order to lower the intrinsic brightness temperature of the source below the theoretical limit[5].

A recent analysis of the historical data set of VLBI images of S5 0716+71 at several frequencies performed by Bach et al. (2005a) showed that Doppler factors ~ 20–30 are consistent with the proper motion of the jet components. These values, which rule out slower kinematic scenarios of the source jet presented previously (Witzel et al. 1988; Gabuzda et al. 1998), could largely account for the above brightness temperature, provided that the source region responsible for the observed flux variability had the same kinematic properties as the VLBI jet components.

The source flux evolution recorded in the centimeter–millimeter domain was always dominated by that of a core of size ≤0.1 mas. Confirmation of this evidence was recently provided by the 15-GHz VLBA measurements during August 2003 (Kovalev et al. 2005) and by the analysis of space-VLBI (VSOP) observations performed in 2000 (Bach et al. 2005b). **The observed variability hence originates from either the sub-parsec jet or regions at the base of the jet itself.**

If the variability comes from one or more jet components moving according to the kinematics described by Bach et al. (2005a), and characterized by inverted or flat radio spectra (possibly becoming steeper as the components move away from the core), the brightness temperature would exceed the IC limit only apparently. The non-detection of the source by INTEGRAL might hence easily be the consequence of the non-occurrence of any Compton catastrophe in the source. This scenario would also **enable us** to reconcile the excessive VLBA brightness temperature of $T_{{\rm b},z=0} > 1.85 \times 10^{13}$ K derived by Kovalev et al. (2005) with a value lower than the IC limit, assuming a Doppler factor $\delta \gtrsim (T_{\rm b}/10^{12}\,{\rm K})\,(1+z) \gtrsim 24$ (note that the VLBA brightness temperature scales by $\delta/(1+z)$).

On the other hand, if the variable core emission is affected by a Doppler enhancement different from that of the resolved VLBI jet components, the IC-limit violation would be real for Doppler factors $\delta \lesssim 8$. **In this case, Compton catastrophes would have occurred in the source: the high-energy non-detection would hence provide a constraint for any model of the source emission taking second-order Compton scattering (e.g. Bloom & Marscher 1996), and hence the possibility of Compton catastrophes, into account.**

Some alternative explanations for the excessive brightness temperature take propagation effects into account. The **correlation between optical brightness and radio spectral index, as well as the simultaneous change of variability timescale** observed during the February 1990 campaign (Wagner et al. 1990; Quirrenbach et al. 1991; Wagner et al. 1996), **have** been **among** the strongest arguments against the extrinsic origin of radio IDV in S5 0716+71 in the past decade. However, the radio and optical intra-day variability observed during our

[5] A more accurate value of the IC limit, and a consequent better estimate of the Doppler factor derived from the brightness temperature, would require the knowledge of the characteristics of the intrinsic spectrum of the source, like the synchrotron upper cutoff frequency, the self-absorption frequency, the radio spectral index, etc. (see e.g. Kellermann & Pauliny-Toth 1969; Blandford 1990; Readhead 1994).

campaign, when the source was in a brighter radio-to-optical state and had an inverted spectrum up to millimeter frequencies, do not appear to be obviously correlated. **This might be the consequence of optical-depth effects (which can modify the shape and amplitude of flares) on a radio emission intrinsically correlated with the optical one; alternatively, the recorded radio and optical radiation might have come from non-cospatial components characterized by different sizes. In absence of correlated radio-optical variations**, the possibility of a contribution of ISS to the observed radio variability **cannot** be completely ruled out, implying that the brightness temperature inferred from variability is not representative of the photon density of the source; in particular, the violation of the IC limit would again be only apparent in an ISS-driven variability scenario.

It is very unlikely that this variability can be explained by scintillation alone. In fact, ISS is **not a** very efficient mechanism in the 32-37 GHz (8-9 mm) regime, to which our brightness temperature refers. Moreover, the simultaneous observations at 86 GHz (3 mm), where the ISS is less efficient than at 32-37 GHz, showed that ISS can definitely be ruled out in the explanation of the observed (comparable) variability and of the **corresponding** excessive brightness temperatures (Agudo et al. 2005). Therefore, if ISS contributed to the observed 32-37 GHz flux evolution, in all likelihood it was not the dominant variability mechanism.

In conclusion, violations of the brightness temperature IC limit were inferred from the radio variability observed at 32-37 GHz. If the recorded radio emission is either intrinsic and beamed with Doppler factors $\delta \gtrsim 8$, or strongly affected by ISS, the violation of the IC limit would be apparent, easily justifying the non-detection of the source by INTEGRAL in the X–γ-ray regime. Intrinsic flux variations affected by lower beaming effects would instead imply a real violation of the theoretical limit; **in this case, the non-detection of corresponding γ-ray avalanches would provide a strong constraint for the modelling of the Compton-catastrophe scenario in this source. At any rate, our unprecedented simultaneous broad-band measurements will help to define the parameter space of the current SSC emission models in detailed studies of the multifrequency emission of S5 0716+71.**

Acknowledgements. We acknowledge the anonymous referee for a careful reading of the manuscript and for helpful advice. We acknowledge support by BMBF, through its agency DLR for the project 50OR0303 (S. Wagner). We acknowledge EC funding under contract HPRN-CT-2002-00321 (ENIGMA). V. M. Larionov and V. Hagen-Thorn acknowledge support from the Russian Foundation for Basic Research under grant 05-02-17562. S. Britzen acknowledges support by the Claussen-Simon Stiftung. A. S. Hojaev acknowledges NSC, Taiwan for invitation and support as Visiting Expert at IoA of NCU.

This research has made use of: optical observations on the WHT, La Palma, made with the ULTRACAM photometer: we acknowledge the support of V. S. Dhillon (University of Sheffield, UK) and T. R. Marsh (University of Warwick, UK); data from the University of Michigan Radio Astronomy Observatory, which is supported by the National Science Foundation and by funds from the University of Michigan; data from the Westerbork Synthesis Radio Telescope, operated by ASTRON with financial support from the Netherlands Organisation for Scientific research (NWO); the NASA/IPAC Extragalactic Database (NED), which is operated by the Jet Propulsion Laboratory, California Institute of Technology, under contract with the National Aeronautics and Space Administration; **the CATS database (Verkhodanov et al. 1997) of the Special Astrophysical Observatory.**

We are grateful to **A. P. Marscher**, A. Mastichiadis and J. G. Kirk for stimulating discussions on the problems of the brightness temperature and IC catastrophes, **to the INTEGRAL Team for useful advice on the INTEGRAL data analysis, and to Y. Y. Kovalev for discussing the paper.**

References

Agudo, I., Krichbaum, T. P., Ungerechts, H., et al. 2005, A&A, submitted
Baars, J. W. M., Genzel, R., Pauliny-Toth, I. I. K., & Witzel, A. 1977, A&A, 61, 99
Bach, U., Krichbaum, T. P., Ros, E., et al. 2005a, A&A, 433, 815
Bach, U., Krichbaum, T. P.,Kraus, A., Witzel, A., & Zensus, J.A. 2005b, in press; astro-ph/0511761
Baker, D. N., Borovsky, J. E., Benford, G., & Eilek, J. A. 1988, ApJ, 326, 110
Benford, G. 1992, ApJ, 391, L59
Bessel, M. S. 1979, PASP, 91, 589
Biermann, P., Schaaf, R., Pietsch, W., et al. 1992, A&AS, 96, 339
Blandford, R. D., Netzer, H., & Woltjer, L. 1990, in Active galactic Nuclei, eds. T. J-L. Courvoisier & M. Mayor (Springer-Verlag, Berlin), 181
Bloom, S. D., & Marscher, A. P. 1996, ApJ, 461, 657
Brandt, S., Budtz-Jørgensen, C., Lund, N., et al. 2003, A&A, 411, L243
Britzen, S., Brinkmann, W., Campbell, et al. 2005, A&A, submitted
Cardelli, J. A., Clayton, C., & Mathis, J. S. 1989, ApJ, 345, 245
Carroll, S. M., Press, W. H., & Turner, E. L. 1992, ARAA, 30, 499
Chang, K. & Refsdal, S. 1979, Nature, 282, 561
Chenevez, J., Lund, N., Westergaard, N.J., et al., Proc. of The 5th INTEGRAL Workshop, The INTEGRAL Universe, Münich, 16-20 Feb. 2004
Cohen, A. S., Lane, W. M., Cotton, W. D., et al. 2002, Bulletin of the American Astronomical Society, 201st AAS Meeting, Vol. 34, p. 1274
Collmar, W. 2005, in Proc. Blazar Variability Workshop II: Entering the GLAST Era, Miller H. R. (ed.), ASP Conf. Ser., in press
Comastri, A., Fossati, G., Ghisellini, G., & Molendi, S. 1997, ApJ, 480, 534
Condon, J. J., & Dressel, L. L. 1973, Ap. Lett., 15, 203
Eckart, A., Hill, P., Johnston, K. J., et al. 1982, A&A, 108, 157
Eckart, A., Witzel, A., Biermann, P. et al. 1986, A&A, 168, 17
Eckart, A., Witzel, A., Biermann, P. et al. 1987, A&AS, 67, 121
de Bruyn, A. G. 1976, A&A, 52, 439
Dhawan, V., Bartel, N., Rogers, A. E. E., et al. 1990, ApJ, 360, L43
Douglas, J. N., Bash, F. N., Bozyan, F. A., Torrence, G. W., & Wolfe, C. 1996, AJ, 111, 1945
Di Cocco, G., Caroli, E., Celesti, E., et al. 2003, A&A, 411, L189
Freedman, W. L., Madore, B. F., Gibson, B. K., et al. 2001, ApJ, 553, 47
Gabuzda, D. C., Kovalev, Y. Y., Krichbaum, T. P., et al. 1998, A&A, 333, 445
Gear, W. K., Stevens, J. A., Huges, D. H., et al. 1994, MNRAS, 267, 167
Ghisellini, G., Villata, M., Raiteri, C. M., et al. 1997, A&A 327, 61
Giommi, P., Massaro, E., Chiappetti, L., et al. 1999, A&A, 351, 59

Goldwurm, A., David, P., Foschini, L., et al. 2003, A&A, 411, L223
Greve, A., Steppe, H., Graham, D., Schalinski, C. J. 1994, A&A, 286, 654
Hales, S. E. G., Mayer, C. J., Warner, P. J., & Baldwin, J. E. 1991, MNRAS, 251, 46
Hales, S. E. G., Waldram, E. M., Rees, N., & Warner, P. J. 1995, MNRAS, 274, 447
Hartman, R. C., Bertsch, D. L., Bloom, S. D., et al. 2000, ApJS, 123, 79
Heeschen, D. S., Krichbaum, T. P., Schalinski, C. J., & Witzel, A. 1987, AJ, 94, 1493
Hoyle, F., Burbidge, G. R., & Sargent, W. L. W. 1966, Nat, 209, 751
Impey, C. D., & Neugebauer, G. 1988, AJ 95, 307
Jones, T. W., O'Dell, S. L., & Stein, W. A. 1974, ApJ, 192, 261
Jorstad, S. G., Marscher, A. P., Mattox, J. R., et al. 2001, ApJS, 134, 181
Kedziora-Chudczer, L., Jauncey, D. L., Wieringa, M. H., et al. 1997, ApJ 490, L9
Kellermann, K. I., & Pauliny-Toth, I. I. K. 1969, ApJ, 155, L71
Kovalev, Y. Y., Kellermann, K. I., Lister, M. L., et al. 2005, AJ, 130, 2473
Kraus, A., Krichbaum, T. P., Wegner, R., et al. 2003, A&A, 401,161
Krichbaum, T. P., Witzel, A., Graham, D. A., et al. 1993, A&A, 275, 375
Kubo, H., Takahashi, T., Madejski, G., et al. 1998, ApJ, 504, 693
Kühr, H., Witzel, A., Pauliny-Toth, I. I. K., & Nauber, U. 1981, A&AS, 45, 367
Kühr, H., & Schmidtt, G. D. 1990, AJ, 99, 1
Lawrence, C. R., Readhead, A. C. S., Linfield, R. P., et al. 1985, ApJ 296, 458
Lebrun, F., Leray, J. P., Lavocat, P., et al. 2003, A&A, 411, L141
Lesch, H., & Pohl, M. 1992, A&A, 254, 29
Lund, N., Budtz-Jørgensen, C., Westergaard, N. J., et al. 2003, A&A, 411, L231
Marscher, A. P. 1977, ApJ, 216, 244
Mattox, J. R. 1998, Bulletin of the American Astronomical Society, 192nd AAS Meeting, Vol. 30, p. 859
McNarown-Brown, K., Johnson, W. N., Jung, G. V., et al. 1995, ApJ, 451, 575
Nesci, R., Massaro, E., & Montagni, F. 2002, Publ. Astron. Soc. Aust., 19, 143
Nørgaard, H. U., Nielsen, C., Budtz, C., et al. 1994, A&A, 284, 705
Ostorero, L., Raiteri, C. M., Villata, M., et al. 2001, Mem. Soc. Astron. Ital., 72, 147
Ott, M., Witzel, A., Quirrenbach, A., et al. 1994, A&A, 284, 331
Perley, R. A. 1982, AJ 87, 859
Perley, R. A., Fomalont E. B., & Johnston, K. J. 1982, ApJ, 255, L93
Pian, E., & Treves, A. 1993, ApJ, 416, 130
Pian, E., Foschini, L., Beckmann, V., et al. 2005, A&A, 429, 427
Polatidis, A. G., Wilkinson, P. N., Xu, W., et al. 1995, ApJS, 98, 1
Qian, S. J., Quirrenbach, A., Witzel, A., et al. 1991, A&A, 241, 15
Quirrenbach, A., Witzel, A., Krichbaum, T. P., et al. 1989, Nat, 337, 442
Quirrenbach, A., Witzel, A., Wagner, S. J., et al. 1991, ApJ, 372, L71
Quirrenbach, A., Witzel, A., Krichbaum, T. P. et al. 1992, ApJ, 258, 279
Quirrenbach, A., Kraus, A., Witzel, A., et al. 2000, A&AS, 141, 221
Racine, R. 1970, ApJ, 159, 99L
Raiteri, C. M., Villata, M., Tosti, G., et al. 2003, A&A, 402, 151
Raiteri, C. M., Villata, M., Ibrahimov, M. A., et al. 2005, A&A, 438, 39
Readhead, A. C., ApJ, 426, 51
Rees, M. J. 1967, MNRAS, 135, 345
Rengelink, R. B., Tang, Y., de Bruyn, A. G., et al. 1997, A&AS, 124,259
Rickett, B. J. 1990, ARA&A, 28, 561
Rickett, B. J., Quirrenbach, A., Wegner, R., et al. 1995, A&A, 293, 479
Riley, J. M. W., Waldram, E. M., & Riley, J. M. 1999, MNRAS, 306, 31
Saikia, D. J., Salter, C. J., Neff, S. G., et al. 1987, MNRAS, 228, 203
Sagar, R., Gopal-Krishna, M. V., et al. 1999, A&AS, 134, 453
Sbarufatti, B., Treves, A., & Falomo, R., ApJ, 635, 173
Schlegel, D. J., Finkbeiner, D. P.. & Davis, M. 1998, ApJ, 500, 525
Schönfelder, V., Bennett, K., Bloom, J. J., et al. 2000, A&AS, 143, 145
Slysh, V. I. 1992, ApJ, 391, 453
Spergel, D. N., Verde, L., Peiris, H. V., et al. 2003, ApJS, 148, 175
Stickel, M., Fried, J.W., & Kühr, H. 1993, A&A, 98, 393
Tagliaferri, G., Ravasio, M., Ghisellini, G., et al. 2003, A&A, 400, 477
Teräsranta, H., Tornikoski, M., Mujunen, A., et al. 1998, A&A 132, 305
Toor, A., & Seward, F. D. 1974, AJ, 79, 995
Ubertini, P., Lebrun, F., Di Cocco, G., et al. 2003, A&A, 411, L131
Vaughan, S., Edelson, R., Warwick, R. S., & Uttley, P. 2003, MNRAS 345, 1271
Vedrenne, G., Roques, J.-P., Schönfelder, V., et al. 2003, A&A, 411, L63
Verkhodanov, O. V., Trushkin, S. A., Andernach, H., & Chernenkov, V. N. 1997, Astronomical Data Analysis Software and Systems VI, eds. G. Hunt & H. E. Payne, ASP Conf. Ser., 125, 322
Villata, M., Raiteri, C. M., Lanteri, L., Sobrito, G., & Cavallone, M. 1998, A&AS 130, 305
Villata, M., Mattox, J., Massaro, E., et al. 2000, A&A, 363, 108
Villata, M., Raiteri, C. M., Kurtanidze, O. M., et al. 2002, A&A 390, 407
Villata, M., Raiteri, C. M., Aller, H. D., et al. 2004, A&A, 424, 497
Wagner, S. J., Sanchez-Pons, F., Quirrenbach, A., & Witzel, A. 1990, A&A, 235, L1
Wagner, S. J. 1992, in Gravitational Lenses, ed. R. Kayser, S. Refsdal & T. Schramm (Springer, Berlin), 189
Wagner, S. J., Witzel, A., Krichbaum, T. P., et al. 1993, A&A, 271, 344
Wagner, S. J., & Witzel, A. 1995, ARA&A, 33, 163
Wagner, S. J., Witzel, A., Heidt, J., et al. 1996, AJ, 111, 2187
Waltman, E., Johnston, K.J., Spencer J.H., et al. 1981, A&A, 101, 49
Westergaard, N. J., Kretschmar, P., Oxborrow, C. A., et al. 2003, A&A, 411, L257
Winkler, C., Courvoisier, T. J.-L., Di Cocco, G., et al. 2003, A&A, 411, L1
Witzel, A. 1992, in Physics of Active Galactic Nuclei, ed. W. J. Duschl & S. J. Wagner (Springer, Berlin), 484
Witzel, A., Heeschen, D. S., Schalinski, C., & Krichbaum, T. P. 1986, Mitt. d. Astron. Gesell., 65, 239
Witzel, A., Schalinski, C., Johnston, K. J., et al. 1988, A&A, 206, 245
Zhang, X., Zheng, Y., Chen, H., et al. 1997, A&AS, 121, 59

Online Material

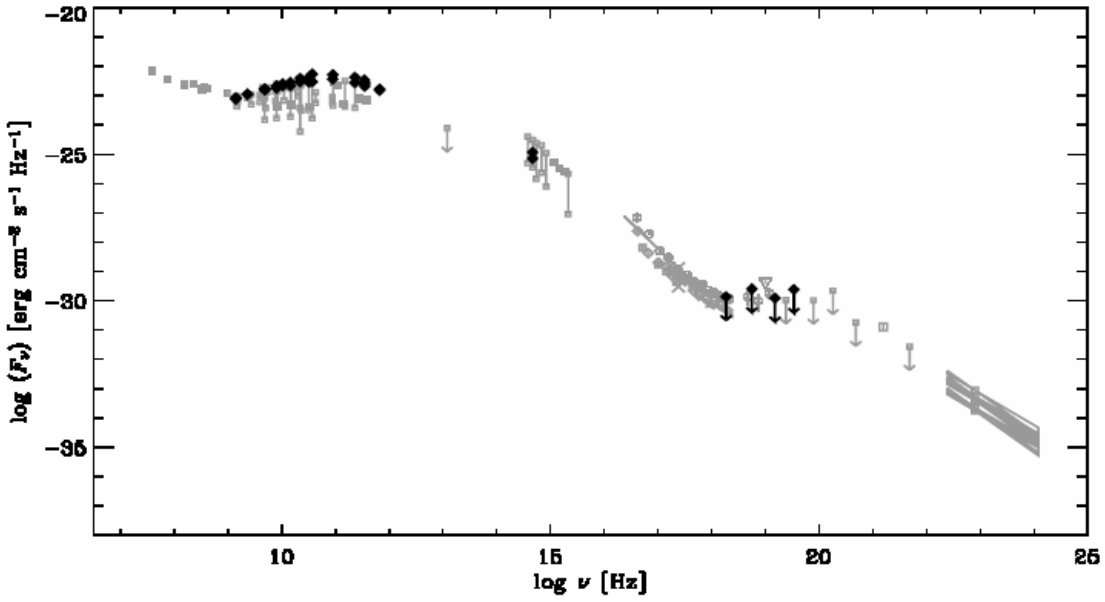

Fig. 3. Broadband spectrum of S5 0716+71: dark diamonds represent data simultaneous with the INTEGRAL pointing, and grey symbols represent historical data; variation ranges are indicated by vertical bars. See caption of Fig. 2 and Sect. 4 for more details.

Mem. S.A.It. Vol. 75, 282

Memorie della

Follow-up observations of pulsating subdwarf B stars

M.D. Reed, A.-Y. Zhou, S.L. Harms, G.W. Wolf[1], D.M. Terndrup, D. An[2], D. Kilkenny[3], C.-W. Chen, H.-C. Lin[4], S. Zola, A. Baran, W. Ogloza, M. Siwak[5], K.D. Gazeas, and P.G. Niarchos[6]

[1] Department of Physics, Astronomy, and Materials Science, Missouri State University, 901 S. National, Springfield, MO, 65804 USA
[2] The Ohio State University, 140 W. 18th Avenue, Columbus, OH 43210, USA
[3] South African Astronomical Observatory, Cape Town, South Africa
[4] Graduate Institute of Astronomy, National Central University, Chung-Li, Taiwan
[5] Mt. Suhora Observatory of the Pedagogical University, ul. Podchorązych 2, PL-30-084 KraKow, Poland
[6] Department of Astrophysics, Astronomy and Mechanics, Faculty of Physics, University of Athens, GR 157 84, Zografos, Athens, Greece

Abstract. We present follow-up observations of pulsating sdB stars as part of our efforts to resolve the pulsation spectra for use in asteroseismological analyses. This paper reports on our overall efforts, but specifically on our results for the pulsating sdB stars PG 1618+563 and EC 05217-3914.

Key words. Stars: pulsating – Stars: asteroseismology – Individual: PG1618+563 – Individual: EC05217-3914

1. Introduction

The scientific goal of this observational study is to resolve the pulsation structure of pulsating sdB stars by combining limited amounts of data from larger telescopes with data from smaller (~0.5 m) telescopes. This combination allows us a long timebase sufficient to resolve closely spaced pulsations and the increased signal-to-noise of the larger telescopes allows us to detect pulsations with low amplitudes. To date we have observed 14 different sdB pulsators over 23 separate campaigns. Though the majority of our data is from Baker, MDM, and McDonald observatories, we routinely participate in multisite collaborations, including the Whole Earth Telescope.

Send offprint requests to: M.D. Reed

2. EC 05217-3914

EC 05217-3914 (hereafter EC 05217) was observed as a 2-site campaign during a Whole Earth Telescope run. 59 hours of observations were obtained in November 1999 from the CTIO 1.5 m and SAAO 1.9 m telescopes. Koen et al. (1999) detected 3 frequencies in their discovery data, while we detect 6, possibly 8. The Fourier transform (FT) is shown in Fig. 1 and frequencies detected are given in Table 1.

Table 1. Periods, frequencies, and amplitudes for EC 05127. Formal least-squares errors are in parentheses. Periods marked with a † may be caused by amplitude variability in a nearby frequency. Periods marked with a ⋆ are near those detected in the discovery data.

Period (s)	Frequency (μHz)	Amplitude (mma)
208.455(0.005)	4797.19(0.11)	0.83(15)
209.274(0.006)	4778.41(0.13)	0.72(15)
213.964(0.005)†	4673.68(0.12)	0.98(15)
214.023(0.003)⋆	4672.39(0.08)	1.45(15)
216.012(0.001)⋆	4629.36(0.03)	3.88(17)
216.146(0.005)†	4626.48(0.11)	1.15(17)
217.629(0.001)⋆	4594.96(0.03)	2.79(15)
221.980(0.007)	4504.90(0.14)	0.69(15)

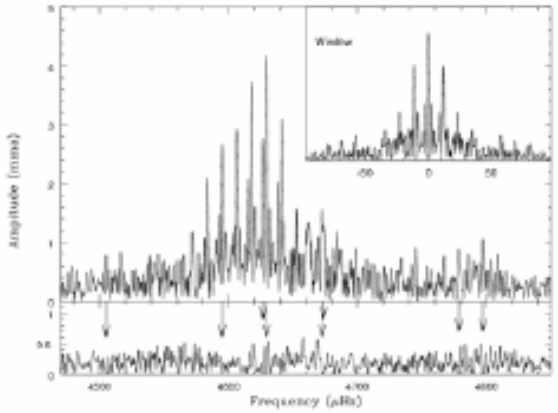

Fig. 1. FT of EC 05217 data. Window is inset and bottom panel shows residuals.

3. PG 1618+563

PG 1618+563 (hereafter PG 1618) was observed from 5 observatories (Baker, MDM, McDonald, Lulin, and Suhora) over a 45 day period in 2005. Silvotti et al. (2000) detected 2 frequencies in their discovery data while we clearly resolve 4 individual frequencies. Figure 2 shows shows an FT of the original data (window function is inset) and prewhitened data (arrows indicate frequencies removed) with the frequencies provided in Table 2.

Table 2. Same as Table 1 for PG 1618.

Period (s)	Frequency (μHz)	Amplitude (mma)
128.9549(0.0008)	7754.64(0.05)	1.71(0.09)
139.0571(0.0008)⋆	7191.28(0.04)	2.04(0.09)
143.9290(0.0011)⋆	6947.87(0.05)	2.22(0.10)
143.9759(0.0014)	6945.60(0.07)	1.64(0.10)

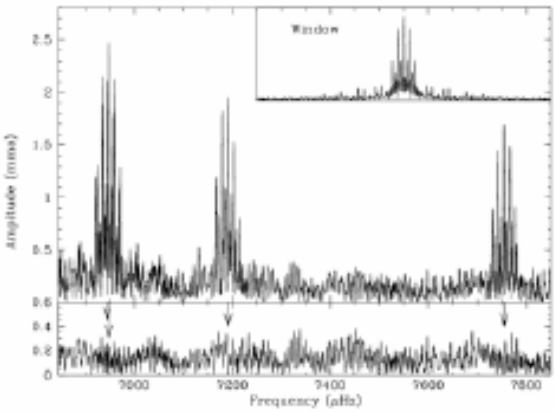

Fig. 2. FT of PG 1618 data. Window is inset and bottom panel shows residuals.

Acknowledgements. We would like to thank the SAAO, CTIO, MDM and McDonald observatory TACS for generous time allocations for this project. This material is based in part upon work supported by the National Science Foundation under Grant Numbers AST007480, and AST9876655. Any opinions, findings, and conclusions or recommendations expressed in this material are those of the author(s) and do not necessarily reflect the views of the National Science Foundation. S.L.H. was supported by the Missouri Space Grant Consortium and an NSF REU supplement grant.

References

Koen, C. O'Donoghue, D., Kilkenny, D., Stobie, R.S., & Saffer, R.A. 1999, MNRAS, 306, 213
Silvotti, R., et al., 2000, A&A, 359, 1068

The Astrophysical Journal, 628:L93–L96, 2005 August 1

OPTICAL AFTERGLOW OBSERVATIONS OF THE UNUSUAL SHORT-DURATION GAMMA-RAY BURST GRB 040924

K. Y. Huang,[1] Y. Urata,[2,3] A. V. Filippenko,[4] J. H. Hu,[1] W. H. Ip,[1] P. H. Kuo,[1] W. Li,[4] H. C. Lin,[1] Z. Y. Lin,[1] K. Makishima,[2,5] K. Onda,[2,6] Y. Qiu,[7] and T. Tamagawa[2]

Received 2005 March 11; accepted 2005 June 9; published 2005 July 14

ABSTRACT

The 1 m telescope at Lulin Observatory and the 0.76 m Katzman Automatic Imaging Telescope at Lick Observatory were used to observe the optical afterglow of the short-duration (1.2–1.5 s) gamma-ray burst GRB 040924. This object has a soft high-energy spectrum, thus making it an exceptional case, perhaps actually belonging to the short-duration tail of the long-duration GRBs. Our data, combined with other reported measurements, show that the early *R*-band light curve can be described by two power laws with index $\alpha = -0.7$ (at $t = 16$–50 minutes) and $\alpha = -1.06$ (at later times). The rather small difference in the spectral indices can be explained more easily by an afterglow model invoking a cooling break than by one with a jet break.

Subject heading: gamma rays: bursts

1. INTRODUCTION

Gamma-ray bursts (GRBs) are among the most powerful explosions in the universe. It is generally believed that the impulsively injected fireball results from core collapse in a massive star (Woosley 1993; MacFadyen & Woosley 1999) or from the merging of either two neutron stars or a neutron star and a black hole (e.g., Ruffert et al. 1997; Popham et al. 1999; Narayan et al. 1992, 2001; Rosswog & Davies 2002; Lee & Ramirez-Ruiz 2002). After the explosion, the relativistic ejecta collide with the ambient interstellar medium (ISM), causing X-ray, optical, and radio emission. These so-called afterglows thus carry important information on the injection mechanism, the configuration of the (possibly collimated) fireball, and the surrounding environment (e.g., Mészáros 2002).

Two kinds of GRBs have been defined according to whether their gamma-ray emission has duration longer or shorter than 2 s. Although their frequency distributions overlap, that of the short-duration GRBs peaks at 0.3 s, while that of the long-duration GRBs peaks at 30–40 s (Kouveliotou et al. 1993). In addition, the duration is weakly correlated with the spectral hardness ratio at high energies: short GRBs tend to be harder and long GRBs tend to be softer (Kouveliotou et al. 1993).

The optical afterglows of short GRBs were elusive until the detection (Fenimore et al. 2004) of GRB 040924 by the *High Energy Transient Explorer 2* (*HETE-2*) on 2004 September 24 at 11:52:11 (UT dates are used throughout this Letter). This event lasted about 1.2 s and was X-ray–rich according to the *HETE-2* flux in the 7–30 and 30–400 keV bands. The Konus experiment on the *Wind* satellite also detected this event with 1.5 s duration in the 20–300 keV band (Golenetskii et al. 2004). Since the high-energy spectrum of GRB 040924 is soft (Fenimore et al. 2004), the object might actually be near the short-duration end of the long GRBs. A detailed study of the associated optical afterglow could provide further information on whether this is indeed the case, thus probing the nature of GRBs in the boundary region.

About $t = 16$ minutes after the burst, Fox (2004) detected the corresponding optical afterglow with an *R*-band magnitude of ~18. This was shortly followed by Li et al. (2004), who reported $R \approx 18.3$ mag at 26 minutes after the burst. From then on, a number of observatories joined in the follow-up observations (Fynbo et al. 2004; Hu et al. 2004; Khamitov et al. 2004a; Terada et al. 2004). Radio observations failed to detect the afterglow at $t = 12.54$ hr and $t = 5.79$ days (Frail & Soderberg 2004; van de Horst et al. 2004a, 2004b). Spectral measurements by the Very Large Telescope of a galaxy located at the position of the optical afterglow indicated a redshift of $z = 0.859$ for this event (Wiersema et al. 2004).

2. OBSERVATIONS AND DATA ANALYSIS

Upon receiving the burst alert message from *HETE-2* and the optical position reported by Fox & Moon (2004), multiband (Johnson *B* and *V*; Bessell *R* and *I*) follow-up observations of GRB 040924 with the Lulin One-meter Telescope (LOT; in Taiwan) were initiated according to the previously approved Target-of-Opportunity procedure (Huang et al. 2005; Urata et al. 2005). Photometric images were obtained with the PI1300B CCD camera (1300 × 1340 pixels, ~11′ × 11′ field of view; Kinoshita et al. 2005) during the interval 14.31–20.89 on September 24 (i.e., 2.4–9.0 hr after the burst). Unfortunately, the earliest observations ($t < 3.1$ hr) were not successful because of poor weather and short exposure times. These problems also affected all of the *B* and *I* data, and many of the *V* and *R* images as well. Nevertheless, our observations reveal unusual early-time evolution of the afterglow brightness, as discussed below.

A standard routine including bias subtraction and flat-fielding corrections with appropriate calibration data was employed to process the data using IRAF.[8] The afterglow was clearly seen in the *V*-band and *R*-band images (Fig. 1). The position of the afterglow (J2000.0) is $\alpha = 2^h6^m22^s.52$, $\delta = +16°6'48''.82$ ($\pm 0''.23$ in each coordinate). Next, the DAOPHOT package (Stetson 1987) was used to perform aperture photometry of the GRB field by choosing 10 field stars for differential photometry. The LOT data were combined with median filtering

[1] Institute of Astronomy, National Central University, Chung-Li 32054, Taiwan (Huang e-mail: d919003@astro.ncu.edu.tw).
[2] RIKEN (Institute of Physical and Chemical Research), 2-1 Hirosawa, Wako, Saitama 351-0198, Japan.
[3] Department of Physics, Tokyo Institute of Technology, 2-12-1 Ookayama, Meguro-ku, Tokyo 152-8551, Japan.
[4] Department of Astronomy, University of California, Berkeley, CA 94720-3411.
[5] Department of Physics, University of Tokyo, 7-3-1 Hongo, Bunkyo-ku, Tokyo 113-0033, Japan.
[6] Department of Physics, Saitama University, Shimookubo, Urawa 338-8570, Japan.
[7] National Astronomical Observatories, Chinese Academy of Sciences, Beijing 100012, China.

[8] IRAF is distributed by the National Optical Astronomy Observatory, which is operated by AURA, Inc., under cooperative agreement with the NSF.

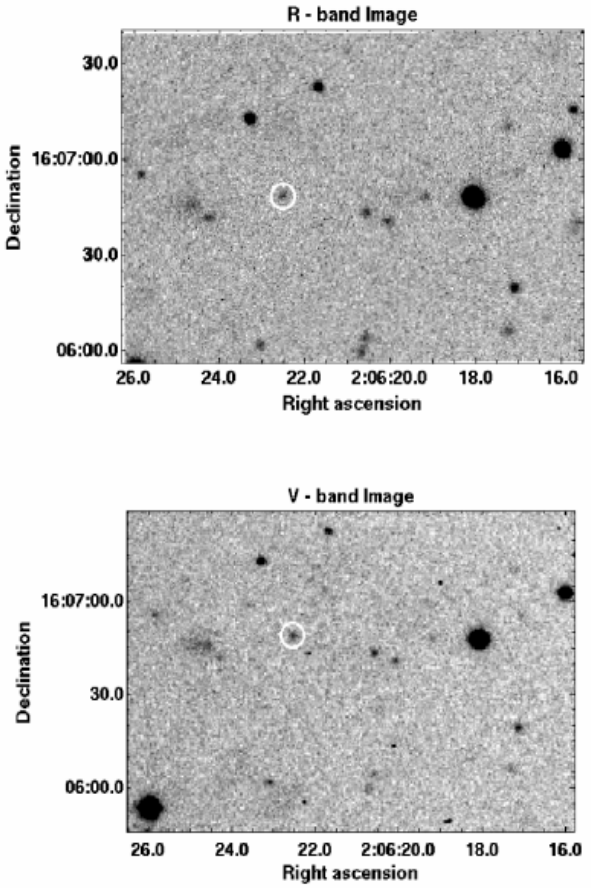

FIG. 1.—*R*-band and *V*-band images of GRB 040924 taken with LOT. The location of the afterglow is indicated by a circle in each image.

to improve the signal-to-noise ratio. For the photometry, the aperture diameter was set to 4 times the FWHM of the objects. The magnitude error was estimated as $\sigma_a^2 = \sigma_{\rm ph}^2 + \sigma_{\rm sys}^2$, where $\sigma_{\rm ph}$ is the photometric error of the afterglow estimated from the DAOPHOT output, and $\sigma_{\rm sys}$ is the systematic calibration error estimated by comparing the instrumental magnitudes of the 10 field stars. Besides the calibration data obtained by the USNOFS 1.0 m telescope (Henden 2004), we used the measurements of four Landolt (1992) standard-star fields (SA 92, PG 2331+055, SA 95, and PG 2317+046) taken by LOT on a photometric night. The difference between the two flux calibrations is within 0.04 mag. The magnitudes derived for the *R* and *V* observations are summarized in Table 1.

In addition to the LOT data, we have also included two early measurements from the 0.76 m Katzman Automatic Imaging Telescope (KAIT; Li et al. 2003b) at Lick Observatory at $t = 0.43$ and 1.06 hr. The KAIT data were taken without filters, but the transformation of the unfiltered magnitude to *R* can be determined from the $V - R$ colors of the GRB field stars and of the optical afterglow (Li et al. 2003a, 2003b). The calibration of the GRB 040924 field is adopted from Henden (2004), and the value $V - R = 0.57$ mag of the afterglow is taken from LOT data at 0.292 days after the burst. KAIT observed the GRB at low air mass (1.26–1.4), and the local standard stars have $V - R$ colors (0.39–0.85 mag) similar to that of the GRB. Moreover, from three photometric nights we found that the coefficient for the second-order extinction is only 0.04; thus, the errors caused by second-order extinction of GRB 040924 are small and are included in the overall uncertainties of the KAIT data.

3. RESULTS

The light curve of GRB 040924 in Figure 2 is a combination of the early observations reported by Fox (2004) at 0.012 and 0.033 days after the burst, the work reported here, and the measurements by Khamitov et al. (2004b, 2004c) at $t = 0.37$, 0.62, and 1.56 days, Fynbo et al. (2004) at $t = 0.73$ days, and Silvey et al. (2004) around $t = 0.9$ days. To put all of the data onto a consistent magnitude scale, we recalibrated the above-mentioned published data by using the Henden (2004) standard stars for the GRB 040924 field. The data of Fox (2004) were calibrated by Guide Star Catalog (GSC; ver. 2.2)[9] stars with F-emulsion magnitude, which corresponds closely to the *R*-band magnitude; the GSC stars are 0.11 mag brighter than the Henden standard stars in the average of our images. Since two reference stars are provided by Khamitov et al. (2004b, 2004c) and Fynbo et al. (2004), we measured these stars from LOT *R*-band combined images and obtained the average magnitudes and rms errors; the results were then used to recalibrate the reported afterglow magnitudes.

The time evolution of the light curve can be expressed in

[9] The GSC 2.2 is a magnitude-selected subset of GSC II, an all-sky catalog based on 1″ resolution scans of the photographic sky survey plates, at two epochs and three bandpasses, from the Palomar and UK Schmidt telescopes (http://www-gsss.stsci.edu/gsc/gsc2/GSC2home.htm).

TABLE 1
LOG OF GRB 040924 OPTICAL AFTERGLOW OBSERVATIONS

UT Date	Start Time	Mean Delay (days)	Exposure (s)	Magnitude	Site
		V Filter			
2004 Sep 24	18:52:37	0.296	300 × 3	22.01 ± 0.13	LOT
	19:46:02	0.333	300 × 3	22.05 ± 0.16	LOT
	20:24:54	0.360	300 × 3	22.18 ± 0.13	LOT
		R Filter			
2004 Sep 24	12:18:21	0.018	120 × 1	18.44 ± 0.05	KAIT[a]
	12:55:21	0.044	120 × 1	19.31 ± 0.15	KAIT[a]
	15:00:55	0.140	600 × 2	20.71 ± 0.13	LOT
	18:34:37	0.284	300 × 3	21.39 ± 0.15	LOT
	19:28:57	0.321	300 × 3	21.47 ± 0.15	LOT
	20:07:48	0.348	300 × 3	21.47 ± 0.14	LOT
	20:42:17	0.372	300 × 3	21.59 ± 0.17	LOT
2004 Sep 25	08:35:00	0.873	300 × 3	>22.47	KAIT[a]

[a] KAIT measurements were unfiltered but transformed to *R* (Li et al. 2003a, 2003b).

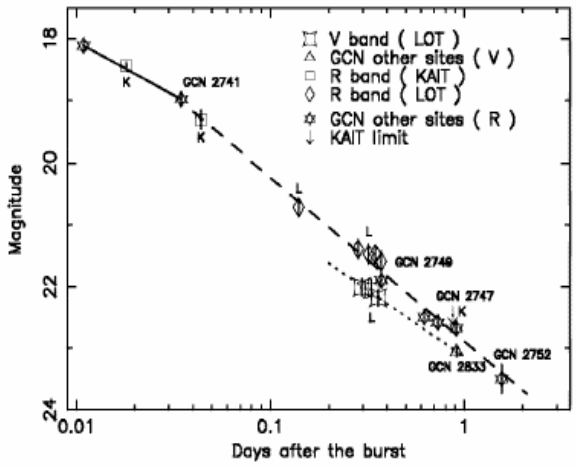

FIG. 2.—*V*-band and *R*-band light curves based on our (LOT and KAIT) observations and the recalibrated data points of Fox (2004), Fynbo et al. (2004), Khamitov et al. (2004b, 2004c), and Silvey et al. (2004). The lines represent the power-law models [$F(t) \propto t^{\alpha}$] fitted to the data points. *Solid line*: *R*-band $\alpha = -0.7$ at early times (based on the first three observations). *Dashed line*: Late-time *R*-band best fit of $\alpha = -1.06 \pm 0.03$ starting from the third observation. *Dotted line*: *V*-band best fit of $\alpha = -0.87 \pm 0.02$ from LOT and Silvey et al. (2004).

terms of a power law with $F(t) \propto t^{\alpha}$, where t is the time after the burst and α is the index. We find $\alpha = -0.87 \pm 0.02$ ($\chi^2/\nu = 0.06$ for $\nu = 2$) for the very sparse *V*-band data (only three closely spaced LOT observations and one later observation from Silvey et al. 2004). Similarly, we derive $\alpha = -0.99 \pm 0.02$ ($\chi^2/\nu = 2.08$ for $\nu = 12$) from all 14 available *R*-band observations. These two values of α fall within the range of long GRBs ($\alpha = -0.62$ to -2.3), so the afterglow of GRB 040924 is consistent with the standard model of cosmic-ray electrons accelerated by the internal and external shocks of the expanding fireball (Mészáros 2002), as in the case of typical long-duration GRBs.

Upon closer scrutiny, the first three *R*-band observations (at $t = 16$–50 minutes) indicate $\alpha = -0.7$, consistent with the conclusion of Fox (2004), while the subsequent data (starting from the third *R*-band observation) give a somewhat steeper value of $\alpha = -1.06 \pm 0.03$ (with $\chi^2/\nu = 1.09$ for $\nu = 10$). (Essentially the same late-time result, $\alpha = -1.06 \pm 0.02$, is found when we use only our own LOT and KAIT data, together with the Silvey et al. [2004] observation at $t = 0.91$ days.) The data thus suggest the presence of a mild break, the significance of which is discussed below.

Finally, our LOT observations of GRB 040924 at $t = 7.10$ hr indicate a color index of $V - R = 0.57 \pm 0.18$ mag, corrected for foreground reddening of $E(B - V) = 0.058$ mag (Schlegel et al. 1998). We have also calculated the color of observations by Silvey et al. (2004) at $t = 0.91$ days (22.1 hr) to be $V - R = 0.35 \pm 0.10$ mag, corrected for foreground reddening. While these two values are consistent with the color of typical long GRBs ($V - R = 0.40 \pm 0.13$ mag; Simon et al. 2001), they also may suggest the interesting possibility of a color change during the time evolution of this afterglow. However, the color change is only marginally significant, given the uncertainties. Future GRB afterglow measurements should shed new light on this tantalizing behavior.

4. DISCUSSION

The brightness variations of the optical afterglows of GRBs potentially yield important information on the expansion of the ejecta. For example, breaks in the light-curve power laws at several hours to several days after the bursts have been observed in a number of GRBs. This effect is generally believed to be associated with the evolution as a collimated jet (Rhoads 1999). In the case of GRB 040924, because of the small variation from $\alpha = -0.7$ to -1.06 around $t = 50$ minutes, the break is not well constrained. On the other hand, this small break could be indicative of some interesting physical process. Note that the amplitude of the break ($\Delta\alpha = \alpha_2 - \alpha_1$; here α_1 and α_2 are the power-law indices before and after the break, respectively) is independent of extinction under the assumption of no color change. In the case of GRB 040924, from $\alpha_1 = -0.7$ and $\alpha_2 = -1.06$ we find $\Delta\alpha \approx -0.36$. According to theoretical work (Rhoads 1999), $\Delta\alpha = -3/4$ for a collimated jet with a fixed angle, and $\Delta\alpha = \alpha_1/3 - 1 \approx -1.23$ for a sideways-expanding jet in the framework of a constant ambient density model. It is clear that the amplitude of the break in GRB 040924 is much smaller than values expected of jet expansion with power-law indices much steeper after the break. The interpretation of a jet break for GRB 040924 is thus uncertain. Next we will explore an alternative possible explanation.

Panaitescu & Kumar (2000) pointed out that a light-curve break could also be caused by the spectral cooling frequency moving through the optical band. This property might be used as a diagnostic tool to differentiate among different possible scenarios of GRB afterglow formation. In the standard GRB afterglow model, it is usually assumed that the synchrotron emission observed in optical bands originates from the expansion of a blast wave of constant energy into an ISM of constant density. However, there is increasing evidence that some GRBs have massive-star progenitors. Consequently, the corresponding relativistic blast waves should actually be expanding into the stellar wind of the progenitor stars with a density variation of $\rho \propto r^{-2}$ (Dai & Lu 1998; Mészáros et al. 1998; Panaitescu et al. 1998). Zhang & Mészáros (2004) listed the broadband optical spectra of the synchrotron radiation from a power-law distribution of energetic electrons with a spectral index p accelerated by the blast wave; accordingly, we can obtain the values of p before and after the cooling break.

As shown in Table 2, the ISM model provides the only possible fit (for $p > 2$) to the GRB 040924 observations that satisfies the requirement that p should remain nearly the same ($p \approx 1.93$–2.08) as the spectrum evolves from $\nu_{\rm opt} < \nu_c$ to $\nu_{\rm opt} > \nu_c$. Note that within the framework of the ISM model, $p = 2.33$ for $\nu_{\rm opt} < \nu_c$ and $p = 2.00$ for $\nu_{\rm opt} > \nu_c$ if the corresponding light curve can be characterized by a single power-law index ($\alpha = -0.99 \pm 0.02$).

Another interesting estimate can be made concerning the relation between the cooling-break frequency ν_c, the break time $t_{\rm days}$ (in units of days), the redshift z, the magnetic energy ϵ_B, the kinetic energy E_{52} (in units of 10^{52} ergs), and the density n_0 of the ISM. According to Granot & Sari (2002),

$$\nu_c = 6.37(p - 0.46)10^{13} e^{-1.16p}(1 + z)^{-1/2}\epsilon_B^{-3/2} n_0^{-1} E_{52}^{-1/2} t_{\rm days}^{-1/2}. \quad (1)$$

Now, with $t_{\rm days} = 0.035$, $\nu_c = 4.7 \times 10^{14}$ Hz in the *R* band, $z = 0.859$, $p \approx 2.08$, and the assumptions that $E_{52} = 1.48$ and $n_0 = 1$ cm^{-3}, we find $\epsilon_B \approx 0.16$. This value is consistent with the normal assumption of a magnetic energy fraction of $\epsilon_B \approx 0.1$, although slightly larger. For the case of a single power-law index ($\alpha = -0.99 \pm 0.02$), $\epsilon_B < 0.01$, which is much smaller than the normal value. Our analysis thus suggests that the observed light curve of GRB 040924 could be the result of the spectral cooling frequency moving through the optical band.

TABLE 2

ELECTRON SPECTRAL INDEX (p) CALCULATED FROM THE MEASURED SPECTRAL INDEX (α)

	$p > 2$			$1 < p < 2$		
FREQUENCY[a]	Relation[b]	p_1[c]	p_2[c]	Relation[d]	p_1[c]	p_2[c]
ISM model:						
$\nu_{opt} < \nu_c$	$p = 1 - 4\alpha/3$	1.93	2.41	$p = -2\alpha - 10/3$	−1.93	−1.21
$\nu_{opt} > \nu_c$	$p = 2/3 - 4\alpha/3$	1.60	2.08	$p = -2 - 16\alpha/3$	1.73	3.65
Wind model:						
$\nu_{opt} < \nu_c$	$p = 1/3 - 4\alpha/3$	1.26	1.74	$p = -6 - 8\alpha$	−0.4	2.48
$\nu_{opt} > \nu_c$	$p = 2/3 - 4\alpha/3$	1.6	2.08	$p = -8 - 8\alpha$	−2.4	0.48
Jet model:						
$\nu_{opt} < \nu_c$	$p = -\alpha$	0.7	1.06	$p = -6 - 4\alpha$	−3.2	−1.76
$\nu_{opt} > \nu_c$	$p = -\alpha$	0.7	1.06	$p = -6 - 4\alpha$	−3.2	−1.76

[a] The frequency at which the spectrum breaks due to synchrotron cooling is ν_c, whereas the typical visible-light frequency is ν_{opt}.
[b] The GRB afterglow model relation of Zhang & Mészáros (2004).
[c] The electron spectral index calculated from $\alpha_1 = -0.70$ and $\alpha_2 = -1.06$.
[d] The GRB afterglow model relation of Dai & Cheng (2001).

In other words, the apparent break in GRB 040924 might not be a jet break but rather a cooling break.

5. CONCLUSION

The 1.2–1.5 s duration of GRB 040924, although formally in the domain of short GRBs, overlaps the short end of long GRBs. Moreover, it has a soft high-energy spectrum, characteristic of long GRBs. Our optical afterglow observations show that the temporal evolution, power-law index, and $V - R$ color of GRB 040924 are also consistent with those of well-observed long GRBs. The signature of a low-amplitude break in the light curve, as suggested by our present data, can be explained by the afterglow model invoking a cooling break at early times. However, note that the jet break usually occurs 1–2 days after the burst, and that there are few observations of GRB 040924 at $t > 1$ days. Thus, we cannot exclude the possibility that the true jet break occurred outside the range of our observations.

Due to the general lack of information on the optical afterglows of short GRBs, we cannot compare our observations of GRB 040924 to this class of objects. The *Swift* satellite, with higher gamma-ray sensitivity and more accurate localization than previous missions, will provide more opportunities to understand the properties of typical short GRBs and of GRBs near the boundary between short and long GRBs.

We thank the staff and observers at the Lulin telescope for various arrangements that made possible the observations reported herein. This work is supported by grants NSC 93-2752-M-008-001-PAE and NSC 93-2112-M-008-006. Y. U. acknowledges support from the Japan Society for the Promotion of Science through a JSPS Research Fellowship for Young Scientists. A. V. F. is grateful for NSF grant AST 03-07894 and for a Miller Research Professorship at UC Berkeley during which part of this work was completed. KAIT was made possible by generous donations from Sun Microsystems, Inc., the Hewlett-Packard Company, AutoScope Corporation, Lick Observatory, the NSF, the University of California, and the Sylvia and Jim Katzman Foundation.

REFERENCES

Dai, Z. G., & Cheng, K. S. 2001, ApJ, 558, L109
Dai, Z. G., & Lu, T. 1998, MNRAS, 298, 87
Fenimore, E. E., et al. 2004, GCN Circ. 2735, http://gcn.gsfc.nasa.gov/gcn/gcn3/2735.gcn3
Fox, D. B. 2004, GCN Circ. 2741, http://gcn.gsfc.nasa.gov/gcn/gcn3/2741.gcn3
Fox, D. B., & Moon, D. S. 2004, GCN Circ. 2734, http://gcn.gsfc.nasa.gov/gcn/gcn3/2734.gcn3
Frail, D. A., & Soderberg, A. 2004, GCN Circ. 2758, http://gcn.gsfc.nasa.gov/gcn/gcn3/2758.gcn3
Fynbo, J. P. U., Hornstrup, A., Hjorth, J., Jensen, B. L., & Anderson, M. I. 2004, GCN Circ. 2747, http://gcn.gsfc.nasa.gov/gcn/gcn3/2747.gcn3
Golenetskii, S., Aptekar, R., Mazets, E., Pal'shin, V., Frederiks, D., & Cline, T. 2004, GCN Circ. 2754, http://gcn.gsfc.nasa.gov/gcn/gcn3/2754.gcn3
Granot, J., & Sari, R. 2002, ApJ, 568, 820
Henden, A. 2004, GCN Circ. 2811, http://gcn.gsfc.nasa.gov/gcn/gcn3/2811.gcn3
Hu, J. H., Lin, H. C., Huang, K. Y., Urata, Y., Ip, W. H., & Tamagawa, T. 2004, GCN Circ. 2744, http://gcn.gsfc.nasa.gov/gcn/gcn3/2744.gcn3
Huang, K. Y., Urata, Y., Ip, W. H., Tamagawa, T., Onda, K., & Makishima, K. 2005, Nuovo Cimento, in press (astro-ph/0506236)
Khamitov, I., et al. 2004a, GCN Circ. 2740, http://gcn.gsfc.nasa.gov/gcn/gcn3/2740.gcn3
———. 2004b, GCN Circ. 2749, http://gcn.gsfc.nasa.gov/gcn/gcn3/2749.gcn3
———. 2004c, GCN Circ. 2752, http://gcn.gsfc.nasa.gov/gcn/gcn3/2752.gcn3
Kinoshita, D., et al. 2005, Chinese J. Astron. Astrophys., 5, 315
Kouveliotou, C., et al. 1993, ApJ, 413, L101
Landolt, A. U. 1992, AJ, 104, 340
Lee, W. H., & Ramirez-Ruiz, E. 2002, ApJ, 577, 893
Li, W., Filippenko, A. V., Chornock, R., & Jha, S. 2003a, ApJ, 586, L9
———. 2003b, PASP, 115, 844
Li, W., Filippenko, A. V., Chornock, R., & Jha, S. 2004, GCN Circ. 2748, http://gcn.gsfc.nasa.gov/gcn/gcn3/2748.gcn3
MacFadyen, A. I., & Woosley, S. E. 1999, ApJ, 524, 262
Mészáros, P. 2002, ARA&A, 40, 137
Mészáros, P., Rees, M. J., & Wijers, R. A. M. J. 1998, ApJ, 499, 301
Narayan, R., et al. 1992, ApJ, 395, L83
———. 2001, ApJ, 557, 949
Panaitescu, A., & Kumar, P. 2000, ApJ, 543, 66
Panaitescu, A., Mészáros, P., & Rees, M. J. 1998, ApJ, 503, 314
Popham, R., Woosley, S. E., & Fryer, C. 1999, ApJ, 518, 356
Rhoads, J. E. 1999, ApJ, 525, 737
Rosswog, S., & Davies, M. B. 2002, MNRAS, 334, 481
Ruffert, M., et al. 1997, A&A, 319, 122
Schlegel, D. J., Finkbeiner, D. P., & Davis, M. 1998, ApJ, 500, 525
Silvey, J., et al. 2004, GCN Circ. 2833, http://gcn.gsfc.nasa.gov/gcn/gcn3/2833.gcn3
Simon, V. 2001, A&A, 377, 450
Stetson, P. B. 1987, PASP, 99, 191
Terada, H., Akiyama, M., & Kawai, N. 2004, GCN Circ. 2745, http://gcn.gsfc.nasa.gov/gcn/gcn3/2745.gcn3
Urata, Y., et al. 2005, Nuovo Cimento, in press (astro-ph/0506233)
van der Horst, A. J., Rol, E., & Wijers, R. A. M. J. 2004a, GCN Circ. 2746, http://gcn.gsfc.nasa.gov/gcn/gcn3/2746.gcn3
———. 2004b, GCN Circ. 2759, http://gcn.gsfc.nasa.gov/gcn/gcn3/2759.gcn3
Wiersema, K., et al. 2004, GCN Circ. 2800, http://gcn.gsfc.nasa.gov/gcn/gcn3/2800.gcn3
Woosley, S. E. 1993, ApJ, 405, 273
Zhang, B., & Mészáros, P. 2004, Int. J. Mod. Phys. A., 19, 2385

RESEARCH ARTICLE

Deep Impact: Observations from a Worldwide Earth-Based Campaign

K. J. Meech,[1*] N. Ageorges,[2] M. F. A'Hearn,[3] C. Arpigny,[4] A. Ates,[5] J. Aycock,[6] S. Bagnulo,[2] J. Bailey,[7] R. Barber,[8] L. Barrera,[9] R. Barrena,[10] J. M. Bauer,[11] M. J. S. Belton,[12] F. Bensch,[13] B. Bhattacharya,[14] N. Biver,[15] G. Blake,[14] D. Bockelée-Morvan,[15] H. Boehnhardt,[16] B. P. Bonev,[17] T. Bonev,[18] M. W. Buie,[19] M. G. Burton,[20] H. M. Butner,[21] R. Cabanac,[22] R. Campbell,[6] H. Campins,[23] M. T. Capria,[24] T. Carroll,[21] F. Chaffee,[6] S. B. Charnley,[25] R. Cleis,[26] A. Coates,[27] A. Cochran,[28] P. Colom,[15] A. Conrad,[6] I. M. Coulson,[21] J. Crovisier,[15] J. deBuizer,[29] R. Dekany,[14] J. de Léon,[10] N. Dello Russo,[30] A. Delsanti,[1] M. DiSanti,[31] J. Drummond,[26] L. Dundon,[1] P. B. Etzel,[32] T. L. Farnham,[3] P. Feldman,[33] Y. R. Fernández,[23] M. D. Filipovic,[34] S. Fisher,[35] A. Fitzsimmons,[36] D. Fong,[37] R. Fugate,[26] H. Fujiwara,[38] T. Fujiyoshi,[39] R. Furusho,[40] T. Fuse,[39] E. Gibb,[41] O. Groussin,[3] S. Gulkis,[11] M. Gurwell,[37] E. Hadamcik,[42] O. Hainaut,[2] D. Harker,[43] D. Harrington,[1] M. Harwit,[44] S. Hasegawa,[45] C. W. Hergenrother,[46] P. Hirst,[21] K. Hodapp,[1] M. Honda,[45] E. S. Howell,[47] D. Hutsemékers,[4] D. Iono,[37] W.-H. Ip,[48] W. Jackson,[49] E. Jehin,[2] Z. J. Jiang,[50] G. H. Jones,[16] P. A. Jones,[51] T. Kadono,[52] U. W. Kamath,[53] H. U. Käufl,[2] T. Kasuga,[54] H. Kawakita,[55] M. S. Kelley,[56] F. Kerber,[2] M. Kidger,[10] D. Kinoshita,[48] M. Knight,[3] L. Lara,[57] S. M. Larson,[46] S. Lederer,[58] C.-F. Lee,[37] A. C. Levasseur-Regourd,[42] J. Y. Li,[3] Q.-S. Li,[50] J. Licandro,[10,59] Z.-Y. Lin,[48] C. M. Lisse,[30] G. LoCurto,[2] A. J. Lovell,[60] S. C. Lowry,[36] J. Lyke,[6] D. Lynch,[61] J. Ma,[50] K. Magee-Sauer,[62] G. Maheswar,[53] J. Manfroid,[4] O. Marco,[2] P. Martin,[22] G. Melnick,[37] S. Miller,[8] T. Miyata,[38] G. H. Moriarty-Schieven,[21] N. Moskovitz,[1] B. E. A. Mueller,[63] M. J. Mumma,[31] S. Muneer,[53] D. A. Neufeld,[33] T. Ootsubo,[64] D. Osip,[65] S. K. Pandea,[53] E. Pantin,[66] R. Paterno-Mahler,[5] B. Patten,[37] B. E. Penprase,[5] A. Peck,[37] G. Petitas,[37] N. Pinilla-Alonso,[67] J. Pittichova,[1] E. Pompei,[2] T. P. Prabhu,[53] C. Qi,[37] R. Rao,[37] H. Rauer,[68] H. Reitsema,[69] S. D. Rodgers,[25] P. Rodriguez,[70] R. Ruane,[26] G. Ruch,[56] W. Rujopakarn,[71] D. K. Sahu,[53] S. Sako,[38] I. Sakon,[38] N. Samarasinha,[63] J. M. Sarkissian,[51] I. Saviane,[2] M. Schirmer,[59] P. Schultz,[72] R. Schulz,[73] P. Seitzer,[71] T. Sekiguchi,[54] F. Selman,[2] M. Serra-Ricart,[10] R. Sharp,[74] R. L. Snell,[75] C. Snodgrass,[36] T. Stallard,[8] G. Stecklein,[5] C. Sterken,[76] J. A. Stüwe,[77] S. Sugita,[38] M. Sumner,[14] N. Suntzeff,[63] R. Swaters,[3] S. Takakuwa,[37] N. Takato,[39] J. Thomas-Osip,[65] E. Thompson,[26] A. T. Tokunaga,[1] G. P. Tozzi,[78] H. Tran,[6] M. Troy,[11] C. Trujillo,[29] J. Van Cleve,[69] R. Vasundhara,[53] R. Vazquez,[79] F. Vilas,[80] G. Villanueva,[16] K. von Braun,[81] P. Vora,[82] R. J. Wainscoat,[1] K. Walsh,[3] J. Watanabe,[54] H. A. Weaver,[33] W. Weaver,[26] M. Weiler,[68] P. R. Weissman,[11] W. F. Welsh,[32] D. Wilner,[37] S. Wolk,[37] M. Womack,[83] D. Wooden,[25] L. M. Woodney,[58] C. Woodward,[56] Z.-Y. Wu,[50] J.-H. Wu,[50] T. Yamashita,[39] B. Yang,[1] Y.-B. Yang,[50] S. Yokogawa,[37] A. C. Zook,[5] A. Zauderer,[3] X. Zhao,[50] X. Zhou,[50] J.-M. Zucconi[84]

On 4 July 2005, many observatories around the world and in space observed the collision of Deep Impact with comet 9P/Tempel 1 or its aftermath. This was an unprecedented coordinated observational campaign. These data show that (i) there was new material after impact that was compositionally different from that seen before impact; (ii) the ratio of dust mass to gas mass in the ejecta was much larger than before impact; (iii) the new activity did not last more than a few days, and by 9 July the comet's behavior was indistinguishable from its pre-impact behavior; and (iv) there were interesting transient phenomena that may be correlated with cratering physics.

The Deep Impact mission was designed so that much of the mission-critical science would be done from Earth-based telescopes. These facilities would observe the comet before, during, and after impact to follow the evolution of the comet in wavelength regimes and time scales inaccessible to the spacecraft. Observations began in 1997 to characterize the nucleus of comet 9P/Tempel 1 for mission planning and to establish a baseline of normal behavior against which impact-induced changes could be assessed (*1*, *2*). From 1997 through 2004, observations on 229 nights were obtained from 14 telescopes at nine observatories. In 2005, since the comet came out of solar conjunction, the worldwide collaboration has involved more than 550 whole or partial nights of observation using 73 Earth-based telescopes at 35 observatories (Fig. 1), plus many (Earth-orbital and Sun-orbital) space-based facilities.

Here we give an overview of the scientific conclusions and collective observations from the Earth-based campaign (*3*). As seen from Earth, the Deep Impact event did not create a new period of sustained cometary activity, and in many ways the artificial impact looked very much like a natural outburst. There were some observable changes after impact in the chemistry of the observed dust and gas as well as in the physical properties of the dust, which may suggest that the material beneath the surface was different in composition from the surface materials.

Ejecta cloud. The ejecta cloud was first resolved ~20 min after impact by Earth-orbiting telescopes at visible and ultraviolet wavelengths. Later, ground-based telescopes worldwide imaged the southwesterly-expanding cloud of dust and gas in the visible and infrared (IR) wavelength regime (λ = 0.3 to 13 μm). Generally, the visible and near-IR wavelengths (0.3 to 2.5 μm) achieved the best spatial resolution and sensitivity; that is, most observations were sampling the reflected sunlight from dust in the cloud, with some contribution from the gas in emission bands (<0.6 μm).

About 1 hour after impact, the ejecta was semicircular and extended across position angles 145° to 325°. The ejecta cloud had a nonuniform light distribution. During the first 20 hours after impact, the time series of images showed the leading edge of the dust cloud expanding outward at a projected speed of ~200 ± 20 m/s (although varying with azimuth). The southward orientation of the ejecta indicates that the impact occurred below the orbital plane of the comet.

From 6 July 2005 (all dates are UT) onward, the expanding dust cloud increasingly changed shape because of the push of solar radiation pressure, forcing the particles into the tail (i.e., antisolar) direction at a position angle of 110°.

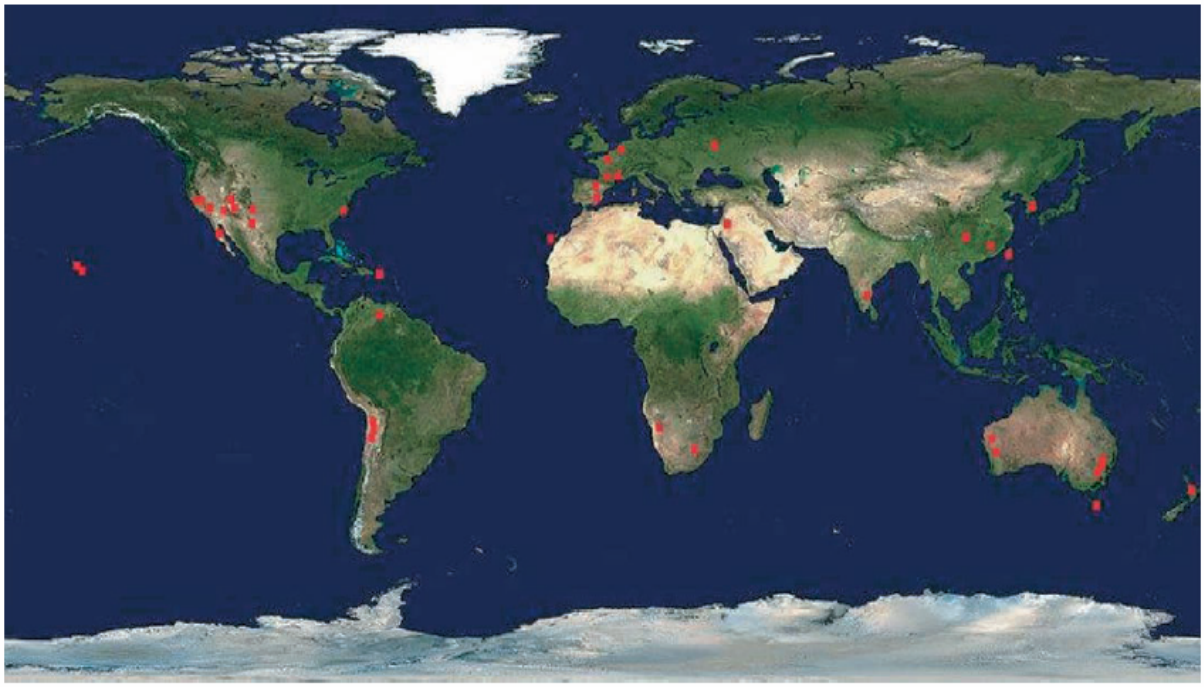

Fig. 1. Map of Earth, showing the locations of observatories collaborating in the coordinated campaign (red dots). World map credit: NASA.

The maximum projected distance in the sunward direction was 30,000 km, achieved on 7 July (Fig. 2). Together, the projected speed and projected distance imply that a typical dust grain experienced a ratio of radiation pressure to gravity of ~0.3.

The size-sorting of the dust grains by radiation pressure led to color changes in the ejecta cloud. Bluer colors on the tailward side of the plume suggested that submicrometer dust grains—which are more sensitive to radiation pressure and less efficient in reflecting red and IR light—were pushed out first. By 9 July, the dust cloud dispersed and had faded below the detection limit of many imaging instruments (Fig. 2).

By assuming a dust albedo and a "typical" grain size (0.5 μm), the flux of the impact ejecta can be converted into a total dust mass. On the order of ~10^6 kg of dust were liberated, equivalent to ~10 hours of normal (pre-impact) dust production.

Coma structures. For the 6 months before impact, the dust coma showed a broad fan to the southeast and other narrow jetlike radial features at various azimuths. Because they did not vary with the rotation of the nucleus, these

[1]Institute for Astronomy, University of Hawaii at Manoa, 2680 Woodlawn Drive, Honolulu, HI 96822, USA. [2]European Southern Observatory, Casilla 19001, Santiago 19, Chile. [3]University of Maryland, College Park, MD 20742, USA. [4]Université de Liège, B-4000 Liège, Belgium. [5]Pomona College, Claremont, CA 91711, USA. [6]Keck Observatory, Kamuela, HI 96743, USA. [7]Australian Centre for Astrobiology, Macquarie University, Sydney, NSW 2109, Australia. [8]University College London, London WC1E 6BT, UK. [9]Universidad Metropolitana de Ciencias de la Educación, Ñuñoa, Santiago, Chile. [10]Instituto de Astrofisica de Canarias, E38200 La Laguna (Tenerife), Spain. [11]NASA/Jet Propulsion Laboratory, Pasadena, CA 91109, USA. [12]Belton Space Initiatives, Tucson, AZ 85716, USA. [13]Radioastronomisches Institut der Universität Bonn, D-53121 Bonn, Germany. [14]California Institute of Technology, Pasadena, CA 91125, USA. [15]Observatoire Paris Meudon, F-92195 Meudon, France. [16]Max-Planck-Institut für Sonnensystemforschung, Katlenburg-Lindau 37191, Germany. [17]University of Toledo, Toledo, OH 43606, USA. [18]Institute of Astronomy, Sofia 1784, Bulgaria. [19]Lowell Observatory, Flagstaff, AZ 86001, USA. [20]University of New South Wales, Sydney, NSW 2052, Australia. [21]Joint Astronomy Centre, Hilo, HI 96720, USA. [22]Canada-France-Hawaii Telescope, Kamuela, HI 96743, USA. [23]University of Central Florida, Orlando, FL 32816, USA. [24]Instituto di Astrofisica Spaziale e Fisica Cosmica, 00133 Roma, Italy. [25]NASA Ames Research Center, Moffett Field, CA 94035, USA. [26]Air Force Research Lab, Kirtland Air Force Base, NM 87117, USA. [27]Mullard Space Science Laboratory, Surrey RH5 6NT, UK. [28]University of Texas, Austin, TX 78712, USA. [29]Gemini Observatory, Casilla 603, La Serena, Chile. [30]Johns Hopkins University Applied Physics Laboratory, Laurel, MD 20723, USA. [31]NASA/Goddard Space Flight Center, Greenbelt, MD 20770, USA. [32]San Diego State University, San Diego, CA 92182, USA. [33]Johns Hopkins University, Baltimore, MD 21218, USA. [34]University of Western Sydney, NSW 1797, Australia. [35]Gemini Observatory North, Hilo, HI 96720, USA. [36]Queen's University, Belfast BT7 1NN, UK. [37]Harvard-Smithsonian Center for Astrophysics, Cambridge, MA 02138, USA. [38]University of Tokyo, Tokyo 113-8654, Japan. [39]Subaru Telescope, Hilo, HI 96720, USA. [40]Waseda University, Tokyo 169-8050, Japan. [41]University of Notre Dame, South Bend, IN 46556, USA. [42]Service d'Aéronomie, CNRS, 91371 Verrières Le Buisson, France. [43]University of California, San Diego, La Jolla, CA 92093, USA. [44]Cornell University, Ithaca, NY 14853, USA. [45]Institute of Space and Astronautical Science, Sagamihara, Kanagawa 229-8510, Japan. [46]University of Arizona, Tucson, AZ 85721, USA. [47]Arecibo Observatory, Arecibo, PR 00612, USA. [48]National Central University, Jhongli, Taoyuan 32001, Taiwan. [49]University of California, Davis, CA 95616, USA. [50]National Astronomical Observatories, Beijing 100012, China. [51]Australia Telescope National Facility, Epping, NSW 1710, Australia. [52]Japan Agency for Marine-Earth Science and Technology, Yokosuka, Kanagawa 237-0061, Japan. [53]Indian Institute of Astrophysics, Bangalore 560 034, India. [54]National Astronomical Observatory of Japan, Tokyo 181-8588, Japan. [55]Kyoto Sangyo University, Kyoto 603-8555, Japan. [56]University of Minnesota, Minneapolis, MN 55455, USA. [57]Instituto de Astrofisica de Andalucía-CSIC, 18080 Granada, Spain. [58]California State University, San Bernardino, CA 92407, USA. [59]Isaac Newton Group of Telescopes, La Palma E-38700, Spain. [60]Agnes Scott College, Atlanta, GA 30030, USA. [61]Aerospace Corporation, Los Angeles, CA 90009, USA. [62]Rowan University, Glassboro, NJ 08028, USA. [63]National Optical Astronomy Observatory, Tucson, AZ 85719, USA. [64]Nagoya University, Nagoya 464-8601, Japan. [65]Las Campanas Observatory, Pasadena, CA 91101, USA. [66]CEA-Service d'Astronomie, Saclay F-91191, France. [67]Fundación Galileo Galilei & Telescopio Nazionale Galileo, La Palma 38700, Spain. [68]Deutsches Zentrum für Luft- und Raumfahrt, Berlin 12489, Germany. [69]Ball Aerospace, Boulder, CO 80306, USA. [70]European Space Agency, Villafranco del Castillo, 28080 Madrid, Spain. [71]University of Michigan, Ann Arbor, MI 48109, USA. [72]Brown University, Providence, RI 02912, USA. [73]European Space Agency, Noordwijk NL-2200 AG, Netherlands. [74]Anglo-Australian Observatory, Epping, NSW 1710, Australia. [75]University of Massachusetts, Amherst, MA 01003, USA. [76]University of Brussels, B-1050 Brussels, Belgium. [77]Leiden Observatory, NL-2300 RA Leiden, Netherlands. [78]Osservatorio Astrofisico di Arcetri, Firenze I-50125, Italy. [79]Universidad Nacional Autónoma de México, Ensenada 22800, Mexico. [80]NASA/Johnson Space Center, Houston, TX 77058, USA. [81]Carnegie Institution of Washington, Washington, DC 20015, USA. [82]College of William and Mary, Williamsburg, VA 23187, USA. [83]St. Cloud State University, St. Cloud, MN 56301, USA. [84]Observatoire de Besançon, 25010 Besançon Cedex, France.

*To whom correspondence should be addressed. E-mail: meech@ifa.hawaii.edu

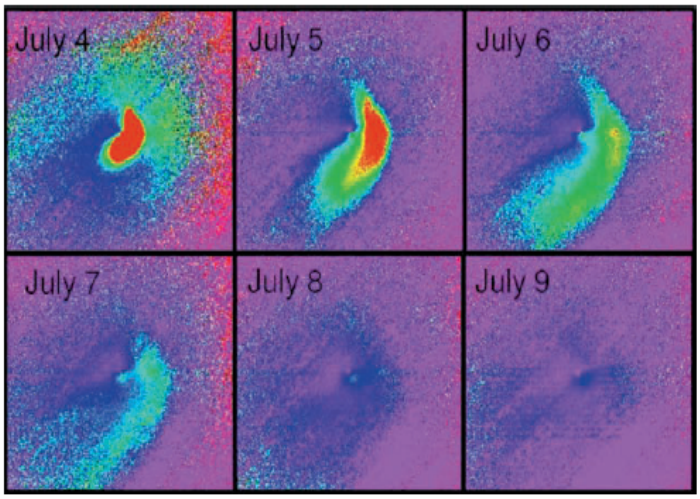

Fig. 2. Sequence of processed post-impact *R* band images of the dust coma of 9P/Tempel 1 acquired from the Nordic Optical Telescope. North is up and east is left. Dates are UT; the first image was taken ~16 hours after impact, and succeeding images were taken around the same time of day on the following nights. The width of each panel is ~120,000 km at the comet. Each image has been divided by a pre-impact 3 July image to accentuate structure in the coma. The evolution of the ejecta cloud is clearly seen.

features are interpreted as a fan coma emanating from localized sources on the nucleus, with the observer point of view being outside the emission cone (*4*, *5*). Neither the number of jets and fans nor their orientations changed during the impact period. In particular, no new long-lived jet or fan has been identified as being from the newly excavated crater.

Fluctuations that were observed in the intensity of some coma structures are possibly related to the impact event itself but could also be due to natural variations in activity. A southwesterly jetlike feature seen one-half rotation period after impact was observed to be brighter than it had been before impact. This could have been caused by gas production from the ejecta dust grains themselves. By just one full rotation period after impact (41 hours), the coma morphology had returned to its pre-impact state, which suggests that the impact site was by this time beginning to cease its activity.

Gas production. The gas species commonly monitored at visible wavelengths in cometary comae—CN, C_2, C_3, NH_2, and CH—were observed in 9P/Tempel 1 before and after impact. During the first 2 days after impact, observations showed the intensity of the species' emission bands increasing by a factor of ~1.5 to 5. An example of the increase in CN as seen through spectroscopy is shown in Fig. 3. Photometry was also used by some groups (*6*). The abundance ratios among the common species stayed at pre-impact levels (*5*). In particular, the C_2-to-CN abundance ratio of ~0.8 classifies 9P/Tempel 1 as a "typical" comet (*7*), as it was before impact. Gas production was back to its pre-impact level by 9 July.

In the near-IR, species not directly detectable before impact—H_2O, C_2H_6, CH_3OH, C_2H_2, and HCN—appeared after impact (*8*). The abundance ratios among these species were consistent with those of typical Oort cloud comets (*8*), although 9P/Tempel 1 is a Jupiter-family comet. There have been relatively few studies of these species among members of the Jupiter family.

Measurements of the CN (0-0) band in the visible spectra revealed isotopic abundances of carbon and nitrogen: The $^{12}C/^{13}C$ ratio was close to the solar value (which is 89), and the $^{14}N/^{15}N$ ratio was half that of Earth's value (which is 272). Hence, comet 9P/Tempel 1 shows the same low nitrogen isotopic ratio that was recently detected in other Jupiter-family comets (*9*).

In addition to near-IR detections of water, other groups monitored the submillimeter transitions of H_2O and the near-ultraviolet transitions of OH. For example, spacecraft observing the 557-GHz transition of water reported a 20% increase in the hours after impact. However, the natural variations in water production that were seen before impact could account for this. On the other hand, there was also a factor of 3 increase in OH production. The reconciliation of these data awaits further analysis.

Several species were monitored from ground-based radio telescopes. HCN at 88.6 and 265.9 GHz and CH_3OH at 145 GHz were detected for only a few days after impact; the production rates later returned to or fell below pre-impact levels. The abundance ratios of HCN and CH_3OH relative to water were similar to those observed in other comets. Post-impact upper limits to production rates were derived for CO, CS, H_2CO, and H_2S; pre-impact upper limits were obtained for OH, CH_3OH, and HCN. All radio detections and upper limits with space-based and ground-based telescopes indicated very little effect on molecular gas production as a result of the impact, whereas somewhat larger effects were noticeable in H-, C-, and N-bearing molecules and in the dust detectable in the visible and near-IR wavelength region. A possible explanation for this different behavior could be gas released from the ejected cometary dust as a consequence of dust fragmentation due to the sublimation of intergrain ices.

Wide-angle imaging in narrowband filters tuned to the fluorescence of H_2O^+ and CO^+ in visible wavelengths was performed. The observations did not reveal any signatures of substantial ion production that could be attributed to the impact.

X-ray observations (0.1 to 1.0 keV) were performed at impact time and afterward. Comets produce x-rays by charge-exchange reactions between the solar wind's highly ionized minor ion population and the neutral cometary gas species (*10*). A ~30% increase in the x-ray counts, lasting for about 1 day, was seen by Earth-orbiting x-ray telescopes after impact. This is interpreted as due to excursions in the comet's gas production rate for a collisionally thin charge-exchange system.

Dust properties. Mid-IR observations can be used to constrain fundamental properties of cometary dust, and 9P/Tempel 1 was no exception, at least after impact. Because of the comet's faintness, pre-impact mid-IR spectra (λ = 8 to 13 μm) obtained from the ground were essentially flat and featureless. Space-based observations gave better signal but yielded a similar pre-impact picture. The grains were generally large (>1 μm) and the 8- to 13-μm emission band was very weak, consistent with previous apparitions (*11*).

Immediately after impact, a short barlike structure extending ~1 arc sec at a position angle of ~225° was seen from ground-based mid-IR imaging. Over the next several hours, the mid-IR flux of the central coma brightened by a factor of ~2 (Fig. 4). Note that the increase in total dust flux (compared to the apparently more modest increase in gas flux) implies that the ratio of dust mass to gas mass in the ejecta was not the same as that seen before impact. This was a dusty impact.

Ground-based mid-IR spectroscopy revealed a substantial growth in the 8- to 13-μm silicate emission feature after impact. The strength of that emission band suggests an emission dominated by submicrometer (0.5 to 1 μm) dust grains. The small size of the grains is consistent with the reports from the spacecraft imaging (*12*). The composition, as derived from modeling the shape of the emission band, is a mix of amorphous olivine and pyroxene, amorphous carbon (which controls the dust temperature), crystalline fosterite, and clino- and orthopyroxene (*13*, *14*). In particular, the resonance peak seen at 11.2 μm is indicative of Mg-rich crystalline olivine. Indeed, the degree of crystallinity in the dust grains was substantially higher in the impact ejecta relative to pre-impact measurements. Organic refractory

material was not needed to model the emission band. The shape of the post-impact silicate feature is strikingly similar to the spectra of active, long-period comets, especially Hale-Bopp. The silicate emission band persisted for about 20 to 26 hours after impact; after that time, the spectral features had disappeared and the comet had returned to its pre-impact mid-IR flux.

Space-based mid-IR observations were performed in phase with the rotation period to ensure that the comet was sampled at similar states of activity. Moreover, in the wavelength segments that are inaccessible from the ground (5 to 8 μm, 13 to 18 μm, and >25 μm), the space-based data filled in the gaps. Imaging at $\lambda = 16$ μm at the time of impact may have revealed thermal emission from the hot impact plume, albeit with a spatial resolution that was poorer than that of the ground-based telescopes by a factor of 5 to 10. Spectroscopic coverage of the entire 5- to 40-μm region after impact revealed compositional and grain temperature information similar to what was seen on the ground. The 9- to 37-μm region showed evidence of crystalline pyroxene in addition to the olivine seen from the ground. Spectral features due to H_2O, CO_2, and carbonaceous material were also seen (*15*).

Polarization of the dust coma was monitored by several groups. Before impact, polarization in visible wavelengths was measured to be 7.0 ± 0.5%. After impact, some variation of polarization with wavelength (0.65 to 0.9 μm) and also with distance from the nucleus was seen, suggesting a change in grain size, porosity, or composition.

Photometric behavior. The transient photometric behavior of the comet's inner coma in the first 15 to 30 min after impact was recorded by many groups. For a small aperture of radius ~1 arc sec, the comet brightened by about 2.3 mag in the visible wavelengths. Note that the nucleus had a magnitude of ~17 in standard Cousins *R* band at the time of impact.

Subtle changes in the light curve can be linked to post-impact phenomena on the comet's surface. A typical light curve with high temporal resolution is shown in Fig. 5. In the first few minutes, there were three distinct rates of brightening. From impact to ~1 min after, the comet brightened sharply. Then, for the next 6 min, the brightening rate was more gradual. However, at ~7 min after impact, the brightening rate increased again, although not as steeply as at first. This rate remained constant for the next 10 to 15 min, at which point the comet's flux began to level off. In the smallest apertures (radius ≈ 1 arc sec), the flux then began to decrease again ~45 min after impact.

This three-sloped light curve as seen in Fig. 5 could be directly linked to the formation of the impact crater, its evolution, and the evolution of the outgassing from it. The falloff in brightness by the first few hours after impact is related to a decrease in the level of activity from the new crater. However, the effect is also partly due to the ejecta moving beyond the edge of the photometric aperture; the peak of the light curve depends strongly on aperture size. Light curves from larger apertures displayed later times of peak brightness; moreover, the comet did not stay at its peak brightness for very long, regardless of aperture. This means that the outgassing from the crater, although much less fecund relative to its activity immediately after impact, had not completely ceased. If it had, light curves with large apertures would show a flat peak flux lasting for the length of time needed for the dust to move out of the aperture.

No group reported seeing an unambiguous, short-duration (<1 s) flash at the exact moment of impact, despite the impact site being visible from Earth. This is likely due to the low contrast of the flash versus the rest of the light from the inner coma as seen in most Earth-based telescopes.

Natural outbursts. The comet was observed to have a series of natural outbursts in addition to the one induced by Deep Impact. These outbursts were identifiable above the comet's normal, gradual brightening as it approached perihelion. The brightness of the comet's dust coma varied with heliocentric distance *r* as $r^{-6.7}$ until early May and dropped thereafter. The first identified outburst occurred on 23 and 24 February (*16*) as the comet brightened by ~40%.

Morphological analysis of an outburst was carried out from visible-wavelength images obtained on 14 June. The outburst showed an arc of material extending over position angles of 215° to 45°. At the peak of the outburst, the comet's brightness was higher than that in previous dates by ~50 to 60%. This outburst was also seen by the Deep Impact spacecraft itself. Observations by multiple telescopes allowed a projected velocity of the dust from the outburst to be calculated: ~200 m/s. Note that this is similar to the speed of the Deep Impact ejecta.

After this discovery, more intense photometric monitoring was initiated, and a series

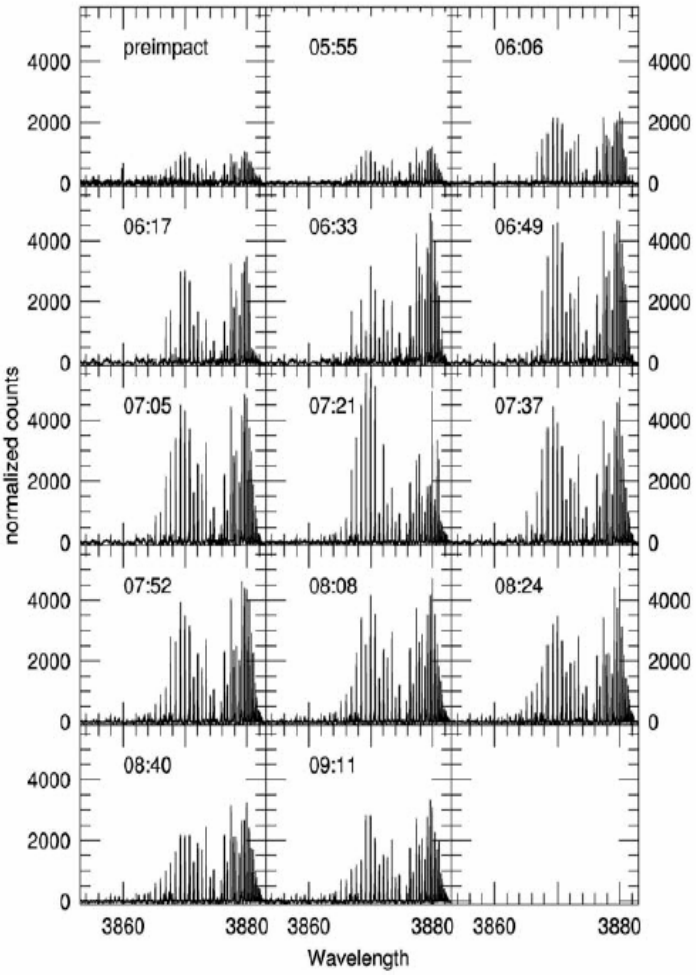

Fig. 3. Spectra (normalized to 1 air mass and 15 min exposure time) of the CN $\Delta v = 0$ emission band ($\delta v = 0$) on 4 July 2005. Data were obtained with the Keck I telescope. The plot shows that the intensity of the CN lines increased by more than a factor of 5 from the pre-impact level to the peak post-impact level (UT 07:21, ~1.5 hours after impact). The emission then begins to decrease; the ejecta must have filled the slit, and the decrease represents the dilution of the gas by expansion. This is consistent with a gas outflow velocity of ~1.1 km/s.

of outbursts occurred approximately every 8 days. On 22 June, there was another outburst and the dust coma morphology was similar to the one on 14 June. On 29 June, mid-IR and x-ray observations revealed another outburst.

On 2 July, another outburst was reported by the spacecraft and by several observers. This was the only event for which a submillimeter continuum detection was obtained; no such detection was reported for the impact event itself. An outburst that was seen by ground-based radio observations of OH occurred on 6 July. Further outbursts were reported on 8 July (in x-rays) and 9 July (in visible wavelengths).

This series of pre- and post-impact natural outbursts bears strong resemblance to the one induced by the impact itself. The projected expansion velocity of the dust cloud has been ~200 m/s for every outburst. The coma morphologies induced by both the natural outbursts and the impact-induced one have been very similar. Specifically, the shape of the ejecta cloud and the ejecta opening angles (~180°) behave similarly, expanding until the radiation pressure starts to dominate the structure.

Summary. The ground-based observing campaign brought together a collaboration of unprecedented size and scope for support of a spacecraft mission. We had worldwide international cooperation, which was critical for addressing fundamental questions revealed by the Deep Impact experiment. Data analysis continues, but several conclusions can be made.

We now have adequate observations to understand the detailed composition of dust in a Jupiter-family comet. Furthermore, this dust comes from deeper subsurface layers than normal, so it is less processed than the cometary dust we normally see. The dust to gas ratio in the ejecta was larger than what was measured before impact, which suggests that the volatile content of the nucleus's material is depleted even several meters below the surface.

The consensus from the observing campaign was that the impact was an impulsive event. A large amount of material was ejected into the coma in a very short time and took no more than 5 days to dissipate, but the amount of material emitted from the impact site was relatively small. Although we cannot conclusively state that the impact did not create a new source, we can conclude that any new source must be small when compared to the sources that already existed on the nucleus.

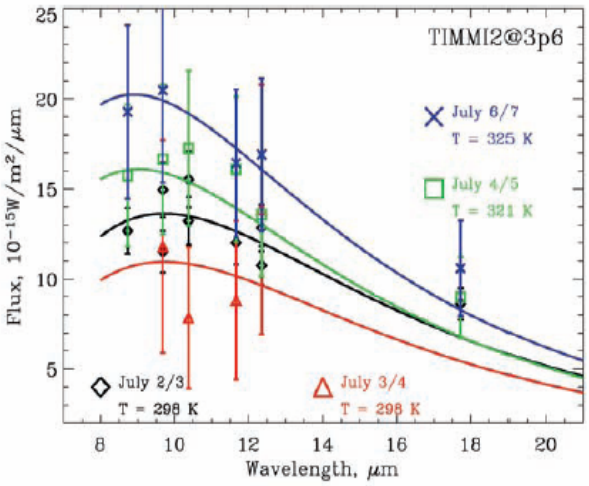

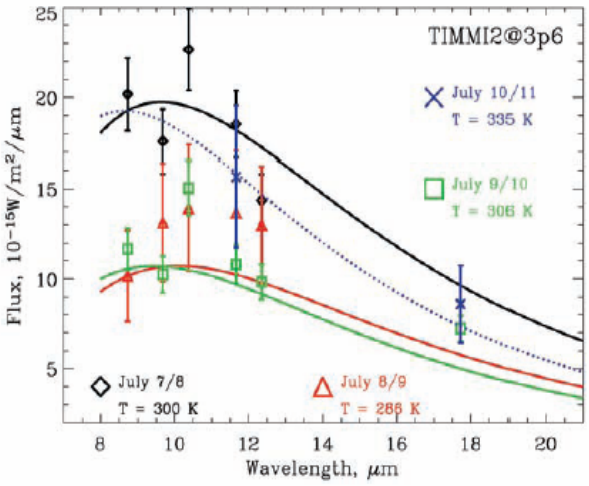

Fig. 4. Synoptic presentation of photometrically calibrated mid-IR fluxes as measured with the European Southern Observatory's 3.6-m telescope. Aperture size was 2500 km at the comet. Data were obtained from 2 days before impact to 7 days after impact. The scatter in the data is due to the "noise" introduced by the normal comet activity. This is consistent with observations done in February and March 2005 (17). Blackbody curves are drawn for each epoch to give an indication of the amount of "nonthermal" flux in the filters sensitive to solid-state features (at 9, 10, and 11 μm).

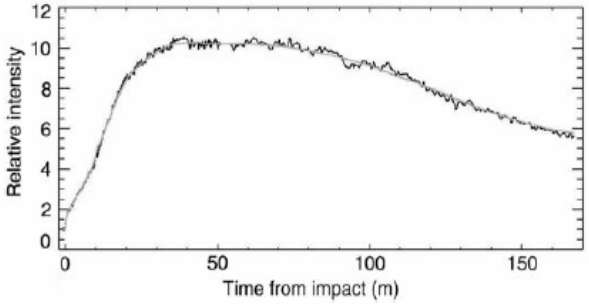

Fig. 5. Impact light curve taken from the charge-coupled device guide camera at United Kingdom Infrared Telescope, sampled at 20 Hz. The triple-slope phenomenon in the first few minutes after impact is clear. The data have been ratioed to the brightness at the time of impact.

References and Notes

1. M. J. S. Belton *et al.*, *Space Sci. Rev.* 117, 137 (2005).
2. K. J. Meech *et al.*, *Space Sci. Rev.* 117, 297 (2005).
3. Note that for succinctness the term "Earth-based" is used to describe observations from ground-based telescopes, Earth-orbiting telescopes, and Sun-orbiting telescopes.
4. Z. Sekanina, H. Boehnhardt, *Earth Moon Planets* 78, 313 (1999).
5. L. Lara *et al.*, in preparation.
6. D. G. Schleicher *et al.*, in preparation.
7. M. F. A'Hearn, R. L. Millis, D. G. Schleicher, D. J. Osip, P. V. Birch, *Icarus* 118, 223 (1995).
8. M. J. Mumma *et al.*, *Science* 310, 270 (2005).
9. D. Hutsemekers *et al.*, *Astron. Astrophys.*, in press (available at http://arXiv.org/abs/astro-ph/0508033).
10. C. M. Lisse, T. E. Cravens, K. Dennerl, in *Comets II*, M. C. Festou *et al.*, Eds. (Univ. of Arizona Press, Tucson, AZ, 2005), pp. 631–643.
11. C. M. Lisse *et al.*, *Space Sci. Rev.* 117, 161 (2005).
12. M. F. A'Hearn *et al.*, *Science* 310, 258 (2005); published online 8 September 2005 (10.1126/science.1118923).
13. S. Sugita *et al.*, *Science* 310, 274 (2005).
14. D. E. Harker, C. E. Woodward, D. H. Wooden, *Science* 310, 278 (2005).
15. C. Lisse *et al.*, *Intl. Astron. Union Circ. 8571* (2005).
16. Amateur Monitoring by the Observadores_Cometas Group (http://astrosurf.com/somyce/c_cometas/9P/9P.htm).
17. H. U. Käufl *et al.*, *Intl. Astron. Union Circ. 8593* (2005).
18. Supported by the University of Maryland and by University of Hawaii subcontract Z667702, which was awarded under prime contract NASW-00004 from NASA. We thank telescope allocation committees everywhere, too numerous to list, for their generous support of time.

17 August 2005; accepted 1 September 2005
Published online 8 September 2005;
10.1126/science.1118978
Include this information when citing this paper.

Astronomy & Astrophysics manuscript no. 3c454
December 22, 2005

The unprecedented optical outburst of the quasar 3C 454.3

The WEBT campaign of 2004–2005⋆

M. Villata, C. M. Raiteri, T. J. Balonek, M. F. Aller, S. G. Jorstad, O. M. Kurtanidze, F. Nicastro, K. Nilsson, H. D. Aller, A. Arai, A. Arkharov, U. Bach, E. Benítez, A. Berdyugin, C. S. Buemi, M. Böttcher, D. Carosati, R. Casas, A. Caulet, W. P. Chen, P.-S. Chiang, Y. Chou, S. Ciprini, J. M. Coloma, G. Di Rico, C. Diaz Lopez, N. V. Efimova, C. Forsyth, A. Frasca, L. Fuhrmann, B. Gadway, S. Gupta, V. A. Hagen-Thorn, J. Harvey, J. Heidt, H. Hernandez-Toledo, F. Hroch, C.-P. Hu, R. Hudec, M. A. Ibrahimov, A. Imada, M. Kamata, T. Kato, M. Katsuura, T. Konstantinova, E. Kopatskaya, D. Kotaka, Y. Y. Kovalev, Yu. A. Kovalev, K. Kubota, M. Kurosaki, L. Lanteri, V. M. Larionov, L. Larionova, E. Laurikainen, C.-U. Lee, P. Leto, O. Lopez-Cruz, A. Lähteenmäki, E. Marilli, A. P. Marscher, I. M. McHardy, S. Mondal, B. Mullan, N. Napoleone, M. G. Nikolashvili, J. M. Ohlert, S. Postnikov, T. Pursimo, M. Ragni, J. A. Ros, K. Sadakane, A. C. Sadun, T. Savolainen, E. Sergeeva, L. A. Sigua, A. Sillanpää, L. Sixtova, L. O. Takalo, H. Teräsranta, M. Tornikoski, C. Trigilio, G. Umana, A. Volvach, B. Voss, and S. Wortel

Whole Earth Blazar Telescope (WEBT) Consortium and other Institutes

ABSTRACT

Context. The radio quasar 3C 454.3 underwent an exceptional optical outburst lasting more than 1 year and culminating in spring 2005. The maximum brightness detected was $R = 12.0$, which should represent the most luminous quasar state ever observed ($M_B \sim -31.4$).

Aims. In order to follow the emission behaviour of the source in detail, a huge multiwavelength campaign was organized by the Whole Earth Blazar Telescope (WEBT).

Methods. Continuous optical, near-IR, and radio monitoring was performed in several bands. Moreover, ToO pointings by the Chandra and INTEGRAL satellites provided information at high energies in May 2005.

Results. The colour-index behaviour (generally redder-when-brighter) during the outburst suggests the presence of a luminous accretion disc. The historical radio and optical light curves reveal a sort of anti-correlation. Up to about 2001.0 only moderate variability characterized the optical regime, while prominent and long-standing radio outbursts are visible at the various radio frequencies, with higher-frequency variations leading the lower-frequency ones. After that date, the optical activity increases and the radio flux becomes less variable. This suggests that the two corresponding jet emitting regions are separated and misaligned, with the inner optical one acquiring a smaller viewing angle during the 2004–2005 outburst. A huge mm outburst has followed the optical one, peaking in June–July. In the meantime the high-frequency (37–43 GHz) radio flux started to increase and reached a maximum at the end of our observing period (end of September). VLBA observations at 43 GHz during the summer strictly confirm the brightening of the radio core and show an increasing polarization. An exceptionally bright X-ray state was detected in May, thus correlating with the rising mm flux and suggesting an inverse-Compton nature of the hard X-ray spectrum.

Conclusions. A further multifrequency monitoring effort is needed to follow the next phases of this unprecedented event.

Key words. galaxies: active – galaxies: quasars: general – galaxies: quasars: individual: 3C 454.3 – galaxies: jets

1. Introduction

The flat-spectrum and highly polarized radio quasar 3C 454.3 at $z = 0.859$ belongs to the blazar class of active galactic nuclei. The dominant non-thermal emission of blazars is ascribed to a plasma jet oriented at a small angle to the line of sight, so that the radiation is relativistically beamed. The broad-band spectral energy distribution (SED) of blazars shows two components: the lower-energy one is attributed to synchrotron radiation by relativistic electrons, while the higher-energy one is com-

Send offprint requests to: M. Villata

⋆ For questions regarding the availability of the data presented in this paper, please contact Massimo Villata (villata@to.astro.it).

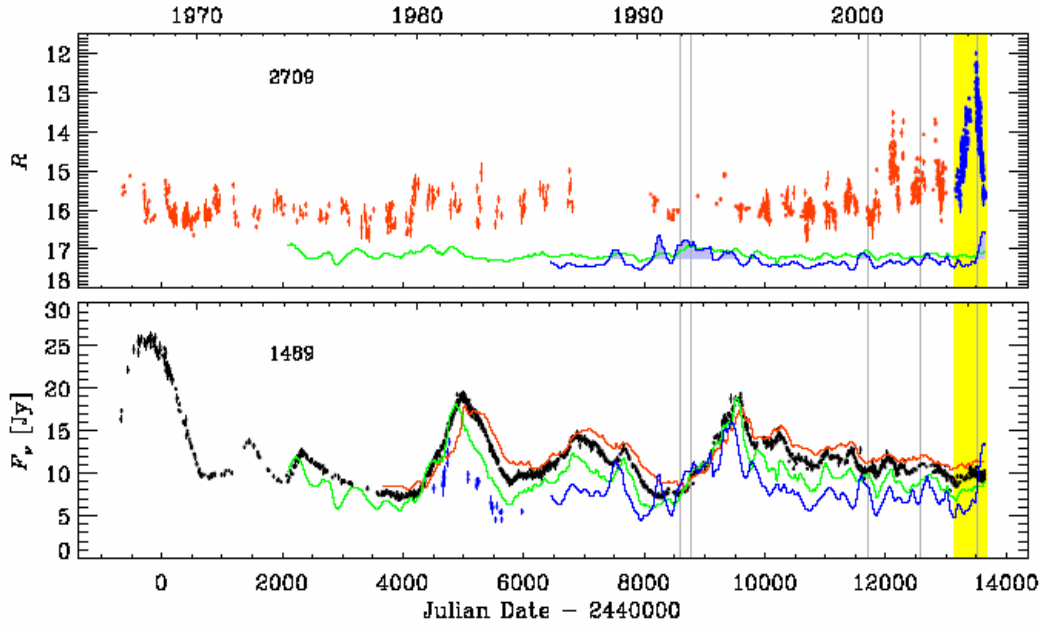

Fig. 1. Optical (top) and radio (bottom) light curves from 1966 to the end of September 2005; the yellow strip indicates the period of the 2004–2005 WEBT campaign, while grey vertical lines show the times of the satellite pointings (see Fig. 4). Bottom panel: black points indicate the 8 GHz light curve (1489 data points); red, green, and blue curves represent the cubic spline interpolations through the 30-day binned light curves at 5, 14.5, and 37 GHz, respectively; blue points are sparse 37 GHz data. Top panel: besides the R-band light curve (2709 data points), the radio hardness ratios $H_{37/8}$ (blue line) and $H_{14.5/8}$ (green line) are plotted as $18 - H$; the light blue shading highlights where $H_{37/8}$ is harder than average.

monly thought to be due to inverse-Compton scattering of soft photons by the same relativistic electrons. In addition to these two components, quasars can also show a "big blue bump" in the UV band, which is interpreted as the signature of the thermal disc feeding the supermassive black hole. This component is mostly visible when the synchrotron emission is faint (see e.g. Pian et al. 1999). One of the main features of blazars is their strong emission variability at all wavelengths, from the radio band to γ-ray energies, on time scales ranging from a few minutes to several years.

2. The WEBT campaign

The historical optical light curve of 3C 454.3 starts from $\sim$ 1900 and in the radio bands the source has been monitored since the 1960s. Figure 1 shows the optical (top) and radio (bottom) light curves over the last $\sim$ 40 years. The historical radio data are from the University of Michigan Radio Astronomy Observatory (UMRAO) and the Metsähovi Radio Observatory (Teräsranta et al. 2005, references therein, and unpublished data), while data from the Crimean (RT-22), MDSCC (PARTNeR), Medicina, Noto, and SAO RAS (RATAN-600) Observatories as well as data from the VLA/VLBA Polarization Calibration Database[1] contribute to the most recent part of the light curves. In the figure the radio data are represented as black points (8 GHz), red line (cubic spline through the 30-day binned 5 GHz data), green line (the same for 14.5 GHz), while blue points/spline indicate the 37 GHz fluxes (including also 36 GHz data). The radio light curves show prominent, long-lasting outbursts, with higher-frequency variations leading the lower-frequency ones, as typically found in many blazars.

On the other side, the optical light curve shows two very different phases. Until $\sim$ 2001.0 only moderate variability is observed, in the range $R \sim 15$–17 (an exception being the higher activity shown in $\sim$ 1940–1955, when R reached $\sim$ 14; see Angione 1968). From 2001 the amplitude of variations started to increase. On May 9.36, 2005 (at the start of the current observing season) the source was observed at $R = 12.0$[2], thus triggering a multifrequency campaign by the Whole Earth Blazar Telescope (WEBT)[3]. In order to have information on both the rising and decreasing phases of the outburst, data were collected from June 2004 to the end of September 2005. In total, 5584 $UBVRI$ observations from 18 telescopes[4]

[1] `http://www.vla.nrao.edu/astro/calib/polar/`.

[2] This outburst peak should represent the most luminous quasar state ever observed: $M_B \sim -31.4$ ($H_0 = 70$ km s^{-1} Mpc^{-1}, $\Omega_M = 0.3$, $\Omega_\Lambda = 0.7$), comparable only with the 3C 279 outburst of 1937 ($M_B \sim -31.2$). For comparison, the bright but nearby quasar 3C 273 has "only" $M_B \sim -26.4$, while the most luminous quasars of the SDSS and of the $z > 4$ sample of Vignali et al. (2003) reach $M_B \sim -29.1$ and $M_B \sim -30.2$, respectively.

[3] `http://www.to.astro.it/blazars/webt/`; see e.g. Villata et al. (2004b); Raiteri et al. (2005).

[4] Kyoto, Osaka Kyoiku, Lulin, Mt. Maidanak, Abastumani, Crimean, MonteBoo, Catania, Armenzano, Michael Adrian, Torino, Sabadell, Teide (BRT), Roque de los Muchachos (KVA

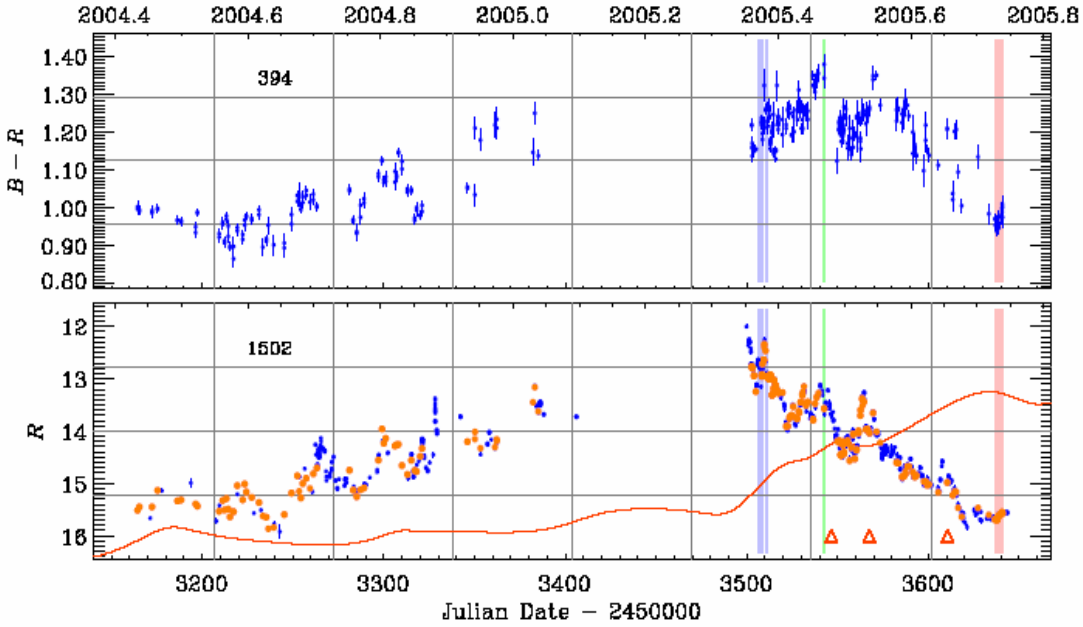

Fig. 2. Time evolution of the $B-R$ colour index (top) during the WEBT campaign compared with the R-band light curve (bottom); orange points in the light curve highlight the R data used to derive the $B-R$ indices; the red curve is a cubic spline interpolation through the 43 GHz light curve, arbitrarily scaled to fit the figure; the light blue strips indicate the epochs of the INTEGRAL (left) and Chandra (right) pointings, while the light green and red ones refer to spectra shown in Fig. 4; the red triangles mark the VLBA epochs of Fig. 3.

were performed in this period; moreover, JHK data were taken at Campo Imperatore, Calar Alto, and Roque de los Muchachos (NOT). Radio data from 1 to 43 GHz were acquired at several antennas, mentioned above. In the top panel of Fig. 1 the R-band light curve from the WEBT campaign is displayed as blue dots (see also Fig. 2): it is composed of 1502 points. In particular, 1146 data were taken in 143.59 days, from May 9.36 to September 29.95, 2005, during the outburst decreasing phase, with a mean time separation of 3.0 hours, and only 4 gaps longer than 36 hours (2–4 days). Previous data are shown as red points; they come from literature (including the recent paper by Fuhrmann et al. 2006) as well as from some WEBT observatories. Here we present some results of this campaign; a more detailed study is deferred to a forthcoming paper.

By looking at Fig. 1 no evident correlation appears between the optical and radio events. In particular, a low radio state characterizes the 2004–2005 optical outburst as well as the previous optical activity, while the past strong radio outbursts do not show any optical counterpart. Even the hardness ratio between the 37 GHz and 8 GHz splines ($H_{37/8} = F_{37}/F_8$, plotted in the top panel as $18 - H_{37/8}$, blue line) does not show correlation with the optical, as instead found by Villata et al. (2004a) for BL Lac. Only during the WEBT campaign one can see a correlation: a fast rise of $H_{37/8}$ to its maximum value (1.43), delayed by several months with respect to the rise of the optical outburst. This growth of $H_{37/8}$ is essentially due to the increase of the 37 GHz flux visible in the bottom panel. The 43 GHz light curve, not plotted there (but in Fig. 2, see below), strictly confirms this trend. In the top panel $H_{14.5/8}$ is also plotted (green line) for comparison. In general, its trend mimics fairly well that of $H_{37/8}$, with some delay and reduced variability amplitude. In particular, just a slight increase can be seen in 2005. The 22 GHz flux and the corresponding $H_{22/8}$ display an intermediate trend, as expected. In conclusion, the general lack of correlation between the radio and optical behaviour suggests that the corresponding emitting parts of the jet are misaligned. It seems that before 2001 the radio part was more aligned with the line of sight and the radio variability was thus enhanced by Doppler effects. On the contrary, in the last 5 years the optical radiation would dominate the scenario due to a smaller viewing angle of the corresponding emitting region. Thus the flux increase we are seeing at the high radio frequencies should be produced close to the optical region. The outburst will probably propagate further out, towards lower-frequency emitting regions. However, we cannot foresee whether it will be visible, since this depends on the jet curvature. A confirmation of the above general picture comes from the source behaviour in the mm bands, where a strong outburst was observed to peak in June–July 2005 (Krichbaum & Ungerechts, private communication).

The time evolution of the $B-R$ colour index during the optical outburst is shown in Fig. 2 (top panel), compared with the R-band light curve (bottom panel). Orange dots in the latter panel highlight the R-band points used to derive the $B-R$ colour indices. In general, a "redder

and Liverpool), Foggy Bottom, Kitt Peak (MDM), and San Pedro Martir Observatories.

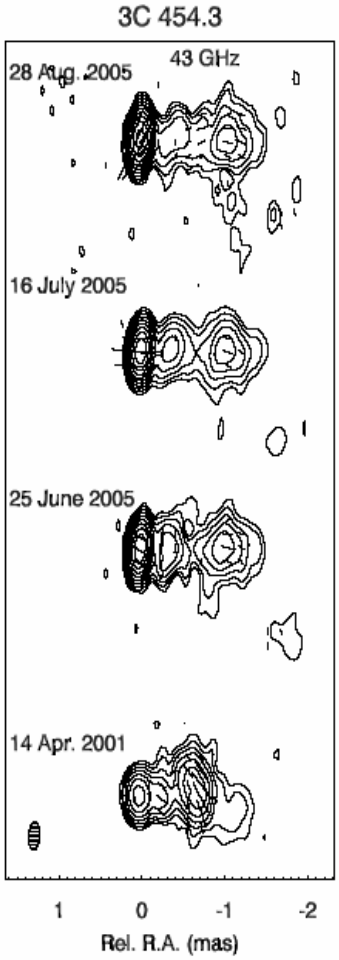

Fig. 3. VLBA maps at 43 GHz.

when brighter" trend can be recognized. Since 3C 454.3 is a quasar, this can be interpreted as due to the contribution given by the thermal emission from the accretion disc, which mainly affects the bluer region of the optical spectrum. However, there seems to be a kind of "saturation" effect in the $B-R$ trend: in the brightest part of the outburst ($R \lesssim 14$) the trend is not visible any more. Most likely, this is due to the dominance of the non-thermal jet emission, which would display its usual "bluer when brighter" behaviour, thus balancing the opposite trend.

The 43 GHz flux-density spline is shown in the bottom panel for comparison, arbitrarily scaled to fit the figure (the range is $\sim$ 4–13 Jy). It peaks in September 2005, i.e. 2–3 months after the mm outburst, which seems to have a similar delay with respect to the optical event.

3. VLBA observations

Figure 3 shows three recent VLBA maps at 43 GHz compared with an older map dated April 2001[5]. The plot is constructed with both total and polarized intensity, normalized to the peak values achieved at epoch August 2005 ($S_{\rm tot} = 9.62$ Jy/beam, $S_{\rm pol} = 0.162$ Jy/beam). The total intensity is shown by contours from 0.15% up to 76.8% of the August 2005 peak value, increasing by a factor of 2. The sticks show the electric vector and their length is proportional to the local polarized intensity. There is a significant increase in both total and polarized intensity of the VLBI core compared with the values in April 2001 (see also Table 1), thus confirming the expectation that the 43 GHz rising flux in 2005 seen in Fig. 2 come from the VLBI core. The three VLBA epochs are indicated in Fig. 2 as red triangles. Since the VLBI core of 3C 454.3 at 43 GHz used to have very low polarization compared to the western feature at 0.7 mas from the core, a strong increase of the core polarization along with the total flux suggests a new component emerging from the core. However, as discussed in the previous section, the emerging feature will be more or less visible depending on the jet bending.

[5] Multiepoch and multifrequency VLBA monitoring of 3C 454.3 (with polarization) was performed between May and December 2005 (Savolainen et al., in preparation).

Table 1. Results of VLBA observations of 3C 454.3 at 43 GHz.

Epoch	Total Int. (mJy)	Polarized Int. (mJy)
April 14, 2001	1710	15
June 25, 2005	6560	74
July 16, 2005	6290	103
August 28, 2005	10200	200

4. Chandra observation

3C 454.3 was observed by Chandra on May 19.7–21.0, 2005 with the HRC-LETG instrumental configuration. The Chandra pointing was performed as part of a ToO program on blazars in outburst, and lasted 112 ks. We used version 3.3 of the CIAO software to reduce and analyse the data. We extracted source and background spectra from the standard HRC-LETG *bow-tie* regions, and then grouped the source spectrum to contain at least 20 counts per channel. We used the fitting-package `Sherpa` to fit the background-subtracted source spectrum in the range $\sim$ 0.2–8 keV. Here we report the result of the continuum spectral analysis, while the study of narrow absorption features due to possible intervening Warm-Hot Intergalactic Medium filaments is deferred to a forthcoming paper (Nicastro et al., in preparation). The 0.2–8 keV spectrum is well described (χ^2/d.o.f. = 1817/2368) by a rather flat power law, with photon index $\Gamma = 1.477 \pm 0.017$, absorbed by a large column density $N_{\rm H} = (13.40 \pm 0.05) \times 10^{21}$ cm^{-2}, exceeding by more than a factor of 2 the Galactic value. We measured de-absorbed fluxes of $F_{0.2-2} = (5.5 \pm 0.2) \times 10^{-11}$ erg cm^{-2} s^{-1} and $F_{2-8} = (8.4 \pm 0.2) \times 10^{-11}$ erg cm^{-2} s^{-1}.

5. Spectral energy distribution and conclusions

In Fig. 4 we show the broad-band SED of the source. The small black crosses in the radio–optical range indicate

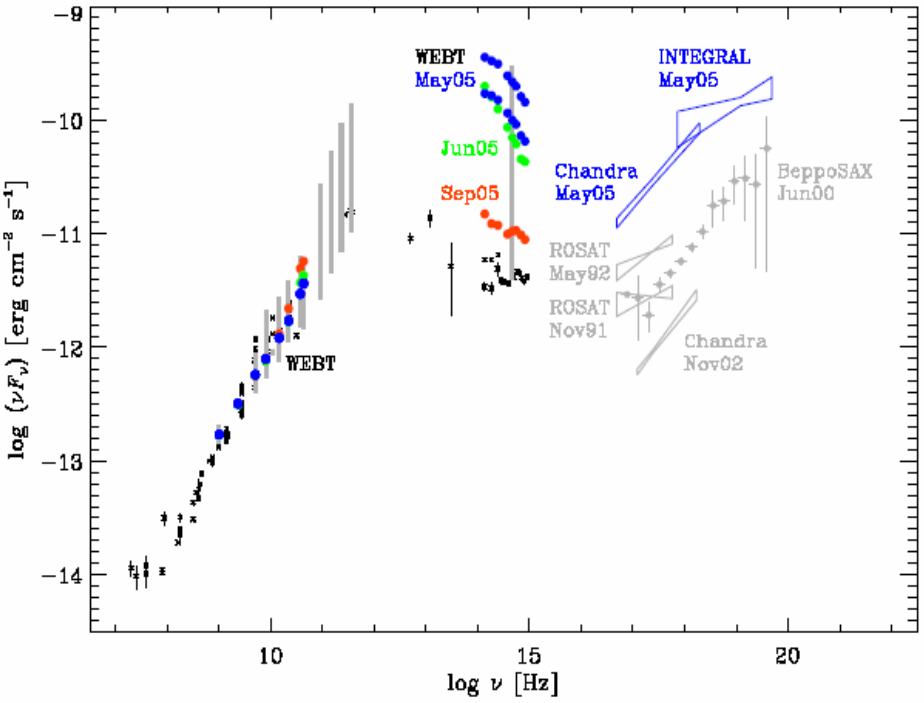

Fig. 4. Spectral energy distribution of 3C 454.3 showing contemporaneous radio, near-IR, optical, and X-ray (Chandra and INTEGRAL) data during May 15–20, 2005. Previous data are also plotted for comparison, together with two other spectra from the WEBT campaign.

archival data taken from NED. In the X-ray band we plotted data from old observations by ROSAT in November 1991 (Sambruna 1997) and in May 1992 (Prieto 1996), as well as data from a BeppoSAX observation in June 2000[6], and data from a pile-up affected Chandra observation in November 2002 (Marshall et al. 2005).

During the brightest phases of the optical outburst, in May 2005, there were other observations by high-energy satellites (RXTE, Swift, INTEGRAL) besides the Chandra one presented in the previous section. The ToO INTEGRAL observation was performed on May 15.8–18.4. In Fig. 4 we show the corresponding 3–200 keV spectrum (Pian et al., submitted to A&A). The Chandra spectrum of May 19.7–21.0 is also plotted, together with radio, near-IR, and optical data from the WEBT in the period of the two pointings (blue symbols). Since in this period the optical brightness varied by $\Delta R = 0.9$, we plot two $UBVRIJHK$ spectra representative of a high and a low state. No significant variation in the spectral slope is seen between the two states, despite their different brightness levels, in agreement with the rather stable colour index found in this period (see Fig. 2, light blue strips). The contemporaneous radio data follow a power law from 1 to 22 GHz, which then breaks due to the just started rise of the 37 and 43 GHz fluxes (see Figs. 1 and 2). The grey vertical strips in Fig. 4 show the historical variation range of the radio and R-band data collected for this paper (and partly displayed in Figs. 1 and 2). For the mm bands an arbitrary range from 3 to 30–40 Jy has been adopted, to mimic the strong recent outburst. One month after the May satellite pointings, around June 21.0, the reddest observed optical state is achieved (light green line in Fig. 2). The corresponding near-IR–optical spectrum is displayed in Fig. 4 with green symbols: it is indeed very steep, crossing the lower May spectrum around the H band, and probably going to connect with the highest parts of the mm strips, since we should be close to the mm outburst peak. Also the 37–43 GHz flux has increased (see also Figs. 1 and 2), while no appreciable variation is seen at lower frequencies. In late September, at the foot of the outburst, the bluest optical state of 2005 is found (light red strip in Fig. 2). The corresponding (red) spectrum in Fig. 4 is the average on 5 days (September 23.0–28.0) of intensive $UBVRIJHK$ monitoring: the thermal component seems to strongly affect the spectrum. At this time also the 22 GHz flux starts to increase and the radio spectral break shifts down, while the top of the outburst is achieved at 37–43 GHz (see also Figs. 1 and 2).

The main feature of the plotted SEDs is the strong variability of the optical–IR (and mm) and X-ray fluxes. In Fig. 1 vertical grey lines indicate the times of the X-ray pointings. The X-ray flux seems to correlate neither with radio flux (always rather low), nor with the optical level (in 2002 it was brighter than during the previous pointings, but the X-ray flux was lower), nor with the radio hardness (higher during the ROSAT pointings and intermediate during the others). It seems instead to correlate with the mm flux, since a big mm outburst was close to its peak during the May X-ray observations. This is expected, due to the probable inverse-Compton nature of the hard X-ray spectrum.

In conclusion, this unprecedented quasar optical outburst led an as well unprecedented mm outburst (accompanied by an exceptionally bright X-ray state) by 2–3 months, and, 2–3 months later, it has fully propagated also to the high radio frequencies. All this has been hap-

[6] http://www.asdc.asi.it/bepposax/.

pening in the VLBI radio core. We cannot foresee whether and when further propagation will be visible at lower frequencies and outside the radio core, due to a probable jet bending. In any case, a further multifrequency monitoring effort is needed to follow the next phases of this exceptional event.

Acknowledgements. This research has made use of the NASA/IPAC Extragalactic Database (NED), which is operated by the Jet Propulsion Laboratory, California Institute of Technology, under contract with the National Aeronautics and Space Administration. This work was partly supported by the European Community's Human Potential Programme under contract HPRN-CT-2002-00321 (ENIGMA). St. Petersburg team acknowledges support from Russian Federal Program for Basic Research under grant 05-02-17562.

References

Angione, R. J. 1968, PASP, 80, 339
Fuhrmann, L., Cucchiara, A., Marchili, N., et al. 2006, A&A, 445, L1
Marshall, H. L., Schwartz, D. A., Lovell, J. E. J., et al. 2005, ApJS, 156, 13
Pian, E., Urry, C. M., Maraschi, L., et al. 1999, ApJ, 521, 112
Prieto, M. A. 1996, MNRAS, 282, 421
Raiteri, C. M., Villata, M., Ibrahimov, M. A., et al. 2005, A&A, 438, 39
Sambruna, R. M. 1997, ApJ, 487, 536
Teräsranta, H., Wiren, S., Koivisto, P., Saarinen, V., & Hovatta, T. 2005, A&A, 440, 409
Vignali, C., Brandt, W. N., Schneider, D. P., Garmire, G. P., & Kaspi, S. 2003, AJ, 125, 418
Villata, M., Raiteri, C. M., Aller, H. D., et al. 2004a, A&A, 424, 497
Villata, M., Raiteri, C. M., Kurtanidze, O. M., et al. 2004b, A&A, 421, 103

List of Objects

Photometric Observations of Asteroids with Comet-Like Orbit at Lulin Observatory

Kinoshita Daisuke[1], Lin Hung-Chin[1], Ohtsuka Katsuhito[2], Sekiguchi Tomohiko[3], Watanabe Jun-ichi[3], Ito Takashi[3], Arakida Hideyoshi[3], Kasuga Toshihiro[3], Miyasaka Seidai[4]

[1] Institute of Astronomy, National Central University, 300, Jhongda Rd., Jhongli, Taoyuan, 32001, Taiwan
[2] Tokyo Meteor Network, 1-27-5 Daisawa, Setagaya, Tokyo, 155-0032, Japan
[3] National Astronomical Observatory of Japan, 2-21-1 Osawa, Mitaka, Tokyo, 181-8588, Japan
[4] Tokyo Metropolitan Government, 2-8-1 Nishi-Shinjuku, Shinjuku, Tokyo, 163-8001, Japan
E-mail(KD): kinoshita@astro.ncu.edu.tw

ABSTRACT

We carried out photometric observations of asteroids with comet-like orbit. These asteroids are thought to be dormant comet, and provide opportunity to reveal properties of bare cometary nuclei which are difficult to be observed by comae contamination due to the cometary activities. A near-Earth asteroid 2005 UD was discovered by Catalina Sky Survey in October 2005. Orbital parameters of this asteroid is similar to those of (3200) Phaethon. (3200) Phaethon has comet-like orbit, and thought to be a parent body of meteor shower. Orbital similarity of these asteroids may suggest that 2005 UD is a fragment of (3200) Phaethon. To test this hypothesis, we carried out photometric observations of 2005 UD. Results of multi-color photometry shows bluish surface of 2005 UD which is consistent with the surface of (3200) Phaethon. We also report the lightcurve of 2005 UD.

1. Introduction

The Apollo-type near-Earth asteroid (3200) Phaethon (= 1983 TB) was discovered by the InfraRed Astronomical Satellite (IRAS) in October 1983 (Green & Kowal 1983). Although, the appearance of (3200) Phaethon is asteroidal, the orbit is highly eccentric as $e = 0.89$ like those of comets. In addition, (3200) Phaethon is thought to be the parent body of Geminid meteor stream (Whipple 1983, Gustafson 1989, Williams & Wu 1993). (3200) Phaethon is likely a dormant cometary nucleus which cometary activity is sporadic or an extinct cometary nucleus which activity is no more seen. Many attempts are made to detect faint coma of this object (Cochran & Barker 1984, Chamberlin et al. 1996, Hsieh & Jewitt 2005). No cometary activity is observed.

On 22 October 2005, an Apollo-type near-Earth asteroid was discovered by Catalina Sky Survey, and the temporal designation of 2005 UD was given to this object (McNaught et al. 2005). Ohtsuka et al. (2005) suggested 2005 UD is likely a parent body of the daytime Sextantids meteor stream based on the orbital similarity. Furthermore, they pointed out the possibility that 2005 UD is a member of Geminid stream complex and a fragment of (3200) Phaethon. Ohtsuka et al. (2006) performed numerical integrations of (3200) Phaethon and 2005 UD both forward and backward using Kustaanheimo-Stiefel regularized equation of motion (Arakida & Fukushima 2000, Arakida & Fukushima 2001). Results of the numerical integrations shows similar behaviors between orbital evolutions of (3200) Phaethon and 2005 UD with the shift of about 4,600 years. This supports the idea that 2005 UD is a km-sized fragment of (3200) Phaethon.

We have carried out the observational studies of the Apollo-type near-Earth asteroid 2005 UD. The aim of our observations is to check the hypothesis that 2005 UD is a fragment of (3200) Phaethon which is supported by dynamical study. We briefly introduce our observations in Section 2, give the data analysis procedures and report results of the observations in Section 3, and summarize in Section 4.

2. Observation

The photometric observations of 2005 UD was carried out at Lulin Observatory of the Institute of Astronomy, National Central University in Taiwan. The Lulin Observatory is located at the peak of Mount Lulin ($120°52'25''$E, $23°28'7''$N, $H = 2862$-m) at the central region of Taiwan. We used 1-m telescope (F/8) and a CCD camera to obtain imaging data. The pixel scale of this system is 0.516 arcsec per pixel, and this is spatially well sampled under the typical seeing size of FWHM $\sim$ 1.5 arcsec. The resultant field-of-view is 11.5×11.2 arcmin. The details of the instrument is reported by Kinoshita et al. (2005).

The data was acquired on six nights from 31 October to 5 November 2005. At the time of observations,

the heliocentric distance of the object ranged from 1.36 to 1.42 AU, and the geocentric distance of the object ranged from 0.51 to 0.62 AU. Non-sidereal tracking was used for imaging of 2005 UD. We used BVRI filters to measure the surface colors of 2005 UD. To avoid the rotational effect, observations were done in the R-B-R-V-R-I-R sequence. This sequence of observation secures at least the rotational lightcurve when the sky condition is unstable. The exposure time was set to 180 sec for R-band, and 300 sec for other bands. When the sky is photometric, standards from the list provided by Landolt (1992) and observed along the night. Photometric standard stars are carefully selected to cover wide ranges of airmass and colors for accurate correction of atmospheric and instrumental signatures.

3. Analysis and Results

The dark subtracting and flatfielding were applied in the standard manner using image analysis software package NOAO IRAF. Then, plate constants were refined by WCSTools (Mink 2002) for astrometric measurements. Refined orbital elements were calculated by Nakano (2005) including our measurements. Those elements are reported by Otsuka et al. (2006).

The differential photometry was performed using R-band images. We applied Lomb's algorithm (Press et al. 1992) to relative magnitudes of 2005 UD to extract the periodicity. The Lomb periodogram os 2005 UD is shown in Figure 1. The periodogram exhibits the maximum at the period of 2.615 hour. Figure 2 is the phase curve assuming the periodicity of 2.615 hour. Considering the lightcurve is due to the irregular shape of the asteroid, the double of the obtained periodicity 5.230 hour is the actual rotational period. The lower limit of the axis ratio is calculated from the amplitude of the lightcurve, if we assume the variability comes from elongated shape of the object. The amplitude of the lightcurve is 0.42 mag which imply the lower limit of axis ratio of $10^{0.4\Delta m} \sim 1.5$.

The multi-color photometry was performed. The transformation coefficients were estimated using the "photcal" package of NOAO IRAF. We defined transformation equatons as

$$B_{std} = B_{inst} + Z_B - k'_B X + C_B(B-V), \quad (1)$$
$$V_{std} = V_{inst} + Z_V - k'_V X + C_V(B-V), \quad (2)$$
$$R_{std} = R_{inst} + Z_R - k'_R X + C_R(V-R), \quad (3)$$
$$I_{std} = I_{inst} + Z_I - k'_I X + C_I(V-I), \quad (4)$$

where $B_{std}, V_{std}, R_{std}, I_{std}$ are the standard magnitudes, B_{inst}, V_{inst}, R_{inst}, I_{inst} are the instrumental magnitudes, Z_B, Z_V, Z_R, Z_I are zero point magnitudes, k'_B, k'_V, k'_R, k'_I are the first-order extinction coefficients, C_B, C_V, C_R, C_I are the color terms, and X is the airmass. The second-order extinction coefficients are found to be small from our previous observations, and are neglected for this study. Obtained transformation coefficients are summarized in Table 1. The surface colors of 2005 UD are $B-V = 0.78 \pm 0.04$ and $V-R = 0.35 \pm 0.03$. These values are plotted in Figure 3 as well as typical colors of major subclasses of asteroids. (3200) Phaethon is known to be B-type asteroid which exhibits bluish surface color. Previous measurement of $B-V = 0.34$ is reporeted for (3200) Phaethon (Skiff et al. 1996). Our measurements of colors of 2005 UD are in good agreement with color of (3200) Phaethon.

Table 1. The transformation coefficients on 3, 4, 5 November 2005 are summarized.

	03/Nov/2005	04/Nov/2005	05/Nov/2005
Z_B	$+22.77 \pm 0.03$	22.85 ± 0.01	22.83 ± 0.01
k_B	0.15 ± 0.02	0.18 ± 0.01	0.17 ± 0.01
C_B	$+0.12 \pm 0.01$	$+0.15 \pm 0.01$	$+0.14 \pm 0.01$
Z_V	$+23.08 \pm 0.03$	23.14 ± 0.01	23.11 ± 0.01
k_V	0.08 ± 0.02	0.10 ± 0.01	0.09 ± 0.01
C_V	-0.09 ± 0.01	-0.07 ± 0.01	-0.06 ± 0.01
Z_R	$+23.04 \pm 0.03$	23.09 ± 0.01	23.05 ± 0.01
k_R	0.06 ± 0.02	0.07 ± 0.01	0.08 ± 0.01
C_R	-0.13 ± 0.02	-0.11 ± 0.01	-0.08 ± 0.01
Z_I	$+22.37 \pm 0.03$	22.38 ± 0.01	22.36 ± 0.02
k_I	0.05 ± 0.02	0.04 ± 0.01	0.03 ± 0.01
C_I	$+0.02 \pm 0.01$	$+0.04 \pm 0.01$	$+0.04 \pm 0.01$

4. Summary

2005 UD is suggested to be associated with daytime Sextandid meteor stream and to be a fragment of (3200) Phaethon. We performed photometric observations of 2005 UD using 1-m telescope at Lulin Observatory in Taiwan to test this hypothesis. Results of multi-color photometry showed bluish surface of 2005 UD which is consistent with (3200) Phaethon, and support the hypothesis that 2005 UD is a km-sized fragment of (3200) Phaethon. The time-resolved photometry in R-band showed rotational period of 5.230 hour. The lower limit of the axis ratio $a/b \sim 1.5$ is estimated from the amplitude of the lightcurve.

Acknowledgement

We would like to express our hearty thanks to Mr. Shih Jun-Shiung, Mr. Du Jing-Chuan, Mr. Shih Hao-Wei, and Mr. Wan Zong-Jing for their local supports at Lulin Observatory. One of the author (KD) thanks to the fellowship from the Japan Society for Promotion of Science (ID: 15-1-2-02681-1) which gives partial support for this study.

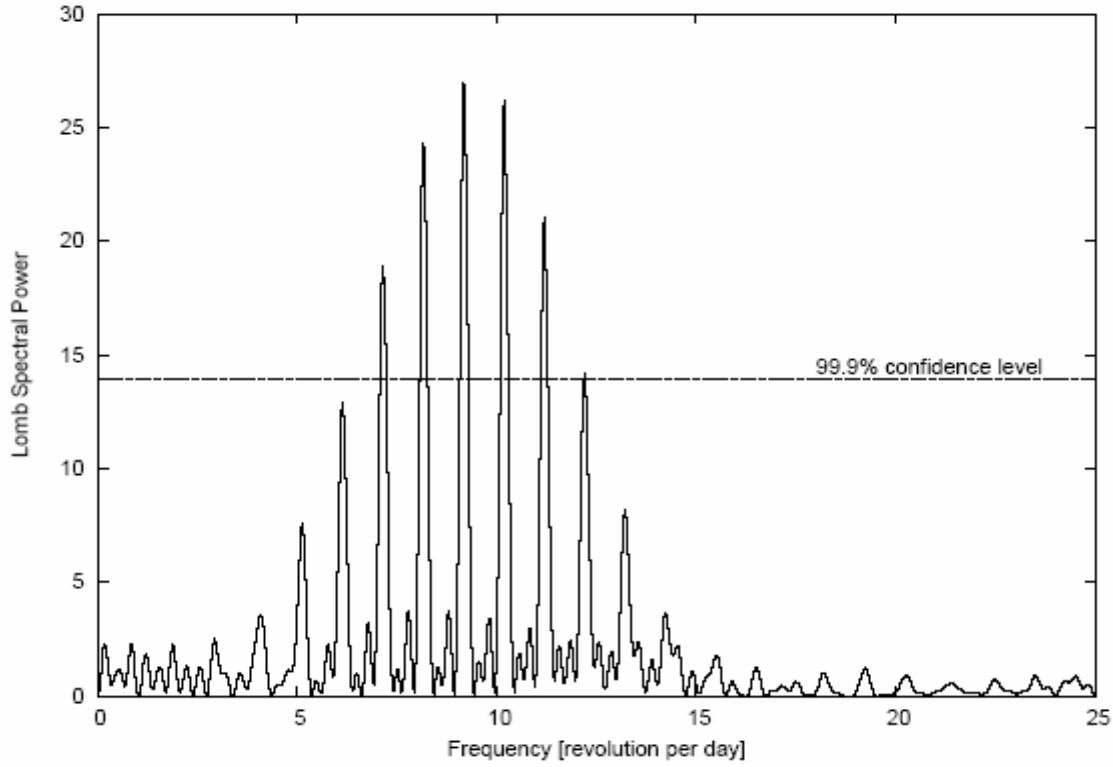

Fig. 1. The Lomb periodogram of 2005 UD is shown.

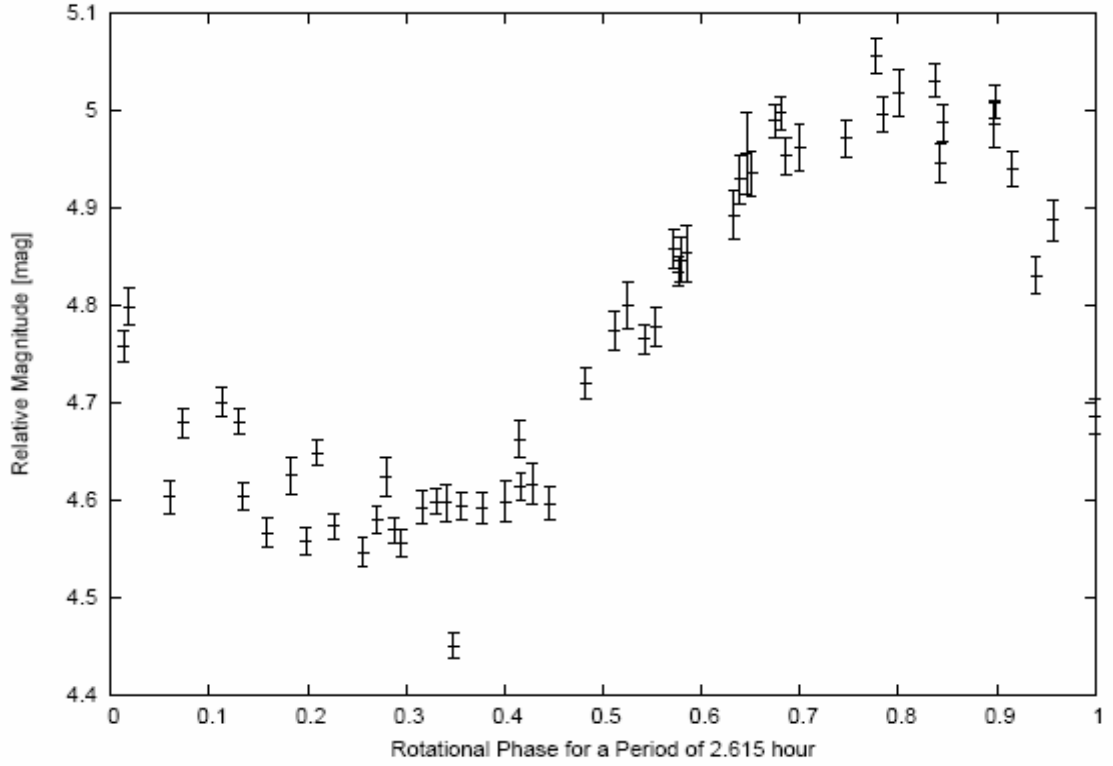

Fig. 2. The rotational phase curve of 2005 UD assuming periodicity of 2.615 hour is shown.

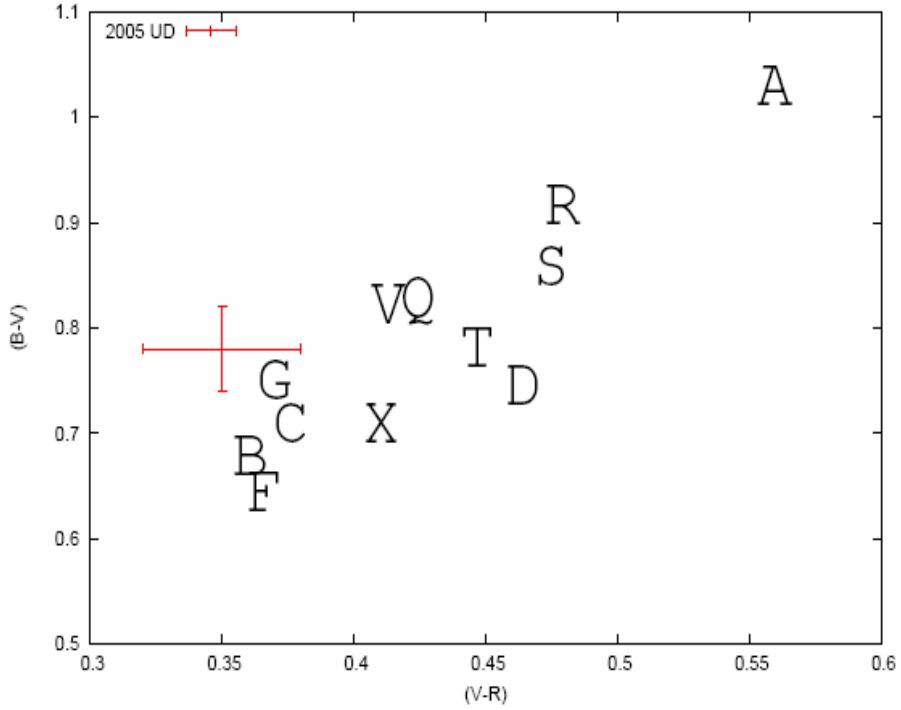

Fig. 3. The (B-V) and (V-R) colors of 2005 UD is plotted as well as subclasses of asteroids. Capital letters in the figure denote typical colors of major subclasses of asteroids.

References

Arakida, H., Fukushima, T., 2000, AJ, 120, 3333.

Arakida, H., Fukushima, T., 2001, AJ, 121, 1764.

Chamberlin, A. B., McFadden, L.-A., Schulz, R., Schleicher, D. G., Bus, S. J., Icarus, 119, 173.

Cochran, A. L., Berker, E. S., 1984, Icarus, 59, 296.

Green, S., Kowal, C., 1983, IAU Circular, 3878.

Gustafson, B. A. S., 1989, A&Ap, 225, 533.

Hsieh, H. H., Jewitt, D., 2005, ApJ, 624, 1093.

Kinoshita, D., Chen, C.-W., Lin, H.-C., Lin, Z.-Y., Huang, K.-Y., Chang, Y.-S., Chen, W.-P., 2005, ChJAA, 5, 315.

McNaught, R. H., McGaha, J. E., Young, J., Christensen, E. J., Beshore, E. C., Garradd, G. J., Grauer, A. D., Hill, R. E., Kowalski, R. A., Larson, S. M., Tibbets, D., Hug, G., Hutsebaut, R., Jacques, C., Pimentel, E., Miles, R., Birtwhistle, P., Marsden, B. G., Minor Planet Electronic Circ., 2005-U22.

Mink, D. J., 2002, Proceedings of *Astronomical Data Analysis Software and Systems XI*, ASP Conference Proceedings, Vol. 281. Edited by Bohlender, D. A., Durand, D., and Handley, T. H., ISBN: 1-58381-124-9, pp. 169.

Ohtsuka, K., Sekiguchi, T., Kinoshita, D., Watanabe, J., 2005, Central Bureau Electronic Telegrams, 283.

Ohtsuka, K., Sekiguchi, T., Kinoshita, D., Watanabe, J., Ito, T., Arakida, H., Kasuga, T., 2006, submitted to A&Ap.

Nakano, S., 2005, `http://www.oaa.gr.jp/~muramatu/mp/2005ud.htm`

Press, W., Flannery, B. P., Teukolsky, S. A., Vetterling, W. T., 1992, *"Numerical Recipes in C: The Art of Scientific Computing"*, Cambridge University Press, ISBN 0521431085.

Skiff, B. A., Buie, M. W., Bowell, E., 1996, American Astronomical Society, DPS meeting No. 28, Bulletin of the American Astronomical Society, Vol. 28, p.1104

Whipple, F. L., 1983, IAU Circular, 3881.

Williams, I. P., Wu, Z., 1993, MNRAS, 262, 231.

Photo-polarimetry of unusual asteroid 1992 UY4 with LOT+PICO

Yusuke Sato (Hokkaido Univ.), Daisuke Kinoshita (NCU),
Hiroyuki Maehara (Univ. of Tokyo) Naoyuki Awajiya, (Tokyo Gakugei Univ.)
Reiko Furusho (Waseda Univ.), Hideyo Kawakita,(Kyoto Sangyo Univ.)
and Munetaka Ueno,(Univ. of Tokyo),

Introduction

Asteroids are considered primordial bodies in the solar system.

We know classify asteroids into several taxonomic types for considering their matter, If we know some value of asteroids from observations.

We often search their color, albedo, Polarization, light curve, and spectrums etc.

Especially, if we can get linear polarization degree variation with phase angle from photopolarimetric observation, we can decide asteroid's albedo, size and type. Those information are very important things for understanding asteroids.

Therefore, we want to observe many asteroids to study for the solar system formation. But, so far, we understood relatively larger asteroids.

However, small asteroids (a few kilometers or below in diameter) are not understood well now. We think that we need to study about small asteroids for understanding the solar system very well.

Observation

We observed asteroid 1992 UY4 with LOT + PICO (Polarimetric Imager for Comet [Ikeda et al. submitting])+AP8 CCD at Lulin observatory, from 31 July 2005 to 3 August 2005. It was close to the Earth last early August.

This asteroid's phase angle (Sun-asteroid-Earth angle) varies so large during short time and it's very useful for determining such asteroid's physical parameters. Its V-band magnitude was 12.3 at that time.

We used i-band filter and we observed several polarimetric standard stars. We used non-sidereal tracking.

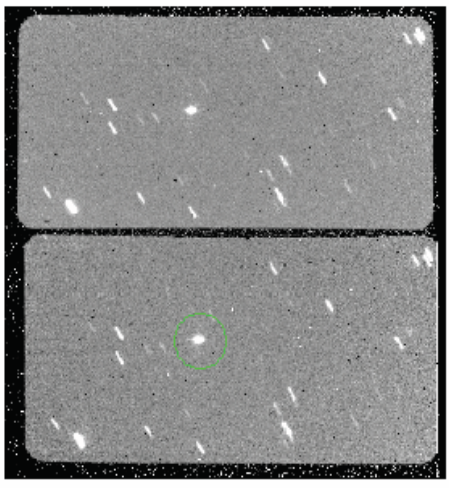

Fig1. This is PICO + AP8 CCD image. Asteroid was center of circle.

Data reduction

Data reduction is accomplished through initial processing to photometry with IRAF. We used APPHOT package. That aperture parameter is 4, annulus is 8, dannulus is 10. And we used our polarimetric degree calculator that we refer Kawabata et al. (1999).

Results

We obtained polarization degree varies from -0.65% to -0.46% , when phaseangle varies from 6.5 degree to 12.8degree during our observations.

Discuss and conclusions

We succeed to observe asteroid LOT + PICO + AP8.

According to our results, we do not consider the object to be M-Type and C-type. We show right figure, our results plotted near zero point at that phase angle. Our results suggest that the asteroid is S-type or V-type. If the asteroid is S-type, It is appropriate that main belt S-type asteroids are inner belt more than all of main belt.

We think that analyze other results of 1992UY4, (light curve, polarization curve, etc) we can obtain varied things.

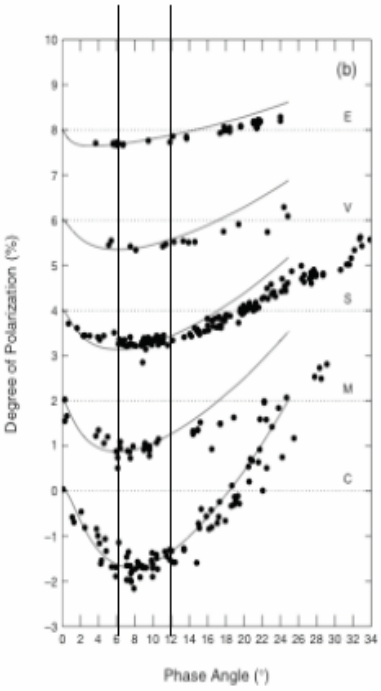

Fig.2 General value of asteroids' Phaseangle vs. polarization degree Muinonen et al. 2003

Acknowledgments

This work is supported by National central Univ. Lulin Observatory and NCU members. Especially, We thank Hung-Chin Lin for his great helpful action while observing this object.

References

B. Zellner and J. Gradie (1976) minor planets and related objects. XX Polarrimetric evidence for the albedos and compositions of 94 asteroids AJ 81 262

- K. Muinonen et al. (2003), Asteroid Photometric and Polarimetric Phase Effects Asteroids III Arizona press

- K. kawabata et al. (1999) A new spectropolarimeter at the Dodaira observatory PASP 111, 898.

A&A 438, L13–L16 (2005)
DOI: 10.1051/0004-6361:200500118

Astronomy & Astrophysics

The cool Galactic R Coronae Borealis variable DY Persei

L. Začs[1], W. P. Chen[2], O. Alksnis[1], D. Kinoshita[2], F. A. Musaev[3,4,5], T. Brice[6], K. Sanchawala[2], H. T. Lee[2], and C. W. Chen[2]

[1] Institute of Atomic Physics and Spectroscopy, University of Latvia, Raiņa bulvāris 19, 1586 Rīga, Latvia
e-mail: zacs@latnet.lv
[2] Graduate Institute of Astronomy, National Central University, Chung-Li 32054, ROC, Taiwan
e-mail: wchen@astro.ncu.edu.tw
[3] Special Astrophysical Observatory and Isaac Newton Institute of Chile, SAO Branch, Nizhnij Arkhyz 369167, Russia
e-mail: faig@sao.ru
[4] ICAMER, National Academy of Sciences of Ukraine, 361605 Peak Terskol, Kabardino-Balkaria, Russia
[5] Shamakhy Astrophysical Observatory, National Academy of Sciences of Azerbaijan, Azerbaijan
[6] 1.State Gimnazium of Riga, Raiņa bulvāris 8, 1050 Rīga, Latvia
e-mail: tamara@r1g.edu.lv

Received 1 March 2005 / Accepted 28 April 2005

Abstract. Results of first CCD photometry during the recent deep light decline, and high-resolution spectroscopy, are presented for DY Persei. The spectra show variable blueshifted features in the sodium D lines. The C I lines are strong whereas neutron-capture elements are not enhanced. The isotopic ^{13}CN(2, 0) lines relative to ^{12}CN are of similar strength with those for the carbon star U Hya. All these confirm the RCB nature of DY Per and the existence of ejected clouds. At least two clouds are revealed at −197.3 and −143.0 km s^{-1}. A star was detected about 0.″4 to the west and 2.″5 to the north from DY Per. This anonymous companion, with observed colour indices $(B-V) = 0.68$ and $(V-R) \simeq 1.1$, may be a foreground star.

Key words. stars: carbon – stars: winds, outflows – stars: fundamental parameters – stars: circumstellar matter – stars: individual: DY Per

1. Introduction

The prototype of R Coronae Borealis (RCB) stars was observed for the first time more than 200 years ago. However, after two centuries of investigations many aspects of the R CrB phenomenon remain mysterious (for a general review, see Clayton 1996). The atmospheres of RCB stars are extremely hydrogen-deficient but rich in carbon and nitrogen (Asplund et al. 2000, and references therein). RCBs seem to be of low mass yet high luminosity. At irregular intervals they manufacture thick dust clouds which can completely obscure the photosphere of the star. During these dust formation episodes the brightness of the star can decrease by 5 to 8 mag in a few weeks and characteristic emission lines are seen in the spectrum. Recently several bright, very large circumstellar dust clouds were detected in RCB variable RY Sgr (de Laverny & Mékarnia 2004). These enigmatic stars seem to be born-again giants, formed either through a final He-shell flash in post-AGB stars or through a merger of two white dwarfs. No RCB star is known to be a binary.

DY Per (CGCS 372) was suspected to be an RCB star based on the photometry by Alksnis (1994). Subsequent photometric monitoring revealed a number of sudden light declines typical for RCB variables superimposed on the 792-day cycle of long-period light variations (Alksnis et al. 2002). However, the temperature of this star is much lower than average for other RCB stars. Moreover, the luminosity of DY Per was suspected to be lower than usually for RCBs. Keenan & Barnbaum (1997) estimated $T_{\rm eff} \simeq 3500$ K using the standard criteria of spectral classification and a giant luminosity. DY Per was classified as R8 (Hardorp et al. 1973), C 4,5 (Yamashita 1975), C 5,4p (Dean 1976) or C-Hd 4.5 C_2 6 (Keenan & Barnbaum 1997). Alcock et al. (2001) revealed four stars similar to the Galactic variable DY Per among eight RCBs discovered in the Large Magellanic Cloud (LMC). They found for RCBs in the LMC a range of absolute magnitudes M_V from −2.5 to −5 mag and a temperature – M_V relationship. The warm RCBs are brighter than the cool one. Therefore DY Per remains an intriguing object with unknown evolutionary status. Here we present the first results of CCD photometry during the recent deep light decline (see Alksnis 2004), and some results of high-resolution spectroscopy for this unique star.

2. Observations and data reduction

The imaging photometry of DY Per was taken with the Lulin 1-m telescope (LOT), equipped with a Princeton Instruments PI 1300B CCD camera. The f/8 optics of the telescope

gives 0.″516 per pixel and an FOV about 11′ on the focal plane. DY Per was monitored in the V band from early October 2004 through late January 2005, for which differential photometry is available. Typical seeing was about 2″. On several nights, in particular on 11 November 2004 for which the sky conditions were good, a complete set of $BVRI$ data were acquired and calibrations of standard stars and extinction were performed. Exposure times ranged from 20 s in the I and R bands, 90 s in the V band, to 300 s in the B band. The Landolt standards, SA92 #245, 248, 249, and 250, were used for flux calibration, with a typical internal photometric accuracy better than ~0.01 mag. Images were processed by standard procedures of bias and dark subtraction and flat fielding with the IRAF package.

High-resolution spectra for DY Per and the comparison star U Hya were obtained with the coudé échelle spectrometer MAESTRO fed by the 2 m telescope at the Observatory on the Terskol Peak in Northern Caucasus equipped with a CCD detector (Musaev et al. 1999) with a resolving power of ~45 000. A total exposure time of 7200 s was made for DY Per on 18 November 2002. The spectrum covered from 3600 to 10 200 Å in 85 wavelength bands overlapping shortward of H_α. Each region spanned from 50 to 140 Å. Because of the energy distribution in carbon stars the S/N ratio shortward of 4800 Å is very low. In addition, for comparison purposes one high-resolution spectrum of similar resolution was adopted from Barnbaum (1994) to reveal possible changes in spectra between two seasons of observations. The reduction of spectra was performed with the standard DECH20T routines.

3. Analysis

3.1. Photometry

Images observed on 11 November 2004 during the deep light decline revealed a nearby star about 0.″4 to the west and 2.″5 to the north from DY Per. Figure 1 shows the images in the B and I bands. Individual fluxes of DY Per and the anonymous star were measured using the IRAF/DAOPHOT for PSF photometry. The carbon star DY Per is much redder than the companion so a clear separation is seen toward shorter wavelengths. The magnitudes for DY Per itself were found to be $m_B \sim 17.89$ mag, $m_V \sim 15.68$ mag, and $m_R \sim 13.89$ mag, respectively. The anonymous star had $m_B \sim 17.48$ mag, $m_V \sim 16.80$ mag, and $m_R \sim 15.66$ mag, respectively. At longer wavelengths, DY Per outshines the companion. In the I band, the pair could no longer be resolved, and the combined flux, predominantly from DY Per, was $m_I \sim 11.85$ mag.

The anonymous star, judging from its observed colours indices $(B-V) = 0.68$ and $(V-R) \simeq 1.1$, is likely a foreground star so not physically related to DY Per. With no prior knowledge of the existence of the anonymous star, previous photometric measurements of DY Per, in particular toward short wavelengths, conceivably could have been influenced.

For the photometry obtained on other nights only the combined fluxes of DY Per and its companion were estimated (see Table 1). DY Per appeared to have brightened between mid-November and mid-December of 2004.

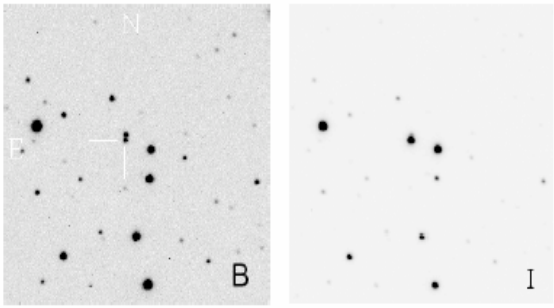

Fig. 1. The star field around DY Per (marked) in the B (*left*) and I (*right*) bands observed with the Lulin 1-m telescope. An anonymous star is seen to the north of DY Per.

Table 1. The combined visual magnitude of DY Per and the nearby star.

Date	JD	V
		mag
2004 Oct. 4	2 453 282.5	15.48
28	306.5	15.26
Nov. 1	310.5	15.28
7	316.5	15.34
11	320.5	15.35
Dec. 17	356.5	14.83
2005 Jan. 21	391.5	14.64
24	394.5	14.55
29	399.5	14.46

3.2. Radial velocity

The radial velocity (RV) for DY Per was measured from the high-resolution MAESTRO spectrum (JD 2 452 597.5) using about 30 relatively clean and symmetric atomic absorption lines selected over the whole spectral region. In addition about 60 uncontaminated CN lines were selected for RV measurements. No significant difference was found in the velocity derived from atomic or molecular lines. The heliocentric correction was calculated to be -0.5 km s^{-1}. Thus the mean heliocentric stellar $RV_\odot$ was found to be -43.7 km s^{-1} with a standard deviation of the mean value of 0.4 km s^{-1}.

Radial velocity for DY Per using the same (common) lines was estimated also in the spectrum observed at Lick Observatory (JD 2 448 141.5), $RV_\odot = -47.2$ km s^{-1}, which is close to that (-46.8) obtained by Barnbaum (1992) using the cross correlation technique against the template of a standard carbon star. The difference between the stellar radial velocities derived for two seasons seems to be significant. We note that Dean (1976) reported $RV_\odot = -39 \pm 5$ km s^{-1} using medium-resolution spectra. The change could be the result of pulsations in this SRb variable. Barnbaum (1992) using cross-correlation analysis found the mean radial velocity to vary about 3 km s^{-1} for SR and Lb variable carbon stars. Spectroscopic monitoring, preferably with simultaneous photometric measurements, is highly desirable to clarify the nature of RV variations in DY Per.

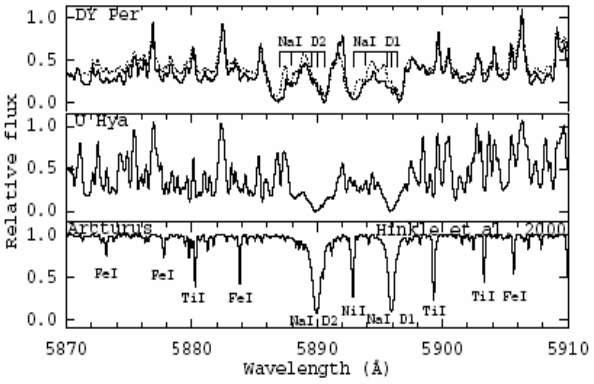

Fig. 2. The observed spectra of DY Per (C 4.5,6) around the Na I D12 lines for two different seasons, November 2002 (solid line) and September 1990 (dotted line; Keenan & Barnbaum 1997), both near light maxima. Also shown are the spectra for a typical carbon star U Hya (C 6,5) and the standard star Arcturus (K 1.5 III). All spectra have been shifted in wavelengths to correct for the stellar radial velocities. The resolved five Na I components are indicated by ticks.

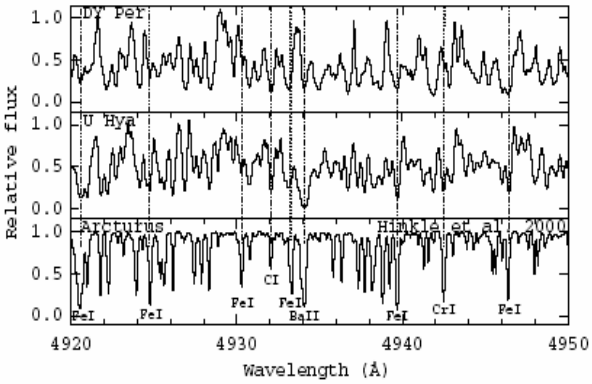

Fig. 3. The observed spectra around the Ba II line at 4934 Å where contamination by molecular lines is relatively low. It is seen that barium is not enhanced in the atmosphere of DY Per. The strong C I line at 4932 Å is marked.

The resulting rectified spectrum for the region around Na I D12 lines along with those for the typical carbon star U Hya (C 6,5) is presented in Fig. 2; also shown is the spectrum for the standard K 1.5 giant Arcturus (Hinkle et al. 2000). Although the spectrum of DY Per is very crowded the spectral features seen in both spectra (seasons) are almost identical. Some discrepancies in the relative intensities seem to be mainly due to uncertainties in the continuum definition. However, significant changes are seen in the sodium lines. At least five components are resolved in each of the spectra. Averaged D1 and D2 velocities of these components on 2002 (phase 0.77) and 1990 (phase 0.15) are (−197.3, −143.0, −57.0, −36.7, −12.8) km s^{-1} and (−214.4, −157.8, −56.8, −36.6, −10.4) km s^{-1}, respectively. The phases are calculated using Max = 2 438 521+792E (Alksnis 1994). Each measured radial velocity refers to the line core, and for an individual line is accurate to about 1.5 km s^{-1}. It is evident that the two most blueshifted components display changes both in the radial velocity and the shape, thus lending support to the assertion (see Keenan & Barnbaum 1997) that the most blueshifted component would be formed in the cloud of dust and gas ejected by DY Per. However, the interstellar origin of the component at −157.8 km s^{-1} was overruled due to significant changes in the profile and velocity. Thus at least two clouds ejected by star are detected. Three components near the stellar velocity of DY Per seem to be non-variable so originate from the photosphere and interstellar medium. The existence of ever-changing thick dust clouds near the surface of the RCB star UW Centauri was discovered by Clayton et al. (1999). De Laverny & Mékarnia (2004) reported the first direct detection of heterogeneities in the circumstellar envelope of the RCB variable RY Sgr. Thus our spectroscopy support the RCB nature of DY Per.

3.3. Chemical peculiarities

The use of traditional method to calculate atmospheric parameters and abundances for DY Per is not possible mainly due to the lack of reliable atmospheric models. Asplund et al. (1997) calculated hydrogen-deficient model atmospheres for typical RCB stars only with effective temperatures higher than 5000 K. Here a few results of qualitative analysis are provided those based mainly on comparison of our high-resolution spectra for DY Per (C 4.5,6), U Hya (C 6,5) and the standard K 1.5 giant Arcturus. In the red spectral region the influence of the nearby star should be negligible, because the spectrum of DY Per was observed near the maximum of light and the companion is much hotter than DY Per itself.

An inspection of the high-resolution spectra of DY Per relative to the normal carbon star U Hya ([Fe] ≃ 0.0, [s/Fe] ≃ +1 dex, $^{12}C/^{13}C = 35$; see Abia et al. 2002) shows that a large number of strong C_2 and CN lines dominate over all the analyzed spectrum, blending significantly with the atomic absorption lines. However, a limited number of relatively uncontaminated atomic lines were selected to check chemical peculiarities revealed for typical RCBs. Our analysis shows that the lines of the iron-peak elements are of similar strength or slightly deficient while features due to the atomic carbon are enhanced (see, for example, Fig. 3), in agreement with that for typical RCB stars. The equivalent widths of strong C I line at 4932 Å in the spectra of DY Per and U Hya are $EW \simeq 500$ and 280 mÅ, respectively. The shape of the spectrum of carbon star determine mainly the absolute abundances of CNO elements and the C/O ratio. The extremely complicated spectrum of DY Per (due to carbon bearing molecules) in comparison with that for the carbon star U Hya support high C/O value for DY Per. However, it is evident that neutron-capture elements are not enhanced. For example, the barium line at 4934 Å in the spectrum of DY Per is relatively weak ($EW \simeq 400$ mÅ; see Fig. 3) in comparison with that for U Hya ($EW \simeq 1$ Å), confirming nearly solar barium abundance. Notice that typical RCB stars show weak hydrogen and strong C(N) lines; the s-process elements usually are mildly enhanced (Asplund et al. 1997). Relative intensities of spectral features due to

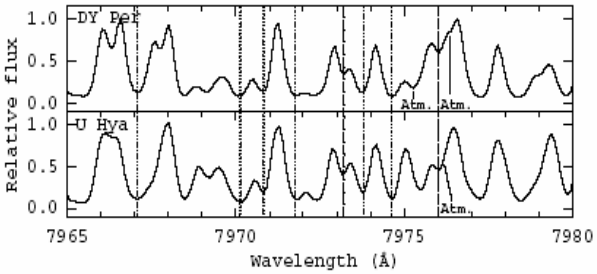

Fig. 4. The spectra of DY Per and U Hya in the spectral region from 7965 to 7977 Å. The isotopic ^{13}CN(2, 0) lines (dashed line) relative to ^{12}CN (dotted line) are of similar strength with those for the carbon star U Hya with $^{12}C/^{13}C = 35$.

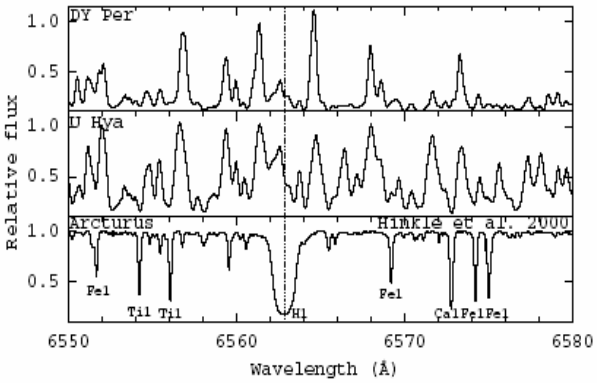

Fig. 5. The observed spectra around the H_α line. The laboratory wavelength of H_α line is marked by the dotted line. The small dip in the spectra of DY Per and U Hya could be the core of H_α. In this case hydrogen deficiency in the atmosphere of DY Per is doubtful.

isotopic molecules were inspected using the C_2 Swan system band heads near 4740 Å and some lines of CN red system (2, 0) at 7975 Å. It is evident that the isotopic ^{13}CN lines relative to ^{12}CN are of similar strength with those for the carbon star U Hya (see Fig. 4). The discrepancy with some previous estimations seems to be due to neglected blends in the used low-resolution spectra. Unfortunately, the regions around H_α (Fig. 5) and H_β lines are too crowded to clarify the level of hydrogen deficiency in the atmosphere of DY Per even in the high-resolution spectrum. An inspection of another lines of the Balmer series was not possible due to very low *S/N* ratio in the blue region of high-resolution spectrum.

4. Discussion and conclusions

1. An inspection of the high-resolution spectrum of DY Per observed near the light maximum relative to the normal carbon star U Hya shows that neutron-capture elements are not enhanced while the features due to atomic carbon are strong, in agreement with that for typical RCB stars. The metallicity was found to be nearly solar. The isotopic ^{13}CN lines are not enhanced in the spectrum of DY Per relative to ^{12}CN. Unfortunately the spectral regions around H_α and H_β are very crowded to clarify the level of hydrogen deficiency in the atmosphere of DY Per.
2. A significant changes are seen in the profiles of sodium D lines between two seasons of observations. At least five components are resolved. Averaged D1 and D2 heliocentric velocities of these components on 2002 (phase 0.77) and 1990 (phase 0.15) are (−197.3, −143.0, −57.0, −36.7, −12.8) km s^{-1} and (−214.4, −157.8, −56.8, −36.6, −10.4) km s^{-1}, respectively. Thus two the most blueshifted components display changes both in the radial velocity and shape while three components near the stellar velocity of DY Per seems to be non-variable. The blueshifted components apparently are formed in the clouds of gas and dust ejected by DY Per. The rest revealed components originate in the stellar atmosphere and interstellar medium.
3. A close nearby star was detected about 2.″5 from DY Per using CCD images during the recent deep light decline. The carbon star DY Per itself is much redder than the companion so a clear separation is seen in the *B* band. At longer wavelengths DY Per starts to outshines the companion. The presence of such companion was not revealed during more than 10 years of the photometric monitoring, however, it was supposed by Alksnis (1994) to interpret the variations of the observed colour indices. This anonymous companion, with observed colour indices $(B - V) = 0.68$ and $(V - R) \simeq 1.1$, may be a foreground star.

Acknowledgements. A. Alksnis is acknowledged for initiation of this research and subsequent discussions. The referee, G. C. Clayton, is thanked for his valuable comments on the paper. We are grateful to Y. T. Chen, P. S. Chiang, H. C. Lin, Z. Y. Lin, and M. C. Tsai for their help with the photometric observations. The Mutual Fund of scientific collaboration among Taiwan (ROC), Latvia and Lithuania is thanked for support. WPC acknolweges the grant from NSC/Taiwan NSC93-2112-M-008-040.

References

Abia, C., Dominguez, I., Gallino, R., et al. 2002, ApJ, 579, 817
Alcock, C., Allsman, R. A., Alves, D. R., et al. 2001, ApJ, 554, 298
Alksnis, A. 1994, BaltA, 3, 410
Alksnis, A., Larionov, V. M., Larionova, L. V., & Shenavrin, V. I. 2002, BaltA, 11, 487
Alksnis, A. 2004, IBVS, 5561, 1
Asplund, M., Gustafsson, B., Kiselman, D., & Eriksson, K. 1997, A&A, 318, 521
Asplund, M., Gustafsson, B., Lambert, D. L., & Rao, N. K. 2000, A&A, 353, 287
Barnbaum, C. 1992, AJ, 104, 1585
Barnbaum, C. 1994, ApJS, 90, 317
Clayton, G. C. 1996, PASP, 108, 225
Clayton, G. C., Kerber, F., Gordon, K. D., et al. 1999, ApJ, 517, L143
Dean, C. A. 1976, AJ, 81, 364
de Laverny, P., & Mékarnia, D. 2004, A&A, 428, 13
Hardorp, J., Lubeck, K., & Stephenson, C. B. 1973, A&A, 22, 129
Hinkle, K., Wallace, L., Valenti, J., & Harmer, D. 2000, Visible and Infrared Atlass of the Arcturus Spectrum 3727-9300 A (San Francisco: ASP)
Keenan, P. C., & Barnbaum, C. 1997, PASP, 109, 969
Musaev, F. A., Galazutdinov, G. A., Sergeev, A. V., Karpov, N. V., & Podyachev, Yu. V. 1999, Kinematika I Fizika Nebesnyh Tel, 15, 282
Yamashita, Y. 1975, Ann. Tokyo Astron. Obs., 15, 47

台灣超新星尋天計劃 (TSS, Taiwan Supernova Survey)

陳英同[a], 陳婷婉[a], 李易錫[a], 黃癸雲[a], 林忠義[a], 林宏欽[a], 葉永烜[a],
陳文屏[a], 裘予雷[b], 胡景耀[b], 李衛東[c]

a Institute of Astronomy, National Central University, IANCU
b Beijing Astronomical Observatory, NAOC
c Department of Astronomy, UC Berkeley

國立中央大學天文所鹿林天文台自 2004 年 7 月首先公布發現 3 個超新星 2004ee, 2004cy, 2003lz 以來，至 2005 年 12 月為止，共發現十顆超新星，此新訊息以時間順序分別發表在國際天文聯合會通告 IAUC(International Astronomical Union Circulars) 第 8364 期、第 8371 期、第 8399 期、第 8407 期、第 8420 期、第 8420 期、第 8454 期上、第 8471 期上、第 8534 期上及第 8567 期上(如表一，圖一)。

Name	Galaxy	Date	R.A.	Dec.	Mag	IAUC	Type
2003lz	ESO 428-G13	2003 10 30	7h16m25s.24	-29°37'4".5	17.1	IAUC 8371	?
2004cy	ESO 403-G9	2004 04 05	21h34m25s.67	-33°23'13".7	15.6	IAUC 8364	?
2004ee	ESO 298-G7	2004 07 31	2h6m14s.62	-37°20'5".4	17.2	IAUC 8399	Ia
2004eq	ESO 404-G12	2004 07 30	21h57m9s.46	-34°34'51".3	16.8	IAUC 8407	Ia
2004fa	MCG -05-48-5	2004 09 05	20h22m35s	-29°49'20".7	16.8	IAUC 8420	Ia
2004fb	ESO 340-G7	2004 10 07	20h15m25s.63	-37°30'34".6	18.3	IAUC 8420	II
2004gv	NGC 0856	2004 10 07	02h13m37s.42	-00°43'05".8	17.6	IAUC 8454	Ib
2005O	NGC 3340	2005 01 16	10h42m18s.32	-00°22'41".2	15.2	IAUC 8471	Ib
2005cd	IC 0651	2005 05 16	10h50m57s.60	-02°08'48".2	17.4	IAUC 8534	?
2005cw	IC 1439	2005 07 11	22h16m39s.61	-21°29'28".7	18.5	IAUC 8567	II

表一：由鹿林天文台發現之超新星資料

由於超新星為大質量恆星演化晚期爆發的現象，所以主要會發生在可見恆星數目最多的星系當中。在本銀河系跟河外星系均有發現超新星的可能性，不過在做超新星尋天工作時，我們對於消光嚴重的銀河盤面做觀測是很沒有效率的，發現超新星的機率也不高，所以我們主要是觀測樣本空間較大的河外星系。

現今在世界上已有不少的研究團隊正在做超新星尋天的計劃，尤其是美國的研究團體最多。以地理位置來看，雖然大致上在各個時區分布都有觀測點，不過都是以北天為主，所以使得目前所發現的超新星都是集中在北天的星系，在南天除了澳洲及非洲之外，少有南天國家在做超新星尋天計劃。由於北京天文台在 2001 年結束超新星尋天計劃，台灣的地理位置剛好可替補亞洲時區的觀測點，台灣的地理位置又位於北緯 23.5 度，可視星場為北天全天，而南天則可到達 40 度以上，我們以新手的經驗去切入超新星尋天計劃，所鎖定的星場為 DEC:0°~DEC:-40°，一來不會與位於較高緯度，而且已經對超新星尋天技術發展純熟的研究團體的觀測星場有所競爭，二來剛好切入南天超新星尋天研究團體少的優勢。

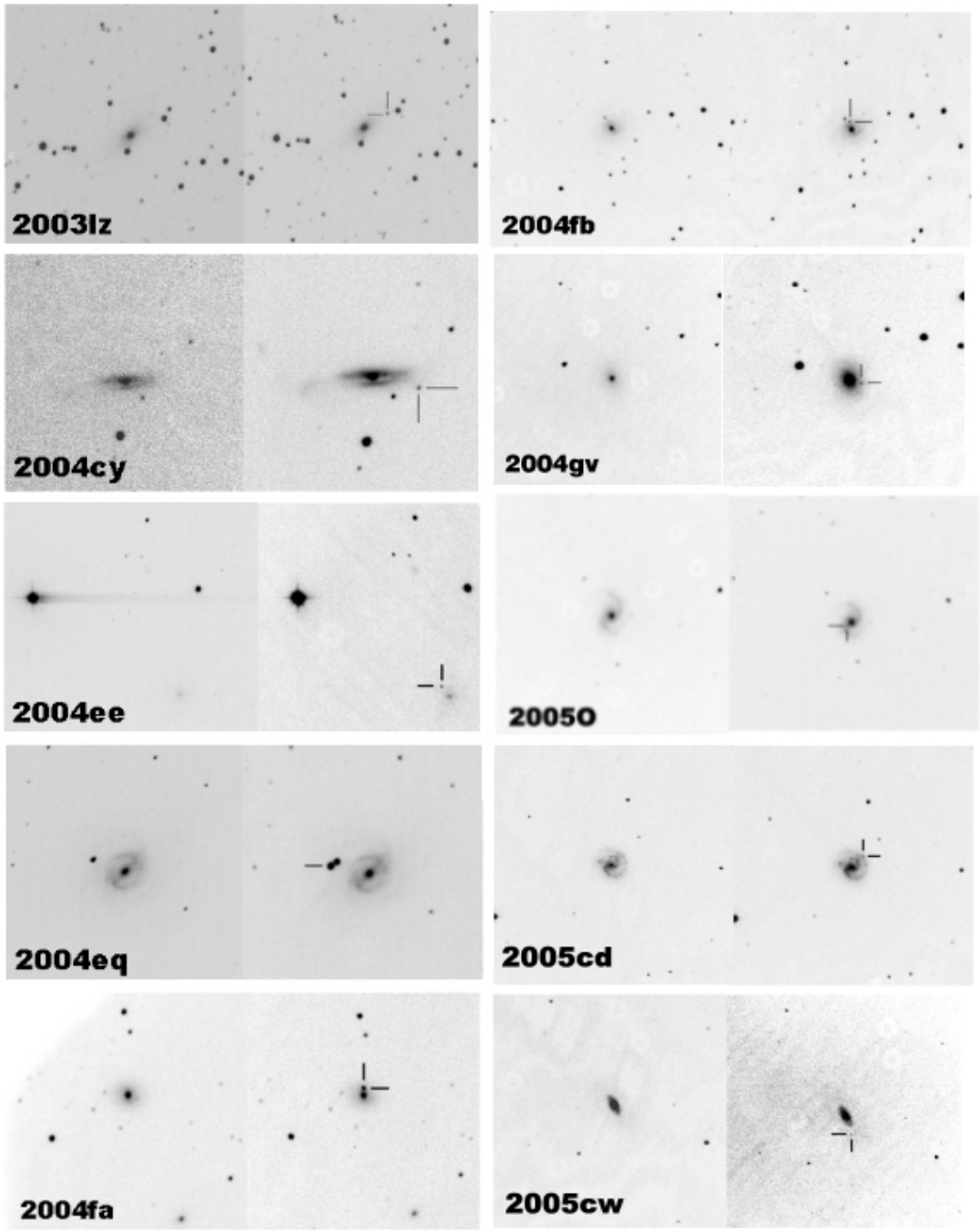

圖一：由鹿林天文台發現之超新星影像

目前台灣超新星尋天計劃是利用中央大學鹿林前山天文台一米望遠鏡(Lulin One-meter Telescope, LOT) 做超新星尋天的觀測，所選的目標均為鄰近星系，主要分布在 DEC:0°~DEC:-40°之間的 1573 個星系。為了讓觀測更有效率，在觀測時不使用濾鏡，一開始所設定的曝光時間為 20 秒，極限星等約 19 等(無濾鏡對照 R-Band)，現在則將曝光時間重新設定為之前的一半(10 秒，極限星等大約差 0.25 個星等)，以提升巡天速率，增加發現超新星的機率，在 2005 年的 LOT 觀測時間分配中，大概是每十多天有一次的觀測時間。以目前的單位時間的觀測速度，平均一分鐘可以觀測 1.8 個目標，目前的每晚觀測星系數目最多可以到達一千多個、橫跨 18 個赤緯。

台灣超新星尋天計畫主要是比較不同時間所得到的影像，在經過強度比例調整對減後，觀察影像有無差異，區別有無超新星出現在新影像裡。在短時間週期內，不同時間所照的影像中，假如沒有特殊發生天文事件的話，兩個時間的影像在對減後應該不會有特別奇怪的星點出現；反之，假如有一個亮度改變的天文事件發生在時間較晚的影像當中，在兩幅影像對減後，就可以發現明顯的不同(圖二)。

在星系中找到有亮度變化超新星候選者後，因為影像當中會有亮度變化的原因有很多種，我們再來就要確定它是否為超新星現象所引起的。引起影像有亮度變化的可能有可能因為宇宙射線(cosmic ray)、變星(Variable Stars)、古伯帶星體(KBO)、超新星等等。一般的確認方法就是在隔天再取一幅新影像做比對，確定不是小行星或是古伯帶星體所短暫引起的亮度變化，或是其他觀測上的問題所引起誤差。

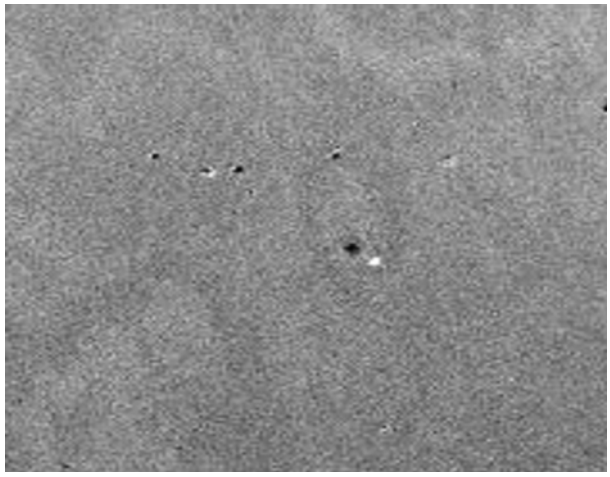

圖二：對減後影像

目前台灣超新星尋天的技術，主要是來自北京天文台(Beijing Astronomical Observatory BAO)的胡景耀老師及裘予雷老師，以及 UC Berkeley 的李衛東老師的技術指導。北京天文台的超新星尋天計劃(BAO Supernova Survey －BAOSS)在 1996 到 2001 年中，就發現了 45 顆超新星，而 UC Berkeley 的 LOSS (Lick Observatory Supernova Survey)，則是現在全世界發現超新星最多也是最有效率的研究團隊，相信我們在充份的合作下，能夠對南天的超新星發現上能有可觀的科學研究貢獻。

行星狀星雲 A14 中心星的光度變化測量

C. H. Hsia[a](夏志浩), W. H. Ip[a](葉永烜), J.Z. Li[b](李金增)
a Institute of Astronomy, National Central University, Taiwan, R.O.C
b Beijing Astronomical Observatory, Beijing, China

雙極型(蝴蝶狀)行星狀星雲的型態一直是眾人所感興趣的話題，尤其是它那對高度對稱的雙極型噴流。目前一般相信雙極型噴流的來源可能來自於中心恆星的磁場或是由雙星系統(可能有一顆伴星爲系外行星)所造成的。由此可知，行星狀星雲的形狀與中心星的演化過程是有一定的關連。而 Sahai 等人於 2003 年，利用 HST 超高解析度的光譜儀，在一顆具有高速雙極噴流的 AGB 星中找到了雙星系統，而且也證實了這些高速噴流的來源；是來自於環繞恆星周圍的吸積盤，但是，盤的中央並不是原來那顆主星，而是環繞其周圍的伴星或巨行星。De Marco, Orsola 等人，利用極高解析度的光譜儀對於行星狀星雲的中心星進行長時間的速度監測(Radial-velocity Survey)，結果，她們在 11 個行星狀星雲當中已經確定有 10 個的中心星爲雙星系統所組成的，這無疑是讓“行星狀星雲的起源”的這個問題有著更進一步的瞭解。

A14(Abell 14) – 這個著名的行星狀星雲，是天文學家 Abell 於 1958 年所發現的，利用窄波段濾鏡 [NⅡ]以及大望遠鏡所拍攝的影像中所顯示：有一對弧狀的結構分佈在其管壁上，這對弧狀結構很可能是 A14（圖一）在漸進水平分支(AGB)時期質量損失所遺留下來的痕跡；我們使用鹿林天文台一米望遠鏡進行 A14 中心星密集的光度觀測(B 波段)，以便於我們能夠找出 A14 中心星的光度變化（表一）。

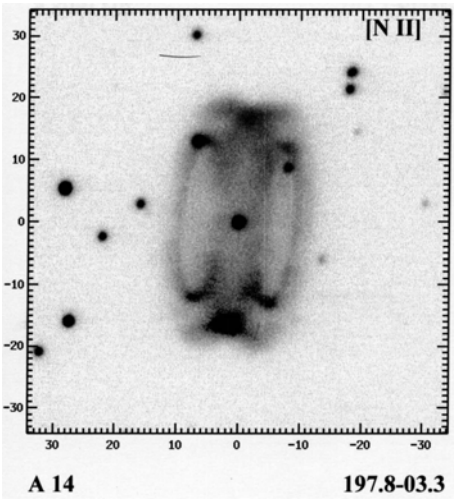

（圖一）雙極型行星狀星雲 A14 於[NII]所拍攝的影像，整張影像的視野為 68 arcsec，我們可以清楚的見到在東、西方向上分佈著這個行星狀星雲在 AGB 時期質量損失所形成的結構。

Table 1. Journal of photometric observations of A14

Observation date	Start (UT)	Start (HJD 2453300 +)	Duration (hrs)	Filter	Number of exposures
2005 January 01	15:42	72.1508	2.2	B	30
2005 January 02	11:07	72.9638	8.1	B	103
2005 January 11	14:09	82.0897	4.8	B	63
2005 January 14	11:58	84.9992	6.5	B	85

（表一）我們使用鹿林天文台一米望遠鏡進行 A14 中心星密集的光度觀測(B 波段)

爲了要得到 A14 中心星的光度變化，我們採取較差測光的方式來進行資料處理的工作；較差測光有別於其他的光度測量工作，主要是在於它能夠避免在觀測時天氣的變化所造成的誤差，同時也能夠避免大氣消光對於光度測量的影響。

於是，我們得到 A14 每天的光度變化（圖二）；從這些光度變化圖裏，可以知道，如果 A14 的中心星爲雙星系統的話，那麼，其週期一定要比 8.1hrs 還要長，所以我們只能證實 A14 的中心星確實有光度的變化，至於到底有沒有週期性或是其週期爲多長，現在還無法確定。

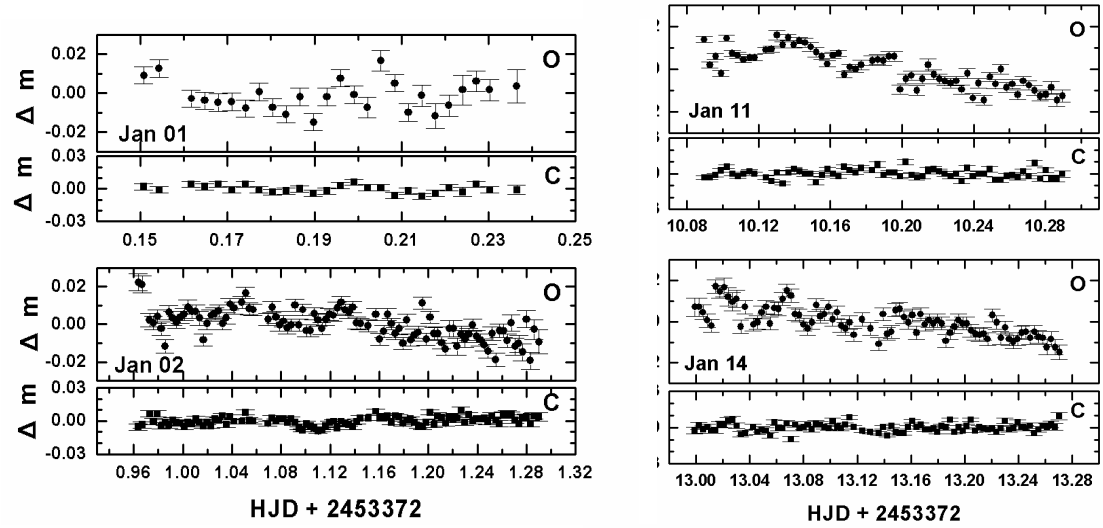

（圖二）我們針對 A14 進行一些光度變化的觀測，可以看出在 1 月 1 日至 1 月 14 日四天內的觀測時間之內其光度在 B 波段有著變化。

Reference:

De Marco, Orsola; Bond, Howard E.; Harmer, Dianne; Fleming, Andrew J. ApJL, 93, 602, 2004

Sahai, R.; Morris, M.; Knapp, G.. R.; Young, K.; Barnbaum, C., 2003,Nature,426,261S.

Photometric variability studies on brown dwarfs

Soumen Mondal, Wen-Ping Chen
Graduate Institute of Astronomy, National Central University

We propose to use CCD R and I bands photometric observations to study brown dwarfs for atmospheric variability. We will observe a sequence of L dwarfs to probe their hour scale variability because of their atmospheric clouds or dust that is expected by some models for these objects. Our new observational results would constrain the physical parameters of the dynamics of the very cool atmospheres.

Large-scale imaging surveys (e.g., 2 Micron All Sky Survey (2MASS), Deep Near-Infrared Survey of the southern sky (DENIS) and Sloan Digital Sky Survey (SDSS)) have resulted in a major revolution in cool star research. From these surveys we have witnessed an avalanche of brown dwarf, pushing stellar temperature below 1000 K. These discoveries have required the definition of two new spectral classes, L and T dwarfs (Kirkpatrick et al. 1999, APJ, 519, 802), the major additions to the widely accepted MK system.

Efforts are still underway the new detection of brown dwarfs from these surveys. Second phase is the understanding of their structure, origin and evolution. One means of probing the atmospheric structure of brown dwarfs has focused on the presence, or lack of photometric variability, which may be tied to circumstellar warm dust clouds properties or magnetic activity (Enoch et al. 2003, AJ, 126, 1006). If any exists, it is unclear on what timescale such variability would occur, or how large a fractional variability amplitude to expect. But limited observational efforts on variability studies have been given idea of such expectations. For example, two L1 dwarfs show a R-band non-periodic variability of amplitude ranging from 0.01 to 0.02 mag (Sengupta et al. 2005, APJ, 619, L183). Another example, a young brown dwarf, S Ori 45 show variability of 34 to 81 millimag at I and J band filters at period of 2.5-3.0 hr (Zapatero Osorio et al. 2003, A&A, 408, 2003).

For photometric observations of brown dwarfs we will use the Lulin 1m Telescope (LOT) and optical CCD camera. A few target lists of brown dwarfs in the spectral type of L dwarfs are assembled in the below list from the published data considering their brightness and good observability from the Lulin observatory during November-December 2005. There is no published R and I band mag for many of those sources, the approximate mag in I-band is calculated from their color-spectral type relation and given in the list. The differential photometric light curves with an accuracy of 20 to 30 millimag will allow us to investigate photometric variability and periodicity on those selected observable samples.

The observational efforts on variability will provide much insight on their atmospheric activity and possible mechanisms (e.g. presence of dust clouds, rotation, binarity and magnetic activity etc), and constrain the atmospheric models of low mass dwarfs. Such considerations drive searches for more

variability measurements, in order to more characterize their atmospheres.

We observed eight brown dwarfs of spectral type early L in R and I bands during Nov 29 - Dec 4 2005 using CCD photometer on LOT. Data analysis is in progress. From these observations, we will look for short-period (over few hours scale) variation, which might be related to rapid evolution of atmospheric features (either clouds or magnetic spot), or the orbital motion of companion at separation of few stellar radii. Our observations might help us better understanding of their variability, e.g. if it is periodic then may be due to orbital motion of a close companion, and if non-periodic then due to atmospheric features.

Two Comets were Observed in 2005

Zhong-Yi Lin
Graduate Institute of Astronomy, National Central University

C/2004 Q2 (Machholz)

On Aug. 27, 2004 the well-known comet hunter Donald Machholz discovered his 10th comet, again visually, with his 15 cm (6 inch) reflector. In mid-December it will start to move rapidly northward, predicted to reach 4-5 mag at the beginning of January 2005, mainly due to the proximity to earth (0.35 A.U.) on Jan. 7 2005. We apply the proposal to observe this comet during the perigee passage and perihelion passage with the narrow-banded filters (C2, NH2, RC, BC).

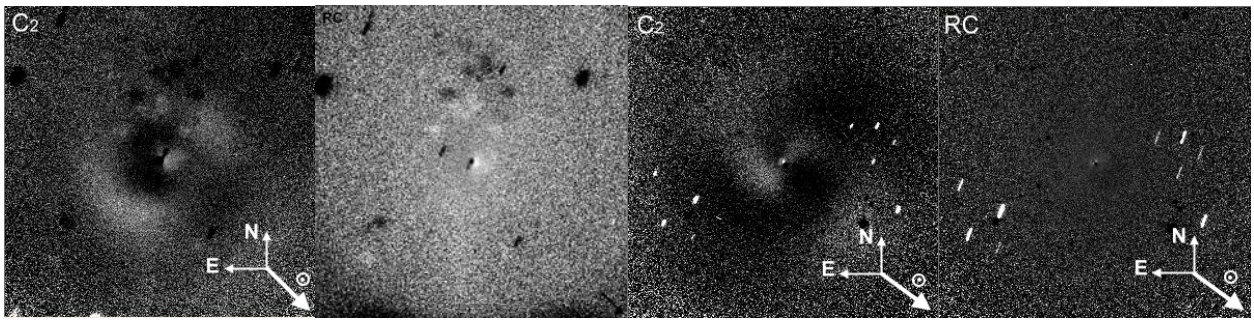

Figure 1: Images produced by "divide" method. (Left: Dec. 5, 2005, Right: Dec. 15, 2005, 10'FOV)

In Figure 1, Twisted jets were clearly detected using the "divide" method in the C2 images, that are clearly not present in the continuum images. To get the clearly coma structures in comet images, the azimuthally average coma intensity profile would be used and applied to continuum image and all C2 images available (before continuum subtraction). In Figure 2, a examples for the jets are shown in C2 images. On Jan 24 and 25, a possible disconnetion of one jet from the comet nucleus was observed. In Figure 3, On one night, a clear change in position angle of the jets could be observed. Nevertheless, the dataset appears to be not sufficient to derive the position of the comets rotational axis.

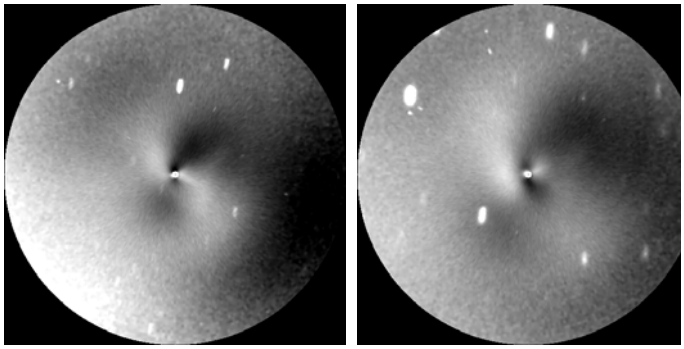

Figure 2: Coma jet structures. Left: C_2 image (Dec 24, 2004 , 4' fov Right: C_2 image (Jan 25, 2005. 4.5' fov)

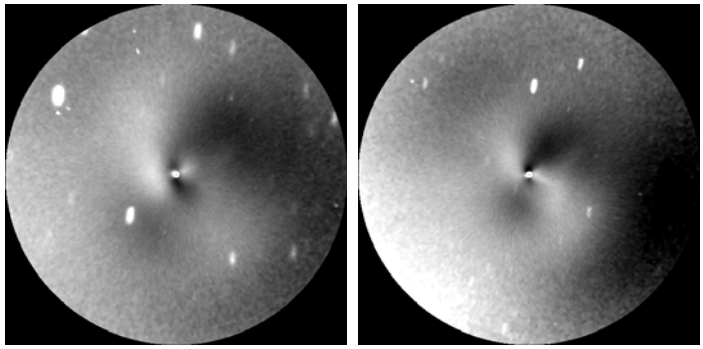

Figure 3: A clear change in position angle of the jets. (Jan 24, 2005. 4.5' fov)

9P/Tempel 1

The periodic comet 9P/Tempel 1 with an orbital period of 5.5 years and a perihelion distance of 1.5 AU will be the target of the Deep Impact mission of NASA. A 370-kg projectile will be fired at its nucleus on July 4, 2005, with the purpose of creating an artificial impact crater with the size of a football field.(Figure 4: the flight system of Deep Impact Mission) It is expected that a burst of gas and dust will be ejected from the surface and interior thus leading to an increase of the coma brightness by several magnitude to m ~ 6. The impact of the Deep Space Probe projectile on July 4 was awaited with much anticipation. The experiment was successful and very interesting results were recorded. However, observers on Earth were widely disappointed, because the impact did not result in any significant brightening of the overall brightness of the coma. Many observers did not even see the comet at all at the time of impact, because at that time it had grown very diffuse at low altitude. Those who were lucky to observe the comet at impact time reported an increase of the degree of condensation and the appearance of a short-lived inner coma. Very few observers with large amateur instruments noticed and documented a brightness increase of the very center by about 1-2 mag within the first hours after impact.

Figure 4 : Flight System

Using the same method reduces the data of 9P/Tempel 1, we found the dust expanding after DI time. (Figure 5.) Unfortunately, there are only a few images for Lulin observatory by testing 40cm telescope although the weather condition is good for observation. On that time, I was in Xinglong Observatory Beijing but the weather was bad for comparison with Lulin Taiwan! In conclusion, we just have a few images during the DI time and we can't get more detail information form these images.

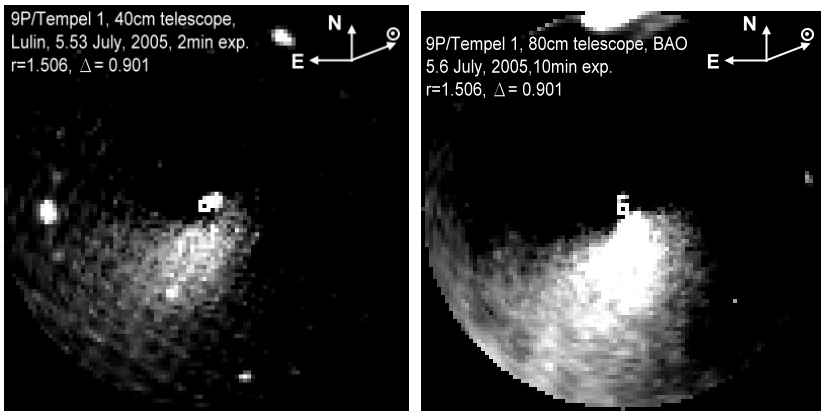

Figure 5 :The dust expanding were found after DI time. (Left : Lulin 40cm, Right: BAO 80cm.)

Age and Distance Determination of the Open Cluster NGC 1857

Wen-Shan Hsiao & W. P. Chen
Graduate Institute of Astronomy, National Central University

NGC 1857 is a poorly studied open cluster located at the anti-Galactic center direction. One early-type star has been previously recognized to have Balmer emission lines. In our study of Herbig Ae/Be stars, i.e., intermediate-mass pre-main sequence (PMS) stars in open clusters, we identified another early-type emission-line star in NGC 1857. Earlier studies of NGC 1857 suggest an age (> 1 Gyr) too old to host such young member stars. This prompted us to conduct a detailed investigation of this star cluster. Our data consist of 2MASS, imaging photometry with the LOT, and optical spectroscopy of the BAO 2 m.

In March, 2005, Chin-Wei Chen took UBV images of NGC 1857. We used a combination of IRAF and IDL to process the data. We found that the U-band images of the LOT show noticeable "halo" structure around bright stars, rendering inferior photometric accuracy. We compared our U magnitudes of the bright stars in NGC 1857 with those published by Mermilliod (1987), and found systematically higher fluxes in our data. We henceforth rescaled our photometry for the subsequent analysis.

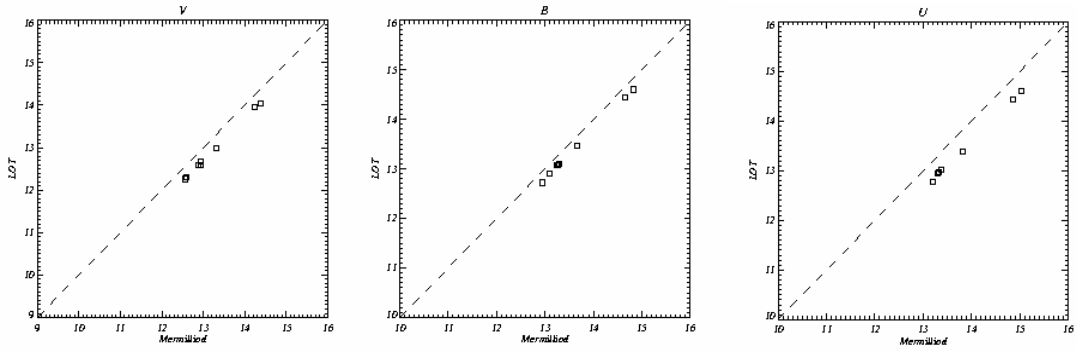

Fig. 1: Comparison between our photometric data (from left to right, for V, B, and U bands) and the published values. In each case the diagonal dashed line represents the equality between our photometry and that of Memilliod (1987). The offset values are V~0.21 mag, B~0.14 mag, and U~0.27 mag, respectively.

The (U-B) versus (B-V) color-color diagram is shown in Figure 2. The reddening of the cluster, determined from the early-type members, is estimated to be ~0.45 mag. The dereddened color-magnitude diagram is then compared with the theoretical evolutionary tracks by Girardi et al. (2000), shown in Figure 3. The age of NGC 1857 is determined to be between $10^{8.35}$ and $10^{8.40}$ years, with a distance of ~5.2 kpc. NGC 1857 is, therefore, a distant open cluster of an intermediate age, for which all massive members should have already evolved off the main sequence. Hence those bright and red sources in the color-magnitude diagram are likely giant members, and the two emission-line stars cannot be PMS sources. In November 2005, deeper images were taken with the LOT. Spectra taken at BAO in December 2005 confirmed the classification of giant stars in this cluster.

Furthermore, we find the two emission-line stars to be classical Be stars. Our data provide a clue to the evolutionary status of this peculiar class of objects. A paper is being drafted and we will report these results in the 2006 CPS meeting.

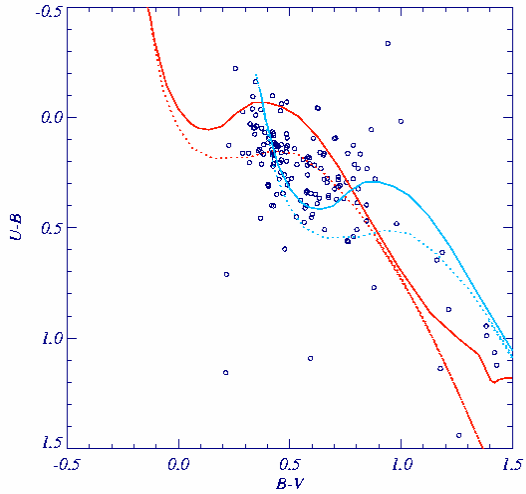

Fig. 2: Color-color diagram of NGC 1857. The red lines represent unreddened ZAMS (solid) and giant (dotted) loci. The blue lines represent those with a reddening of E(B-V) = 0.45 mag.

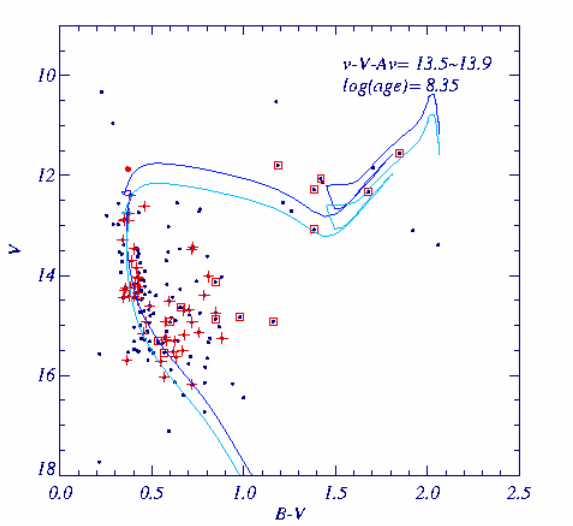

Fig. 3: Color-magnitude diagram of NGC 1857, with the isochrone overlaid. The red symbols represent photometric members.

Report on Galactic High Latitude Open Cluster Study 2006

Chin-Wei Chen
Graduate Institute of Astronomy, National Central University

I totally got 25 nights in 2005, but returned 7/25-29 when I was in Europe for an international conference this summer. For the remaining 20 nights, none of them are clear enough to get photometric data on open clusters. Even so, I still took some galaxy images to make pseudo-color images for the 2007 calendar as Fig.1-4.

Fig.1 M65

Fig.2 M74

Fig.3 M81

Fig.4 M82

Instead of my own run, Wen-Shan Hsiao and Fong-Yi Huang observed 12 open clusters under clear sky in another run. These clusters are NGC305, NGC7193, Dol-Dzim 1, NGC 6980, NGC 7801, White 1, NGC 1891, Be 50, Dol-Dzim 9, eso485-20, IC1590 and NGC7833. Fig. 5 is the reduced V-band image of NGC 7193 with 3 sec exposure time. Fig .6 is the color-color diagram and color magnitude of NGC 7193. This cluster may not be a bona fide open cluster but just a density enhancement of field stars. Data of other clusters are being processed and the data reduction will be

finished before the end of Jan 2006.

Fig.5 reduced V-band image of NGC 7193 with 3 sec exposure time

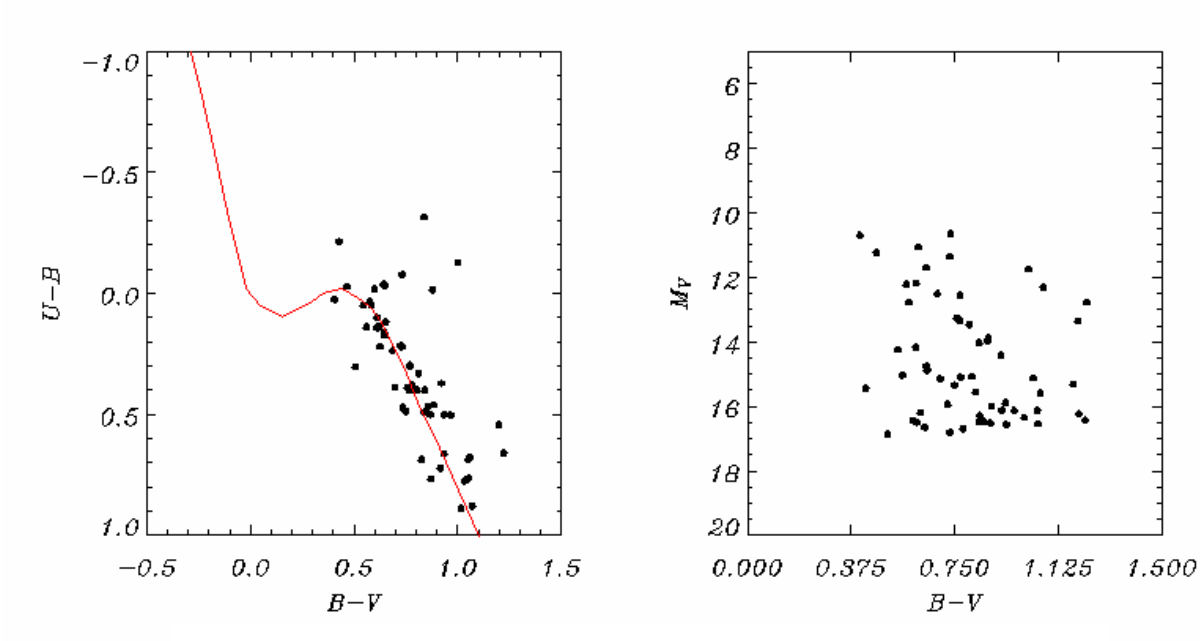

Fig.6 left) Color-color diagram of NGC 7193. The red curve is the theoretical track of zero-age main-sequence stars.
right) Color-magnitude diagram of NGC 7193. The uniformly distributed stars may imply that this is only the projected effect of field stars rather than a real open cluster.

TAOS at Lulin in 2005

S. K. King[a] (金升光), C. Alcock[b], T. Axelrod[c], F. B. Bianco[d,b], Y. I. Byun[e], Y. H. Chang[f] (張永欣), W. P. Chen[f] (陳文屏), K. H. Cook[g], R. Dave[d], J. Giammarco[d], T. Lee[a] (李太楓), M. Lehner[b,d], J. Lissauer[h], S. Marshall[i], S. Mondal[f], I. de Pater[j], R. Porrata[k], J. Rice[l], M. E. Schwamb[d], A. Wang[a] (汪仁鴻), S. Y. Wang[a] (王祥宇), C. Y. Wen[a] (溫志懿) and Z. W. Zhang[f] (張智威)

[a] Institute of Astronomy & Astrophysics Preparatory Office, Academia Sinica, Nankang, Taiwan, ROC
[b] Harvard-Smithsonian Center for Astrophysics, Cambridge, MA, USA
[c] Steward Observatory, University of Arizona, AZ, USA
[d] Department of Physics & Astronomy, University of Pennsylvania, PA, USA
[e] Department of Astronomy, Yonsei University, Korea
[f] Institute of Astronomy, National Central University, Chung-Li, Taiwan, ROC
[g] Institute of Geophysics & Planetary Physics, Lawrence Livermore National Laboratory, CA, USA
[h] NASA Ames Research Center, Mountain View, CA, USA
[i] Stanford Linear Accelerator Center, Stanford, CA, USA
[j] Department of Astronomy, University of California, Berkeley, CA, USA
[k] Department of Physics, University of California, Berkeley, CA, USA
[l] Department of Statistics, University of California, Berkeley, CA, USA

TAOS started taking simultaneous long zipper data regularly since the winter of 2004. There are some hardware improvement and software upgrading every now and then. Here is a summary of some major activities and progresses at Lulin site in 2005.

1. Real-time tracking using zipper image is available since July.
2. Simultaneous long zipper data from two or three telescopes were analyzed using aperture photometry. The hold time was usually 0.25 s. The length of the long zipper of each observed field varied from 20 minutes (before April 20), 30 minutes (till June), to 1.5 hours (since July). The list of analyzed fields in Table-1 is provided by Z. W. Zhang. Some observed fields in January, February and October might be missing. Some fields were observed several (n) times per night (labeled as "*n"). A telescope might be down during an observation. A long zipper could be stopped due to system crash or twilight (not shown in the table). Some preliminary light curves are available at taos.asiaa.sinica.edu.tw/~kiwi.
3. TAOS C mirror was re-polished and (temporarily) re-coated in Korea in June. It was installed on site in August. However, the edge (about 1-2 cm) of this mirror seems have poorer optical quality. A temporary mask might help.
4. One arm of TAOS D lid was broken and fixed in September. TAOS B lid was replaced because of leakage in heavy rain.
5. The A/D circuit of TAOS B camera (800-106) lost one bit in its dynamic range. The TAOS C camera (800-111) was used as a replacement.
6. A status report "Status of the TAOS Project and a Simulator for TNO Occultation" will be published in *Advances in Geosciences 2005 (Volume 3: Planetary Science)*, World Scientific Pub. Co., Singapore, 2006.

2005	Analyzed Fields	TAOS
15-Feb	54, 62, 71, 74, 82, 88, 97, 102, 117, 118, 137, 165	ABD
16-Mar	146, 147, 150	ABD
4-Apr	81, 90, 113, 117, 119, 120	ABD
7-Apr	95, 98, 108, 117, 120, 146, 90(AD)	ABD
11-Apr	110, 113, 114, 115, 116, 151, 154, 167	ABD
19-Apr	147, 148, 151(*2)	ABD
20-Apr	151	ABD
22-Apr	88, 95, 147, 148, 151(*2), 88(AB)	ABD
29-Apr	74, 82, 88, 97, 147(AB), 148(AB), 151(AB*3)	ABD
30-Apr	147, 151	ABD
1-May	107, 147, 148, 151(*3)	ABD
4-May	147, 148	ABD
16-May	147, 148, 151(*4)	ABD
21-May	14	ABD
26-May	107, 147, 148(*2), 151(*2), 93(A)	ABD
30-Jun	28(A), 28(AB)	
1-Jul	28, 121(*2)	A
4-Jul	121(*2), 147, 151	A
5-Jul	121(*2), 151(*3), 138(B)	AB
6-Jul	28, 138, 151	AB
8-Jul	121, 138, 151	AB
9-Jul	28, 121(*2), 151	AB
10-Jul	121, 151	AB
11-Jul	147, 151	AB
13-Jul	147, 151	AB
15-Jul	121(*3), 138	AB
16-Jul	150, 151(*3)	AB
24-Jul	121, 28	AB
25-Jul	121(A), 121(AB)	
26-Jul	28	AB
30-Jul	121, 138	AB
31-Jul	28, 121	AB
1-Aug	121(*2), 124, 151, 138(B)	AB
2-Aug	121(*2), 124, 138, 151	AB
7-Aug	28, 124	AB
29-Aug	126	AB
9-Sep	129	AB
11-Sep	30, 126, 134, 138	AB
13-Sep	51, 124, 129, 138	AB
14-Sep	28, 30, 126, 134	A
15-Sep	30, 53, 121, 130, 138	A
16-Sep	28, 121, 124, 130, 134	A
28-Sep	53	AB
29-Sep	136	AB
30-Sep	68, 134	AB
4-Oct	68, 123, 134	AB
6-Oct	50	ABD
23-Nov	130, 162	AD
24-Nov	18	ABD
25-Nov	23, 49, 52, 57, 62	AB
26-Nov	53, 60, 162	AB
27-Nov	22, 50, 125	AB
28-Nov	19, 48, 54, 130, 160	AB
29-Nov	43, 60, 126, 18(AB), 69(A)	ABD
30-Nov	24, 53	ABD
1-Dec	20, 39, 52, 137	ABD
2-Dec	38, 68, 125, 160	ABD
9-Dec	71, 137, 162(AB)	ABD
15-Dec	126, 57(AB)	ABD
16-Dec	68, 84	A
17-Dec	130, 51(AB)	ABD
22-Dec	23	AB
23-Dec	18, 61, 82, 160	ABD
25-Dec	71, 74	ABD

Table 1. Summary of TAOS long zipper data (analyzed) in 2005. (summarized by Z. W. Zhang)

鹿林天文台的紅色精靈觀測-2005 年度報告

紅色精靈研究團隊
國立成功大學物理系

成大物理系紅色精靈團隊在 2005 年所進行的高空閃電地面觀測，總觀測日數爲 26 天，其中有 19 天的觀測地點位於鹿林天文台。總計觀測到事件的天數則爲 11 天，其中在鹿林天文台的有 10 天。這 10 天當中，總共觀測到 168 個高空閃電現象，參考圖一。

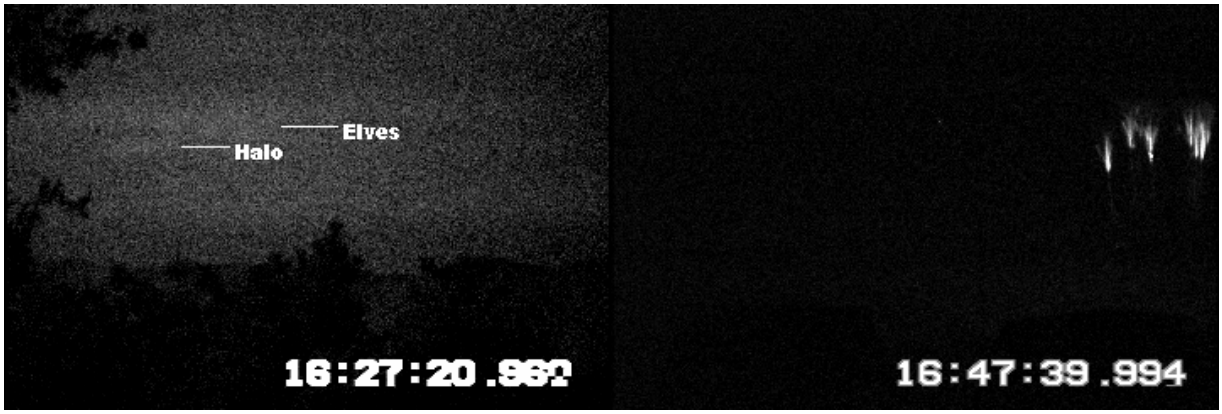

圖一：左邊是在鹿林山所攝得的 elves+halo。右邊是在鹿林山所攝得的 sprite。

以事件類型來區分，在這 168 個事件當中，以 sprite 爲最多，共有 158 個。其次爲 sprite+halo，共 6 個。另有 halo 2 個，elves 和 elves+halo 各 1 個。在所觀測的事件當中，以產生於海陸交界系統的爲最多，共 123 個。陸地系統則次之，有 43 個。海洋系統最少，只有 2 個。其中海洋系統出現單一 sprite 的比率較高, 陸地系統則以成群 sprite 的出現率較高，與歷年的觀測結果相符，參考表一。

表一、歷年所觀測到的紅色精靈，其型態與發生地點的關係。

	2001		2002		2003		2004		2005	
	有出現單一sprite的事件	有出現成群sprite的事件	有出現單一sprite的事件	有出現成群sprite的事件	有出現單一sprite的事件	有出現成群sprite的事件	有出現單一sprite的事件	有出現成群sprite的事件	有出現單一sprite的事件	有出現成群sprite的事件
海	14(77.78%)	4(22.22%)	3 (60.00%)	2 (40.00%)	35 (53.03%)	31 (46.97%)	11 (64.71%)	6 (35.29%)	3 (60.00%)	2 (40.00%)
交界	15(35.71%)	27(64.29%)	2 (100.00%)	0 (0.00%)	25 (46.30%)	29 (53.70%)	27 (24.32%)	84 (75.68%)	29 (24.17%)	91 (75.83%)
陸	0 (0.00%)	0 (0.00%)	0 (0.00%)	1 (100.00%)	3 (25.00%)	9 (75.00%)	2 (18.18%)	9 (81.82%)	8 (18.60%)	35 (81.40%)

本期計畫的主要目的是從事巨大噴流的多波段觀測與高速觀測，但是由於所觀測的天氣系統並未產生巨大噴流。因此只觀測到多波段(如圖二)與高時間解析度的紅色精靈影像。有關多波段的觀測，也因爲 sprite 的發生地點相距太遠，受大氣散射的影響，因此只觀測到紅色的影像，並未觀測到藍色波段的影像，因此無法用以探討發生 sprite 時大氣的游離層度，瞬間電子密度分佈與瞬間電場強度等物理性質。觀測結果不如往年豐富。

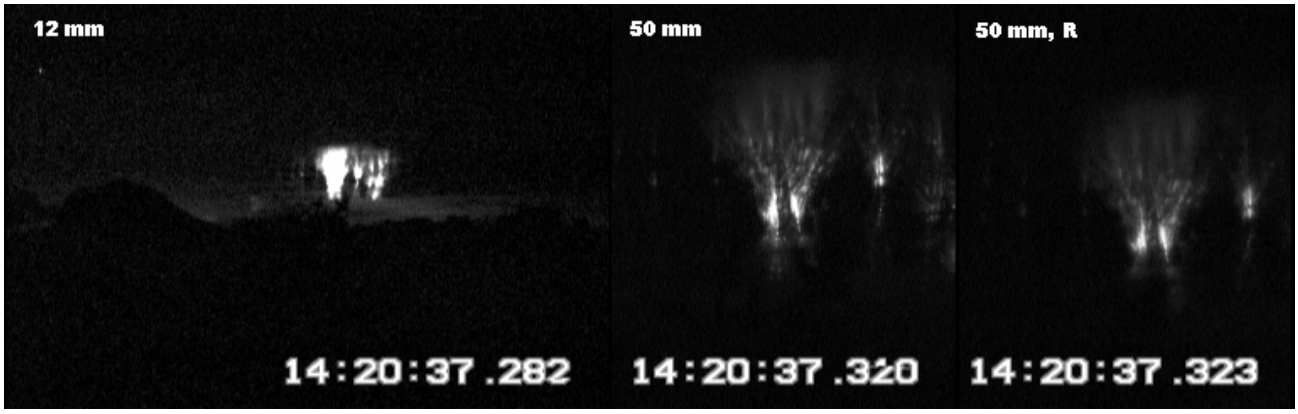

圖二：紅色精靈的多波段影像。2005 年 7 月 30 日所攝得的 sprite。由左至右，拍攝鏡頭各爲 12mm、50mm、50mm 加紅光波段濾鏡，另外加藍色波段濾鏡的攝影機並無相關的訊號。

另外，團隊也在 2005/09/09-11 兩個晚上，進行低光度光譜儀(圖三)的測試觀測。其中包含儀器的測試、星光的光譜量測，並對可能的對流胞進行紅色精靈的光譜測量。由於當時的對流系統並沒有紅色精靈，因此我們就以天狼星（Sirius）、星宿四（Alpha Orionis）當作測試的對象。所得的星光光譜測量如圖四，與已知的光譜相比較，可知除了在 550nm 以下有強烈的吸收，其餘是相當一致的。這是因爲低光度光譜儀採用穿透式的光柵稜鏡與鏡頭特性的關係。接著，我們將繼續從事低光度光譜儀的相對強度的校正，並考慮使用反射鏡來增加藍光的穿透率，但會增加光學組裝的困難。

圖三：鹿林天文台的測試低光度光譜儀。

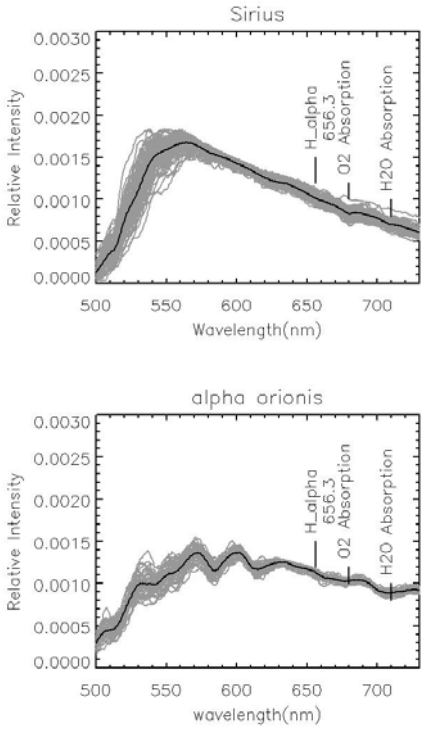

圖四：低光度光譜儀所量到的天狼星（Sirius）、星宿四（Alpha Orionis）的光譜。

Low-latitude ELF-whistlers observed in Taiwan

Yun-Ching Wang
Department of Physics, National Cheng Kung University, Tainan, Taiwan

Kaiti Wang
Division of Natural Sciences, Department of General Education, Ming Hsin University of Science and Technology, Hsin-Chu, Taiwan

Han-Tzong Su and Rue-Ron Hsu
Department of Physics, National Cheng Kung University, Tainan, Taiwan

Received 11 January 2005; revised 19 March 2005; accepted 25 March 2005; published 23 April 2005.

[1] Detections of ELF whistler-like events at a low latitude location are reported. Events with frequencies between 60 and 100 Hz were recorded by the ELF station at the Lulin Observatory in Taiwan from August 26, 2003 to July 13, 2004. The most distinguished feature for these events is the frequency descent in the frequency-time spectrograms, resembling terrestrial whistlers. Other notable features include (a) a long event duration averaging up to two minutes, (b) a daytime diurnal maximum occurring around 10 am, (c) a dominant magnetic field polarization in the north-south direction with strength of a few to tens of pT, and (d) no detection of vertical electric fields. Similar events were only reported twice for the past thirty years: one at an auroral latitude site in Alaska and the other at a mid-latitude site in California. Possible source mechanisms including magnetosheath lion roars and lightning-generated whistlers are discussed. **Citation:** Wang, Y.-C., K. Wang, H.-T. Su, and R.-R. Hsu (2005), Low-latitude ELF-whistlers observed in Taiwan, *Geophys. Res. Lett.*, *32*, L08102, doi:10.1029/2005GL022412.

1. Introduction

[2] Observations of lightning-generated whistlers by satellites and ground stations showed that the detected frequency for terrestrial whistlers ranges from about 2 kHz to 10 kHz, with peak occurrence around 5 kHz [*Helliwell*, 1965]. Based on the data acquired in this type of studies, *Heacock* [1974] and *Sentman and Ehring* [1994] reported detections of whistler-like events at much lower frequencies between 60 to 200 Hz in the ELF band. Heacock's measurements were made in Alaska (65°N, 256°E, geomagnetic) at high latitude. These events were detected to possess a frequency range similar to lion roars observed in the magnetosheath [*Smith et al.*, 1967, 1969], but their spectral forms are quite different [*Heacock*, 1974]. Sentman and Ehring's measurements were made in California (34.4°N, 117.7°W) at mid-latitude. They called these events ELF-whistlers and remarked that the most probable interpretation would be whistler-mode waves of magnetosheath lion roars entering into the ionosphere. Both studies ruled out lightning-generated whistlers as a source because the observed dispersions cannot be accounted for under normal plasma environmental conditions.

[3] In this paper, we report the first low-latitude observations of ELF-whistler events at Lulin Observatory in Taiwan. These events are similar to those observed previously at high and middle latitudes by *Heacock* [1974] and *Sentman and Ehring* [1994].

2. Instruments and Observations

[4] In this study, both electric and magnetic ELF antennas were used. The ELF magnetic field antenna (EMI-BF4) was located at Lulin Observatory (23.47°N, 120.87°E; 2862 m) in the Yu-Shan National Park, Taiwan. This site was built far away from residential and industrial regions to reduce background noises. The antenna is in operation since August, 2003. The range of receiving frequency is from 1 Hz to 200 Hz and notch-filtered at both 60 Hz and 120 Hz. The response of the receiver drops below 10% for signals with frequencies higher than 100 Hz. The signals were sampled by a 16-bit A/D converter at a rate of 400 Hz. Both north-south (H) and east-west (D) components of magnetic fields on the horizontal plane were measured.

[5] The 60-meter long wire ELF electric field antenna was constructed at National Cheng Kung University (23.00°N, 120.22°E, 32 m) about 100 km south of Lulin. The preamplifier has a gain of 100 and 50 dB notch filters at 60 and 120 Hz. The system receives electric fields at the same frequency range as the magnetic ELF system by using the same signal condition and notch filtering module. The electric ELF antenna only measured fields in the local vertical direction, same as that of *Sentman and Ehring* [1994].

[6] Whistler-like events were recorded between 26 August 2003 and 13 July 2004. Figure 1 shows examples of events in the frequency-time (*f*-*t*) spectrograms that were assembled from the recorded signals. The H and D components of magnetic fields are plotted on the top and the bottom panels, respectively. The color bar on the right represents the scale of intensity in dB. On these spectrograms, two background features should be noted: periodically-occurring horizontal signals with stronger intensities at lower frequencies (<40 Hz) are from Schumann resonances; vertical fine, enhanced signals covering almost all frequencies often come from global lightning. In Figures 1a

0094-8276/05/2005GL022412$05.00

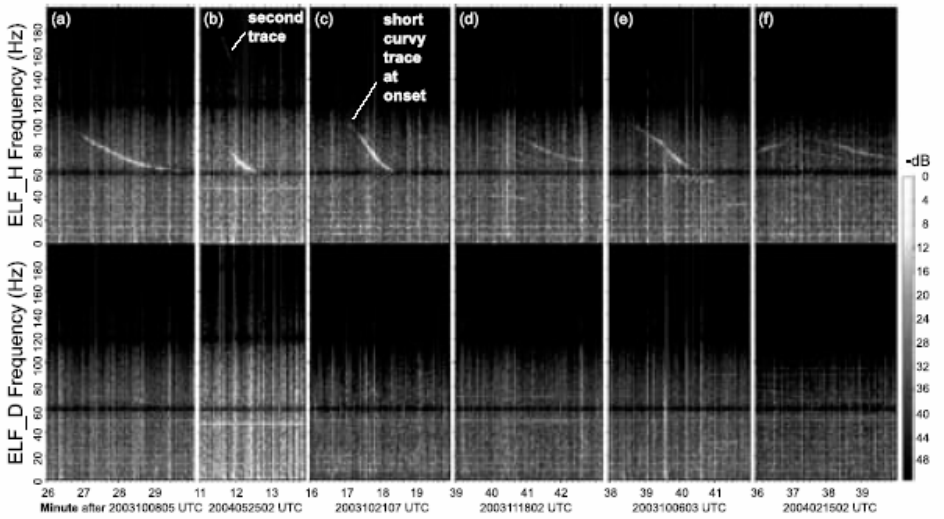

Figure 1. (a) A type-I ELF-whistler, (b) a type-I ELF-whistler containing two traces of signals between 60–100 Hz and 150–180 Hz, (c) a type-II ELF-whistler, (d) a multi-trace type-II ELF-whistler, (e) a type-III ELF-whistler, and (f) a multi-trace type-II ELF-whistler. A short curvy trace at onset distinguishes the type-II ELF-whistler from the type-I. There are no discernible signals in the magnetic east-west direction (ELF_D) for the events depicted in Figures 1a, 1b, 1e and 1f.

and 1b, the brightest-colored event traces resemble conventional lightning-generated "whistlers" patterns: descendent frequencies with increasing time. In addition to the classical or the type-I ELF "whistlers", other types of patterns were also found. Figures 1c and 1d demonstrate the type-II ELF-whistlers, which basically are "type-I whistlers" but with a short curvy trace at onset. This type of events were also appeared in the spectrograms of *Heacock* [1974] and *Sentman and Ehring* [1994] but were not specifically indicated therein. Figures 1e and 1f illustrate the type-III ELF whistlers with signal traces like the silhouettes of "mountains", with an ascending trace, a crest, and a descending trace. There are cases of these three types of events but containing two or more signal traces as shown in Figures 1b, 1d and 1f. In all, 296 such events around 60 to 100 Hz were detected during the observation period. Among them, 135 events are classified as "type-I" ELF-whistlers, 125 are "type-II", and 36 are "type-III".

[7] In addition to events between 60 and 100 Hz, there were also single-trace events with frequencies ranging from 30 to 40 Hz. This type of low-frequency events were also reported by *Heacock* [1974]. Since our data contains only 23 of these low-frequency events, therefore, the following analysis is based on the 296 events occurred between 60 and 100 Hz. Their frequencies, durations, fields, occurrence times are analyzed.

3. Data Analysis

[8] In our ELF events, the average lower cutoff frequency is 62 Hz, and the upper cutoff frequency is 94 Hz. Whereas for *Heacock* [1974] and *Sentman and Ehring* [1994], their observed frequencies reached up to 200 Hz. Since our instruments are less responsive above 100 Hz, the existence of signals with frequencies extending up to 200 Hz cannot be excluded. A comparison chart for the key results from *Heacock* [1974], *Sentman and Ehring* [1994], and this paper can be found in Table 1.

[9] Time durations for these detected events range from 40 seconds to 5 minutes. The average duration is 124 seconds, longer than those in previous studies which were around 40 s to 1.5 minutes. For comparison, the duration of whistlers observed on Earth typically lasts a few seconds. All dispersions shown in these signals exhibit no echoes, same as previous two reports. There are 69 events exhibiting multi-trace, approximately 23% of the total events. These multi-trace events can also be found in the work by *Heacock* [1974].

Table 1. Comparisons of ELF-Whistlers Observations at Different Locations

Data Source	*Heacock* [1974]	*Sentman and Ehring* [1994]	This Work
Geographic Location	auroral latitude 65°N	midlatitude 34°N	low latitude 23.5°N (λ_m = 18°N)
Frequency	40–200 Hz	60–180 Hz	60–100 Hz
Duration	40 s–1.5 mins	40 s–1.5 mins	40 s–5 mins
Dispersion	no echoes	no echoes	no echoes
Local Time	daytime maximum	daytime maximum	daytime maximum
Amplitude	a few pT	1–20 pT $Hz^{-1/2}$	a few pT to 70 pT
Magnetic Field	E-W	E-W	N-S
Vertical Electric Field	No measurement	Null	Null
Correlation with Ap	anticorrelated	insufficient samples	not obvious

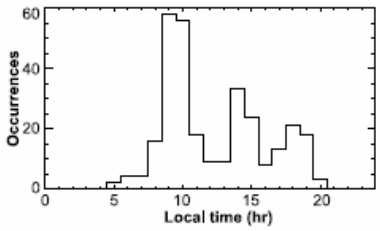

Figure 2. Events occurrence vs. local time. Note that all events occurred between 6 am to 8 pm.

[10] All 296 events possess the H component of magnetic fields, and 137 events also possess a weak D component. Therefore, the observed signals have linear polarizations dominated by north-south directions. Previous observations in Alaska and California showed linear polarization in E-W direction, probably due to variations of local geomagnetic field directions. As to electric fields, no distinguishable signals in the local vertical direction were detected for these events. This is similar to features observed by *Sentman and Ehring* [1994] in which the vertical electric fields weren't detected either.

[11] Figures 2, 3, and 4 show the statistical graphs for these events. The relation between event occurrences time vs. local time is plotted in Figure 2. Please note that all events occurred between 6 am to 8 pm, consistent with previous observations in which occurrences were detected only at local daytime. The peak occurrence happened at around 9 to 10 am, about 3 hours earlier than previous observations. There is also a very clear night to dawn gap, the same as that of *Heacock* [1974] and *Sentman and Ehring* [1994]. There are also another two distinguished peaks occurring at local time around 2–3 pm and 6–7 pm, which were not reported in previous studies.

[12] Figure 3 shows the relation between occurrence and A_p index. *Sentman and Ehring* [1994] mentioned that there was no strong correlation on the base of fewer observations. However, *Heacock* [1974] showed anti-correlations between A_p index and occurrences. Most events occurred at quiet ($A_p < 29$) and minor storm times ($29 < A_p < 50$). Only one event occurred at major storm time with $A_p = 70$, but it has the same features as signals detected at other times. Figure 4 shows event durations vs. A_p index. The upper limit of event durations tends to decrease at greater value of A_p, which is a feature not reported in previous studies.

[13] Please note that even though we categorize these events into three patterns, their statistical characteristics such as frequency range, occurrence time, correlation with A_p index, durations are fundamentally similar. There is no unique or distinctive feature can be found for any of these patterns.

4. Discussions

[14] Striking similarities between our observed ELF events and those recorded in previous studies on frequency ranges, daytime occurrences, wave field strengths, linear polarizations, long durations, and signal patterns on *f-t* spectrograms have suggested that they should have been generated from the same source mechanism. Whistler-mode waves were believed to be the most possible wave modes. Two probable source mechanisms, magnetosheath lion roars and lightning-generated whistlers, are discussed.

[15] Magnetosheath lion roars were found to have frequencies below 120 Hz, field strengths of ~0.1 nT and signal duration of ~1s [*Smith et al.*, 1967, 1969; *Smith and Tsurutani*, 1976; *Tsurutani et al.*, 1982; *Zhang et al.*, 1998; *Baumjohann et al.*, 1999]. Basing on frequency ranges and dayside occurrence of the observed ELF-whistlers, *Sentman and Ehring* [1994] suggested they were induced by lion roars that entered the Earth-ionosphere waveguide.

[16] However, the lion roar emission is incoherent and contains a band of frequencies, whereas the ELF-whistlers observed on the ground are very narrow-banded and coherent. It is unclear that how magnetosheath lion roars could be converted into the ELF-whistlers. Furthermore *Smith and Tsurutani* [1976] had shown that the percentage of occurrences for lion roars increases as storm index Kp increases. In our data, the correlation between occurrence percentages of ELF-whistlers and Kp are not as evident as that in the lion roars studied. All these imply that if lion roars are indeed the source, some unknown processes may need to be considered.

[17] Previous studies had questioned how lightning-generated whistlers could generate ELF events with such a long durations and dispersions. The average dispersion *D* of Lulin events is 5500 sec $Hz^{1/2}$, whereas the dispersion for lightning whistlers observed on Earth ranges from 12 to 400 sec $Hz^{1/2}$ [*Helliwell*, 1965]. To metamorphose the

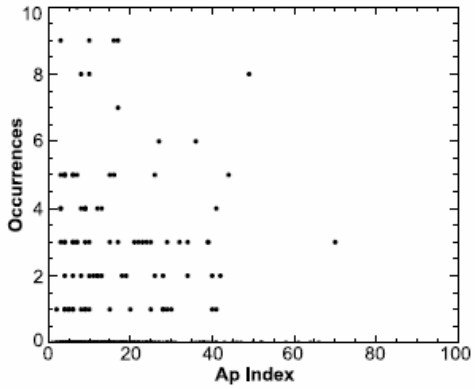

Figure 3. Occurrences vs. Ap Index.

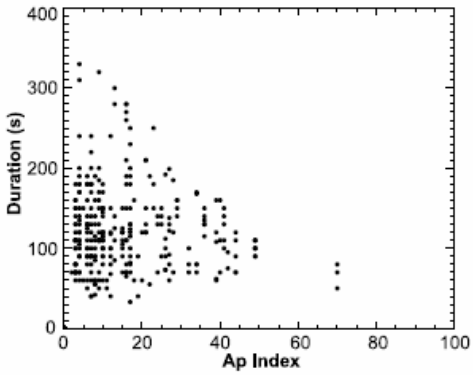

Figure 4. Event duration vs. A_p index.

lightning-generated whistlers into the observed ELF-whistlers, a long propagation path is required for the dispersion to accumulate. Here we examine a mechanism which was suggested to generate the very-long-dispersion whistlers ($D > 26000$ sec $Hz^{1/2}$) observed near Neptune by Voyager 2 [*Gurnett et al.*, 1990]. The constraint of total path l needed to produce the ELF-whistlers can be estimated basing on field-aligned propagation [*Gurnett et al.*, 1990]:

$$l = 2c\frac{f_c^{1/2}}{f_p}D.$$

Where f_c is electron cyclotron frequency, f_p is plasma frequency, and c is the light speed. They are all assumed to be constant.

[18] The magnetic L-shell for our station is 1.09 derived from IGRF field model with Earth radius (R_e) 6371 km. The geomagnetic latitude and longitude are 16.76° and 192.73°, respectively. The field line length S corresponds to $L = 1.09$ can be estimated from $S = R_e(2.76L - 2)$ [*Volland*, 1984] to be $1.0084R_e$. The field line completely sinks in the ionosphere so that the electron density is assumed to be $10^5/cm^3$. Using f_c derived from the weakest field strength of 0.300 Gauss to the strongest field strength of 0.446 Gauss at this field line, l is deduced to range from 166 R_e to 202 R_e, corresponding to 83 to 101 times of the back-and-forth bounce motion along the field line. However in this propagation pathway, highly-dispersed ELF-whistler echoes are expected in *f-t* spectrograms. The observed ELF events at Lulin, contain no echoes, and hence are not likely to be formed from whistlers bouncing along the same field line.

[19] Alternatively, the ELF-whistlers may be generated from non-ducted whistlers propagated from other longitudes with azimuthal crossing as suggested by *Gurnett et al.* [1990]. The whistlers propagate in a zigzag fashion reaching required path length l, accumulating dispersion via repetitively-integrated electron densities. However, besides needing to perform a large numbers of hops in the plasmasphere that was never observed, it is not clear how these whistlers could re-enter the Earth-ionosphere waveguide; because they are very oblique and cannot be easily trapped in a duct. Hence, for the lightning-generated whistlers to undergo the mode conversion into the observed ELF-whistlers, some exotic processes may be needed for them to happen.

[20] *Heacock* [1974] indicated a reason that these events were only detected in Alaska probably was due to low latitudes of other sites. Nevertheless, this type of events was detected at a lower latitude site in California, and now was observed in Taiwan as well. Recently, similar ELF emissions were also detected at Antarctica during January of 2004 [*Kim et al.*, 2004]. Therefore, the low frequency and long dispersed ELF-whistlers maybe widely distribute across the globe. As for the source mechanisms, magnetosheath lion roars, field line bouncing and non-ducted whistlers all have great deficits and likely are not the sources of the ELF-whistlers. Further study has been taken to elucidate the multi-ion effects of the ionosphere on the whistlers, and the potential role of the multi-ion plasma in converting lightning-generated whistlers into the observed ELF-whistlers. We hope that the work reported here could invoke the interest of other ELF researchers and contribute their effort in resolving the mysterious ELF-whistlers, after thirty years since their first detection.

[21] **Acknowledgments.** Yun-Ching Wang and Kaiti Wang contributed equally to this work. The authors thank Drs. D. D. Sentman, L. C. Lee, W. S. Kurth, H. C. Yeh, C. H. Lin, Y. H. Yang, and R. M. Thorne for the valuable discussions. We thank the Lulin Observatory, National Central University for hosting our ELF station and for logistic supports. Assistance from S. C. Wang, H. F. Rong, Y. H. Lin, P. J. Yang, J. Y. Lee, and R. I. Oyang are gratefully acknowledged. This work was supported in part by research grants NSC93-2111-M-159-001, 93-NSPO(B)-ISUAL-FA09-01, NSC93-2112-M-006-007, and NSC93-2111-M-006-001.

References

Baumjohann, W., R. A. Treumann, E. Georgescu, G. Haerendel, K.-H. Fornacon, and U. Auster (1999), Waveform and packet structure of lion roars, *Ann. Geophys.*, *17*, 1528.

Gurnett, D. A., W. S. Kurth, I. H. Cairns, and L. J. Granroth (1990), Whistlers in Neptune's magnetosphere: Evidence of atmospheric lightning, *J. Geophys. Res.*, *95*, 20,967.

Heacock, R. R. (1974), Whistler-like pulsation events in the frequency range 20–200 Hz, *Geophys. Res. Lett.*, *1*, 77.

Helliwell, R. A. (1965), *Whistlers and Related Ionospheric Phenomena*, Stanford Univ. Press, Stanford, Calif.

Kim, H., M. R. Lessard, J. LaBelle, J. R. Johnson, and A. T. Weatherwax (2004), Observations of narrow-band 60–100 Hz waves at high auroral latitudes, *Eos Trans. AGU*, *85*(47), Fall Meet. Suppl., Abstract SM23A-0464.

Sentman, D. D., and D. A. Ehring (1994), Midlatitude detection of ELF whistlers, *J. Geophys. Res.*, *99*, 2183.

Smith, E. J., and B. T. Tsurutani (1976), Magnetosheath lion roars, *J. Geophys. Res.*, *81*, 2261.

Smith, E. J., R. E. Holtzer, M. G. Mcleod, and C. T. Russell (1967), Magnetic noise in the magnetosheath in the frequency range 3–300 Hz, *J. Geophys. Res.*, *72*, 4803.

Smith, E. J., R. E. Holzer, and C. T. Russell (1969), Magnetic emissions in the magnetosheath at frequencies near 100 Hz, *J. Geophys. Res.*, *74*, 3027.

Tsurutani, B. T., E. J. Smith, R. R. Anderson, K. W. Ogilivie, J. D. Scudder, D. N. Baker, and S. J. Bame (1982), Lion roars and nonoscillatory drift mirror waves in the magnetosheath, *J. Geophys. Res.*, *87*, 6060.

Volland, H. (1984), *Atmospheric Electrodynamics*, Springer, New York.

Zhang, Y., H. Matsumoto, and H. Kojima (1998), Lion roars in the magnetosheath: The Geotail observations, *J. Geophys. Res.*, *103*, 4615.

R.-R. Hsu, H.-T. Su, and Y.-C. Wang, Department of Physics, National Cheng Kung University, Tainan 70101, Taiwan.

K. Wang, Division of Natural Sciences, Department of General Education, Ming Hsin University of Science and Technology, Hsin-Chu County 30401, Taiwan. (ktwang@must.edu.tw)

整合性中尺度環境評估系統子計畫三--亞洲環境背景站

林能暉教授 國立中央大學大氣物理研究所
李崇德教授 國立中央大學環境工程研究所
王家麟教授 國立中央大學化學系

1. 計畫目的

近年來亞洲地區大氣污染物(包含酸性物染物、亞洲沙塵、生質燃燒、有害物質)對台灣的長程輸送已受到相當廣泛的注意，每當沙塵暴、生質燃燒或酸雨發生時，均受到民眾普遍重視與關切。除了台灣之空氣品質受到衝擊外，亦可能會導致區域環境與氣候衝擊。

臺灣位處於亞洲大陸東南隅，由氣候條件看，大範圍氣象條件很容易將上游亞洲之污染物輸送到臺灣的上空。亞洲酸雨現象隨工業化與經濟成長而日漸顯著，致酸因子硫酸鹽與硝酸鹽長程傳送過程中產生之雲雨交互作用、輻射效應等，不但對局部降水產生影響，更對區域輻射平衡有一定的干擾。此外，最近幾年臺灣空氣品質幾次急遽惡化就與中國沙塵暴南移至臺灣附近有關，因此相關研究逐漸受到各界的重視。而近幾年來「大氣褐雲」，亦受到國際科學界的重視，除大量生質燃燒，導致於溫室氣體增加，加速全球變暖外，霾害產生的煙霧，飄散到大氣中，直接影響雲內的成分，或直接反射太陽光，造成到達地面的太陽輻射減少，因而影響全球輻射效應，使得地面的溫度及海溫降低，改變區域氣候特性。

東南亞與南亞所排放的生質燃燒量相當驚人，僅次於南美洲和非洲，這些排放物很有可能產生臭氧或臭氧前驅物長程輸送至下游地區，造成高臭氧值，台灣南部有時會發生高污染日，可能與東南亞霾害之低層傳送有關。

我國正好位於東亞大氣污染物下風處及南亞生質燃燒傳送路徑之下風處，過去環保署雖在全國設置超過 76 個採樣之監測站，但多為代表地區性之特性，目前仍無代表一區域型之觀測地點，因此在若干境外污染物傳送影響之議題上，常受到地區性污染物干擾，採樣分析的結果往往難以量化受境外影響之程度。相對的，考量中部高山乃為大氣背景站之絕佳之觀測點。

事實上，亞洲大氣污染物長程傳送對台灣已形成相當衝擊，其對區域環境與氣候干擾亦可能間接影響台灣。國科會卓越計畫支持本研究團隊與環保署合作興建鹿林前山大氣背景站，測站完成後，進行持續性的觀測實驗，探討亞洲大氣污染物之長程輸送與其對區域環境及氣候衝擊。

2. 實驗內容

PM_{10} 懸浮微粒採樣

ANDERSEN Dichotomous 的採樣儀器裝設 37mm 的濾紙採樣，濾紙使用配置為兩張鐵氟龍濾紙 (PM_{10} 與 $PM_{2.5}$) 或是兩張石英濾紙 (PM_{10} 與 $PM_{2.5}$)，以進行後續的化學分析。左旋葡萄聚糖(levoglucosan)、甘露聚糖(mannosan)、半乳聚糖 (galactosan)為植物纖維素燃燒微粒的特徵成分，分析這些成分對於生質燃燒微粒能掌握其影響程度。

降水化學觀測

設置酸雨採樣器，當降水發生時，採樣器自動採樣，天文站人員協助每週二上午九時固定收集累積一週之雨水，分瓶後保存至冰箱，經宅配送回中大實驗室進行離子成份分析。由雨水中化學成份可以進一步探討其污染來源。

微量氣體分析

目前進行不定期 CO 量測，以了解此背景大氣成份，以及其伴隨南亞生質燃燒傳至台灣情形。未來將陸續增加 CFCs、O_3、CO_2 等量測，以監測區域溫室氣體與污染排放。

3. 國際合作

美國 NASA 戈達中心於 2005 年 5 月至 2008 年 4 月進行東南亞生質燃燒國際觀測計畫(Biomass-burning Aerosols in South East-Asia：Smoke Impact Assessment, BASE-Asia)，結合地面監測、飛機觀測、衛星遙測技術以量化東南亞生質燃燒所產生之氣膠、溫室效應氣

體，及其他污染物的排放清冊，及其在源與匯之物理與化學特性，並探討其在長程傳送過程的變化情形。該計畫邀請泰國、寮國、柬埔寨、越南、香港、中國及台灣等在煙塵傳送路徑上的國家參與觀測實驗，共同建構完整的資料庫，並發展區域大氣化學模式，進一步了解其對區域氣候與環境的衝擊。

本研究團隊則延伸我們的興趣與研究項目以與 BASE-Asia 合作，並提出中部鹿林前山的大氣化學觀測。吾人負責強化在大氣氣膠的觀測、雲及降水化學的觀測，以及大氣環境場的氣流預測與分析，以提供實驗時機(2-5 月間)及事件日的判斷。樣本化學分析及相關物理量測(如輻射)則有助於我們了解生質燃燒經由源區排放後的特性變化。

4. 鹿林大氣背景站建置

鹿林大氣背景站(Lulin Atmospheric Background Station, LABS)之建置乃為環保署重大施政建設，經報行政院核准設置，並規劃配合外交部科技外交，列入參與聯合國地球觀測整合系統(Earth Observing System of Systems, EOSS)之敲門磚。本團隊則獲得國科會卓越計畫支持高階儀器與科學研究，環保署則出資興建背景站及基本觀測儀器，以及未來維護運轉。中央大學與環保署簽署備忘錄，進行十年合作，期能發展此東南亞最高大氣背景站，與國際接軌，並納入聯合國觀測系統。測站主體已於 2005 年 12 月完成，正待電力、通訊、採樣管線整合，預計 2006 年 2 月底完工，4 月正式啟動。

LELIS at Lu-Lin

LELIS : Lu-Lin Emission Line Imaging Survey

W.-H. Sun (孫維新), B.-W. Wang (王斌威), C.-C. Liu (劉治軍)
Y.-W. Cheng (鄭以文), H.-H. Ma (馬學輝), H.-Y. Mong (蒙宏堯)

We have established a narrow-band, wide-field imaging system to survey the northern sky in 3 major emission lines, H_α、[OIII]，and [SII], at the Lu-Lin Observatory since 2004. This survey will provide a comprehensive database for various studies of Interstellar Medium (ISM), such as supernova remnants (SNRs), planetary nebulae (PNe), star formation regions (SFRs), and HII regions.

In the year of 2005, we have replaced the FLI CCD cameras with the more reliable ST-10XME CCDs which, when combined with the new 400mm/F2.8 camera lens, give a field of view of 3 x 2 square degrees. To carry out a systematic calibration, we carried out observing runs using the 2.16m telescope at the Xinglong station of the National Astronomy Observatory near Beijing in March and September, 2005, to obtain spectra of a sample of PNe and white dwarfs, in order to obtain standards for both line and continuum observations.

In the preliminary phase, we have obtained 3-color images for a number of emission nebulae, such as the Rosette, and the head portion of the Orion constellation. As to the flat-fielding, we have accumulated both twilight and night sky flats. To remove the large-scale gradient of the sky brightness, we have carried out a self-consistent division. Since the filed of view is less than the previous setting of 7.2 by 7.2 square degree, the large scale inhomogeneity is not severe. In addition to the ISM studies, we have also obtained 3-color images of the nearby large galaxies, such as M31. Attached please find the images of M31 and North America Nebula in various wavebands.

Figure 1. 在 [OIII] 波段，對「北美洲星雲」十分鐘的曝光影像。

Figure 2. 在 [SII] 波段，對「北美洲星雲」十分鐘的曝光影像。

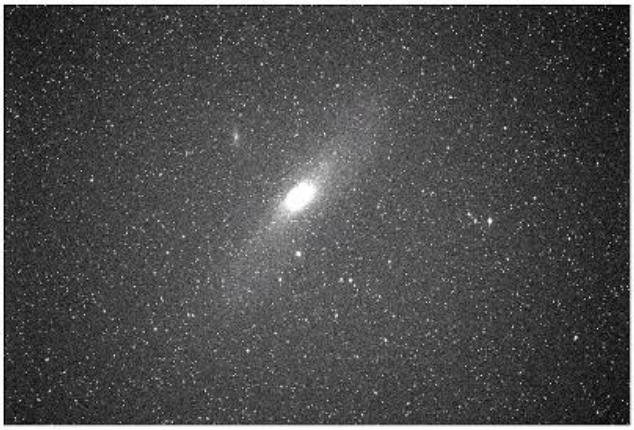

Figure 3. 在 [SII] 波段，對 M31「仙女座大星系」十分鐘的曝光影像（未處理）。

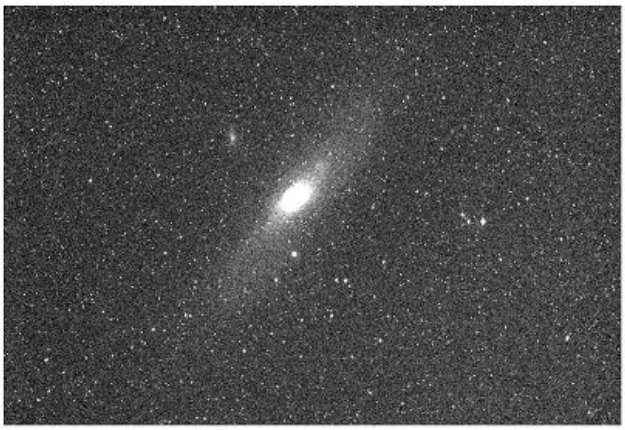

Figure 4. 在 [SII] 波段，對 M31「仙女座大星系」十分鐘的曝光影像（經影像校正）。

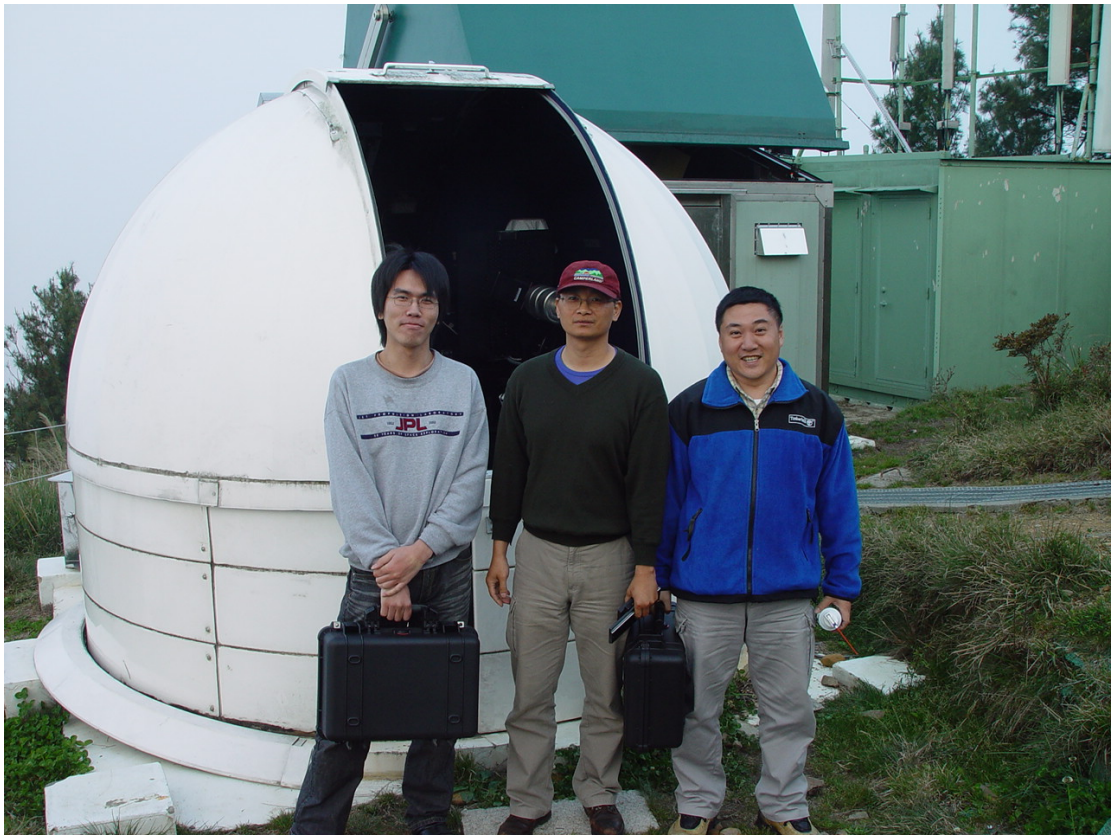

Figure 5. 三位專任助理在 LELIS 圓頂前，由左至右爲王斌威、劉治軍，和馬學輝。

This page intentionally left blank.

工作報告

基地統計資料及儀器設施報告

林宏欽、張明新、張永欣、吳宇立、林啓生

鹿林天文台的一米望遠鏡經過 3 年的運作後，已進入穩定期，累積大量的觀測資料，科學成果產出亦隨著資料的累積、國際合作擴增而逐漸增多。在基地內今年還新建了由環保署與中央大氣物理所合作設置的空氣背景監測站，預計 2006 年春季可以正式開始運作，比起目前以臨時架設進行的採樣方式，將可提昇採樣的品質與時間涵蓋範圍。紅色精靈的地面觀測也計劃在鹿林增設自動觀測系統，顯示鹿林已是國內高山地區的重要科學研究基地。以下就鹿林天文台在 2005 年的一些統計數字、基礎設施改進、增加的觀測儀器、人員營運狀況以及未來規劃提出總結報告。

觀測統計

藉由 LOT 觀測者填寫之觀測回報，可以約略統計出總觀測時數，2005 年總計有效觀測時數約 1,655 個小時，若以平均每天 10 小時觀測時數計，可觀測天數約爲 165 天，對照 2003 年總觀測時數 1,738 小時、2004 年總觀測時數 1,756 小時，2005 年的觀測時數少了近 100 小時，12 月的觀測時數明顯較前兩年低了許多，因爲該月連續五波的冷氣團鋒面南下，爲台灣地區帶來不少水氣及降雨，鹿林雖然降雨不多，但雲霧籠罩的情況較往年晴朗乾冷的型態爲多，使觀測時數大幅降低。下圖爲 2003 年至 2005 年的每月觀測時數統計

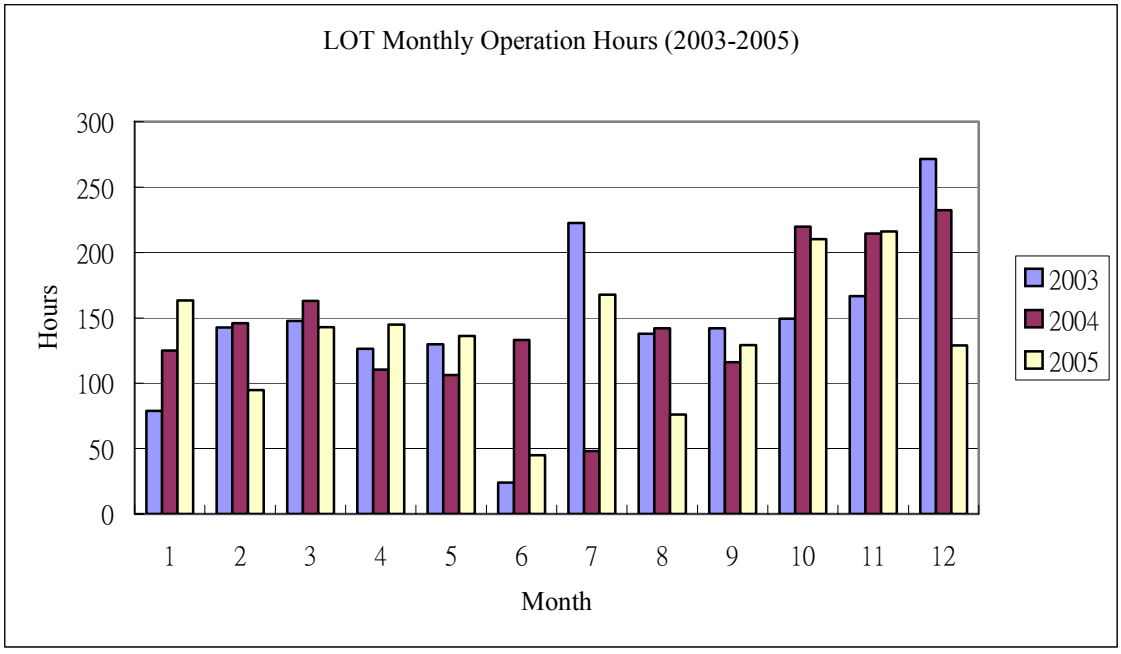

由於目前觀測回報的統計數字是由觀測者自行填寫，難免會有誤填或補填錯誤的情況，且簡單的觀測時數統計和實際的觀測情況會有落差，爲使統計能更爲精準及自動化，未來擬建立視相監測儀、水氣儀等自動化的監測設備，能夠確實對天文台的視相值、水氣含量等有長期客觀的測量。

氣象資料統計(2003-2005)

CAMPBELL 自動氣象站原設於玉山西峰供 TAOS 計畫資料收集之用，2002 年中遷到鹿林天文台，目前鹿林較完整的氣象紀錄從 2002d351 開始。2005 年 3 月(2005d66)增設溫濕度計，始有濕度記錄。2005 年底在同一氣象竿上新增了 DAVIS Vantage Pro2 氣象站，提供即時氣象上網。

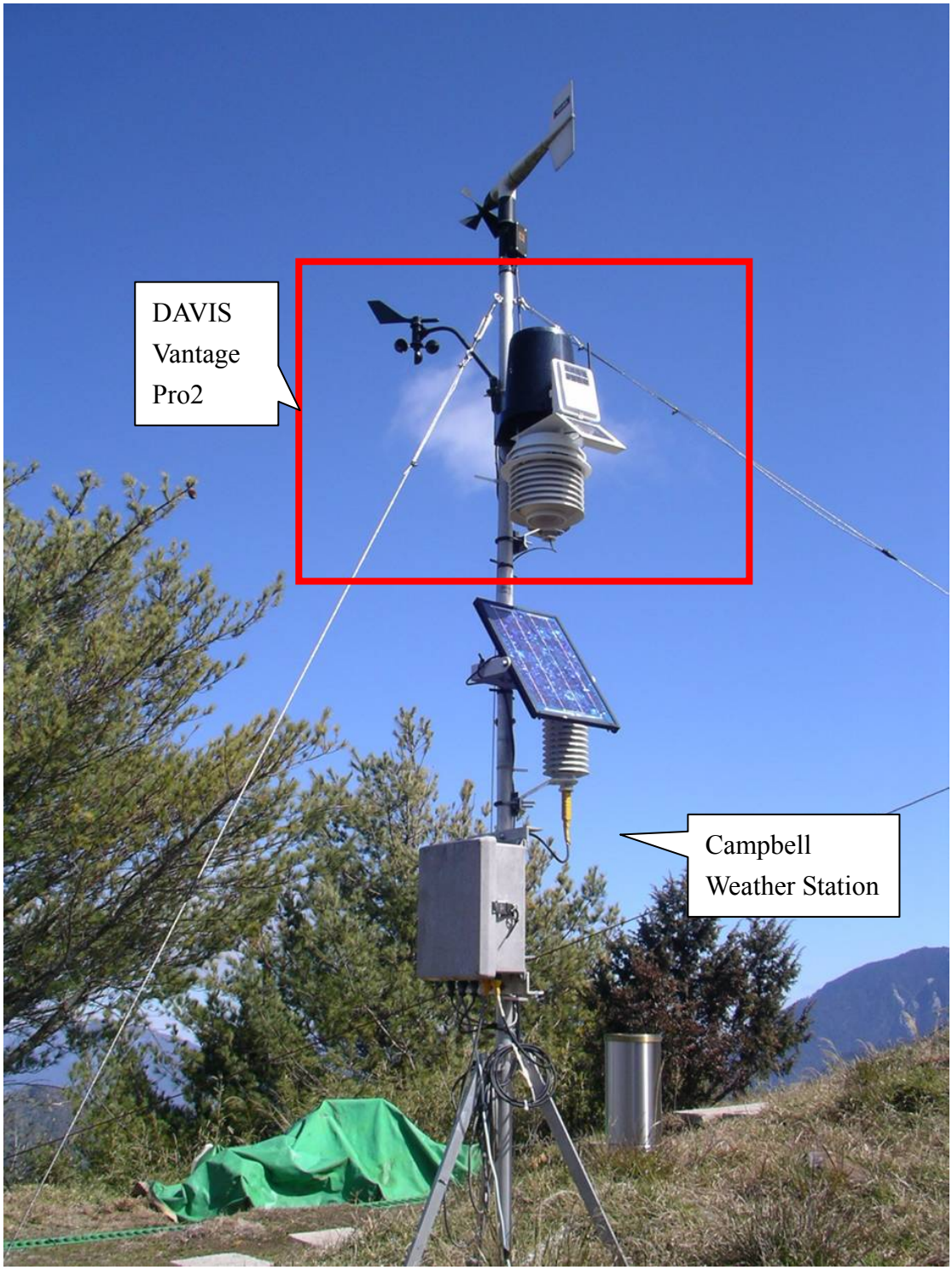

鹿林天文台 CAMPBELL 自動氣象站與 DAVIS Vantage Pro2 氣象站(紅框內)

氣象站設置位置

據 CAMPBELL 氣象站 2003-2005 三年資料紀錄，統計圖示如下：

a.溫度

- 最高溫出現在白天中午前後
- 最低溫出現在下半夜凌晨
- 夏季溫度介於 10～25℃之間
- 冬季溫度介於 0～10℃之間
- 冬夏溫差約 10℃
- 每年 12 月到翌年 2 月間最冷，最低溫可低到零下

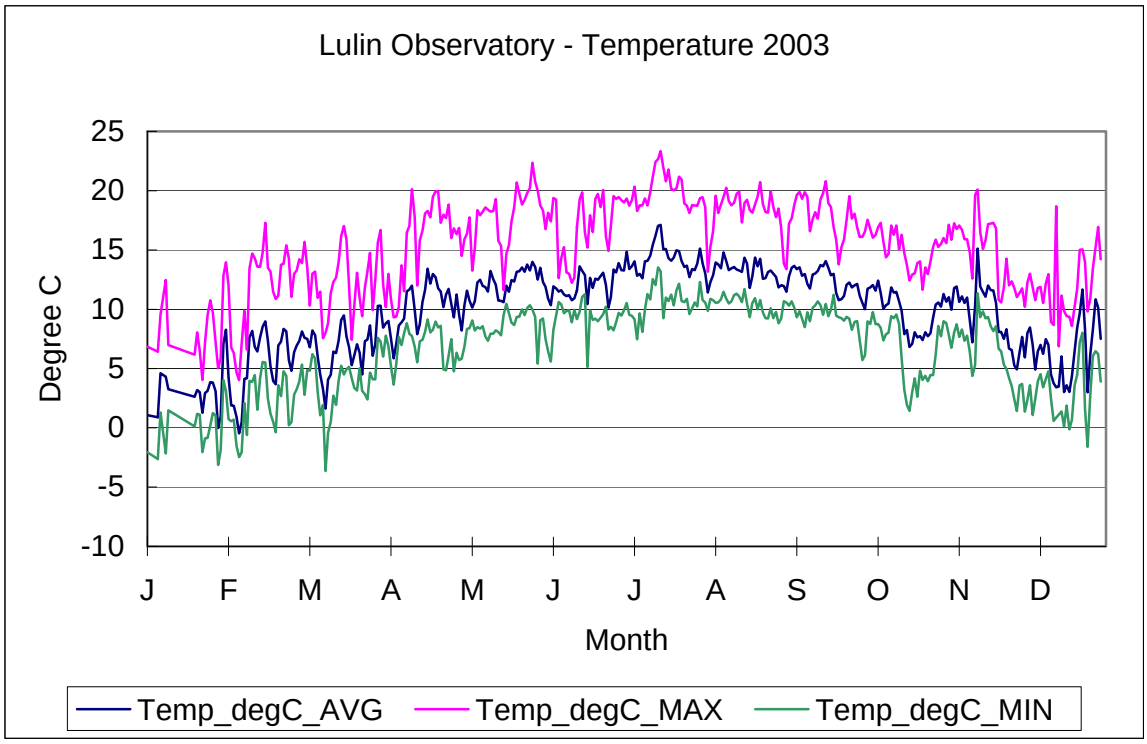

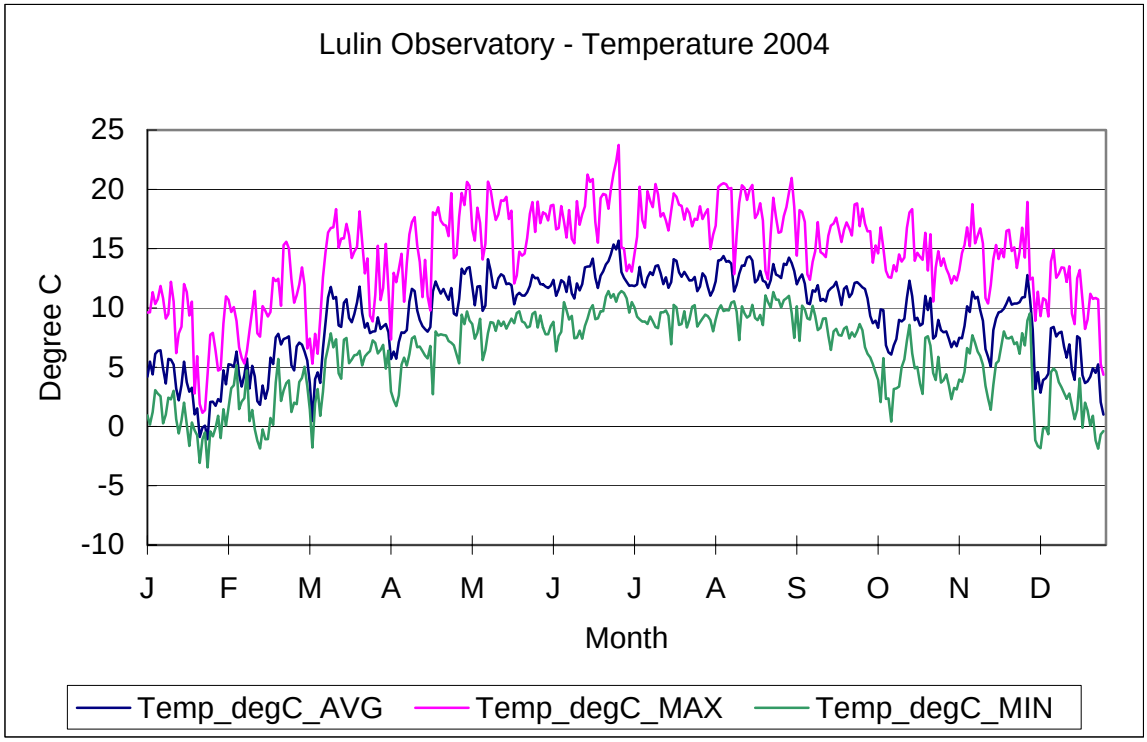

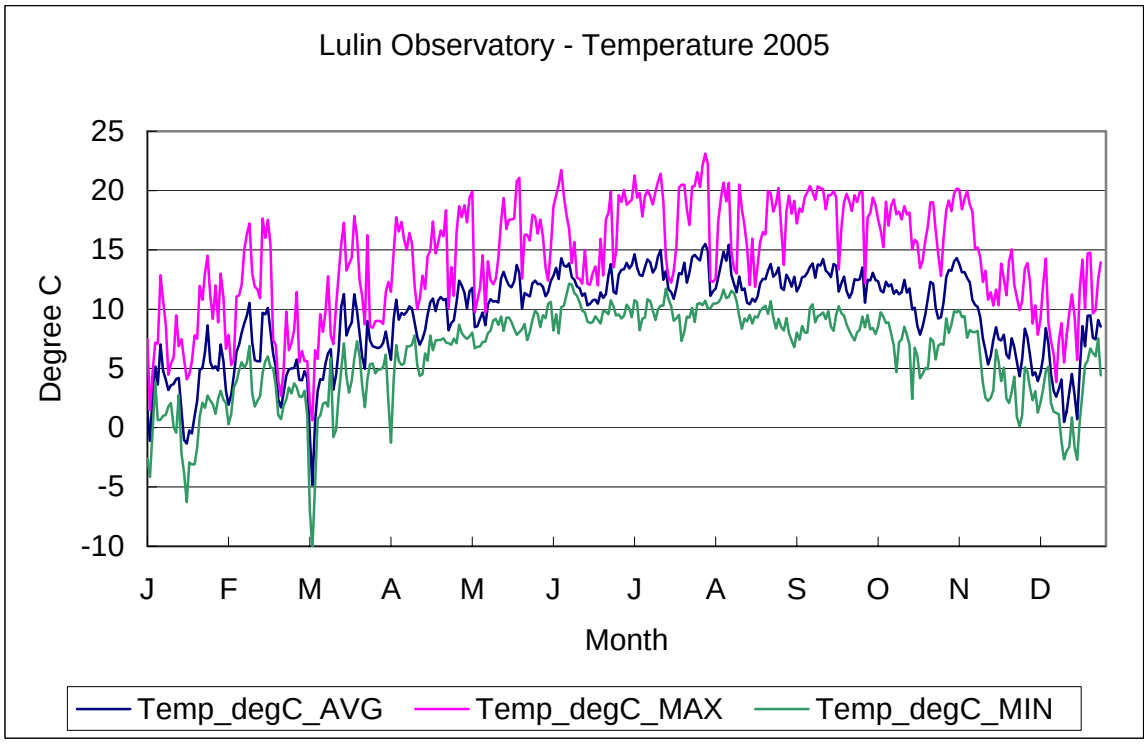

*2005 年 3 月 4 日罕見的大雪，溫度陡降至 -10℃以下，雪經過一週才完全融化

b.風

風速計的設置高度離地面僅約 2 公尺，遠低於設置標準（離地 10-20 公尺），且位於鹿林前山山頂山坳之間，受附近地形影響，故風速一般偏低，又受附近山谷間上升氣流影響，有時記錄到的風向與山區大範圍的風不同，所以風向變化僅供參考

- 鹿林天文台終年吹西南風，即使冬季亦然，僅偶有其它方向的風
- 除颱風期間外，最大風速一般低於 10m/s

➢ 平均風速<2m/s，但如 LOT 圓頂位處 3 層樓高處，風速應不止如此

杜鵑颱風（風速>30m/s）造成很大損害，LOT 位於山頂靠北側，當颱風期間吹起東及北風時，應該加強戒備

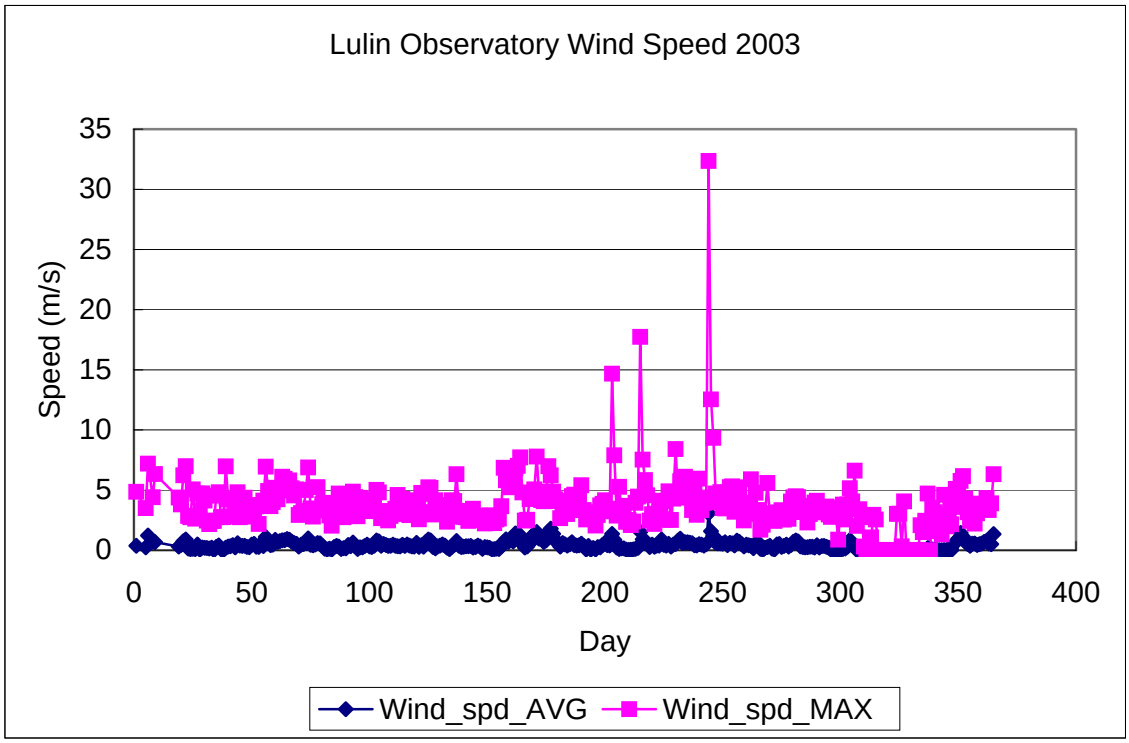

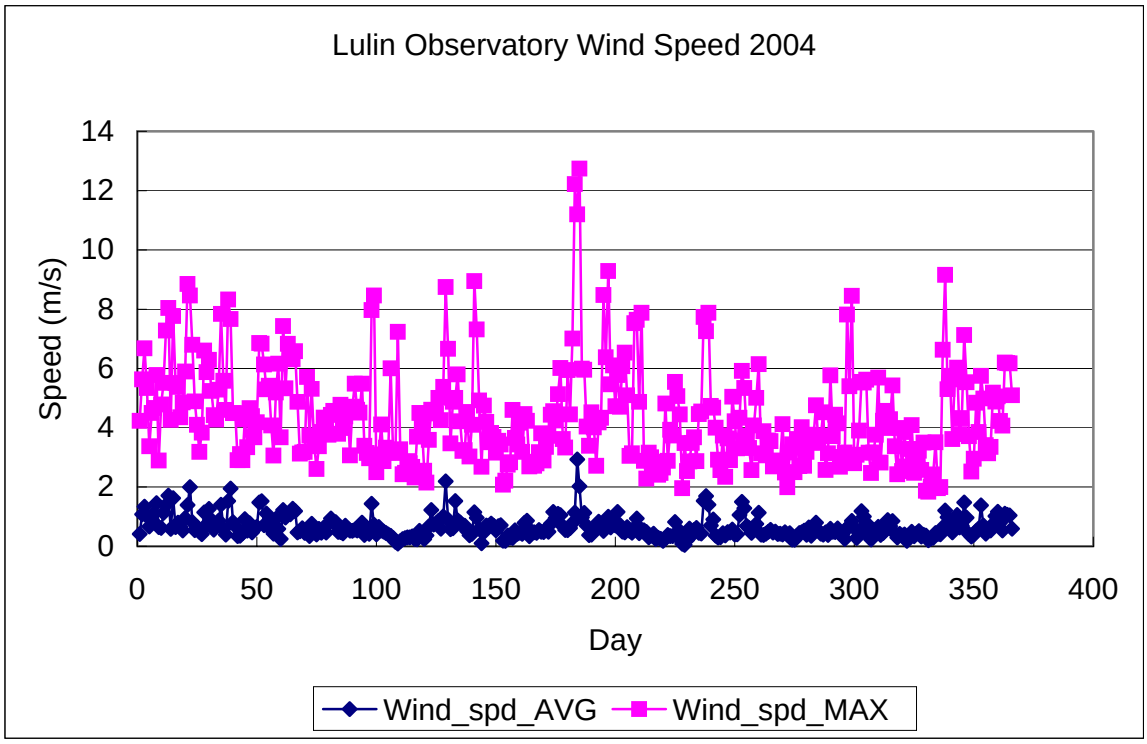

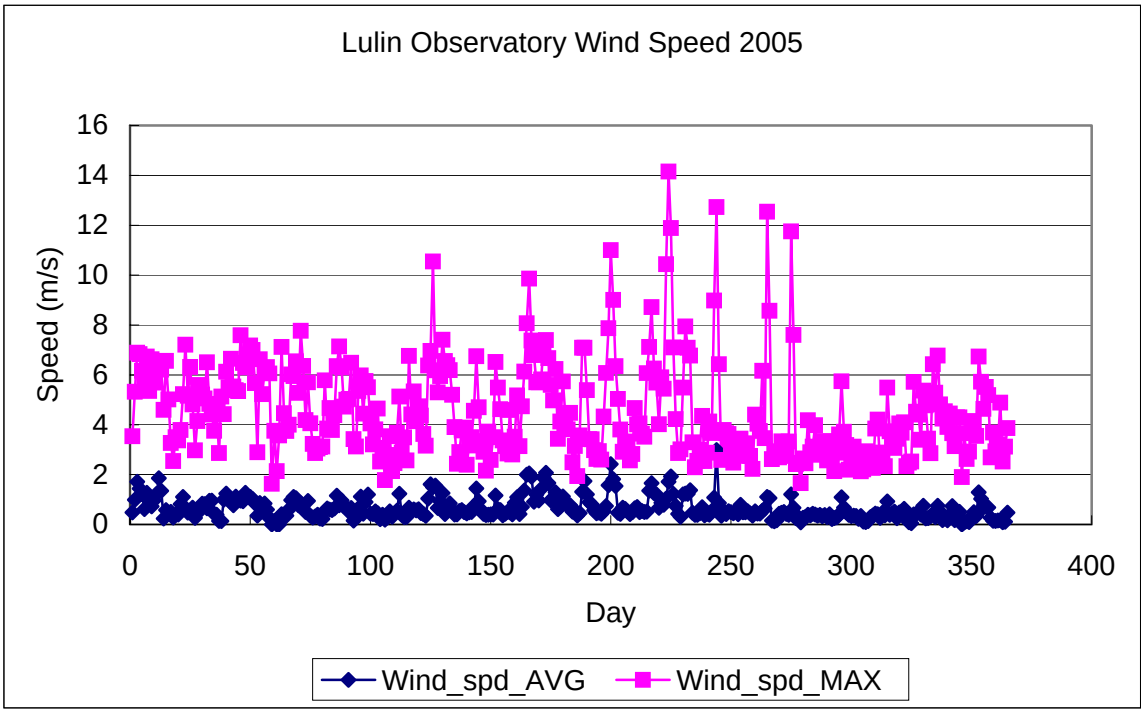

c.雨量

- 主要雨量起始於春雨到夏秋之交，尤其是颱風期間的豪大雨量爲最。
- 當夏季的太平洋高壓籠罩時，雲系退到長江華北一帶，本地山區幾不下雨，如圖(1)
- 當夏季的太平洋高壓消退時，山區常有午後雷陣雨，強度大但時間短，不構成災害。
- 秋天到春天，蒙古冷高壓強盛，華南到琉球之間經常橫著一條雲系，本區僅會下毛毛雨，少有大的雨勢，如圖(2)
- 秋季雨量最少，晴天數最多。

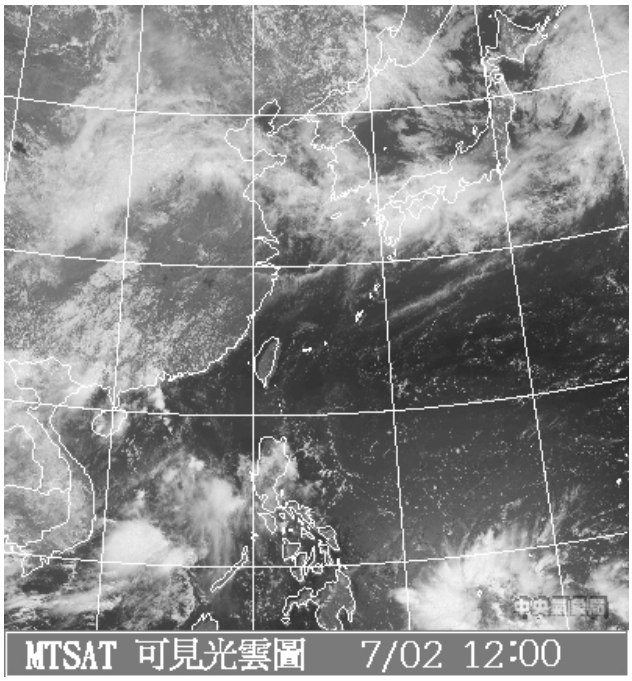

圖(1) 取自中央氣象局網站

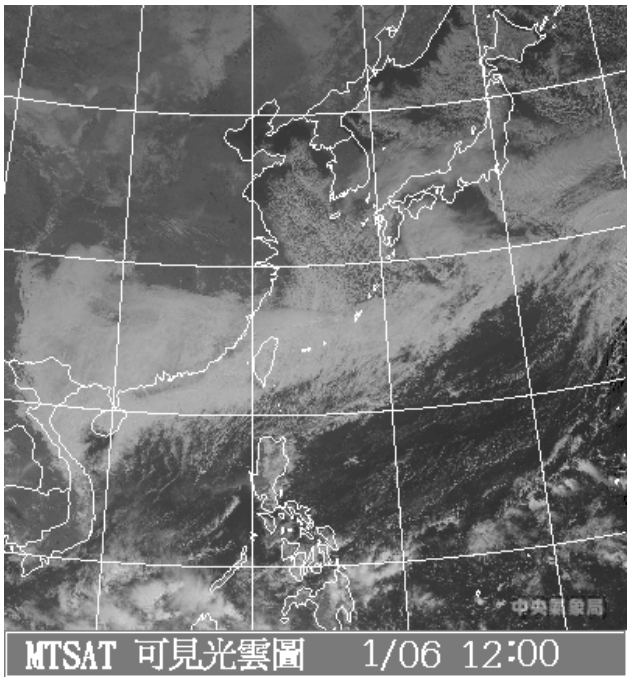

圖(2) 取自中央氣象局網站

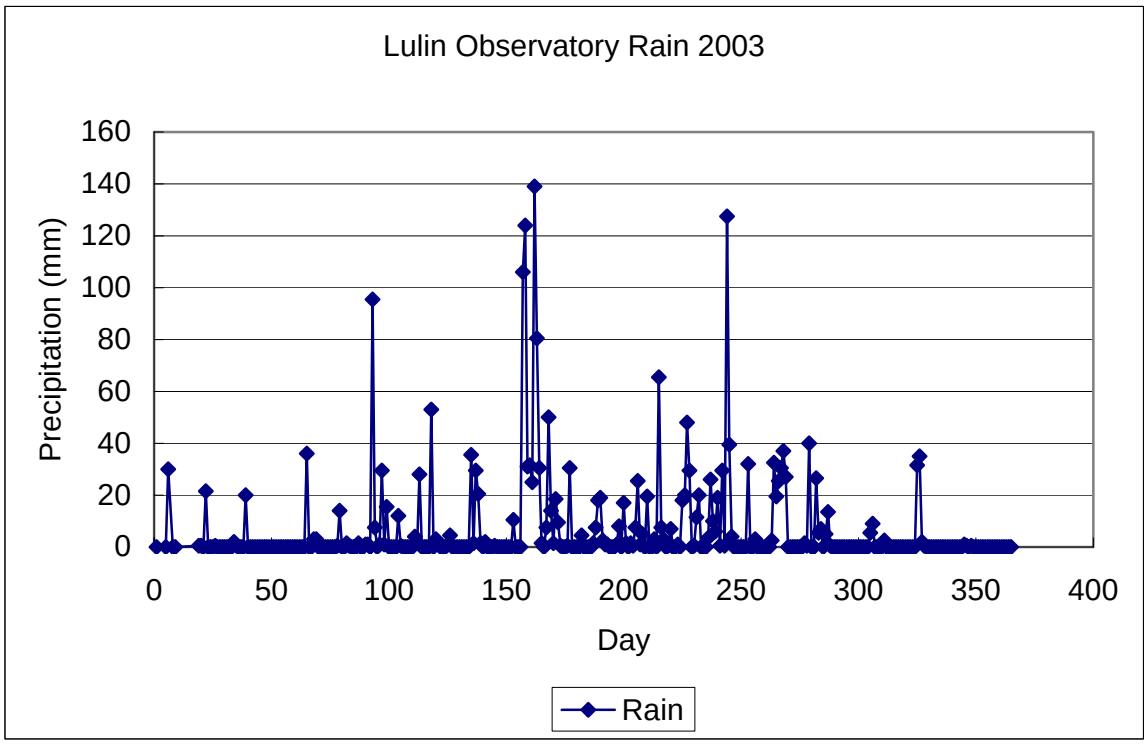

*2003 年總雨量 2240.5mm

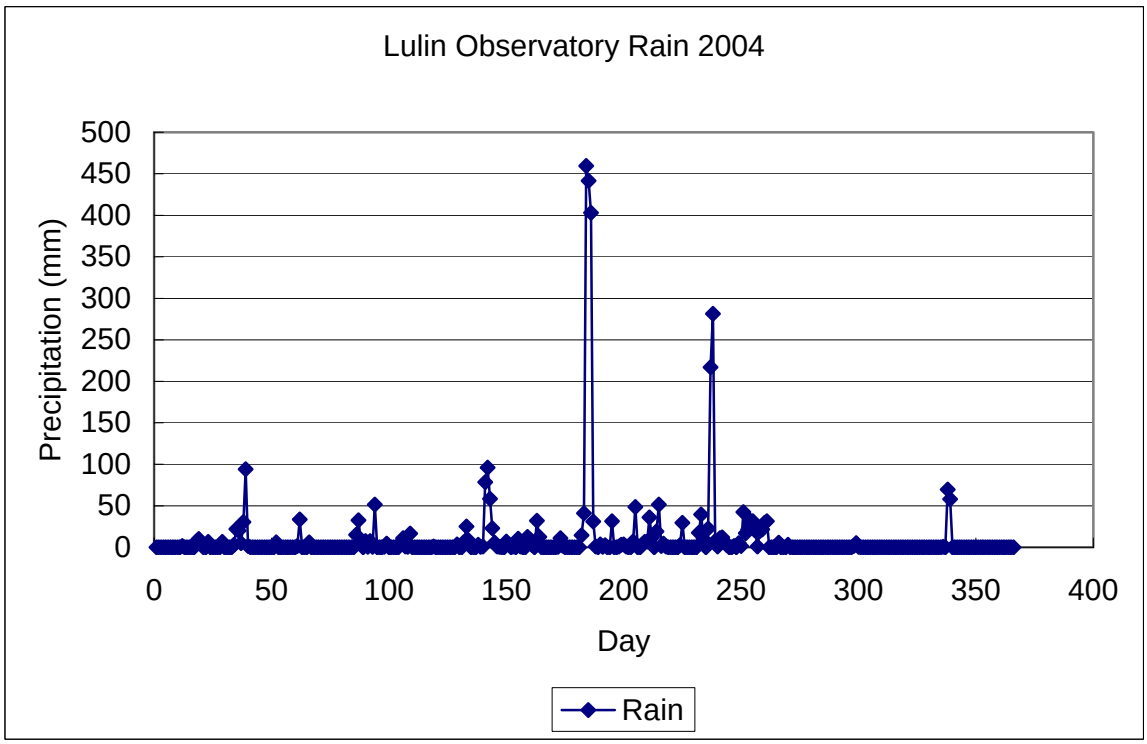

*2004 年總雨量 3554.5mm

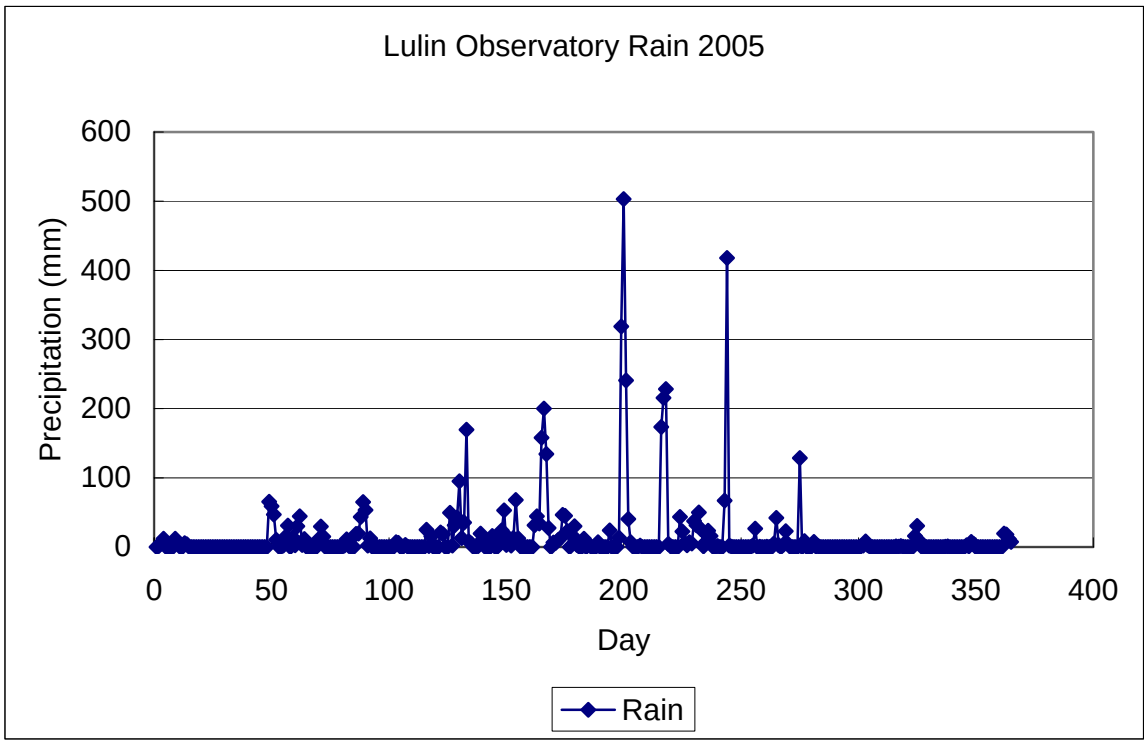

*2005 年總雨量 5260mm

鹿林天文台剛好位在玉山和阿里山之間，大環境的長期氣候可以參考這兩地的中央氣象局測站資料(http://www.cwb.gov.tw)。根據玉山和阿里山測站長期降雨量統計，每年降雨期主要爲 4-9 月，尤其集中在 5-8 月(颱風、西南氣流…)。每年 10 月雨量開始驟減，到隔年初山區會開始出現缺水現象，到 4-5 月始得抒解。

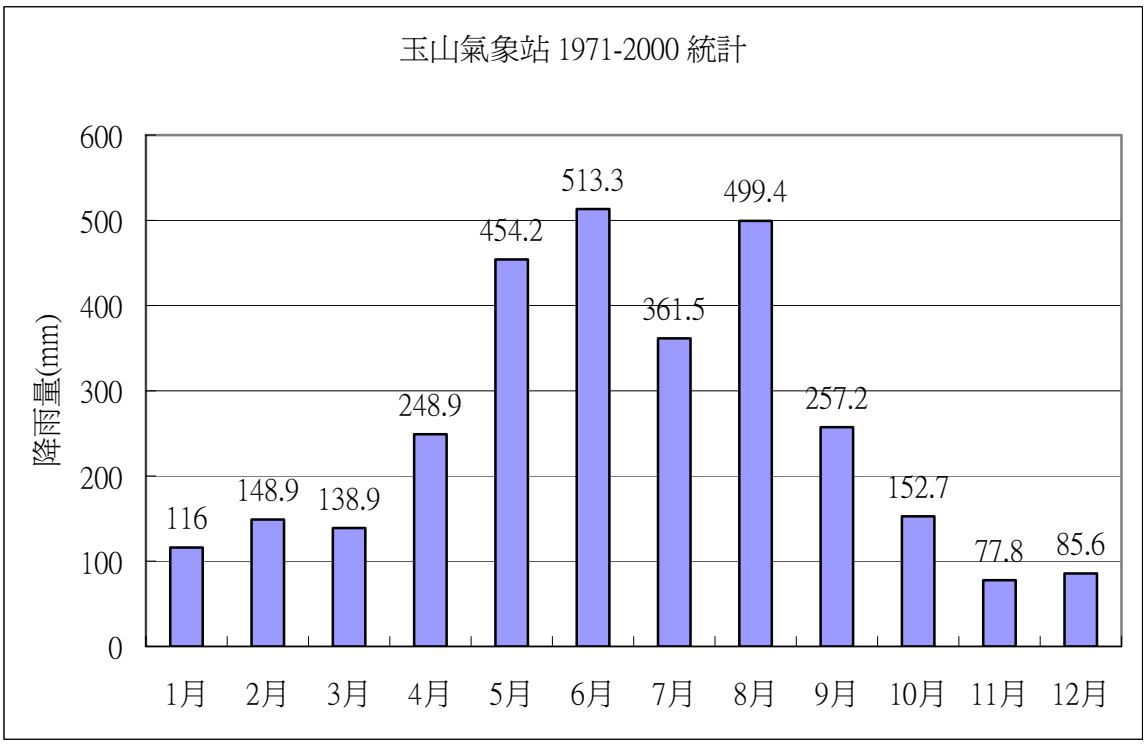

*平均年雨量 3054.4mm

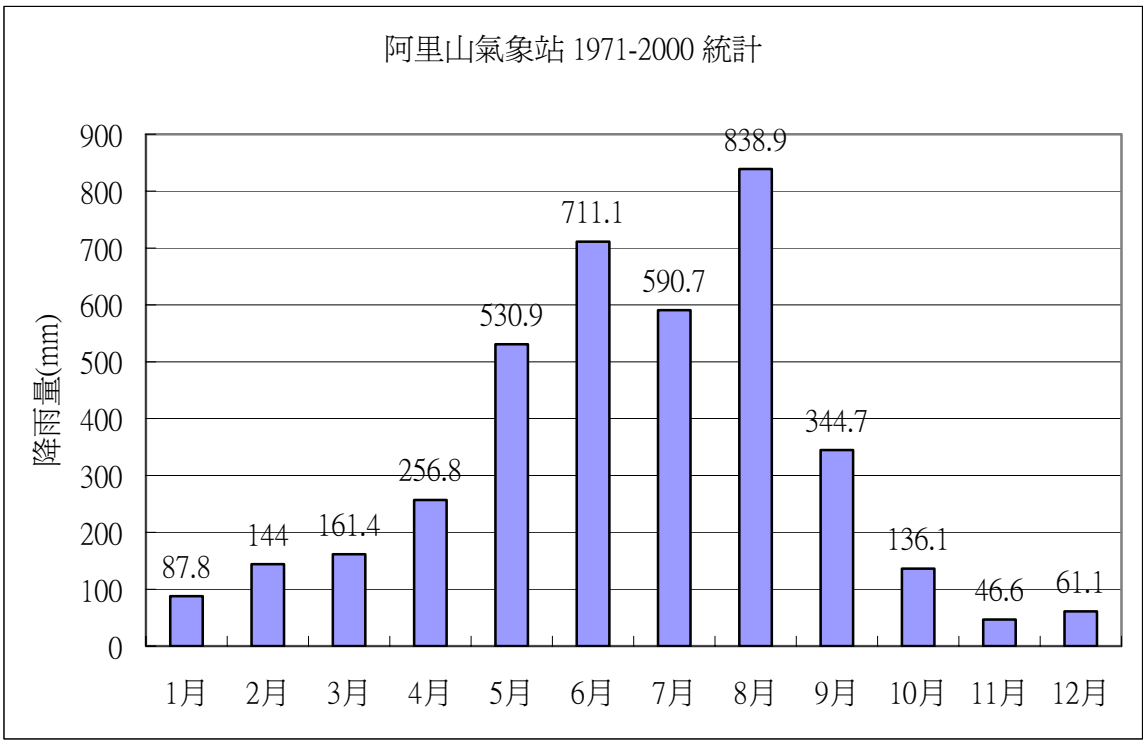

*平均年雨量 3910.1mm

d.相對濕度

CAMPBELL 濕度計於 2005 年初設置，目前尚不滿一年，資料從缺。因最低濕度通常出現在白天日曬時段，不能作爲夜間觀測參考。故只取夜間 21:00, 24:00, 03:00 三個時間點資料作圖。

- 鹿林相對濕度偏高，沒有明顯低濕度的季節，僅有零星低濕度的短暫時段。
- 受到南邊沿著山坡爬升氣流影響，使得相對濕度提高。
- 晴朗的晚上後半夜濕度大都會低於前半夜

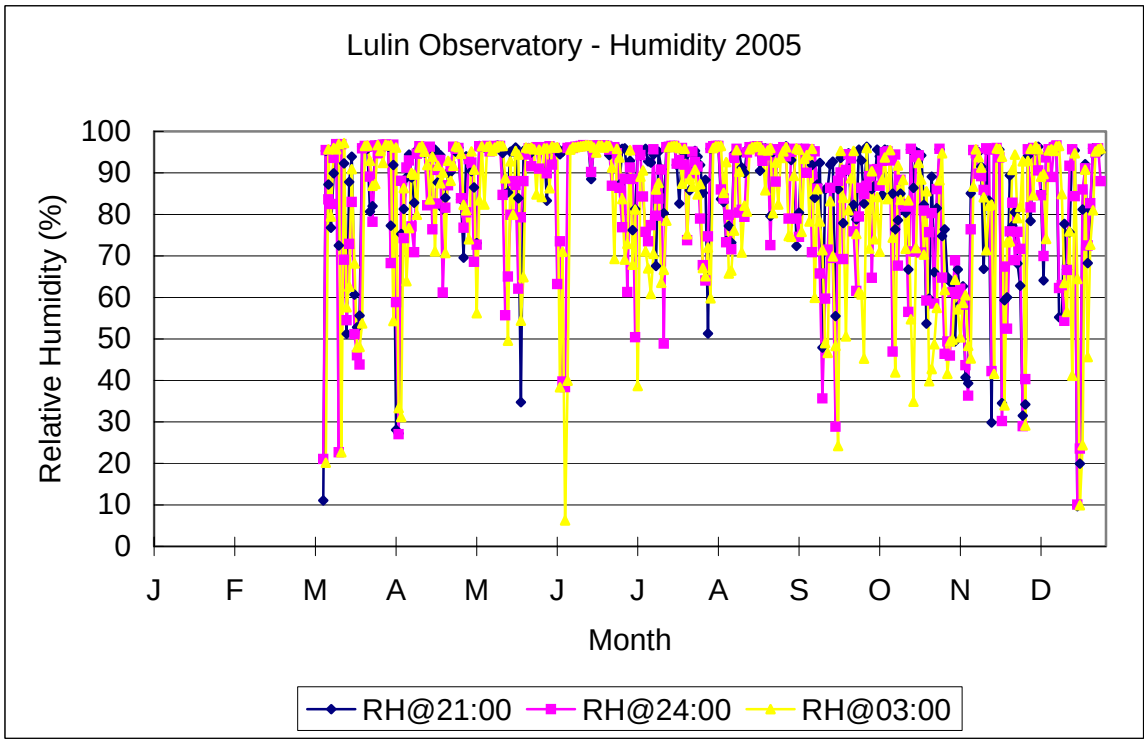

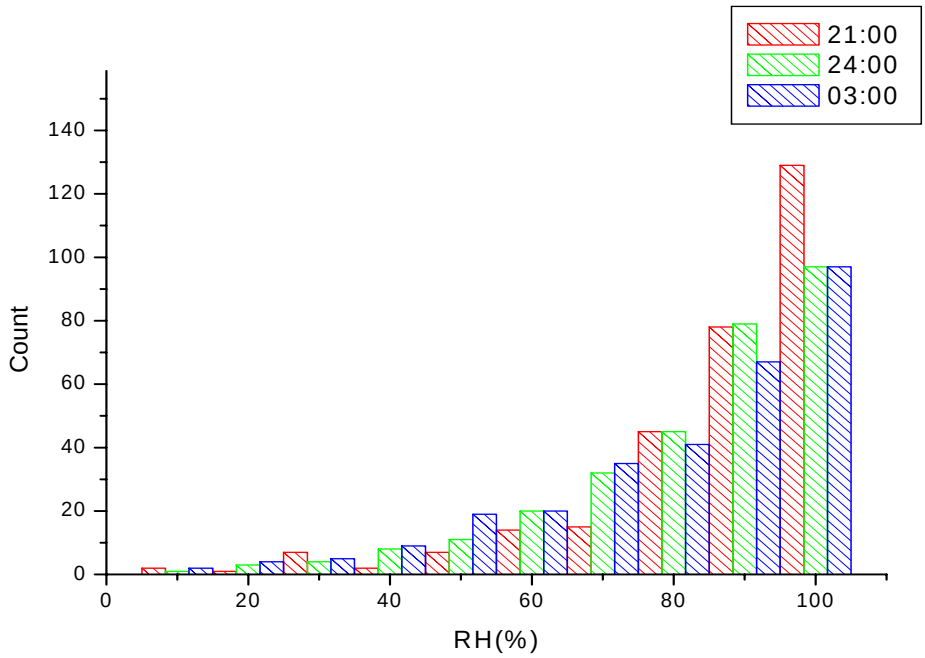

LOT 觀測計劃

LOT 在 2005 年共執行 34 個觀測計劃（上半年 19 個、下半年 25 個），觀測的課題涵蓋小行星、彗星、超新星、恆星演化、星際物質以及協同觀測七月的 Deep Impact 太空任務。除了研究計劃以外，鹿林也提供大學部及研究所的天文觀測教育訓練使用。在今年的 34 個任務中，3 個屬教學教育訓練、5 個是國際合作觀測、其他則爲個人研究計劃；而申請者除了中大、成大、師大等國內天文研究單位以外，還包括來自東京大學、夏威夷大學等國外學術研究單位，分別以日本偏振儀（PICO）或鹿林之 PI CCD 進行彗星、小行星研究。下表列出 LOT 於 2005 年進行的觀測計劃：

IANCU/LOT Observing Time 2005A (January - June)

No.	Project	PI
01	Time-resolved photometry for superhumpers	Alfred Chen
02	Astroseismology of extreme horizontal branch stars	ChinWei Chen
03	Supernovae Search and Follow-up Observations	Wing-Huen Ip
04	UBV photometry on galactic open clusters	ChinWei Chen
05	Search for Exoplanets and variable stars in the Open Cluster	Hu Juei-Hwa
06	Extreme Trojans	David Jewitt
07	Asteroseismology of the pulsating DA white dwarf EC 14012-1446	Kaushar Sanchawala
08	Studies and Observations of X-ray Binaries	Yi Chou
09	天文觀測(II)戶外教學	Yi Chou
10	Halpha survey of nearby and Seyfert galaxies	Sebastien Muller
11	BVRI Photometric Study of (832) Karin	Wing-Huen Ip
12	Observations of Deep Impact Comet 9P/Templel	Zhong-Yi Lin

13	Target of Opportinuity of GRBs and XRFs follow-up Observation	Kui-Yun Huang
14	Ground based observation of asteroid sample	Daisuke Kinoshita
15	The Origin and Evolution of Bipolar type planetary nebula–Abell 14	Chih-Hao Hsia
16	Search for Exoplanets Following Microlensing Alerts	Lee, Chien-Hsiu
17	Calibration Program 4: PI1300B and Focal Reducer	Kinoshita Daisuke
18	Rotational Lightcurve of Centaurs	Kinoshita Daisuke
19	The multi-wavelength observation of planetary nebulae	Trung Hua

IANCU/LOT Observing Time 2005B (July - December)

No.	Project	PI
1	World-Wide monitoring campaign of the sdB star BA09	陳文屏
2	天文觀測教學	陳文屏
3	The photometry of selected eight open clusters with differential age, distant, and poor known.	傅學海
4	H-alpha and [SII] imaging of Triggered Star Formation in Per OB1 association	李晌岱
5	Ground based observation of asteroid sample return mission target	安部正真
6	Photometry and Dynamics Study of Selected Open Clusters	吳志剛
7	Search for Exoplanets Following Microlensing Alerts.	李見修
8	Imaging Polarimetry of Comet 9P/Tempel 1 at Lulin Observatory: Ground-based Observation for NASA Deep Impact Mission	FURUSHO Reiko
9	Observations of ‘unusual’ comet 9P/Temple1 after Deep Imapct time	林忠義
10	Photometric variability studies on brown dwarfs	Soumen Mondal
11	UBV photometry on galactic open clusters with poor age and distance determination: Formation and evolution of high galactic latitude open clusters	陳錦威
12	Search for Active Main-Belt Asteroids	Hsieh Hong-Li
13	觀測天文學教學及實習	黃崇源
14	The Origin and Evolution of Bipolar type planetary nebula – Abell 14	夏志浩
15	LOT-MOA Microlensing Project	葉永烜
16	H-alpha and [SII] Mosaic Imaging of L1551	李晌岱
17	Rotation Periods and Surface Color Measurements of Large EKBOs	葉永烜
18	The Hα Survey of bright galaxies in the Coma Cluster	黃崇源
19	Calibration Program 5: Apogee U42 and Focal Reducer	Daisuke
20	Multi-Color and Time-Resolved Photometric Observation of Damocloid 2004 YH 32	Daisuke
21	A test of star formation theories in galaxies from near-infrared and Hα imaging	葉永烜
22	Supernovae Search and Follow-up Observations	葉永烜
23	Photo-polarimetry of unusual asteroid 1992 UY4	SATO
24	Target of Opportunity of GRBs and XRFs follow-up observation	黃癸雲
25	Galactic structure from apparent luminosity function	高仲明

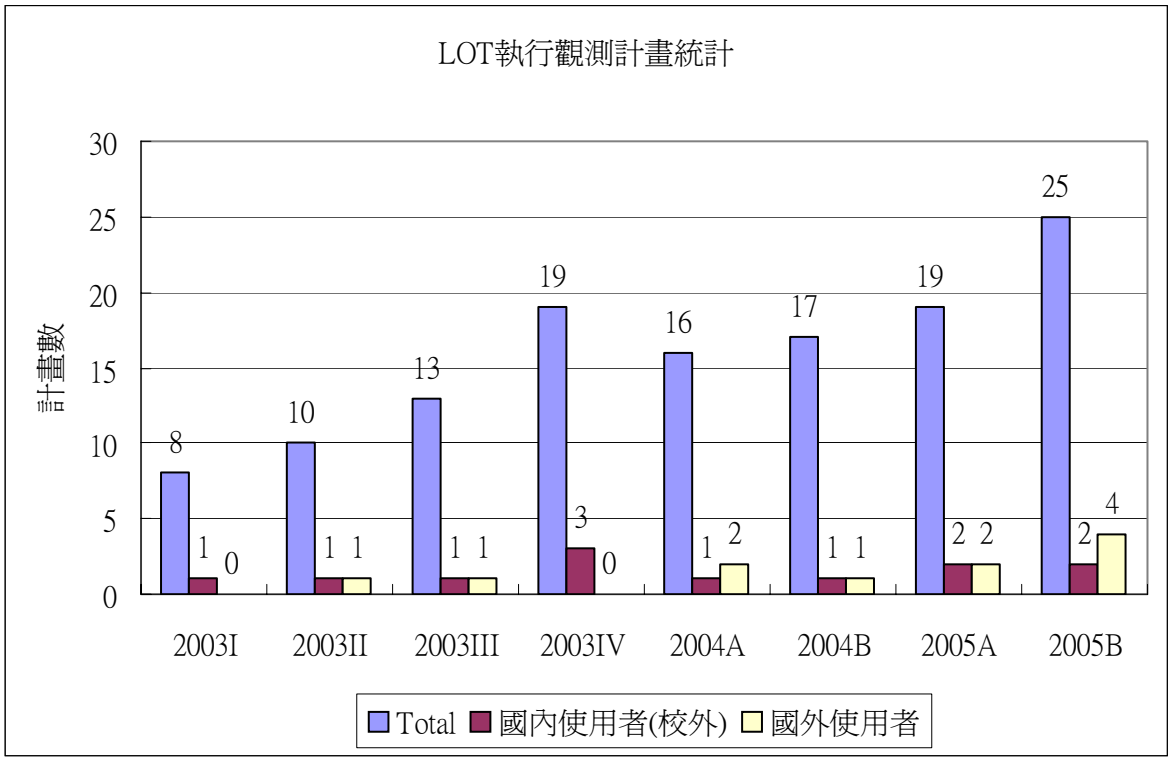

- LOT 於 2002 年 9 月安裝完成，2003 年起開放國內外申請觀測。
- 2003 年觀測計畫以每三個月(季)爲單位申請及執行(I=1-3 月、II=4-6 月、III=7-9 月、IV=10-12 月)。
- 2004 年起觀測計畫改爲以每半年爲單位申請及執行(A=上半年、B=下半年)。
- 2003-2005 三年來執行計畫總數 127 個，中大使用者佔 82%，中大以外的國內使用者佔 9%，而國外使用者佔 9%。

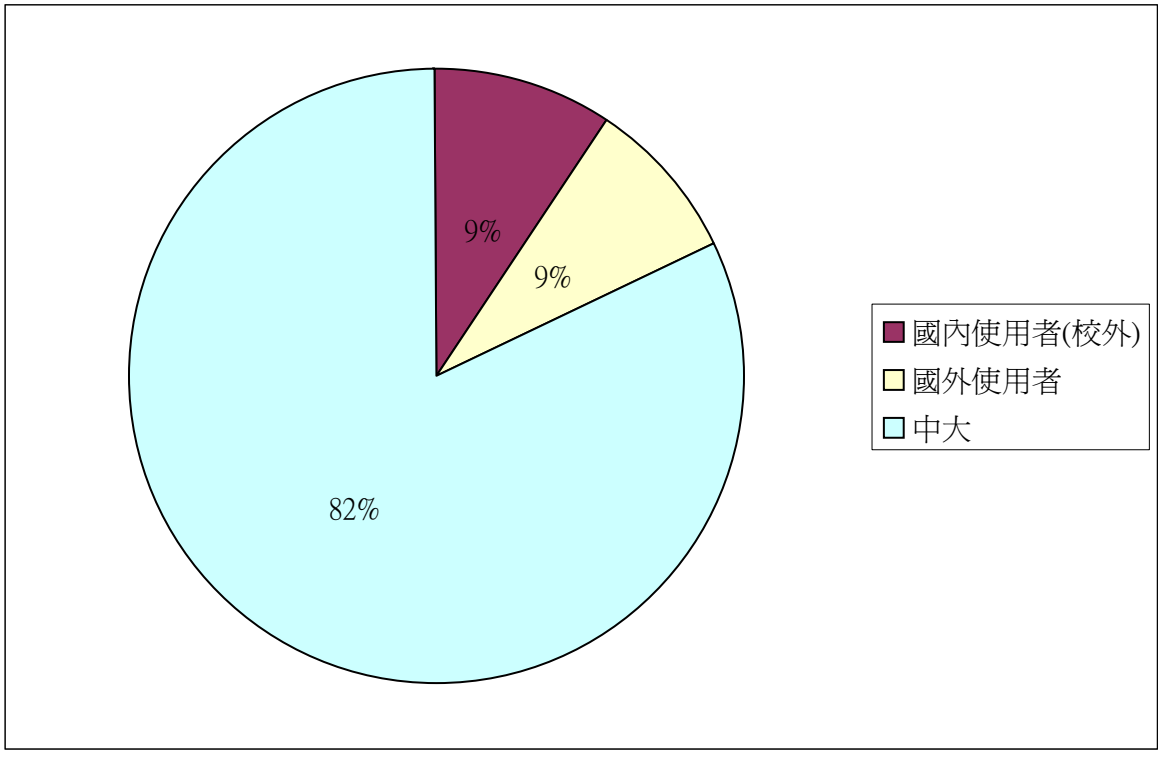

人員

駐站人員與觀測助理對天文台運作發揮很大的幫助，駐站人員處理所有的庶務，例如食宿準備、環境維護、人員接駁、設備運補…等，使觀測人員能心無旁騖地執行觀測計劃，也使鹿林各種狀況都有人能迅速處理、回報，對營運及維護工作都發揮極大的效用。此外由於國科會通過了營運計劃的經費申請，鹿林自 2005 年三月份開始，增聘一位觀測助理，除了負責在台內值班協助解決觀測時發生的問題外，也支援部分服務觀測，協助無法抽調人員進行觀測的研究計劃，獲取所需要的觀測資料，並對即時發生的天象事件，配合相關團隊進行迅速的觀測程序；此外還協助位於原 SLT 圓頂內的新 40 公分超新星巡天望遠鏡配置、測試及操作等各種儀器整備工作，使 40 公分望遠鏡已具備可由中大校園進行遠距遙控觀測的能力。

觀測助理對 LOT 及尋天望遠鏡的運作助益不小，但 10 月份營運計劃結束後，礙於經費未能續聘，觀測助理的培訓與經驗累積均耗時甚久，未能續聘有經驗的人員對天文台而言殊爲可惜。幸而後來國科會核定了鹿林新年度的營運計劃，於是在 12 月份聘請林啓生先生爲續任的觀測助理，2006 年一月份增聘觀測助理楊庭彰先生，期能更全面性地協助各項觀測研究，並對未來的國際合作計劃做先期準備工作。

基礎設施改善

今年度鹿林天文台新設由環保署與中大大氣物理所、環工所、化學系合作的中尺度環境研究背景站（見研究報告章節），基於安全考量，背景站電力系統與天文台分開獨立設置，背景站爲兩層樓建築，設有氣體採樣口及氣象塔，未來相關的儀器設備將由戶外移至戶內，提供更好的採樣品質，並降低非必要的人員干擾。其他的各項基礎設施並無重大變更，僅進行了電力系統避雷措施補強與消防設備補強等兩項改進工作，而針對 LOT 即將進行的主鏡重鍍工作，則預先建立了所需的吊運設備。

末端增設之雷擊保護裝置

戶外增設之導電銅板

鹿林天文台地處落雷區，易受雷擊或感應電流影響，造成儀器受損並有危及人員安全的問題，在營運計劃及校補助款共同分攤經費的情況下，針對這些問題加以改善。首先在室內各重要儀器迴路的末端開關加裝雷擊突波保護器，減少感電時進入敏感儀器的電流量，總計

在各建物（包含控制中心、SLT 及 TAOS 遮罩等）的電源系統開關箱中裝設雷擊保護器 28 個，在弱電系統（網路、RS232 訊號、同軸電纜等系統）中，也增設了 16 個雷擊感應電流保護裝置；而在戶外的部分，則提升原有避雷針與整個電力系統的接地性能，增加地棒，加速電流的洩放，降低遭受雷擊或感電的損壞範圍與人員危害的直接風險。

LOT 的主鏡工作至今已經三年多，由於氧化及落塵、濕氣等影響，反射率降低，爲了提升反射率，預計在 2006 年將主鏡卸載下來，進行表面反射層重鍍的工作，由於鏡片含鏡室重量將近一公噸，非人力所能進行，而安裝用的大型吊車並不適合進行單獨的鏡室吊運，因此爲了配合 LOT 主鏡重鍍所需的吊運工作，預先在望遠鏡室內進行了結構補強，並設置負載可達 1 公噸以上的小型吊車，加上原有 LOT 安裝時的基座與機械設備，以解決要進行主鏡重新鍍膜時的卸載及運送問題。

儀器維護與更新

本年度的 LOT 儀器部分新增了 0.5x 減焦鏡一組，提供需要大視場的觀測使用，可涵蓋一般影像的四倍視場，對於星際物質或星團等目標可提升不少觀測效率，並減少後處理拼接工作。周邊的輔助設施也進行了擴充或增補，例如擴增伺服器的儲存空間，便於觀測資料存取、氣象監測系統的升級、CCD 快門更換等等。2005 年夏，LOT 的濾鏡盤因不明原因故障，必須送回美國檢修，這段期間因缺乏適當的替代儀器，導致必須以舊的 AP-8 CCD 及僅能安裝五片濾鏡的 FLI CFW-1 濾鏡盤工作，造成不小影響，針對這個部分將在明年增購備用濾鏡盤，平常可提供 40 公分望遠鏡觀測，當主要儀器有問題時則可遞補，減少發生類似情況時的影響程度。

在原有 SLT 天文台圓頂內，新設了專供超新星搜尋及系外行星搜尋、口徑 40cm 的望遠鏡系統，已達到可遠距遙控觀測的能力，本所研究生可於校內操作進行觀測，節省人員往返時間與費用（詳見 40 公分望遠鏡報告，P）。

LOT 於五月份新購 BVRI 濾鏡組一組及 Hα 濾鏡，請光電所協助檢測該濾鏡之穿透曲線，結果圖示如下：

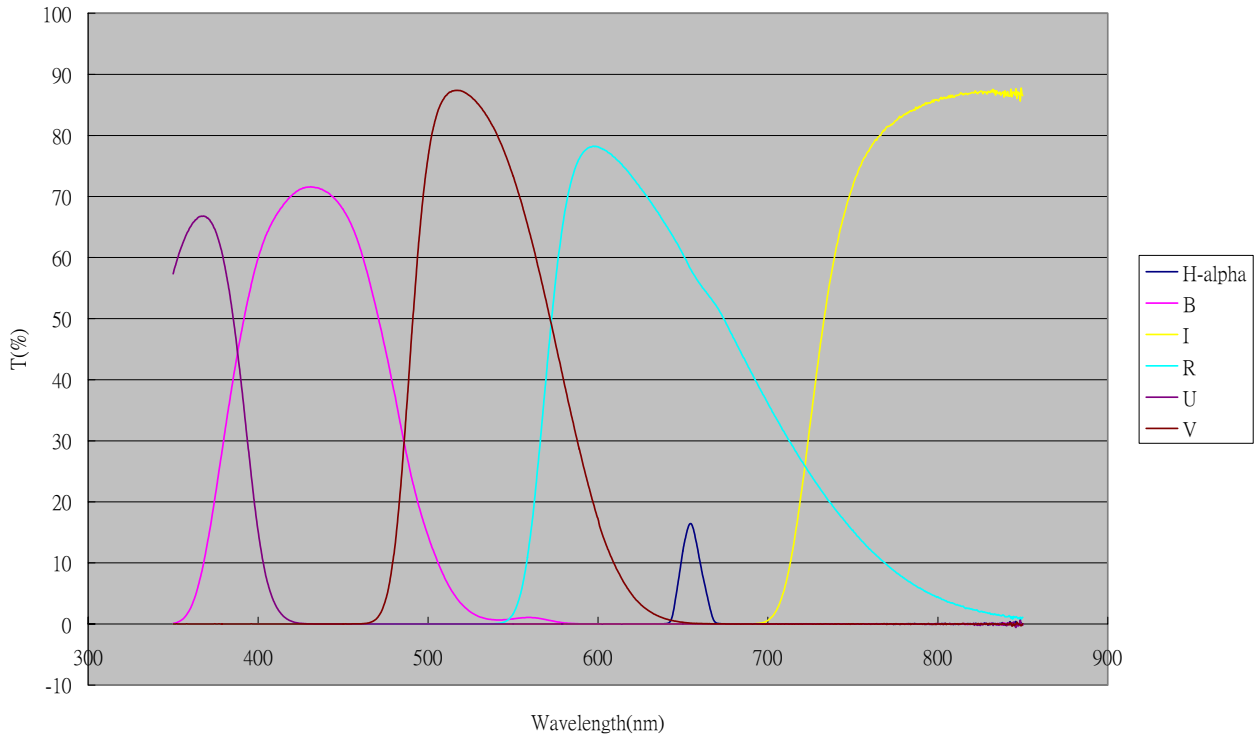
100
90
80
70
60
50
40
30
20
10
0
-10
T(%)
300
400
500
600
700
800
900
Wavelength(nm)
H-alpha
B
I
R
U
V

PI-1300B CCD Window 結露解決方法

張永欣、林宏欽

當 PI-1300B CCD 晶片冷卻至零下 50℃時，由於晶片外部僅處於近真空封裝，加上真空室結構的金屬傳導，封裝的窗口玻璃會有降溫的情形，雖然沒有降到與 CCD Chip 一樣的冷度，但此時玻璃外側接觸的潮濕空氣，便立即凝結水滴在玻璃表面，阻擋光線的進入。

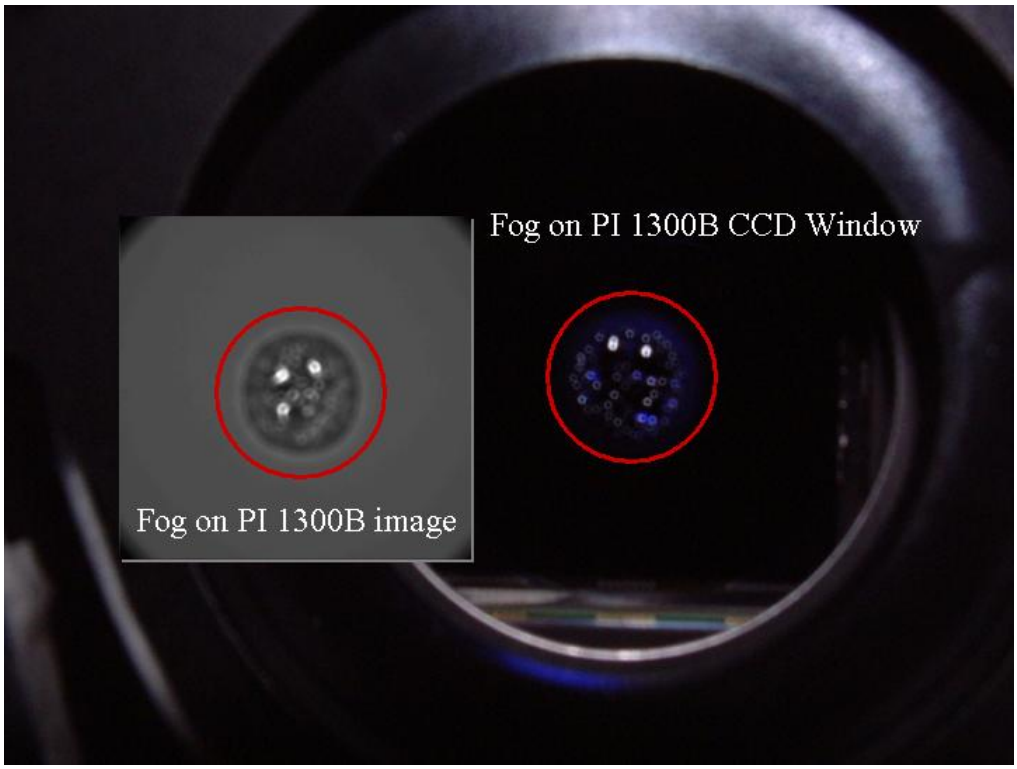

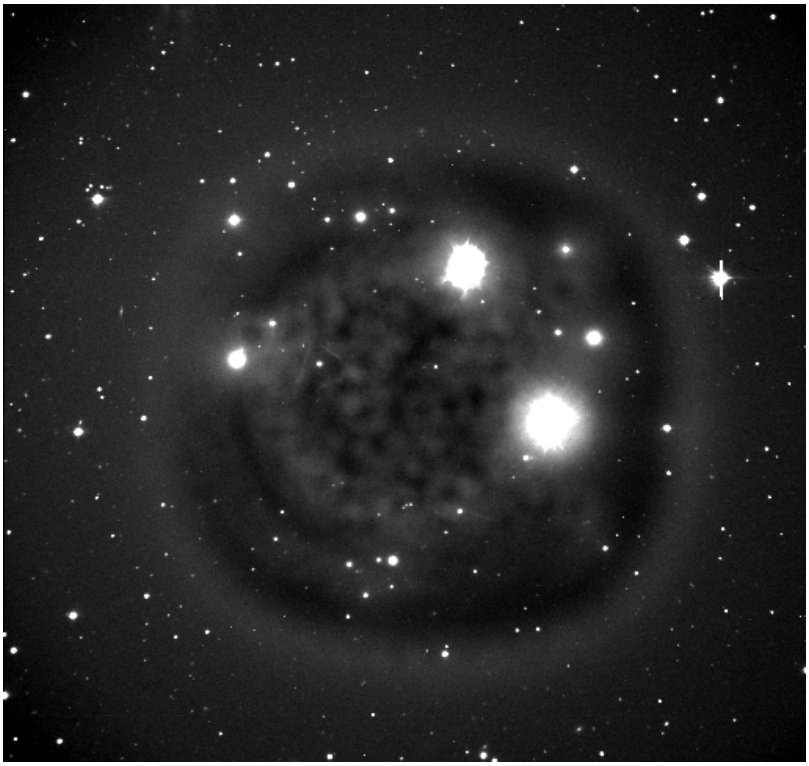

CCD Window 中央結露(上圖)，造成影像中央產生圓形不規則減光、星像暈化現象(下圖)爲解決這一個現象，我們採用在 CCD 窗口玻璃外側提供一足夠乾燥空氣之空間的方式；由窗口玻璃往外還有機械快門、濾鏡（盤）兩層阻隔，雖然沒有達到密閉的條件，但並未完全

直通接觸環境空氣，所以只要持續提供一足夠之小流量的乾燥空氣，便可以維持這個空間乾燥，避免結露。

如何持續獲得乾燥的空氣呢？我們在網際網路上找到奧地利一個天文台(http://www.harpoint-observatory.com/)，採用空氣管線流經過冷凍庫，將空氣冷卻到-25℃的方式，以取得含水量 0.7047 g/m³的乾燥空氣，可是這要消耗極高的能量，還要解決管線內冷凝水結冰的問題。因此我們改由飽和蒸汽壓的方式來獲得乾燥空氣，我們從壓力露點與一大氣壓露點換算，當空氣壓縮爲 8 大氣壓時，再將壓縮空氣冷卻到 2℃，以保持管線內冷凝水的流動性，如此可以得到相當於露點 -23℃的飽和蒸汽，亦即玻璃表面必須低於-23℃時才會發生結露現象，這是目前最爲經濟的選擇，若需要更低濕度的乾燥空氣，可以再經二次增壓加大壓力或是經由交換吸附式空氣乾燥機處理。

壓縮空氣淨化系統配置建議 (摘自 http://www.hyperdryer.com.tw/)

實際系統說明如下，使用一般空氣壓縮機將空氣壓縮到~8 Kg/cm2，先經過前置過濾器(prefilter)將壓縮空氣內大部分水氣濾除，再經三道精密過濾器(SMC AF4000 + AFM4000 +AFD4000)將壓縮空氣中的微量油氣精密濾除至 0.001PPM，同時濾除空氣中雜質顆粒至 0.01MICRON，以達到無油標準的高品質壓縮空氣。最後利用一流量計調整進入 CCD 相機的空氣量，實測找出適當流量防止結露產生，目前系統使用的空氣流量估計約 500 cc/min。空氣壓縮機馬達每隔約 12 分鐘自動充氣。

系統中原本裝置有冷凍式空氣乾燥機將壓縮空氣冷卻，實際使用發現只要將空氣流量調大即可完全杜絕結露現象，故將空氣乾燥機移除。冷凍式空氣乾燥機使用壓縮機冷卻，既耗電又發熱，移除之有利無害。

最後整理幾點注意事項如下，

- ●改用無油式空氣壓縮機，避免對 CCD 相機可能的油氣污染，並降低空壓機的維護需求 (e.g. 機油更換...)。
- ●CCD 端進氣口位置必須在快門下方的 CCD Window 區域，保持這個空間乾燥，才能有效防止 Window 結露。
- ●CCD 端進氣口宜用 L 形彎管，並將進氣端管線約 30cm 段包覆黑色膠帶，避免漏光。

●空氣流量寧大勿小，確保 CCD window 不會結露，以免觀測資料出問題。

●我們目前使用的流量計(Dwyer RMA-150-SSV Air)指示範圍爲 10~100 cc/min，然實測發現 100 cc/min 流量太小，無法阻止結露產生，需調大至轉鈕白線指到約 10 點鐘方向才行(最小流量 10 cc/min 約在 3 點鐘方向)，估計實際所需空氣流量約 ~500 cc/min，待更換較大範圍流量計(100-1000 cc/min)便知。

●Dwyer RMA-150-SSV Air 流量計最大壓力上限爲 100psi，故在 prefilter 處降壓至 100psi 以下，或調降空壓機壓力至 100psi 以下也可。

●流量計範圍不可太大，以防 CCD 快門因高壓空氣而受損。

●空氣壓縮機及過濾器宜加裝自動排除水器(閥)，減少人工維護需求。

●空氣壓縮機宜選用較大的儲氣桶，降低打氣頻次，以減少馬達負擔。

●空氣壓縮機打氣噪音很大，宜放置於無人隔間或遠離人員工作場所之處。

●空氣壓縮機需定期(每 1-2 個月)洩除儲氣桶內積水/油垢。

●一般使用機油潤滑的空氣壓縮機需定期(每 300 小時)更換機油。

●LN2 冷卻 CCD 相機因 CCD 晶片冷卻程度達 -100 度 C，CCD window 溫度勢必更低，可能需要更大流量換氣或使用更乾燥的空氣(加裝冷凍式空氣乾燥機)。

PI 1300B CCD 相機目前使用的 Window 防結露系統圖

REFERENCE

http://www.harpoint-observatory.com/

http://www.hyperdryer.com.tw/

http://www.kinequip.com/PDF/SMC/AFD.PDF

http://www.hyperdryer.com.tw/Precise-filter.htm

http://www.swarmtop.com/p1.htm

http://www.dwyer-inst.com/

駐站人員工作報告

石俊雄、杜進全、汪榮進、石皓偉

本年度駐站工作人員進行工作包含下列項目：

1.協助觀測：協助觀測人員之食衣住行.固定每週採買，並協助簡單維修，讓其能安心觀測無後顧之憂。

2.天文台清潔：天文台之內部及周邊整潔、換洗床被單套、垃圾帶下山、花木種植，雜草修整之工作。

3.防颱工作：今年颱風甚多，做好防颱工作，使天文台的災害降到最低。

4.接待：接待校友部落及天文台兩日遊及協助天文營完成天文教學活動。

5.工程監督：林道駁崁工程及環保署，背景站工程適時提供工作進度及工程照片。

6.協助 TAOS：每晚協助 TAOS 進行觀測及簡單維修。

7.榮譽榜：參加學校運動會協助理學院獲得拔河第一名。

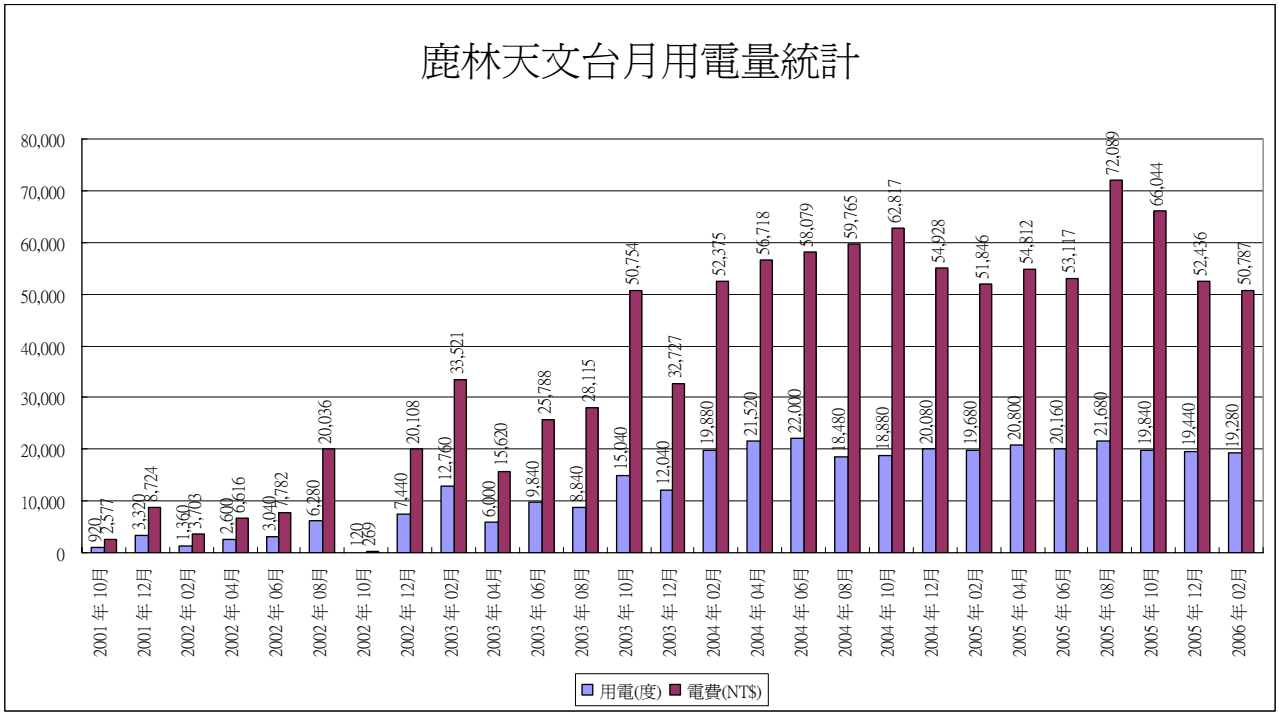

- 2002 年 9 月之前只有每個月不定期的觀測及維護，無人員常駐，用電量相對較少。
- 2002 年 9 月一米望遠鏡安裝完成暨控制中心落成啓用，才開始人員 24 小時常駐。因此 2003 年用電量比 2002 年增加了約 210%。
- 2003 年 12 月基地台開始正式運作，因此 2004 年用電量比 2003 年增加了約 87%。
- 天文台陸續有新設施加入，但基地台因公司合併撤掉部分機組，故 2004、2005 兩年用電量約持平，沒有明顯變化。
- 4 年來年用電量成長了約 6 倍。
- 2002、2003、2004、2005 電費平均分別約爲 2.81、2.89、2.85、2.88 元/度

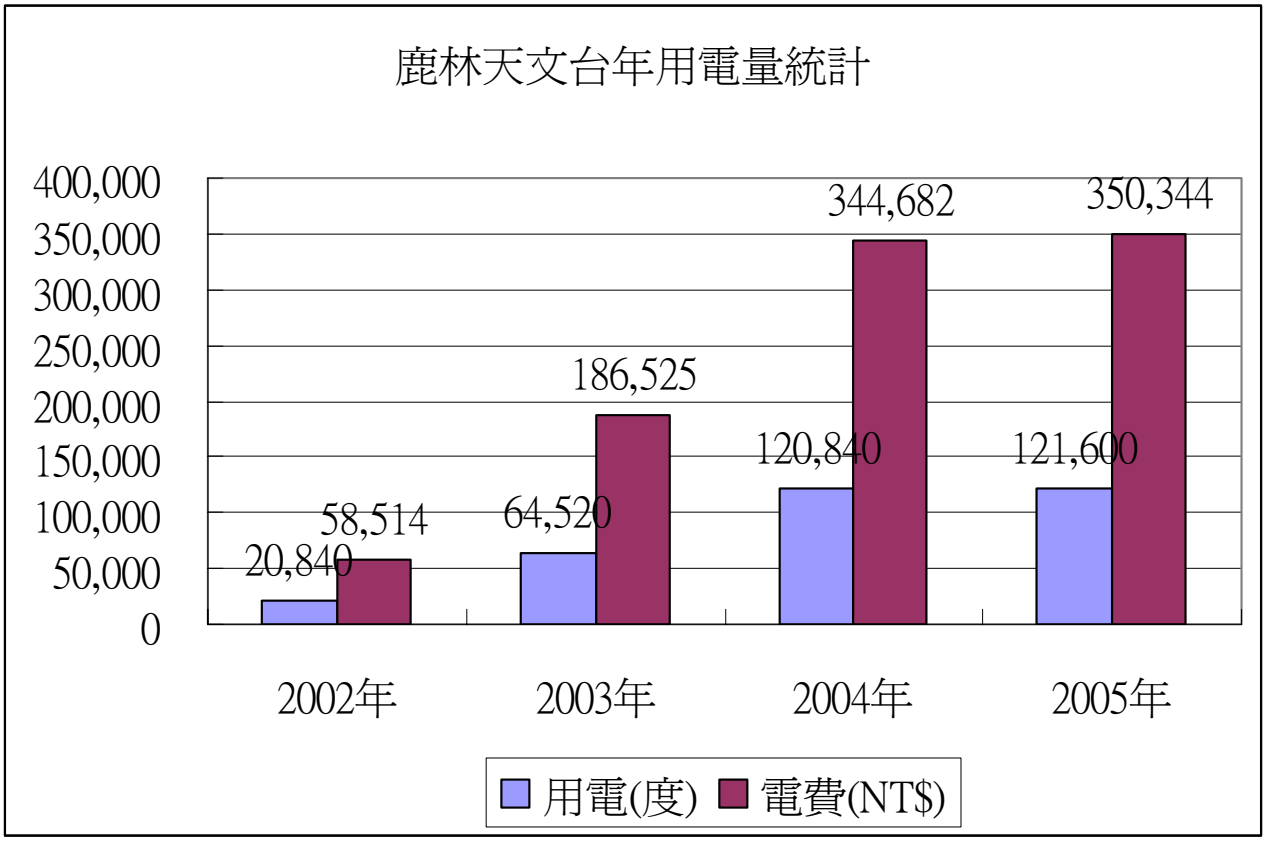
鹿林天文台年用電量統計
400,000
350,000
300,000
250,000
200,000
150,000
100,000
50,000
0
20,840
58,514
64,520
186,525
120,840
344,682
121,600
350,344
2002年
2003年
2004年
2005年
用電(度)
電費(NT$)

40 公分遠距遙控望遠鏡

胡瑞華、林宏欽、陳英同、李見修、陳鑭津、鄭宇棋 & 葉永烜

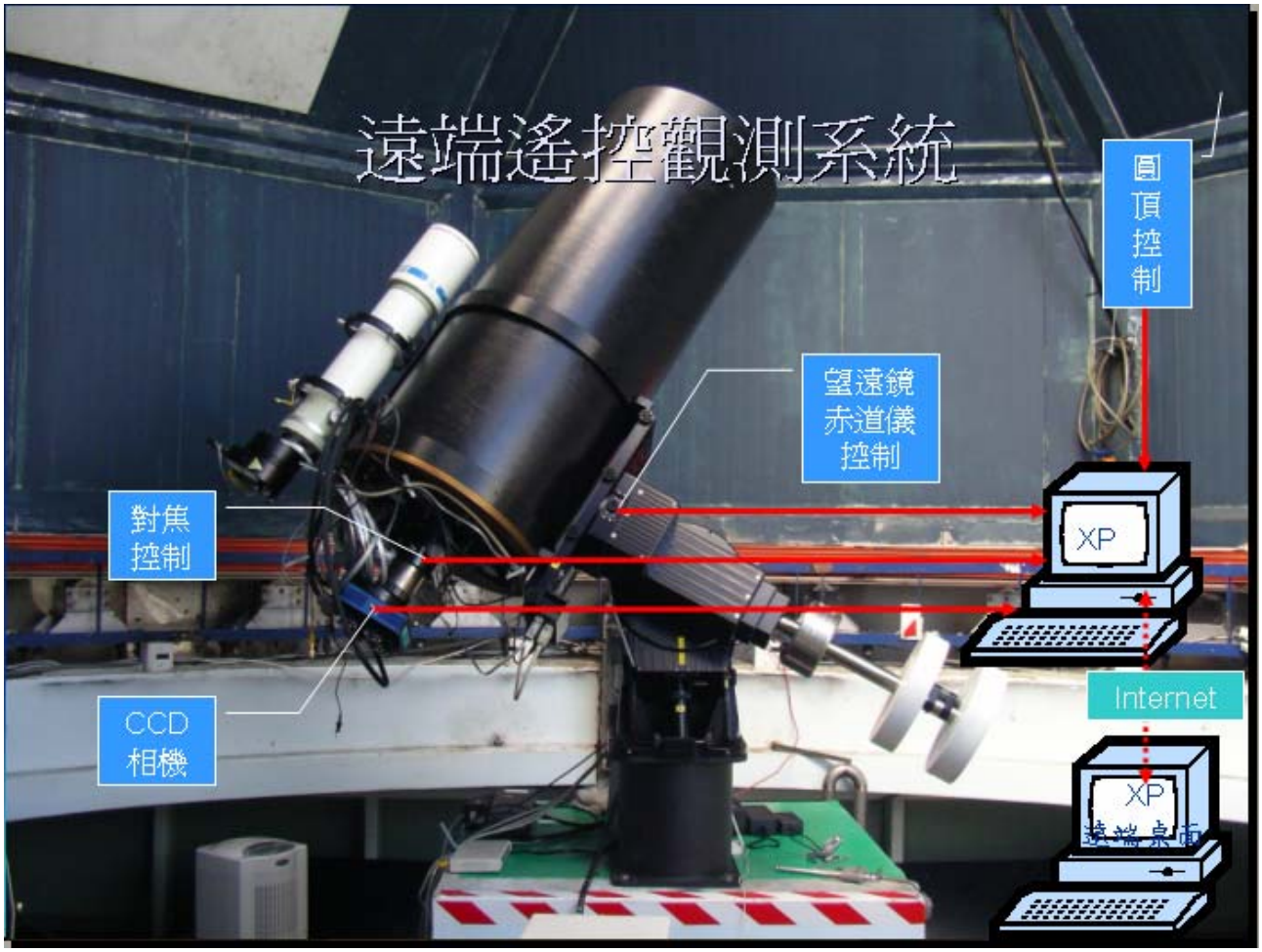

40 公分遠距遙控望遠鏡是在原 SLT (Super Light Telescope)天文台新架設的望遠鏡。此望遠鏡主要的觀測目標是超新星的搜尋、尋找系外行星、Gamma-ray 爆發的後續觀測以及有特殊天文現象時與 LOT (Lulin One-meter Telescope) 的同步觀測。圖一爲 9P/Tempel 1 彗星深撞(Deep Impact)，撞擊 6 小時後由 40 公分望遠鏡所攝得的影像。

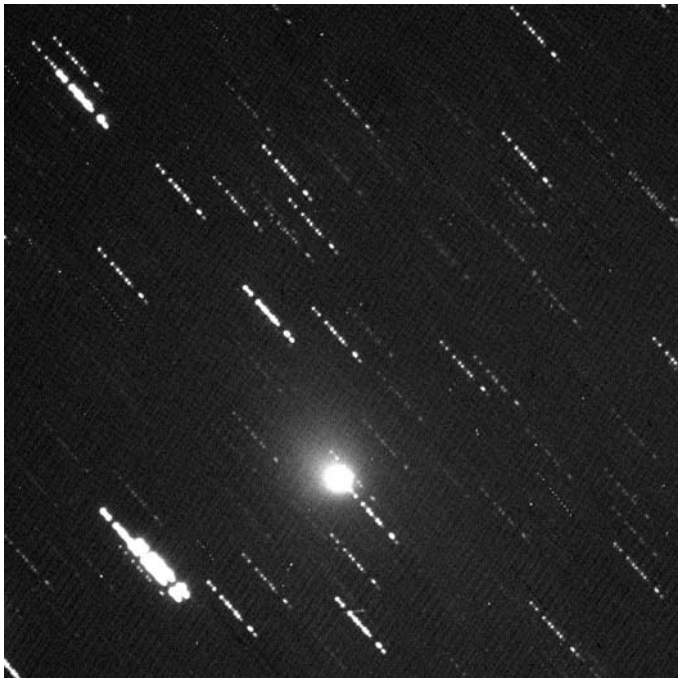

目前系統經過 94 年 11、12 月兩個月的遠距遙控觀測測試，觀測人員可以不用往返鹿林天文台，便可以在任何有網際網路的地方連線進行觀測。下階段將測試進一步的自動化觀測，即不需觀測人員在旁控制，直接交由電腦依排程觀測，預計 95 年 6 月可以達到自動化。圖二及圖三分別爲遠距觀測的監視畫面及遠端控制桌面。

圖一、9P/Tempel 1 彗星深撞(Deep Impact)，使用 40 公分望遠鏡於 2005/07/04 19:46 - 20:45 (CST) 拍攝 (13 張影像合

成)。

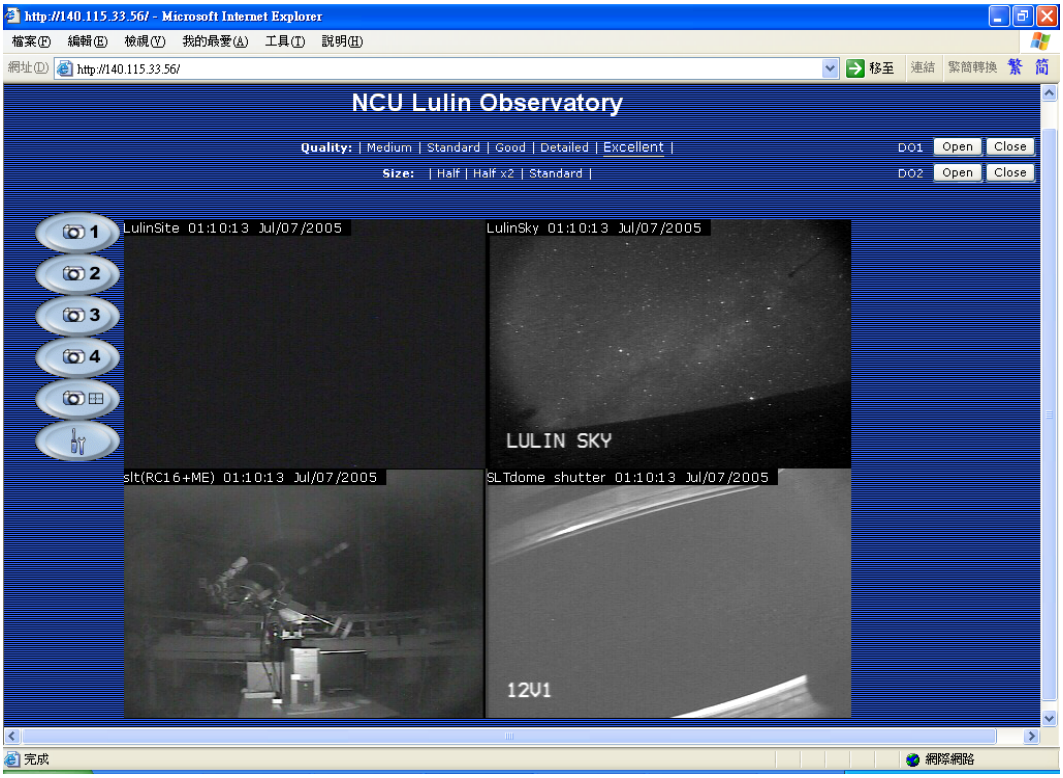

圖二、遠距觀測的監視畫面，左上爲鹿林觀測站的監視畫面、右上爲鹿林的天空、左下的畫面監控 40 公分望遠鏡的狀況，右下爲圓頂天窗

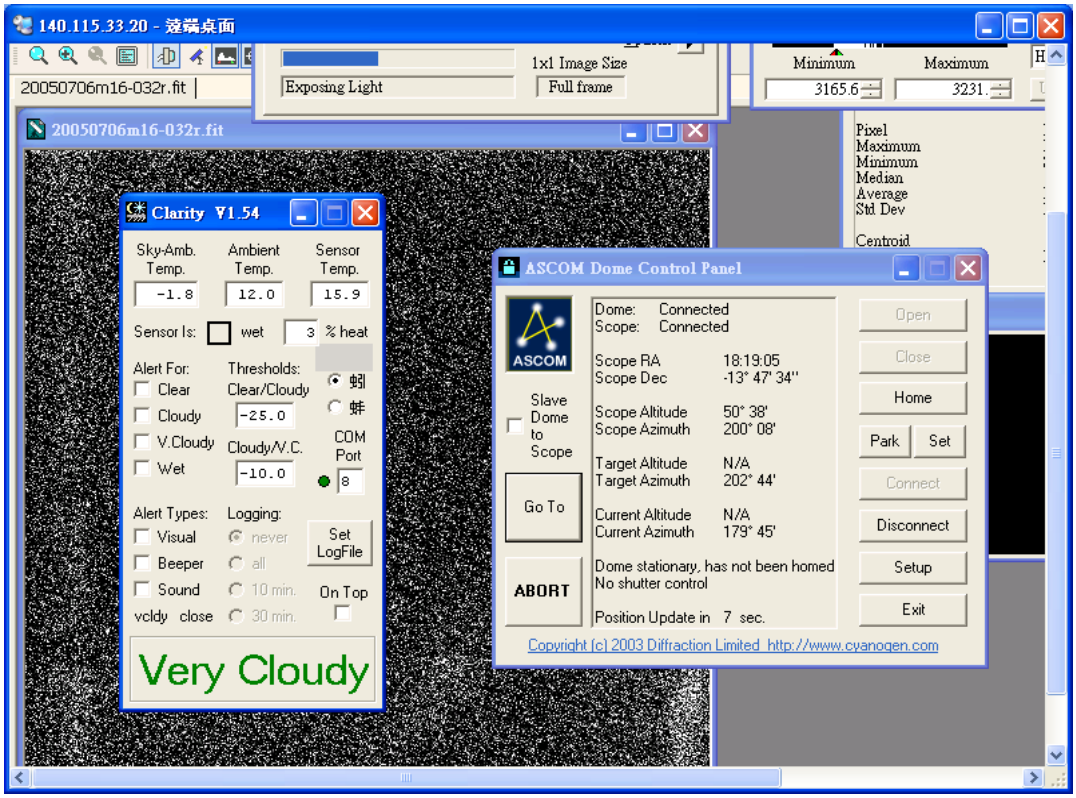

圖三、遠端控制桌面

附錄

全文原載於【台北星空 27 期第 32 頁~第 35 頁】

中大天文所鹿林山開發經驗
——發表於西藏國際天文選址研討大會

文、圖/張光祥

2004年7月5日至9日中國在拉薩召開了「大陸西部天文選址國際研討會」，目地為推動大陸地面天文學的發展和確定未來20年國家天文學科的發展策略及其重要基礎工作，與會人士包括了有來自臺灣、美國、德國、法國、丹麥、澳大利亞、印度、日本等各國具有天文台選址經驗和專門技術的觀測天文學家和研究人員，以及氣象、地質、地理和衛星遙測等與天文台選址相關領域的專家，此研討會對大陸天文事業的發展具有極其重要意義，為國際天文界所矚目。

會議結束後，由24位中外專家組成的探勘隊，從拉薩出發-日喀則-桑桑-措勤-改則-葛爾-新疆葉城-塔什庫爾幹-喀什，沿新藏公路（世界海拔最高的公路），共計八天的行程，穿越崇山峻嶺，一望無際的戈壁荒漠無人區，翻越皚皚冰山冰峰的雪山。

本文作者全程參與，下文是他在研討會中發表的中央大學鹿林天文臺的開發經驗。

新疆塔什庫爾幹（海拔4300公尺）：經視相度觀測後，目前已選定此處爲預定地，即將在此打開一扇探索宇宙的窗口。

考察路線圖

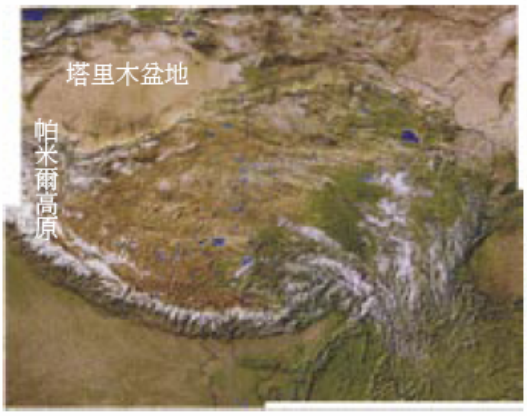

塔里木盆地

帕米爾高原

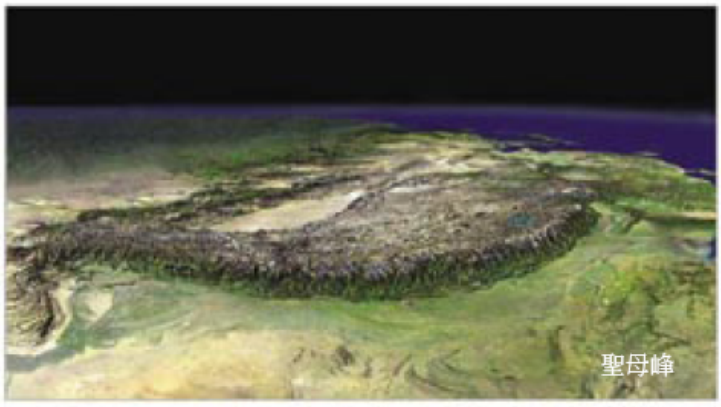

聖母峰

（一） 鹿林山天文臺發展沿革：

三年選址（1989~1992 site survey）

天文台的選址工作，首先要考慮選在高山上（超過逆溫層以上的山頂），接著考慮該地點的晴天數、天空透明度、天空背景、大氣視相度等因素，找尋良好的天文台台址是非常重要的前置作業。綜合考量氣候交通等因素後，中大天文台的選址重點放在鹿林前山、鹿林山、石水山、石山這區域。經過三年監測後，已有平坦腹地的鹿林前山比起其他地點來得優越。

四年規劃（1992~1996）

首先進行臺灣光學望遠鏡的前期評估研究，基本上著重於三點：（1）在科學目的上，邀請國內外華裔天文學者規劃專精的科學研究主題。（2）就目前選定的適當台址，規劃台址與連外道路的地質探勘，以及就台址用地、道路、交通、水電、補給等方面進行開發規劃評估。（3）參考國外著名天文台及望遠鏡規劃經驗及專家意見，研究符合我們所需要的望遠鏡系統。並參訪望遠鏡製造廠商，就設計製造能力與價格方面進行評估。

五年籌建（1997~2002）歷十二年完成鹿林天文臺基地建設

在鹿林前山上建造一座標準形式，又能符合自動望遠鏡連動的天文台，是整個計畫中經費最浩大且工程最艱鉅的部分。為了配合能安放76公分先導型望遠鏡，並預留以後可以安置口徑1.5公尺的經緯式望遠鏡，我們嘗試採用國內首座直徑六公尺的八角型天文台。經歷種種困難，我們才得以完成中大鹿林前山天文台。

（二） 鹿林山天文臺各類基礎建設：

就鹿林前山天文台的基礎工程來說，以下幾項是特別重要的：（1）地下共同管溝，可保


探勘人員合影


雪地紮營

護水電通訊管線。（2）安全的交通動線，可有效完成觀測任務與天文臺營運。（3）充足的電力可兼顧未來發展與儀器正常運作。（4）良好通訊可有效掌握訊息並達成遠距遙控觀測的任務（5）便利的生活機能，可讓駐站人員以及不遠千里而來的觀測人員提升工作效能。

基礎工程的改善會使觀測人員的生活便利，進而提昇工作效能

（三） 鹿林山天文臺未來發展：

我們利用CosPAI（教育部追求卓越發展計畫第五分類子計畫-國內天文研究大環境軟硬體系統之建立）所建立的鹿林天文臺設備，對鄰近明亮星系中產生的超新星進行深入研究。本計劃與國際上此領域之研究群合作，一方面高效率搜尋剛爆發之超新星；另一方面展開即時之光度與光譜之後續觀測。尤其針對Ia型超新星的研究乃是宇宙大尺度距離測量之基礎。我們將探討不同種類超新星與宿主星系類型之間的關係。本計劃結合鹿林天文臺之地理優勢，多波段即時追蹤觀測，以及全自動觀測望遠鏡設備，預期可將本國超新星研究以及其在宇宙學應用方面，推向國際前沿。（本計畫至目前已搜尋到七顆剛爆發之超新星）

鹿林前山天文台軟硬體設備的配合，以及整個超新星爆發的搜尋過程

藏新公路

巧遇牧民，令人興奮（已經兩天沒有看見別人），牧民是無人區看守土地的偉大遊民。

（四） 經驗分享

(1) 依個人在鹿林山天文臺開發之經驗，應從下列幾個工作重點同時展開並依序建設。工作重點有：天文臺址土地取得、選址、評估、基礎建設。基礎建設又分?道路、控制中心、通訊、電力、望遠鏡設計組裝測試、生活機能、維護、觀測營運、後續發展、視像度及氣候之監測長期監測。

(2)八角組合式天文臺的優點：

1. 可分成較小區塊，搬運方便。
2. 可小區域地更換及維護。
3. 組合簡單。
4. 造價比傳統圓頂便宜。

除此之外，天文臺還需要具備通訊、機電、網路、防雷擊設備，以及能穩固地承載望遠鏡的基座。基底必須和其他建築物隔離，才有避震效果。而且不管是經緯儀或赤道儀，望遠鏡運作時的不動點要落在天文臺中心。另外還必須具備防凍功能，維持天文臺的溫度，避免望遠鏡受到溫度的影響而損壞，干擾觀測的品質。

(3)自然生態環境的維護：

基於保護自然生態的立場，有些工作在天文台建造的過程中是非常需要注意的。首先就是設站前後的生態調查及地質鑽探調查，建造過程要注意水土保持。污水及廢棄物的處理也要有妥善的規劃，避免污染原來乾淨的環境。再者是太陽能的使用及雨水、雪水的再利用可以讓在資源較缺少的山上增加水電的來源。像鹿林前山天文台位在玉山國家公園的範圍內，這些考量更是不可或缺！

結語

大陸西部地區天文臺開發成功後，將是晴夜數最高、受光害干擾最少，觀測條件將優於夏威夷、南美智利等地區之天文臺，期望國際合作開發推動的工作能順利展開，屆時觀測的成果，能滿足人類進步的原動力：「好奇心」。

參考資料：
臺北星空第18期北半球最後一個可能安放超大型口徑望遠鏡的地方-西藏。—作者：張光祥
林嵐老師赴藏參加國際天文臺選址活動紀錄。—作者：林嵐

作者：國立中央大學天文所技士

交通建設爲天文臺的重要發展之一，在無人區如果發生交通中斷將會有生命危險！（此圖是在考察過程中，因路況惡劣常造成爆胎，換胎後再上路！）

在研討會中發表：中央大學天文所鹿林前山天文臺的建設發展過程。

登高望遠在鹿林—天文台的現在與未來

作者：葉永烜（國立中央大學天文所教授）

全文原載於【科學月刊 2005 年 10 月號第 800 頁~第 805 頁】

跨國的天文研究中心

如果你在中央大學天文所門前，搭乘每星期的定時班車南下，途中經過新竹、苗栗和台中的平地，從南投水里開始轉入跨山過河的彎路。一路上，你不但可以看到台灣的秀麗風光，也看到土石流帶來怵目驚心的災害。在高度漸增的途中，周遭的植被和景象也跟著變化。經過 5~6 小時的車程，便到達位於玉山國家公園的鹿林前山。把隨身攜帶的儀器和物件背在肩上，沿著一節節的石階，便要作 600 公尺的高陡度攀登，直到海拔 2862 公尺。

在喘息之餘，腦中還在思索「仁者樂山，智者樂水」的意涵時，便已看到一個豁然開朗的平台。順步進去，你的注意力便會被一個高達四層樓的控制中心，和數個大小不一的圓頂建築物所吸引。這便是中央大學鹿林天文台的一米望遠鏡（Lulin One-meter/Optical Telescope，簡稱 LOT）、超新星望遠鏡，和中美掩星合作計畫（Taiwan-American Occultation Survey，簡稱 TAOS）的基地（圖一）。

在天文台周遭走走，你會看到更多的天文觀察儀器，其中包括中央大學天文所的窄波巡天計畫、中央大學大氣系的亞洲大氣污染物的長程輸送與衝擊研究站，及成功大學物理系的紅色精靈極低頻無線電波偵測系統。其中，一米望遠鏡開放給國內外天文學家申請應用，而中美掩星合作計畫則是中央大學、中央研究院及美國加州大學羅倫斯利佛摩國家實驗室（Lawrence Livermore National Laboratory, LLNL）的合作計畫。鹿林天文台現在已經是一個跨校以及跨國的天文研究中心，整個規模的起源如登山之路，有點崎嶇，也有點柳暗花明又一村的感覺。

一步一腳印的打造

鹿林天文台的建設，是中央大學不斷地投入十多年的精神和心血而成。現今在天文台埋頭工作的研究人員，可能無法想像在 4~5 年前，天文台還沒有水電供應，而通訊系統更是極度缺乏的狀況。由於還沒有鋪上木頭階梯，那一條步道更顯漫長。對參加觀察工作的人員而言，每一次任務都是體力和意志力的挑戰。

幸好在 2000 年起，我們有機會與台灣大學和中研院合作，參加教育部的「追求卓越」計畫，提出「宇宙學和粒子物理學」計畫方案。其中，中央大學負責建立國內天文學研究環境的大架構。是在這個契機著力之下，我們才得以進行有關道路、通訊和水電的工程。計畫執行過程中，更有機會得中央大學校方支持，使原提案中的控制中心得以完成。

另一項關鍵性的發展，便是陳文屏教授物色到一部剛用過不久的一米望遠鏡，可以半價購置。從德國搬運到台灣後，也很順利在 2002 年 9 月正式啓用，上線運作。現在說來這些好像都帶點運氣，實際上，在過去的年月裡，我們是一步一腳印，沒有天文所同仁不折不撓、同心協力的精神，鹿林天文台的一切可能還是遙遙無期。

鹿林天文台是由林宏欽站長負責當地各項後勤和技術性事務。此外，還有四名當地鄒族

的青年助理協助。他們的勤奮工作，讓國內和外地訪問學者留下很深刻的印象。事實上，美國哈佛史密遜天文台（Smithsonian center for Astrophysics）台長 Charles Alcock，在一次科學會議中，敘述鹿林天文台的從無到有，以致各項事情的井然有序，可稱許爲一件英雄事蹟。不到鹿林非好漢，大概就是這個意思（圖二）。

至於望遠鏡時間的分配，則由中央大學、成功大學等院校教授所組成的委員會，針對每季（一年中分爲 1 月~6 月及 7 月~12 月兩季）國內外各研究小組提出的計畫加以審查，根據科學目標的優劣及可行性，作觀測時間的分配。根據統計，鹿林天文台每季平均都有 18 個計畫在進行。這表示 LOT 已成爲國內天文學教育和研究的一個重要工具。

南天觀測獨領風騷

鹿林天文台的觀察工作可以歸納爲幾個主題，這些都是利用到小型望遠鏡和台灣觀測條件的優勢。因爲小型望遠鏡的運作及時間的分配，都比口徑二米以上的大型望遠鏡更具有彈性。所以 LOT 可以用來研究天文物體亮度，長達數小時以致數天的連續時間變化。

由於台灣的緯度靠近赤道，經度則與夏威夷遙遙相隔幾千里。因此我們一方面可以集中注意力在南方天空的目標，對於瞬間發生的天文現象（如超新星及伽瑪爆），更是在全天 24 小時占了 5~6 小時的便宜，獨領風騷。我們在文後便會提到，如何在這個基礎上，盡量發揮台灣的科學資源，和天文研究的特色。

當 LOT「開光」不久之後，便派上用場。成功大學、中央大學，以及美國耶魯大學的天文單位有個合作計畫，是利用 LOT 和 RXTE 衛星的 X 光天文望遠鏡作同步觀測。這次的觀察工作非常順利，也有很好的結果。此外，在全球性的 WEBT（Whole Earth Blazar Telescope）計畫中，鹿林天文台也扮演一個重要的角色。這兩個例子，讓我們對台灣的天空觀測，在時空的優勢更有信心。兩年的功夫下來，鹿林天文台有好幾個具前瞻性的天文觀察計畫，已經有一些重要的成果，分述如下。

中美掩星合作計畫

這個原本由中央大學天文所、中研院天文及天文物理研究所籌備處，和美國利佛摩國家實驗室合作的方案，現有韓國延世大學天文系的加入。所以共有四個 50 公分的廣角望遠鏡，聯合且同時監測數個恆星亮度的變化。

觀測原理在於如果從一個恆星到地球的光線路徑中，偶然受到一個小物體的遮掩，產生爲時很短的掩星效應，把亮度降低。3~4 個望遠鏡同時觀測，便可以大幅增加這些瞬間掩星現象的可像性（圖一）。

此計畫的主要科學目標，是普查海王星軌道外的柯伊伯帶（Kuiper belt）中 10 公里左右的小物體。最近有科學家找到一個在海王星軌道以外運行，直徑約爲 2600 公里，名爲 2003 UB313 的物體。在柯伊伯帶外，很可能還保留著許多太陽系形成時所餘留的物質。這對太陽系來源的理論有很大的挑戰。

經過 5~6 年的埋頭苦解，TAOS 已展開正式的科學工作。除了柯伊伯帶物體的普查，還

有一些預料之外的大發現。想風流人物，還看今朝，它的成果衝擊力實可預期。

鹿林發射線影像普查計畫

鹿林發射線影像普查計畫簡稱 LELIS 計畫，是孫維新教授主導的另一個別具特性的計畫。主要由三台 10 公分的廣角望遠鏡（視場＝2.8×4.2 平方角度）所組成。每一座望遠鏡都配有特定濾光片（SII、OIII、Hα）。LELIS 的特殊功能在於能在短時間內，作大幅天區的巡天觀察工作。由於短焦距的緣故，低亮度的恆星星際空間的物質全都一覽無遺。因爲類似的多波段設備，仍是鳳毛麟角，所以已經引起國際間天文界不少的注意。

低質量雙星系統 X 射線源

在雙星系統演化過程中的吸稱過程，會導致強烈的 X 光輻射。從它們的光度變化，可以推導整個物理過程。一個特別有趣的目標便是 XTE J1118＋ 480。它的 X 光射線輻射的時間變化，指向存有超駝峰（Superhump）現象，此由圍繞一個中子星的吸稱盤所產生。中央大學天文所周翊教授的研究小組，利用 LOT 進行歷時一年半的觀察，在 2005 年 1 月中的觀察資料中得到很有趣的重要結果。

彗星和小行星的觀測

1 公尺口徑的天文望遠鏡用於明亮彗星的觀察已綽綽有餘。在 2005 年初，研究人員用 LOT 拍攝到彗星 2004 Q2（Machholz）的 H2O＋離子尾結構的時間變化，這一筆資料將有助科學家了解彗星離子尾的來源和演變。

在小行星的研究方面，我們除了中央大學天文所同仁的計畫外，並極力推動國際合作，其中包括了美國夏威夷大學 David Jewitt 教授的團隊，和日本宇航研究所的小行星太空探測部門的阿部教授，協同觀測將來小行星計畫可能目標的物理性質。此外，中央大學天文所的觀測員也發現了兩個新的小行星。

超新星巡天計畫

如前文所述，鹿林天文台的主要軟硬體架構，都是透過教育部以及國科會「追求卓越」計畫的支援才得以完成。經過多方考慮，我們便敲定以「超新星的巡天觀察」作爲相關後續計畫的科學工作。一方面，這個計畫可以借重台灣的地理位置，專注在南方天空的星系目標。從這個天時地利的條件，切入宇宙學研究的一個焦點。

1998 年兩個在美國柏克萊加州大學（University of California, Berkeley）的超新星研究小組，不約而同地公布一個重要結果：從 Ia 型超新星的觀察可以推論宇宙在加速膨脹之中。由此證明，愛因斯坦覺得鑄成大錯的「宇宙常數」確有其事。這個結果在一夕之間，將暗能量（dark energy）這個匪夷所思的名詞，變成宇宙中無所不在的事物。

中央大學天文所也是趁著這股銳氣，把握機會開墾超新星這個多采多姿的課題。從 2003 年底至今，已發現了 10 個超新星（圖三）。相關研究小組也和美國柏克萊加州大學、大陸北京天文台團隊建立合作關係。除了超新星爆發的監察外，還對「各類超新星亮度的時間變化作追蹤」，和「超新星的發生和星系環境的關係」等題目展開深度研究。

伽瑪爆可見光餘暉的認定

在宇宙深空中，有一種比超新星爆發還更劇烈的能量釋放，爲時不過數秒，可以把整個星系都照亮。這種謎樣的伽瑪射線和 X 射線的高能現象，往往會產生長達幾分鐘到幾十分鐘的可見光餘暉。這些餘暉的亮度變化帶有伽瑪爆（Gamma-ray bursts）機制，和其火球擴張過程的主要資訊。所以在太空中的 X 光或伽瑪射線望遠鏡，若偵查到這些瞬時事件，便會即時通知地面上的天文台，希望能有機會在第一時間偵查到這些突然出現的光點。鹿林天文台的 LOT 在 2004 年便投入這項工作。

這種龐大的國際合作計畫要得到成績，便在於天文台的觀察人員能否通力合作和任勞任怨，將手頭上要進行的觀測暫時放下，主動轉移目標，替伽瑪爆餘暉計畫爭取這千載一時的資料。當我聽到研究生們敘述這些默契和緊密合作關係時，不禁對「仁者樂山」這句話略有所悟。至少在鹿林前山是如此！

中央大學天文所、日本東京的理化研究所宇宙線實驗室，以及大陸北京天文台共同合作，組成一個伽瑪爆餘暉觀察網。經過多月來的努力，終於在近日連續得到數個餘暉的資料，將鹿林天文台放入了伽瑪爆研究的版圖。整體而言，在這種大規模國際科學合作中，重要的是團隊精神的建立。有了這些有形和無形的架構，現在的我們充滿信心追求更崇高的科學目標。

與夏威夷大學合作

在十年前，大概還沒有人會猜想到，台灣本土的半導體製作技術可以超越美國。台灣本土的科學資源極爲豐富，現在更添加了事在人爲的精神，所以我們應該更有企圖心。在我們的藍圖中，鹿林天文台是攀登高峰、追求卓越的第一步。在規畫「台灣超新星巡天計畫」時，我們已經注意到這類的研究工作在十年內的發展了。

美國夏威夷大學天文所，和美國空軍合作的泛星計畫（ Pan-STARRS），是由四個二米口徑的廣角望遠鏡組成。在 4 天時間內便能把整個天區攝照一遍。主要的任務，是偵查可能對地球構成碰撞威脅的近地物體。但超新星的發現和亮度變化的監控、伽瑪爆餘暉、柯伊柏帶物體普查，以至重力效應和大尺度結構也都是重要課題。

所以泛星計畫的科學任務，和鹿林天文台的部分工作非常一致。我們希望能有機會和美國夏威夷大學天文所建立合作關係，當這個計畫在 2006~2007 年上線後，這邊的研究團隊就更有英雄用武之地。

資料爆炸和資訊氾濫

美國的國家光學天文台（National Optical Astronomy Observatory, NOAO）與相關學術隊伍，也在規畫一個更大（8.4 米口徑）的廣角望遠鏡，如果一切順利，可能在 2010 左右便開始操作。這個稱爲「暗物質望遠鏡」的計畫有個非常特別的地方，便是將得到的觀察資料，以近似即時的速度，公開給科學界使用，供相關人員從中擷取需要的資料作進一步的研究工作。

這種做法對研究人員極有幫助，也是目前天文學界的大趨勢。現在太空中有多架太空望

遠鏡在不同的波段，日夜不停地錄取資料。地面上大大小小的望遠鏡也是如此。天文學已經面臨資訊爆炸和資料氾濫的情況。一小段時間內得到的影像或光譜，可能需要十倍甚至百倍的時間來作整理和分析。所以有些太空計畫或天文台便索性把觀察資料都放在網站，供有興趣的大眾取用。

架構虛擬天文台

當中一個有趣的例子，便是台灣一位業餘天文學家，利用歐洲太空總署（ESA）的太陽鑒太陽圈太空站（Solar and Heliospheric Observatory, SOHO）太空船提供的圖片，發現了一顆近日彗星。這是在台灣發現的第一顆彗星，而且沒有使用到望遠鏡！這種只在網站上存在，把資訊科學和天文學的尖端發展結合在一起，以軟體爲主的「虛擬天文台」的架構，現在已成爲各個國家天文台的主流思潮。

台灣在這個新興領域應該極力發展一片天地，因爲在「虛擬天文台」的高效益、低成本投資，可部分抵銷大型硬體設備和儀器研發的不足；另一方面，也可以利用台灣在資訊科技以及資料分析的優勢，激發天文研究另外的兩個重要方向。理論工作和數值模擬的發展，配合著 e 科學的雷厲風行，國內產業更可由此提升。這實在值得國家科學委員會和經濟部重視。我們在此只是藉著中央大學鹿林天文台的一些計畫加以簡略說明。

培育天文人才的急迫

最後，我們要探討一個重要的課題。根據最近一項調查，台灣的小學生對科學的興趣越來越薄弱，這實在是一大警訊。事實上，在其他先進國家也存在同樣的現象，大家都在設法扭轉這個局面，如美國航太總署（NASA）的太空計畫便一直想盡辦法，把行星探測的有趣結果放入中小學的教材。認知科學的專家更指出，幼稚園和國小的小朋友，如果在 7~8 歲前未能引起科學的興趣，以後可能會越來越困難。

比起其他的太空天文教材，火星、彗星、木星和土星，可以說是最容易引起小孩子的好奇心與想像力，更不用說超新星殘骸和行星狀星雲的圖片。單就教育層面來看，美國航太總署、歐洲太空總署、日本宇航局，以及其他國家的天文太空科學計畫，雖是耗資極鉅，但實在都物有所值，我們有什麼理由不作同樣的思考？

從天文學研究大架構的建立，到以鹿林天文台作爲培育人才的搖籃，以及凝聚研究能量的中心，又談到天文教育在社會將來發展的功能，情況確實是有點緊迫。

來趟奇妙之旅吧！

在今日的世界裡，哪個國家的年輕一代可以在科技出頭，便可以掌握國家的命運，下一代能不好好培養嗎？在過去，可能只有強大的國家才能推動相關天文研究。但是在未來，可能要以天文研究和教育來確保國富邦強。天文研究和教育，便是整個國家科技創新的磐石之一。

因此，歡迎大家有機會來到中央大學參觀，在這裡，你可以看到其他五花八門的天文研究工作，也可以和我們一齊勾勒鹿林之路，從山下到山上，一步步地從一無所有到峰迴路轉、豁然開朗，再到達最新進的技術，好仰視宇宙時空。這將是一個充滿奇妙事物的旅程。

登高望遠在鹿林—天文台的現在與未來

葉永烜

現在的鹿林天文台是個跨校、跨國的天文研究中心，
回想整個天文台從無到有的純屬過程，讓真的是柳暗花明又一村。

跨國的天文研究中心

如果你在中央大學天文所門前，搭乘每星期的定時班車南下，途中經過新竹、苗栗和台中的平地，從海拔水里開始轉入到山過河的彎路，一路上，你不但可以看到台灣的秀麗風光，也看到土石流帶來慌目驚心的災害。在高度的增的途中，周遭的植被和景象也跟著變化。經過 5~6 小時的車程，便到達位於玉山國家公園的鹿林前山。把隨身攜帶的儀器和物件背在肩上，沿著一節節的石階，便要作 600 公尺的高陡攀登，直到海拔 2862 公尺。

在喘息之餘，醫中還在思索「仁者樂山，智者樂水」的意義時，便已看到一個酷然開朗的平台，順步走去，你的注意力便會被一個高達四層樓的控制中心，和數個大小不一的圓頂建築物所吸引。這便是中央大學鹿林天文台的一米望遠鏡（Lulin One-meter/Optical Telescope，簡稱 LOT）、超新星望遠鏡，和中美掩星合作計畫（Taiwan-American Occultation Survey，簡稱 TAOS）的基地（圖一）。

在天文台周遭走走，你會看到更多的天文觀察儀器，其中包括中央大學天文所的寧波巡天計畫、中央大學大氣系的亞洲大氣污染物的長程輸送與衝擊研究站，及成功大學物理系的紅色精靈極低頻無線電波偵測系統。其中，一米望遠鏡開放給國內外天文學家申請應用，而中美掩星合作計畫則是中央大學、中央研究院及美國加州大學經費斯利佛摩國家實驗室（Lawrence Livermore National Laboratory, LLNL）的合作計畫。鹿林天文台現在已經是一個跨校以及跨國的天文研究中心，整個規模的起首如玉山之腳，有點崎嶇，也有點柳暗花明又一村的感覺。

一步一腳印的打造

鹿林天文台的建設，是中央大學不斷地投入十多年的精神和心血而成。現今在天文台裡頭工作的研究人員，可能無法想像在 4~5 年前，天文台還沒有水電供應，而通訊系統更是極度缺乏的狀況。由於還沒有鋪上木頭階梯，那一條步道更顯漫長。對參加觀察工作的人員而言，每一次任務都是體力和意志力的挑戰。

幸好在2000年起，我們有機會與台灣大學和中研院合作，參加教育部的「追求卓越」計畫，提出「宇宙學和粒子物理學」計畫方案。其中，中央大學負責建立國內天文學研究環境的大架構。是在這個架構著力之下，我們才得以進行有關通訊、通訊和水電的工程。計畫執行過程中，更有幾會得中央大學校方支持，使原提案中的控制中心得以完成。

另一項關鍵性的發展，便是陳文屏教授物色到一部剛用過不久的一米望遠鏡，可以半價購置。從德國搬運到台灣後，也很順利在2002 年 9 月正式啟用，上線運作。現在說來這些好像都帶點運氣，實際上，在過去的年月裡，我們是一步一腳印，沒有天文所同仁不折不撓、同心協力的精神，鹿林天文台的一切可能還是遙遙無期。

鹿林天文台是由林宏欽站長負責當地各項後勤和技術性事務。此外，還有四名當地鄒族的青年助理協助，他們的勤奮工作，讓國內和外地訪問學者留下很深刻的印象。事實上，美國哈佛史密遜天文台（Smithsonian center for Astrophysics）台長 Charles Alcock，在一次科學會議中，敘述鹿林天文台的從無到有，以致各項事情的井然有序，可稱許為一件英雄事蹟。不到鹿林非好漢，大概就是這個意思（圖二）。

至於望遠鏡時間的分配，則由中央大學、成功大學等院校教授所組成的委員會，針對每季（一年中分為 1 月~6 月及 7 月~12 月兩季）國內外各研究小組提出的計畫加以審查，根據科學目標的優劣及可行性，作觀測時間的分配。根據統計，鹿林天文台每季平均都有 18 個計畫在進行。這表示 LOT 已成為國內天文學教育和研究的一個重要工具。

南天觀測獨領風騷

鹿林天文台的觀察工作可以歸納為幾個主題，這些都是利用到小型望遠鏡和台灣觀測條件的優勢。因為小型望遠鏡的運作及時間的分配，都比口徑二米以上的大型望遠鏡更具有彈性。所以 LOT 可以用來研究天文物體亮度，長達數小時以致數天的連續時間變化。

由於台灣的緯度靠近赤道，經度則與夏威夷遙遙相隔幾千里。因此我們一方面可以集中注意力在南方天空的目標，對於瞬間發生的天文現象（如超新星及伽瑪爆），更是在全天 24 小時占了 5~6 小時的便宜，獨領風騷。

我們在文後便會提到，如何在這個基礎上，盡量發揮台灣的科學資源，和天文研究的特色。

當 LOT「開光」不久之後，便派上用場。成功大學、中央大學，以及美國耶魯大學的天文單位有儀合作計畫，是利用 LOT 和 RXTE 衛星的 X 光天文望遠鏡作同步觀測。這次的觀察工作非常順利，也有很好的結果。此外，在全球性的 WEBT（Whole Earth Blazar Telescope）計畫中，鹿林天文台也扮演一個重要的角色。這兩個例子，讓我們對台灣的天空觀測，在時空的優勢更有信心。兩年的功夫下來，鹿林天文台有好幾個具前瞻性的天文觀察計畫，已經有一些重要的成果，分述如下。

中美掩星合作計畫

這個原本由中央大學天文所、中研院天文及天文物理研究所籌備處，和美國利佛摩國家實驗室合作的方案，現有韓國延世大學天文系的加入。所以共有四個 50公分的廣角望遠鏡，聯合且同時監測數個恆星亮度的變化。

觀測原理在於如果從一個恆星到地球的光錐路徑中，偶然受到一個小物體的遮掩，產生為時很短的掩星效應，把亮度降低。3~4 個望遠鏡同時觀測，便可以

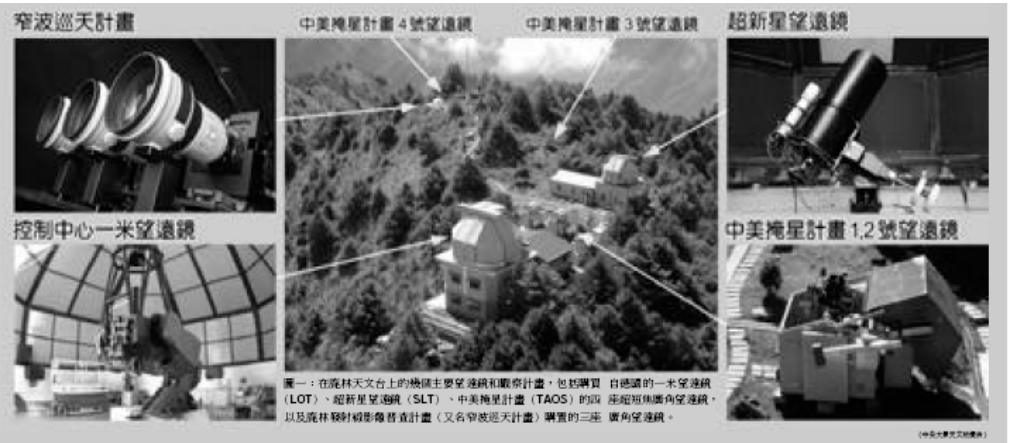

圖一：在鹿林天文台上的機儀主要望遠鏡和觀察計畫，包括購買自德國的一米望遠鏡（LOT）、超新星望遠鏡（SLT）、中美掩星計畫（TAOS）的四座超短焦廣角望遠鏡，以及鹿林發射線影像普查計畫（又名寧波巡天計畫）購置的三座廣角望遠鏡。

（中央大學天文所提供）

大幅增加這些瞬間掩星現象的可像性（圖一）。

此計畫的主要科學目標，是普查海王星軌道外的柯伊伯帶（Kuiper belt）中10公里左右的小物體。最近有科學家找到一個在海王星軌道以外運行，直徑約為 2600 公里，名為 2003 UB313 的物體。在柯伊伯帶外，很可能還保留著許多太陽系形成時所餘留的物質。這對太陽系來源的理論有很大的挑戰。

經過 5~6 年的埋頭苦幹，TAOS 已開展正式的科學工作。除了柯伊伯帶物體的普查，還有一些預料之外的大發現。想風流人物，還看今朝，它的成果衝擊力實可預期。

鹿林發射線影像普查計畫

鹿林發射線影像普查計畫簡稱 LELIS 計畫，是薛絳新教授主導的另一個別具特性的計畫。主要由三台 10 公分的廣角望遠鏡（視場＝2.8×4.2 平方角度）所組成。每一座望遠鏡都配有特定濾光片（SII、OIII、Hα）。LELIS 的特殊功能在於能在短時間內，作大幅天區的巡天觀察工作。由於短焦距的緣故，低亮度的恆星際空間的物質全都一覽無遺。因為類似的多波段設備，仍是鳳毛麟角，所以已經引起國際間天文界不少的注意。

低質量雙星系統 X 射線源

在雙星系統演化過程中的吸積過程，會導致強烈的 X 光輻射。從它們的光度變化，可以推導整個物理過程。一個特別有趣的目標便是 XTE J1118 + 480。它的 X 光射線輻射的時間變化，指向存有超黑峰（Superhump）現象，此由圍繞一個中子星的吸積盤所產生。中央大學天文所周御教授的研究小組，利用 LOT 進行歷時一年半的觀察。在 2005 年 1 月中的觀察資料中得到很有趣的重要結果。

彗星和小行星的觀測

1 公尺口徑的天文望遠鏡用於明亮彗星的觀察已綽綽有餘。在2005年初，研究人員用LOT拍攝到彗星 2004 Q2 (Machholz) 的 H_2O^+ 離子尾結構的時間變化，這一筆資料將有助科學家了解彗星離子星的來源和演變。

在小行星的研究方面，我們除了中央大學天文所同仁的計畫外，並極力推動國際合作，其中包括了美國夏威夷大學 David Jewitt 教授的專隊，和日本宇航研究所的小行星太空探測部門的阿部教授，協同觀測將來小行星計畫可能目標的物理性質。此外，中央大學天文所的觀測儀也發現了兩個新的小行星。

超新星巡天計畫

如前文所述，鹿林天文台的主要軟硬體架構，都是透過教育部以及國科會「追求卓越」計畫的支援才得以完成。經過多方考慮，我們便決定以「超新星的巡天觀察」作為相關後續計畫的科學工作。一方面，這個計畫可以借重台灣的地理位置，專注在南方天空的星系目標。從這個天時地利的條件，切入宇宙學研究的一個焦點。

1998 年兩個在美國柏克萊加州大學（University of California, Berkeley）的超新星研究小組，不約而同地公布一個重要結果：從 Ia 型超新星的觀察可以推論宇宙在加速膨漲之中。由此證明，愛因斯坦曾經成大錯的「宇宙常數」確有其事。這個結果在一夕之間，將暗能量（dark energy）這個匪夷所思的名詞，變成宇宙中無所不在的事物。

中央大學天文所也是趁著這股銳氣，把握機會開墾超新星這個多采多姿的課題。從 2003 年底至今，已發現了 10 個超新星（圖三）。相關研究小組也和美國柏克萊加州大學、大陸北京天文台廣泛建立合作關係。除了超新星爆發的監察外，還對「各類超新星亮度的時間變化作追蹤」，和「超新星的發生和星系環境的關係」等題目開展深度研究。

伽瑪爆可見光餘暉的認定

在宇宙深空中，有一種比超新星爆發還更劇烈的能量釋放，為時不過數秒，可以把整個星系都照亮。這種謎樣的伽瑪射線和 X 射線的高能現象，往往會產生長達幾分鐘到幾十分鐘的可見光餘暉。這些餘暉的亮度變化帶有伽瑪爆（Gamma-ray bursts）機制，和其火球膨脹過程的主要資訊。所以在太空中的 X 光或伽瑪射線望遠鏡，若偵查到這些瞬時事件，便會即時通知地面上的天文台，希望能有機會在第一時間偵查到這些突然出現的光點。鹿林天文台的LOT在2004年便投入這項工作。

這種龐大的國際合作計畫要得到成績，便在於天文台的觀察

圖二：2001年11月中旬獅子座流星雨，中研院李遠哲院長與鹿林天文台工作人員。

人員能否通力合作和任勞任怨，將手頭上要進行的觀測暫時放下，主動轉移目標，替值瑪爆餘暉計畫爭取這千載一時的資料。當我聽到研究生們敘述這些默契和緊密合作關係時，不禁對「仁者樂山」這句話略有所悟。至少在鹿林前山是如此！

中央大學天文所、日本東京的理化研究所宇宙線實驗室，以及大陸北京天文台共同合作，組成一個值瑪爆餘暉觀察網，經過多月來的努力，終於在近日連續得到數個餘暉的資料，將鹿林天文台放入了值瑪爆研究的版圖。整體而言，在這種大規模國際科學合作中，重要的是團隊精神的建立。有了這些有形和無形的架構，現在的我們充滿信心追求更崇高的科學目標。

與夏威夷大學合作

在十年前，大概還沒有人會猜想到，台灣本土的半導體製作技術可以超越美國。台灣本土的科學資源極為豐富。現在更添加了事在人為的精神，所以我們應該更有企圖心。在我們的藍圖中，鹿林天文台是攀登高峰、追求卓越的第一步。在規畫「台灣超新星巡天計畫」時，我們已經注意到這裏的研究工作在十年內的發展了。

美國夏威夷大學天文所，和美國空軍合作的泛星計畫（Pan STARRS），是由四個二米口徑的廣角望遠鏡組成。在 4 天時間內便能把整個天區攝照一遍。主要的任務，是偵查可能對地球構成碰撞威脅的近地物體，但超新星的發現和亮度變化的監控、值瑪爆餘暉、柯伊柏帶物體普查，以至重力效應和大尺度結構也都是重要課題。

所以泛星計畫的科學任務，和鹿林天文台的部分工作非常一致。我們希望能有機會和美國夏威夷大學天文所建立合作關係，當這個計畫在 2006~2007 年上線後，這邊的研究團隊就更有英雄用武之地。

資料爆炸和資訊氾濫

美國的國家光學天文台（National Optical Astronomy Observatory, NOAO）與相關學術隊伍，也在規畫一個更大（8.4 米口徑）的廣角望遠鏡，如果一切順利，可能在 2010 左右便開始操作。這個稱為「暗物質望遠鏡」的計畫有個非常特別的地方，便是將得到的觀察資料，以近似即時的速度，公開給科學界使用，供相關人員從中擷取需要的資料作進一步的研究工作。

這種做法對研究人員極有幫助，也是目前天文學界的大趨勢。現在太空中有多架太空望遠鏡在不同的波段，日夜不停地錄取資料。地面上大大小小的望遠鏡也是如此。天文學已經面臨資訊爆炸和資料氾濫的情況。一小段時間內得到的影像或光譜，可能需要十倍甚至百倍的時間來作整理和分析。所以有些太空計畫或天文台便索性把觀察資料都放在網站，供有興趣的大眾取用。

架構虛擬天文台

當中一個有趣的例子，便是台灣一位業餘天文學家，利用歐洲太空總署（ESA）的太陽雲太陽圈太空站（Solar and Heliospheric Observatory, SOHO）太空船提供的資料，發現了一顆近日彗星。這是在台灣發現的第一顆彗星，而且沒有使用到望遠鏡！這種只在網站上存在，把資訊科學和天文學的尖端發展結合在一起，以軟體為主的「虛擬天文台」的架構，現在已成為各個國家天文台的主流思潮。

台灣在這個新興領域應該極力發展一片天地。因為在「虛擬天文台」的高效益、低成本投資，可部分抵銷大型硬體設備和儀器研發的不足；另一方面，也可以利用台灣在資訊科技以及資料分析的優勢，激發天文研究另外的兩個重要方向。理論工作和數值模擬的發展，配合著 e 科學的蓬勃風行，國內產業更可由此提升。這實在值得國家科學委員會和經濟部重視。我們在此只是藉著中央大學鹿林天文台的一些計畫加以簡略說明。

培育天文人才的急迫

最後，我們要探討一個重要的課題。根據最近一項調查，台灣的小學生對科學的興趣越來越薄弱。這實在是一大警訊。事實上，在其他先進國家也存在同樣的現象，大家都在設法扭轉這個局面。如美國航太總署（NASA）的太空計畫便一直想盡辦法，把行星探測的有趣結果放入中小學的教材。認知科學的專家更指出，幼稚園和國小的小朋友，如果在 7~8 歲前未能引起科學的興趣，以後可能會越來越困難。

比起其他的太空天文教材，火星、彗星、木星和土星，可以說是最容易引起小孩子的好奇心與想像力，更不用說超新星殘骸和行星狀星雲的圖片。單就教育層面來看，美國航太總署、歐洲太空總署、日本宇航局，以及其他國家的天文太空科學計畫，雖是耗資極鉅，但實在都物有所值，我們有什麼理由不作同樣的思考？

從天文學研究大架構的建立，到以鹿林天文台作為培育人才的搖籃，以及凝聚研究能量的中心，又談到天文教育在社會將來發展的功能，情況確實是有點緊迫。

來趟奇妙之旅吧！

在今日的世界裡，哪個國家的年輕一代可以在科技出頭，便可以掌握國家的命運。下一代能不好好培養嗎？在過去，可能只有強大的國家才能推動相關天文研究。但是在未來，可能要以天文研究和教育來確保國富邦強。天文研究和教育，便是整個國家科技創新的磐石之一。

因此，歡迎大家有機會來到中央大學參觀，在這裡，你可以看到其他五花八門的天文研究工作，也可以和我們一齊勾勒鹿林之路，從山下到山上，一步步地從一張所有到雞逃踏轉、豁然開朗，再到達最新進的技術，好仰視宇宙時空。這將是一個充滿奇妙事物的旅程。

葉永烜：任教
中央大學天文所及太空研究所

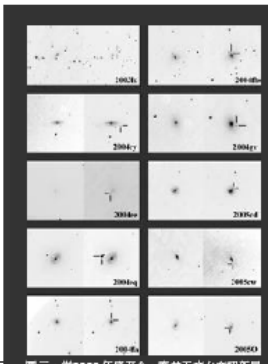
圖三：從2003 年底至今，鹿林天文台在超新星巡天計畫中發現的十顆超新星。

This page intentionally left blank.

相關報導

台日國際合作觀測 Deep Impact 任務

原載於日本【星空月刊 2005 年九月號】

台湾でのディープインパクト観測

台日国際協力

2005年7月4日にアメリカの探査機ディープインパクトがテンペル第1彗星に衝突体をぶつけた。彗星核の表面や内部を調べるこの野心的な探査計画を受けて、台湾の國立中央大學天文研究所と、日本の国立天文台、早稲田大学、東京大学などからなる研究グループは東アジアでの観測を協力して行うことにした。ディープインパクトにあたっての、台湾と日本の国際共同観測について報告する。

文／木下大輔（日本学術振興会特別研究員）、台日国際協力チーム

7月初めの日本は梅雨である。一方、台湾ではすでに梅雨は終わり、本格的な夏を迎える時期となる。我々はこの点に目をつけ、日本の偏光撮像装置PICO（Polarimetric Imager for COmet）を台湾の國立中央大學の鹿林天文台の1m望遠鏡に取り付けて観測を行うことを計画した。PICOは、早稲田大学の古荘玲子助手らによって製作された、彗星から放出された塵による偏光を測る装置である。視野内の平均的な偏光度を測るのではなく、画像を取得し偏光度を得るので、彗星コマのなかの偏光度の空間分布を調べることが可能である。PICOによる観測から、彗星の塵の組成やサイズ分布や形状などの物理的特性などを明らかにすることを狙った。

鹿林天文台は、台湾の最高峰である玉山のそばにある天文台である。国立公園の中にあるため道路を作ることができず、最後の30分は歩いて登らなければたどり着けない。我々は、天文台の先住民（鄒族）スタッフの力も借りて、人力でPICOを観測所まで運び上げた。調整に時間がかかったが、なんとか現象の前後でのデータ取得に成功した。観測データの詳細な解析は現在、精力的に行われているところだが、輝度分布からは彗星から放出された塵が広がっていく様子が見え、また、偏光度分布からは彗星コマ中の偏光度が衝突の前後で空間的に変化していることがとらえられている。

近年、天文学における地域協力の必要性が叫ばれ始めている。今回の観測では、台湾側が現象の時期に天候に恵まれそうなサイトと望遠鏡とCCDを、日本側が偏光撮像モジュールを提供し、協力が成立した。国を越えた協力により、より科学的な意義の高い観測を実現できる場合には、今後も積極的に国際協力を模索したいと考えている。

メンバー（アルファベット順、敬称略）
張明新（國立中央大學）／古荘玲子（早稲田大学）
池田優二（Genesia, Co.）／葉永助（國立中央大學）
春日敬測（総研大）／河北秀世（京都産業大学）
木下大輔（國立中央大學、国立天文台）
林宏欽（國立中央大學）／林忠義（國立中央大學）
佐藤祐介（東京大学）／渡部潤一（国立天文台）

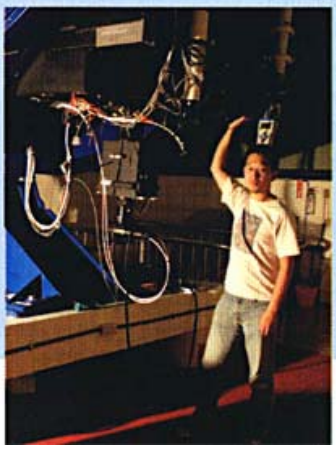

鹿林1メートル望遠鏡に取り付けたPICO。右は筆者。

7月3日12:51～15:00（UT）総露出時間120分

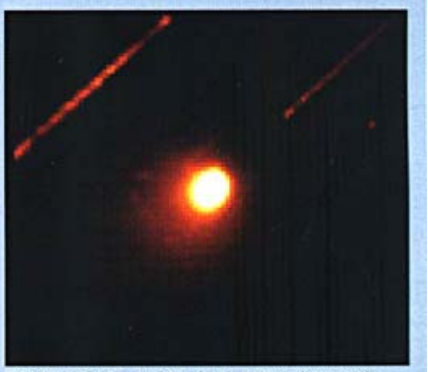

7月4日12:12～15:05（UT）総露出時間160分

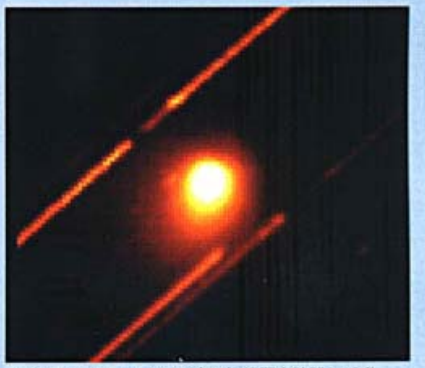

7月5日12:27～14:56（UT）総露出時間140分

【共通データ】鹿林1m望遠鏡（口径1m F8）＋偏光撮像装置PICO、写野角3.7′×3.7′

13

中央大學鹿林天文台發現他們的第八顆超新星

原文轉載自【2005-01-21/台北市立天文科學教育館電子報】

中央大學天文研究所「臺灣超新星巡天計畫（Taiwan Supernova Survey）」從開始加入超新星搜尋戰局至今，在不到一年的時間內且觀測時間不多的情形下，已經發現了他們的第八顆超新星--SN 2005O（SN 爲超新星 Supernova 的縮寫，2005 爲發現年，英文字母 O 爲 2005 年當中全球發現的第 15 顆超新星）。

中央大學天文研究所研究生陳英同利用中大鹿林山天文台 1 米望遠鏡 LOT (Lulin One-meter Telescope) 進行超新星搜尋工作，於國際標準時 1 月 16.78 日發現這顆位在 NGC 3340 星系中的超新星，發現時亮度約爲 16.1 等（未加濾鏡，如下右圖短線標示處），並在 1 月 20.650 日增亮至 15.2 等。在先前 2004 年 12 月 27 日的觀測影像中（下左圖）中並未有這顆星的存在，因此確認爲超新星。

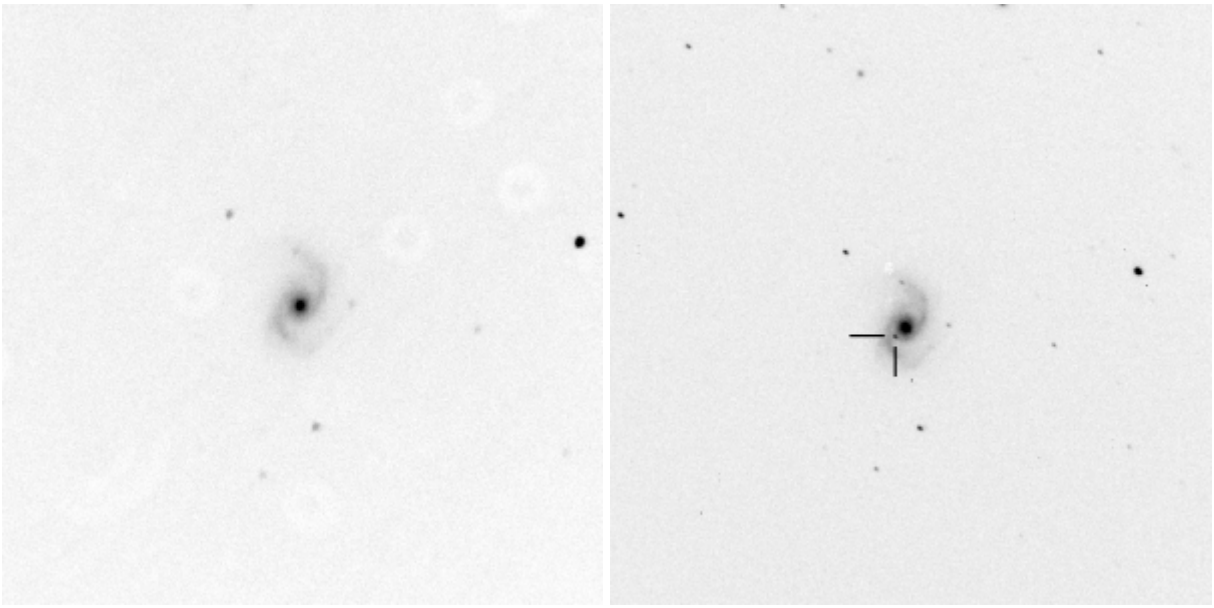

20041227　　20050116

「臺灣超新星巡天計劃」在葉永烜教授主持下，由林忠義、黃癸雲、陳英同及林宏欽等成員共同執行觀測任務，利用 LOT 定期地進行超新星巡天工作。超新星大部分是在外星系中被發現，平均每個晚上可以觀測 300 個以上的候選星系，並即時將新的星系影像與以前觀測過的星系影像進行比對，如找出疑似超新星候選者的星體則可以進一步確認。臺灣超新星巡天計劃採國際合作模式，合作單位包括美國加州柏克萊大學天文系 KAIT 及大陸北京國家天文台。由於國外的超新星搜尋計畫集中於北半球，如 KAIT 與北台觀測天區皆以北天球天區爲主。利用台灣低緯度的地理優勢，選擇偏南天的星系，可以發現更多新的超新星，使超新星的研究課題能有更多的觀測目標與資料，大幅推動國際水平。

參考資料來源：鹿林天文台第 8 顆超新星 SN2005O，IAUC No. 8471。

瑞雪紛飛　鹿林山天文台降下罕見三月雪

原文轉載自【2005-03-21/中央大學電子報】

【本報訊】三月初持續低溫特報，海拔近三千公尺的中央大學鹿林天文台降下罕見的三月雪，氣溫一路盪到零度以下，積雪達十餘公分厚，屋外一片銀白世界，工作人員興奮地堆起雪人、打雪仗，僅管冷到發抖，但看到這場罕見的三月雪，大家都大呼「值得」！

相較於合歡山、太平山聚集了大批遊客，鹿林山天文台由於是學術觀測地點，因此「遊

客止步」，一片片瑞雪不斷從天而降，四週道路、天文台都覆蓋了皚皚白雪。工作人員仰望繁星點點同時，還能擁抱白色世界，都顯得奮興莫名。

鹿林天文台位於鹿林前山，緊鄰玉山國家公園，海拔高 2862 公尺，位於大氣逆溫層之上，白日雲層籠罩，但傍晚後隨著氣溫下降，雲層逐漸下降，因此可露出晴朗夜空，遮擋山下光害，特別適合天文觀測。一般入夜後氣溫約爲 5℃～10℃，連續幾波冷氣團發威，可降到零下 6-7 ℃。

今年慶祝本校九十週年校慶，5 月 28、29 日將由劉全生校長、張昭焚理事長領隊進行「參訪鹿林天文台活動」，鹿林山天文台附近風景秀麗，原住民部落民風淳樸，熱情好客，本次參訪除了可以飽覽天文科學新知與欣賞山林自然美景，更可以親身體驗原住民的風俗與文化。

鹿林天文台目前設有中大 0.76 公尺口徑反射式望遠鏡，另有我國與美國等國家合作之「中、美掩星計畫」0.5 公尺口徑超廣角望遠鏡構成的監測網。2002 年完成台灣最大口徑一公尺望遠鏡上線，使鹿林山天文台成爲台灣天文學術研究的聖殿。

物理年接力點燈 419 台灣九處發光

轉載自【2005-04-12/聯合報】

紀念愛因斯坦發表相對論 100 周年暨逝世 50 周年發起的「讓物理光耀世界」活動，全球物理迷將在愛因斯坦逝世的 4 月 18 日 (美國時間)點燈，台灣物理同好則準備在 19 日晚上 7 時在九個地方接力點燈。

中華民國物理學會表示，活動同時另有線上點燈活動，參加者可到「讓物理光耀世界」網站登錄個人資料，登錄成功後依照主辦單位規定的程序點燈，主辦單位網站上的世界地圖，台灣就會多一盞燈。

至於全球連線點燈將從美國紐澤西州愛因斯坦的故居啓動。台灣部分會在 19 日晚上 6 時 40 分由東岸花蓮縣立棒球場啓動，依序傳到高雄科工館、台南市運河、台南縣縣府廣場、彰化八卦山大佛、台中科博館、新竹同步輻射中心，晚上 7 時在台北 101 大樓及玉山鹿林天文台同時點燈。在 101 大樓上亮出全球最高的 E=mc2（相對論公式)。

「讓物理光耀世界」全球網頁 http://www.wyp2005.at/glob1-light.htm

記者孫蓉華／台北報導

紀念愛因斯坦 讓物理光耀世界

原文轉載自【2005-04-19/聯合報/C8 版/教育・文化】

全世界紀念愛因斯坦發表相對論 100 周年暨逝世 50 周年，今天將有一連串的「讓物理光耀世界」活動，今晚台灣有十個地點接力點燈，台北 101 大樓也將打出世界最高的 E=MC2，德國電視台將來台轉播此一盛事。

「讓物理光耀世界」活動聯絡人蔡美惠表示，如果不能親臨點燈現場，也可以上 www.419.com.tw 網站參加「世界線上點燈競賽」活動，民眾可先上網註冊，在今晚七點以前，以簡訊傳送註冊時獲得的密碼到+43 676 800 676 777，台灣地圖上就會亮一個燈，只要台灣的亮燈密度最高，就可以到瑞典接受世界表揚。

蔡美惠說目前估計已經有一萬人上網註冊，有趣的是，此次有近 50 個國家參加這次的活動，但網路點燈活動時台灣與大陸是分開計算亮燈密度，大會總網頁上還特地註明「This project must not be used in any way for political purposes!」即這個活動不涉及政治。

除了網路及台灣實地點燈，如果最近在ＭＳＮ上看到顯示名稱前出現一個燈泡，這也是參加相對論 100 周年的紀念活動，主辦單位也號召大家放上燈泡，跟世界一起點燈。

蔡美惠表示，台灣的起始站花蓮將以原住民鑽木取火的方式啓動點燈，還會到彰化八卦山大佛，並在玉山鹿林天文站點亮台灣最高的燈，估計全台將有數萬民眾參與。

全球的點燈連線，將從美國紐澤西州普林斯頓城愛因斯坦故居開始，第一道雷射光束劃破黑暗夜空，橫越美國國界及太平洋向亞洲挺進。接著分別往北沿著俄羅斯及往南同時繞經日本與台灣，回程在奧地利會合，最後再回到起始點普林斯頓城。

記者林怡婷／台北報導

鹿林天文台光束上雲霄

原文轉載自【2005-04-20/台灣日報】

東南亞最高的中央大學鹿林天文台昨晚配合全球 2005 物理年的「讓物理光耀世界」（Physics Enlightens the World）點燈活動，在晚間 7 時點亮直達雲霄的光束，表達對愛因斯坦卓越貢獻的敬意與辭世 50 週年的悼念，並慶祝該校 90 週年校慶。

爲了紀念愛因斯坦發表光電效應理論、布朗運動、相對論 100 週年，以及愛因斯坦逝世 50 週年，聯合國特地將今年定爲全球物理年。奧地利兩位教授發起的「讓物理光耀世界」點燈活動在愛因斯坦逝世的 4 月 19 日當天，由他生前最後工作的普林斯頓大學開始，在校園全面熄燈後以雷射啓動點燈活動，一路往美國西部傳遞，跨越太平洋後到達日本、台灣、中國等地區，然後持續往歐洲傳遞，跨越大西洋再回到美國，整個活動將環繞地球延續兩天，爲 2005 物理年掀起第一波高潮。

記者許瀚文/信義報導

全台發光 直沖三千公尺天文台

原文轉載自【2005-04-20/中國時報】

紀念愛因斯坦發明相對論一百周年，物理年系列活動之「讓物理光耀世界」，十九日晚間將在全台各地同步點燈。海拔將近三千公尺的中央大學鹿林天文台，成爲這一波點燈活動的最高據點。

此次傳遞燈火的活動，獲全球四十四國的響應，台灣在十九日晚上六點四十分開始由東岸花蓮啓動，依序傳到高雄科工館、台南市運河、台南縣縣府廣場、彰化八卦大佛、台中科博館、新竹同步輻射中心，晚上七點整在台北一０一大樓及玉山鹿林天文台接力點燈，隨後再由東南亞各國及中國大陸、蒙古等地接力。

此次活動由中華民國物理協會、工業技術研究院主辦，位在玉山上的中央大學鹿林天文觀測站，是國內最高的天文觀測站，因此也獲選爲傳遞燈火地點。

爲參加此次傳遞燈火活動，共計有四組重達一千公斤的燈具，從高雄北運至鹿林山登山口，再透過索道吊上去，工程浩大。而且每盞燈有四千瓦，光束打向十一公里的高空，照亮鹿林山夜空，遠從阿里山風景區、新中橫公路都可看到這項歷史景觀。

「如果沒有愛因斯坦，新竹科學園區可能會晚二十年出現！」竹科同步輻射中心十九日晚上，用同步加速器打出光束線，直接詮釋愛因斯坦對文明的影響力。並安排神秘嘉賓「愛因斯毯」，台下八百多位學生及來賓立即爲這位貌似大師的來台研究學者歡呼，「笑」果十足。

昨晚七點零五分，「物理學光耀世界」的聖火傳遞到彰化；科學之神愛因斯坦的相對論，在八卦山上碰到宗教之神的大佛。考試院長姚嘉文等人按鈕，大佛頓時光亮起來。百盞天燈也從後邊升起，像物理學造福世界一般地，爲這塊土地上的子民祈福。

台南市政府，昨晚七點零二分在今年台灣燈會「鳳鳴玉山」會場，和世界同步行動，由市長許添財、教育局長王水文、和成功大學物理系主任傅永貴，以飛箭方式點燃愛因斯坦提出的相對論原理。亮起「E=MC2」。台南縣長蘇煥智打扮成愛因斯坦模樣，帶隊以騎協力車發電方式，順利將燈點亮。

記者鄭滄杰、陳愛珠、陳志成、葉明憲、楊淑芬、鄭緯武/綜合報導

太空探索新發現 2005 GW60 小行星　鹿林天文台第二顆

原文轉載自【2005-04-21/東森新聞報】

國立中央大學天文研究所博士後研究員木下大輔博士與博士生黃葵雲，利用鹿林天文台 1 米望遠鏡，發現一顆新的小行星，目前已獲國際小行星組織確認並給予暫訂編號 2005 GW60。

木下（Kinoshita Daisuke）博士受黃葵雲之託，於 2005 年 4 月 8 日晚上觀測 SWIFT 觀

測衛星通報之伽瑪射線爆發源 GRB 20050408 的餘暉。由於預報位置的預差範圍頗大，因此他們利用 LOT 總共觀測了 4 幅影像，才將整個預報範圍全部涵蓋。

通常 SWIFT 衛星偵測到 GRB 爆發後，會立即通報全球相關單位進行後續觀測。黃葵雲利用 DSS（Digital Sky Survey 數位星圖）查驗影像，發現兩個 GRB 的疑似目標。因此，她與木下博士再度針對這兩個疑似目標進行確認，經兩小時的觀測後，卻發現其中一個目標「會移動」--這是一顆小行星！經過與所有已知小行星比對之後，確定這顆小行星是以前從未發現過的新小行星。經過 Vaisala 軌道程式計算位置與軌道元素之後，木下博士估計這顆小行星的 V 亮度約爲 19 等。

爲了取得新小行星的暫訂命名，必須連續觀測 2 晚以上的資料。不過 4/9 天氣不佳，讓木下博士相當擔心；4/10 按 Vaisala 的預測位置再度進行觀測，終於成功地監測到這顆新小行星，並立即進行小行星的天文位置測量，再將測量結果通報給國際天文聯合會（IAU）所屬的國際小行星組織（Minor Planet Center，MPC）。MPC 確認後，於臺灣時間 4/11 發佈公告，並給予暫訂編號 2005 GW60。

這是鹿林天文台 1 米望遠鏡成立 2 年多來，所發現的第二顆小行星。木下博士目前擁有這顆小行星的命名權，他表示考慮將這顆小行星命名爲「中央大學 90（NCU90）」，以紀念恰於今年邁入 90 周年的中央大學。

東新新聞報訊

中大發現小行星　鹿林天文台三年內連見兩顆

原文轉載自【2005-05-13/大學報/7 版/地球紀實】

中央大學天文研究所博士後研究員木下大輔（Kinoshita Daisu-ke），利用鹿林天文台一米望遠鏡（Lulin One-meter Telesco-pe， LOT），在太陽系發現一顆小行星。這項發現純粹是個偶然。

當時木下待在玉山海拔二千八百公尺的鹿林天文台，忽然聽到一陣鈴聲，原來是天文所博士生黃葵雲來電，請木下協助觀測伽瑪射線爆發源 GRB 20050408（目前宇宙中除大霹靂之外，已知最劇烈的天體爆發現象）的餘暉。

木下一口答應，馬上利用一米望遠鏡觀測餘暉。彙整資料後，他發現二個 GRB 可疑目標，趕緊打電話給黃葵雲，而她請木下再確認一次。經過二小時觀測，木下有了大發現，按耐不住興奮之情，火速通知黃葵雲。電話嘟嘟響了幾聲，黃葵雲接起電話還來不及說「喂」，就聽到話筒那頭爆出這麼一句：「其中一個可疑目標居然會移動，它是顆小行星！」黃葵雲憶及當時大木對她說的話，仍感到相當驚訝。她說：「萬萬沒想到天外竟飛來這麼一『球』。」

木下上網搜尋已發現小行星資料，確定這顆「可疑目標」確實是新發現。他運用軌道程式計算小行星位置，推估小行星未來的運行方向，以利後續觀測。

據木下觀察，小行星位於太陽系小行星帶，距離地球二點三個天文單位（一個天文單位是地球與太陽的單程距離），鄰近獅子座。星等爲十九點八等，是相當暗的小行星。而太陽光

經小行星反射後，需過十九分鐘才會抵達地球。鎖定小行星軌道後，木下將繼續探測光度變化以測知運轉週期。另外，他也將進一步觀察外部顏色，推測小行星可能的組成元素。

目前這顆小行星已獲國際天文聯合會（International Astro-nomical Union，IAU）所屬的國際小行星組織（Minor PlanetCenter，MPC ）確認，暫定編號 2005GW60。擁有命名權的木下博士，考慮將小行星名爲「中央大學 90（N-CU90）」，以紀念中大創校九十週年。

二年多前鹿林天文台剛成立時，中大天文所研究生張智威與陳秋雯，就曾用同一台望遠鏡發現一顆小行星，並命名爲「鹿林一號」，而木下發現的小行星是鹿林天文台觀測史上的第二顆。

記者翁英傑台北電話報導

亮燈密度 全球第一 物理年點燈 台灣「光」耀世界

原文轉載自【2005-06-21/中國時報/A8 版/社會脈動】

紀念愛因斯坦，台灣光耀國際！全球今年發起「讓物理光耀世界」點燈活動，紀念愛因斯坦發表相對論一百周年暨逝世五十周年，台灣在四十七個參賽國中，同時贏得世界線上點燈競賽亮燈數最高密度國家、全球最高樓１０１點燈的榮耀，勇奪兩個世界第一，預計七月十三日在瑞士伯恩接受榮譽表揚。

全球四十七國參與「讓物理光耀世界」活動，總計六萬五千個線上點燈成功，台灣民眾的熱情參與，更讓台灣亮燈數贏得最高密度，在世界地圖上成爲最亮的發光點，點燈當晚的高品質活動設計更脫穎而出，吸引全球注目。

根據世界物理年大會規定，參與二００五世界物理年世界線上點燈競賽的國家民眾在網站上完成註冊後，大會會傳送一組密碼，並以電子郵件通知一組電話。點燈當晚七點，將密碼以簡訊方式傳送至大會通知的電話號碼，大會就會替參與民眾的國家點亮一顆小燈。

「讓物理光耀世界」活動在台灣時間四月十九日晚上七點登場，全球同步進行線上點燈競賽簡訊活動，總計四十七國登記註冊，收到來自世界各地卅二個國家、超過六萬五千封簡訊。台灣民眾的團結與熱情，爲台灣點亮了六千多顆小燈，亮燈密度最高（相對於總人口數的線上點燈比例），勇奪世界第一。

此外，世界最高樓台北１０１也點燈打上相對論公式（E=mc2）、海拔近三千公尺的中央大學鹿林天文台更點亮直達雲霄的光束紀念愛因斯坦。

前五名得獎的國家依序爲台灣、奧地利、多明尼加共和國、拉脫維亞及斯洛伐克，保加利亞排名第六，中國大陸第七、日本第八。全球線上點燈競賽得獎公佈網頁 http://www.wyp2005.at/glob1-light.htm。

中華民國物理學會理事長張慶瑞表示，台灣參與點燈的人數遠遠超過物理學會的會員數，對這些熱情支持科普活動的民眾，該會致上最高謝意。

陳洛薇/台北報導

台灣鹿林天文台第二個觀測重鎮

原文轉載自【2005-07-03/聯合晚報/3 版/話題新聞】

美國航空暨太空總署 (NASA)探測「坦普爾彗星一號」的深撞彗星計畫，除了美國夏威夷天文台之外，台灣的中央大學設在玉山的鹿林天文台將是第二個觀測重鎮。

中央大學指出，夏威夷的天文台，就如同天文劇院的前排座位一般，是在撞擊發生時，看得最清楚的地方。而在夏威夷的天文台觀測後，便由在台灣的鹿林天文台接手觀測，將爲此次太空任務留下珍貴的研究資料。

雖然不是在第一排的位置，但中央大學表示，科學家預測撞擊產生的灰塵，以及可能從內部噴發出的氣體，將造成明亮閃焰。由於估計撞擊後約六小時，亮度可能有明顯變化，當時正值臺灣晚上 8 時左右，鹿林天文台因地理位置特殊，反而位於最佳監測地理位置。

中央大學天文所教授葉永烜表示，此次彗星深撞太空計畫，370 公斤的撞擊體將以 3 萬 6 千公里時速撞擊坦普爾彗星一號，產生相當於 4.8 噸黃色炸藥的威力，預期將產生一個美式足球場大小，深 7 層樓的坑洞。屆時搭配美國國慶日，等於上演一場太空煙火秀。

記者袁世忠/台北報導

天文奇景　七月四日深撞彗星計畫（Deep Impact）

原文轉載自【中央大學電子報】

美國航空暨太空總署 (NASA) 所發射的太空船預計在台灣時間 7 月 4 日下午 1 點 52 分，深度撞擊並探測「譚普彗星一號」(Comet Temple 1)。觀測這次任務的最佳位置在美國夏威夷天文台，下一站便是台灣的中央大學鹿林天文台，預料爲此次太空任務留下珍貴的研究資料。中央大學天文所七月初也將和台北市立天文館合辦推廣活動，帶領民眾更了解這項任務的科學意義。

中央大學天文所教授葉永烜表示，此次彗星深撞太空計劃（Deep Impact），美國 NASA 歷時六年方有成果。370 公斤的撞擊體將以 3 萬 6 千公里時速撞擊譚普彗星一號，產生相當於 4.8 噸黃色炸藥的威力，預期將產生一個美式足球場大小，深 7 層樓的坑洞。屆時搭配美國國慶日，進行一場太空煙火秀。

全世界的天文台當天都會觀察此實驗，其中夏威夷的天文台將扮演關鍵角色，夏威夷的居民將如同電影前排座的最好位置，在撞擊發生時，看得最清楚。而在夏威夷的天文台觀測後，便由台灣的中央大學鹿林天文台接手觀測，將爲此次太空任務留下珍貴的研究資料。

科學家預測撞擊產生的灰塵，以及可能從內部噴發出的氣體，將造成明亮閃焰。由於估計撞擊後約 6 小時，亮度可能有明顯變化，當時正值臺灣晚上 8 時許，故中央大學鹿林天文台因地理位置特殊，將位於最佳監測地理位置。故鹿林天文台的觀測資料將具特殊重要地位。

彗星是由太陽系行星在 45 億年前形成後，所剩下的物質所構成，因此彗星有如化石般保留了歷史訊息。藉由研究彗星內部結構，將有助於我們瞭解太陽系形成初期及演化的過程。

爲把握這項難得的天文奇景，中央大學天文所將與台北市立天文館合辦推廣活動，包括自己動手做彗星、模擬撞擊實驗、天文所葉永烜教授專題演講等。7 月 4 日晚間七點半，於中央大學科四館，天文所陳文屏教授也將以「看地球人還手─2005 痛擊彗星！」爲題進行演說，歡迎對此次活動有興趣的民眾踴躍參加。

中央大學秘書室

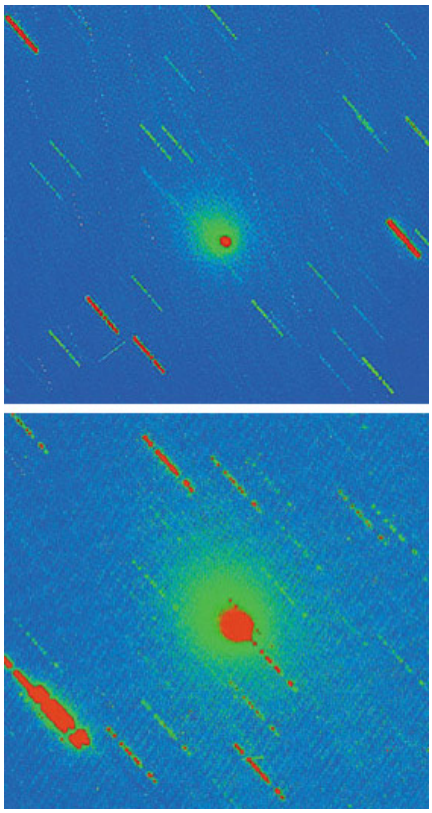

彗星被撞後 6 小時 南投最佳觀測點

原文轉載自【2005/07/05 聯合報】

昨晚夜空能見度良好，南投縣中央大學鹿林山天文台人員以天文望遠鏡，觀測彗星被深撞六小時後的灰塵及亮度變化，並利用高感度數位相機連續拍攝畫面，希望留下珍貴研究資料。

撞前(上)鹿林天文台昨晚觀測彗星被撞後的亮度變化，這是被撞前所拍的畫面。撞後(下)彗星被撞後六小時，光點更亮了。照片／中央大學提供

中央大學天文所教授葉永烜表示，全世界天文台都在觀察這項實驗，其中夏威夷天文台是最好的觀測位置，如同電影銀幕前排座位，看得最清楚；但估計彗星遭撞擊後六小時，內部噴發出來的氣體閃焰，開始產生亮度變化，這時鹿林天文台因地理位置特殊，成爲最佳觀測點。 昨晚八時，鹿林天文台搭配北京天文台興隆觀測站兩米十六望遠鏡，同時進行光譜與光度的觀測。

這次天文觀測任務除了中央大學駐台人員外，還有五位日本天文觀測人員參與，他們空運價值三、四百萬元的「偏光攝像儀」到台灣，開車運到鹿林山腳下，再由原住民以人力搬運上山，因山路坎坷難行，搬運工作艱險。

記者余炎昆／南投縣報導

觀撞擊彗星 中大鹿林天文台最佳

原文轉載自【2005-07-06/聯合報/C2 版/桃園縣新聞】

美國航空暨太空總署發射的太空船前天成功撞擊「譚普彗星一號」，經由中大和日本「ＰＩＣＯ」天文團隊合作，以 1 公尺口徑偏光望遠鏡觀測，發現彗星在撞擊後形狀稍有拉長，亮度也增加了 3 至 4 倍。

中大太空研究所教授葉永烜表示，美國航空暨太空總署 所發射的太空船前天成功撞擊「譚普彗星一號」，中大鹿林天文台透過日本空運來台具有「偏光攝像儀」功能的 1 公尺口徑望遠鏡，拍攝到撞擊後的珍貴畫面，發現彗星形狀拉長，呈現橢圓狀，亮度增加 3 至 4 倍，透過塵埃的分布和變化，對瞭解太陽系形成初期及演化的過程有重大意義。

日本「ＰＩＣＯ團隊」首席科學家木下大輔說，中大鹿林天文台因地理位置特殊，處於最佳監測位置，反觀日本目前處於梅雨季節，緯度較高，觀測條件不如台灣，因此選擇鹿林天文台測監，從 7 月 1 日至 7 月 9 日爲期 10 天。

葉永烜指出，20 多年前太空任務開始之際，都是以大行星爲對象，但目前小行星及彗星已經取而代之成爲主要研究對象，因爲從隕石分析，彗星含有形成生命起源的有機分子，地球上的生命很可能是從其他彗星和小行星來的。

記者游文寶/中壢報導

中大觀星：呈橢圓狀改變 亮度增三至四倍

原文轉載自【2005-07-06/中國時報/A14 版/國際新聞】

美國航空暨太空總署（ＮＡＳＡ） 發射太空船成功撞擊「坦普爾彗星一號」，國內觀測研究同步啓動，國立中央大學鹿林天文台第一時間拍攝及紀錄，對照深擊前照片，初步發現彗星行進形狀呈橢圓狀改變，亮度增加三至四倍。

位於玉山國家公園的鹿林天文台，海拔近三千公尺，配合這次「Deep Impact」任務，不僅有中大天文所研究團隊觀察，包括日本國立天文台、東京大學、早稻田大學等師生所組成「PICO 團隊」，也遠渡重洋來台，跨國聯手合作，完成觀測紀錄。

PICO 團隊最大優勢，就是帶來造價三百萬「偏光攝像儀」，直接由日本空運來台，透過人力背運上山，專門研究撞擊後的塵埃分布和變化，加上中大全國最大口徑一米望遠鏡，相輔相成。「PICO 團隊」的首席科學家木下大輔說，日本目前梅雨季節，緯度高，觀測條件不如台灣。

黃文杰/中壢報導

深撞彗星計畫　臺日合作觀測

原文轉載自【2005-07-07/中央日報/A14 版/教育・藝文】

美國航空暨太空總署（ＮＡＳＡ）所發射的太空船七月四日成功撞擊「譚普彗星一號」（CometTemple1）。全國最高的中央大學鹿林天文台扮演重要角色，透過日本空運來臺貴重的「偏光攝像儀」和全國最大口徑一米望遠鏡，拍攝到珍貴畫面，發現彗星形狀稍有拉長，呈現橢圓狀，且亮度增加三至四倍，透過塵埃的分布和變化，對於了解太陽系形成初期及演化的過程有重大意義。

包括日本國立天文台、東京大學、早稻田大學等師生所組成「ＰＩＣＯ團隊」，遠渡重洋來臺，空運造價三百多萬的「偏光攝像儀」，透過人力揹運上山，運抵海拔近三千公尺的中

大鹿林天文台，目的就是要記錄此次人類首次的撞擊彗星計畫。

「ＰＩＣＯ團隊」的首席科學家木下大輔（中大天文所助理教授）說，中大鹿林天文台因地理位置特殊，處於最佳監測位置。日本目前處於梅雨季節，緯度較高，觀測條件不如臺灣，因此選擇鹿林天文台進行測監計畫，從七月一日至七月九日，爲期十天密集監測。

中大天文所教授葉永烜表示，人類首次撞擊彗星是天文科技上重要成就，扭轉過去太空科技爲軍事戰爭競賽的方向，未來太空天文科技發展應該以「地球村」的概念，非但全世界的天文台都在觀測，所觀測到的資訊也會透過網路分享。

另一個重要意義，就是人類把彗星從遠地觀測，變成第一次可在實驗室用人工做成的太空船撞擊後予以改變。彗星是由太陽系行星在四十五億年前形成後，所剩下的物質所構成，因此彗星有如化石般保留了歷史訊息。藉由研究彗星內部結構，將有助於我們了解太陽系形成初期及演化的過程。

徐乃義/中壢報導
